

**Development of Novel Tandem Mass Spectrometric Strategies
towards LC/FT-ICR MS-Based Structural Determination in
Metabolomics and Peptidomic Analysis**

By

Hyun Ju Yoo

**A dissertation submitted in partial fulfillment
of the requirements for the degree of
Doctor of Philosophy
(Chemistry)
in The University of Michigan
2010**

Doctoral Committee:

**Associate Professor Kristina I. Håkansson, Chair
Professor Robert T. Kennedy
Professor Michael D. Morris
Assistant Professor Peter J. Woolf**

© Hyun Ju Yoo
All Rights Reserved 2010

To My Dear Family

Acknowledgments

I would like to express the deepest appreciation to my committee chair and advisor, Professor Kristina Hakansson. Without her unflinching encouragement, support, guidance and persistent help, this dissertation would not have been possible. I would like to thank my committee members, Professor Morris, Professor Kennedy, and Professor Woolf, who devoted their time to overview all my thesis work and gave valuable advice through this journey. In addition, I would like to thank Professor Opiari and Professor DiRita of the Medical School at the University of Michigan, who provided me with samples and scientific advice for mass spectrometry-based metabolomics work. I also would like to give a special thanks to the Department of Chemistry, University of Michigan for supporting me as GSI and with generous fellowships through my thesis study.

In my daily work I have been blessed with a friendly and supportive group of fellow students. I have worked with so many awesome people in Hakansson's group. It is a pleasure to convey my gratitude to them including all former and current group members (Haichuan, Jason, Jiong, Hye Kyung, Natasa, Julie, Jingjie, Bo, Katie, Hangtian, Wen, Yibing, Ashley, Di, and Ning). I am truly indebted to all of these people. I also would like to thank my collaborators, Lara and Jyl, for their help and discussions for metabolomics and lipid work.

Most of all, many thanks should go in particular to my husband, Sung Hoon and lovely daughter, Su Bin for their sacrifice, patience, and thoughtful support through my study. I am also heartily thankful to my parents who love me and pray for me everyday.

Hyun Ju Yoo

May 11, 2010

Ann Arbor, MI

Table of Contents

Dedication.....	ii
Acknowledgments.....	iii
List of Tables.....	x
List of Figures.....	xi
List of Schemes.....	xiv
List of Appendices.....	xv
List of Abbreviations.....	xvii
Abstract.....	xix
Chapter	
1. Introduction.....	1
1.1. Metabolomics.....	1
1.2. Mass Spectrometry-based Metabolomics.....	3
1.3. Fourier Transform Ion Cyclotron Resonance Mass Spectrometry.....	5
1.4. Alternative MS/MS strategies available in FT-ICR MS.....	9
1.4.1 MS/MS via Vibrational Excitation.....	10
1.4.2 MS/MS via Electron Based Reactions.....	11
1.5. Dissertation Overview.....	13
1.6. References.....	16

2. Metabolic Profiling of Jurkat T Cells by Hydrophilic Interaction Liquid Chromatography/Fourier Transform Ion Cyclotron Resonance Mass Spectrometry (HILIC FT-ICR MS).....	20
2.1. Introduction Identification.....	20
2.2. Experimental Section.....	22
2.2.1. Sample Preparation.....	22
2.2.2. HILIC Separation.....	23
2.2.3. Fourier Transform Ion Cyclotron Resonance Mass Spectrometry.....	24
2.2.4. Data Analysis.....	24
2.3. Results and discussion.....	25
2.3.1. HILIC/FT-ICR MS Method Development and Reproducibility.....	25
2.3.2. Evaluation of Cell Washing Conditions.....	29
2.3.3. LC/FT-ICR MS for Untreated and Drug-treated Jurkat Cells.....	32
2.3.4. Comparison between Untreated Jurkat cells and 2-deoxyglucose-Treated Jurkat cells.....	37
2.4. Conclusions.....	38
2.5. References.....	45
3. Infrared Multiphoton Dissociation and Electron Induced Dissociation as Alternative MS/MS Strategies for Metabolite Identification.....	47
3.1. Introduction.....	47
3.2. Experimental Section.....	51
3.2.1. Sample Preparation.....	51
3.2.2. Fourier Transform Ion Cyclotron Resonance Mass Spectrometry.....	51
3.3. Results.....	53
3.3.1. CID, IRMPD, and EID of Phosphorylated Carbohydrates Involved in Glycolysis.....	53
3.3.2. CID, IRMPD, and EID of Adenosine 5'-triphosphate (ATP).....	56
3.3.3. CID, IRMPD, and EID of Adenosine 5'-diphosphate-ribose (ADP-ribose).....	59

3.3.4. CID, IRMPD, and EID of Nicotineamide Adenine Dinucleotide (NAD).....	59
3.3.5. CID, IRMPD, and EID of Nicotinic Acid-Adenine Dinucleotide phosphate (NAADP).....	60
3.4. Discussion.....	64
3.5. Conclusions.....	67
3.6. References.....	68
4. Determination of Double Bond Location in Fatty Acids by Manganese Adduction and Electron Induced Dissociation.....	71
4.1. Introduction.....	71
4.2. Experimental Section.....	74
4.2.1. Sample Preparation.....	74
4.2.2. Fourier Transform Ion Cyclotron Resonance Mass Spectrometry	75
4.3. Results and Discussion.....	76
4.3.1. EID of Metal-adducted Arachidonic Acid.....	76
4.3.2. Charge-Remote Fragmentation in EID of Ni(II), Mg(II), Ca(II), Fe(II), and Mn(II)-adducted Arachidonic Acid.....	79
4.3.3. Charge-Remote Fragmentation in EID of Mn(II)-Adducted Fatty Acids..	85
4.3.4. EID vs. IRMPD of Mn-adducted Fatty Acids.....	86
4.4. Conclusions.....	87
4.5. References.....	88
5. Determination of Phospholipid Regiochemistry by Ag(I) Adduction and Tandem Mass Spectrometry.....	91
5.1. Introduction.....	91
5.2. Experimental Section.....	96
5.2.1. Sample Preparation.....	96
5.2.2. Fourier Transform Ion Cyclotron Resonance Mass Spectrometry.....	97
5.3. Results and Discussion.....	98
5.3.1. CID of Protonated Phospholipids.....	98
5.3.2. CID and IRMPD of Ag-adducted Phospholipids.....	100

5.3.3. CID and IRMPD of Cu-adducted Phospholipids.....	109
5.4. Conclusions.....	111
5.5. References.....	112
6. Electron Capture Dissociation of Divalent Metal-Adducted Phospholipids..	115
6.1. Introduction.....	115
6.2. Experimental Section.....	118
6.2.1. Sample Preparation.....	118
6.2.2. Fourier Transform Ion Cyclotron Resonance Mass Spectrometry.....	119
6.3. Results and Discussion.....	120
6.3.1. ESI of Divalent Metal Ion-adducted Phospholipids.....	120
6.3.2. ECD of Divalent Meta Ion-adducted Phospholipids.....	121
6.4. Conclusions.....	134
6.5. References.....	135
7. Electron Capture by Peptide Anions: Direct Dissociation and Radical-Driven MS³	138
7.1. Introduction.....	138
7.2. Experimental Section.....	142
7.2.1. Sample Preparation.....	142
7.2.2. Fourier Transform Ion Cyclotron Resonance Mass Spectrometry.....	142
7.3. Results and Discussion.....	144
7.3.1. Electron Capture by Negatively Charged Peptides.....	144
7.3.2. Effect of Electron Energy on Electron Capture Efficiency.....	146
7.3.3. IRMPD MS ³ of Distonic Radical Anions generated by Electron Capture vs. MS/MS of Even-electron Peptide Anions of the Same Charge State.....	149
7.3.4. niECD of Peptide Anions	152
7.4. Conclusions.....	158
7.5. References.....	159

8. Conclusions and Future Directions	161
8.1. Conclusions.....	161
8.2. Future Directions.....	164
8.2.1. Applications of Developed Alternative MS/MS Strategies and LC/FT-ICR MS/MS.....	164
8.2.2. Study of niECD Mechanism.....	165
8.2.3. Application of niECD to Other Biomolecules.....	166
8.3. References.....	166
Appendices.....	168

List of Tables

Tables

Table 2.1. Intra- and interday retention time reproducibility in HILIC/FT-ICR MS.	27
Table 2.2. Intra- and interday peak area reproducibility in HILIC/FT-ICR MS.....	28
Table 2.3. Comparison of metabolite signal abundances from Jurkat cells after washing with water, 10 mM Tris buffer, or 10 mM phosphate buffer	30
Table 2.4. Metabolic changes after 2-deoxyglucose treatment of Jurkat cells.....	39
Table 6.1. Observation of $[R_2COO - H + Met]^+$ and $[M - R_2COOH]^+$ for PC, and the ratio of the sum of total product ion abundances involving bond cleavage at the sn-2 to that of total product ion abundances involving bond cleavage at the sn-1 esterification site in ECD spectra of divalent metal-adducted phospholipids.....	130
Table 7.1. Observation of radical species, $[M - H]^{2-\bullet}$ or $[M - 2H]^{3-\bullet}$, generated from electron capture by negatively charged peptides.....	150
Table 7.2. Backbone bond fragmentation observed in niECD and CID of phosphorylated and sulfated peptides.....	156
Table A.1. Phosphate-containing metabolites and their structures.....	171
Table A.2. The concentrations of phosphate-containing metabolites in standard metabolite mixture.....	177

List of Figures

Figures

Figure 1.1. Schematic diagram of the 7T-Q-FT-ICR mass spectrometer used for the experiment presented in this thesis.....	6
Figure 1.2. Excitation and detection events in an ICR cell and generation of the time domain signal.....	9
Figure 2.1. Comparison of metabolite signal abundances from Jurkat cells washed with water, 10 mM phosphate buffer, or 10 mM tris buffer.....	31
Figure 2.2. TIC and EICs for metabolites in standard metabolite mixture (a) and 40 million Jurkat cells (b).....	33
Figure 2.3. 3D profiles, reconstructed with MS Excel, for untreated, oligomycin-treated, and 2-deoxyglucose-treated Jurkat cells.....	35
Figure 2.4. PCA analysis for (a) untreated vs. oligomycin-treated or 2-deoxyglucose-treated Jurkat cells; (b) untreated vs. Bz-423-treated Jurkat cells; (c) stimulated vs. stimulated and Bz-423-treated Jurkat cells.....	36
Figure 3.1. CID, IRMPD, and EID MS/MS spectra of glucose 6-phosphate.....	55
Figure 3.2. CID, IRMPD, and EID MS/MS spectra of adenisine 5'-triphosphate...	57
Figure 3.3. CID, IRMPD, and EID MS/MS spectra of adenisine diphosphate-ribose.....	58
Figure 3.4. CID, IRMPD, and EID MS/MS spectra of nicotinamide adenine dinucleotide.....	61
Figure 3.5. CID, IRMPD, and EID MS/MS spectra of nicotinic acid adenine dinucleotide.....	62
Figure 4.1. EID of metal-adducted arachidonic acid	78
Figure 4.2. Normalized product ion abundances of $[C_xH_yO_2 + Met]^+$ vs. C_n	80
Figure 4.3. EID of Mn(II)-adducted fatty acids.....	83
Figure 4.4. Normalized product ion abundances of $[C_xH_yO_2 + Met]^+$ vs. C_n	84
Figure 4.5. EID and IRMPD of Mn(II)0adducted arachidonic acid.....	86

Figure 5.1. CID of protonated phospholipids	99
Figure 5.2. CID and IRMPD of Ag-adducted phosphatidylethanolamine.....	101
Figure 5.3. CID and IRMPD of Ag-adducted phosphatidylserine.....	103
Figure 5.4. CID and IRMPD of Ag-adducted phosphatidylcholine.....	104
Figure 5.5. IRMPD of Ag-adducted phospholipids.....	107
Figure 5.6. IRMPD of Ag-adducted [(C18:1/C16:0-PC) + Ag] ⁺	108
Figure 5.7. IRMPD of Cu-adducted phospholipids.....	110
Figure 6.1. ESI mass spectra of phosphatidylcholine from divalent metal- containing solutions.....	122
Figure 6.2. ECD of Ca ²⁺ -adducted phospholipids.....	123
Figure 6.3. ECD of Mg ²⁺ -adducted phospholipids.....	124
Figure 6.4. ECD of Co ²⁺ -adducted phospholipids.....	126
Figure 6.5. ECD of Zn ²⁺ -adducted phospholipids.....	127
Figure 6.6. ECD of Ni ²⁺ -adducted phospholipids.....	128
Figure 6.7. ECD of Ba ²⁺ -adducted phospholipids.....	133
Figure 7.1. Activation and dissociation of coumarin-tagged angiotensin I.....	145
Figure 7.2. Activation and dissociation of untagged angiotensin I.....	147
Figure 7.3. Electron capture efficiency as function of electron energy and electron irradiation time.....	148
Figure 7.4. Comparison of IRMPD MS ³ of the radical species, [M – H] ^{2•} , with MS/MS of the doubly deprotonated form of a tyrosine-phosphorylated peptide.....	151
Figure 7.5. niECD, EID, and CID spectra of singly deprotonated angiotensin I.....	153
Figure 7.6. niECD and CID of tyrosine-phosphorylated peptide.....	155
Figure 7.7. niECD and CID of a serine-phosphorylated β-casein tryptic peptide (residues 48-63).....	157
Figure A.1. Comparison of signal abundances of phosphate-containing metabolites before and after TiO ₂ enrichment using 7 % CH ₃ COOH as loading solution.....	174
Figure A.2. Comparison of signal abundances of phosphate-containing metabolites before and after TiO ₂ enrichment using 3.3 % HCOOH as loading solution.....	175
Figure A.3. Quantitative comparison of enrichment performance using an internal standard (ADP-ribose).....	178
Figure A.4. Effect of acetonitrile in loading and washing solution.....	179
Figure B.1. Mass spectra of lipid A from four strains of <i>V. cholerae</i> (two wild	189

types and two mutants).....	
Figure B.2. MS/MS of lipid A _{penta} from <i>V. cholerae</i> O395.....	190
Figure B.3. MS/MS of lipid A _{hexa} from <i>V. cholerae</i> O395.....	191
Figure B.4. MS/MS of lipid A _{penta} from <i>E. coli</i> K-235.....	193
Figure B.5. MS/MS of lipid A _{hexa} from <i>E. coli</i> K-235.....	194
Figure B.6. MS/MS of doubly deprotonated lipid A _{hexa} from <i>E. coli</i> K-235.....	197

List of Schemes

Schemes

Scheme 3.1. Structure and observed MS/MS fragmentation of glucose 6-phosphate.....	55
Scheme 3.2. Structure and observed MS/MS fragmentation of adenosine 5'-triphosphate.....	57
Scheme 3.3. Structure and observed MS/MS fragmentation of adenosine diphosphate-ribose.....	58
Scheme 3.4. Structure and observed MS/MS fragmentation of nicotinamide adenine dinucleotide.....	63
Scheme 3.5. Structure and observed MS/MS fragmentation of nicotinic acid adenine dinucleotide phosphate.....	63
Scheme 5.1. Structure of phospholipids.....	92
Scheme 6.1. Structure of phospholipids.....	116
Scheme B.1. Lipopolysaccharide (LPS) of <i>V. cholerae</i>	186

List of Appendices

Appendix

A. Phosphate-containing Metabolite Enrichment using TiO₂ Micro-tips.....	168
A.1. Introduction.....	168
A.2. Experimental Section.....	170
A.2.1. Sample Preparation.....	170
A.2.2. Fourier Transform Ion Cyclotron Resonance Mass Spectrometry.....	172
A.3. Results and Discussion.....	172
A.3.1. Comparison of Signal Abundances of Phosphate-containing Metabolites Before and After Enrichment.....	173
A.3.2. Quantitative Comparison of Enrichment Performance using Internal Standard.....	176
A.3.3. Effect of Acetonitrile in Loading and Washing Solution.....	178
A.3.4. Comparison of the Enrichment Performance of Phosphate-containing Metabolites Between DI/MS and LC/MS	180
A.4. Conclusions.....	181
A.5. References.....	182
B. Comparison of Collision Induced Dissociation and Infrared Multiphoton Dissociation for Structural Characterization of Lipid A.....	183
B.1. Introduction.....	183
B.2. Experimental Section.....	186
B.2.1. Sample Preparation.....	186
B.2.2. Fourier Transform Ion Cyclotron Resonance Mass Spectrometry.....	187
B.3. Results and Discussion.....	188
B.4. Conclusions.....	195

B.5. References..... 198

List of Abbreviations

Abbreviations

AMP	Adenosine monophosphate
ADP	Adenosine diphosphate
ADP-ribose	Adenosine diphosphate-ribose
ATP	Adenosine 5'-triphosphate
CDF	Charge driven fragmentation
CRF	Charge remote fragmentation
CID	Collision induced dissociation
dGMP	Deoxyguanosine monophosphate
ESI	Electrospray ionization
ECD	Electron capture dissociation
EDD	Electron detachment dissociation
EI	Electron impact
EID	Electron induced dissociation
ETD	Electron transfer dissociation
EIC	Extracted ion chromatogram
FAB	Fast atom bombardment
FT-ICR	Fourier transform ion cyclotron resonance
GC	Gas chromatography
G3P	Glycerol 3-phosphate
HPLC	High performance liquid chromatography
HILIC	Hydrophilic Interaction Liquid Chromatography
IRMPD	Infrared multiphoton dissociation
LA _{hexa}	Lipid A _{hexa}
LA _{penta}	Lipid A _{penta}
LA _{tetra}	Lipid A _{tetra}
LA _{tri}	Lipid A _{tri}

LPS	Lipopolysaccharide
LC	Liquid chromatography
m/z	Mass-to-charge ratio
MALDI	Matrix assisted laser desorption/ionization
MS	Mass spectrometry
MS/MS	Tandem mass spectrometry
niECD	Negative ion electron capture dissociation
NAD(H)	Nicotinamide adenine dinucleotide
NAADP	Nicotinic acid-adenine dinucleotide phosphate
NP	Normal Phase
NMR	Nuclear magnetic resonance
3PG	3-Phosphoglyceric acid
ppm	parts per million
PL	Phospholipid
PC	Phosphatidylcholine
PE	Phosphatidylethanolamine
PS	Phosphatidylserine
PTMs	Post-translational modifications
PCA	Principal component analysis
RSD	Relative standard deviation
RP	Reverse phase
Q	Quadrupole (mass filter)
S7P	Sedoheptulose 7-phosphate
Std	Standard deviation
SORI	Sustained off-resonance irradiation
T	Tesla, a unit of magnetic field
TCA	Tricarboxylic acid
TIC	Total ion chromatogram
UDP	Uridine diphosphate
UMP	Uridine monophosphate
<i>V. cholerae</i>	<i>Vibrio cholerae</i>

Abstract

Development of Novel Tandem Mass Spectrometric Strategies towards LC/FT-ICR MS-Based Structural Determination in Metabolomic and Peptidomic Analysis

by

Hyun Ju Yoo

Chair: Kristina Håkansson

Mass spectrometry (MS)-based metabolomics offers quantitative analyses with high selectivity and sensitivity, and the potential to identify metabolites. MS is often combined with separation techniques such as liquid chromatography (LC). Metabolic profiling of Jurkat T cells was performed with hydrophilic interaction liquid chromatography (HILIC)/Fourier transform ion cyclotron resonance (FT-ICR) MS in collaboration with Dr. Oipari's group in the Medical School, University of Michigan. The developed HILIC/FT-ICR MS could detect metabolic changes of T-cells following metabolic perturbation. However, many of the observed metabolites could not be

identified using currently available metabolic databases, which reflects a major challenge encountered in mass spectrometric metabolite analysis. Currently, mass spectral libraries are not diverse enough to allow identification of the hundreds to thousands of detected metabolites.

FT-ICR MS can provide improved metabolite identification due to its accurate mass capabilities and alternative MS/MS fragmentation techniques, including infrared multiphoton dissociation (IRMPD) and electron capture dissociation (ECD). These techniques can often provide complementary structural information compared to collision induced dissociation (CID) for various kinds of biomolecules. However, they have seen very limited, if any, application to metabolite characterization. Thus, most of the work in this thesis was devoted to method development for structural characterization and identification of small organic molecules including metabolites and peptides. Alternative strategies available in FT-ICR MS were successfully applied to provide structural information of phosphate-containing metabolites, fatty acids, and phospholipids with and without metal adduction. In addition, it is shown, for the first time, that negatively charged peptide ions can capture electrons, resulting in unique radical species, which dissociate via peptide backbone bond cleavages while retaining posttranslational modifications. Other work includes phosphate-containing metabolite enrichment with TiO₂ micro-tips to overcome ion suppression caused by highly abundant polar metabolites, and structural determination of lipopolysaccharide (LPS) using IRMPD.

Chapter 1

Introduction

1.1. Metabolomics

Metabolomics is the systematic identification and quantification of all metabolites in a biological system.¹ The metabolome represents the collection of all metabolites (such as metabolic intermediates, hormones and other signaling molecules, and secondary metabolites in a cell, tissue, organ, or organism), which are the end products of cellular processes.²⁻³ Thus, while mRNA gene expression data and proteomic analyses do not reveal complete details regarding cellular processes, metabolic profiling can provide an instantaneous snapshot of the physiology of a cell.¹

⁴⁻⁹ The metabolome is dynamic and changes every second. There are approximately 2,500 metabolites, 1,200 drugs, and 3,500 food components that can be

found in the human body, as reported in the literature.¹⁰ This information is available in the Human Metabolome Database (www.hmdb.ca) and is still far from complete based on analysis of information available in the scientific literature.¹¹⁻¹² Much more is known about the metabolomes of other organisms. For example, over 50,000 metabolites have been characterized from the plant kingdom, and many thousands of metabolites have been identified and/or characterized from single plants.¹³

Global metabolite analysis, metabolomics, involves the identification and quantification of all intracellular and extracellular metabolites using different analytical techniques. Metabolites possess wide variations in chemical (molecular weight, polarity, acidity) and physical (volatility) properties. This complexity renders it difficult to analyze various metabolites simultaneously.^{1, 7, 14} Mass spectrometry (MS), nuclear magnetic resonance (NMR) spectroscopy, Fourier transform-infrared (FT-IR) spectroscopy, and Raman spectroscopy are all used for metabolite analysis.^{4, 15-20} FT-IR and Raman spectroscopy can provide rapid, nondestructive, and high-throughput analysis of a diverse range of sample types. These spectroscopic techniques are generally used for metabolic profiling, and absorption spectra can be used for identification of unknown metabolites. However, the sensitivity and selectivity of FT-IR and Raman spectroscopy are not as high as those of other methods.⁴ NMR

spectroscopy is also a rapid and non-destructive, high-throughput method that requires minimal sample preparation. Chemical shifts can be used for metabolite identification, however, NMR requires millimolar to high micromolar concentration of samples, thereby limiting its sensitivity. Another major weakness of NMR is its poor dynamic range (10^3), which results in only the most abundant components being observed.^{4, 21} Mass spectrometry is a highly suitable technique for metabolite measurements due to its wide dynamic range (10^4 - 10^6), good sensitivity (nM), and its ability to detect a diverse number of molecular species.¹⁶ Gas chromatography (GC)/MS has been the most commonly used method for small molecule analysis although this technique is limited to volatile and relatively non-polar molecules. Chemical derivatization can improve volatility, however, such strategies are not always successful. Therefore, liquid chromatography (LC)/MS has become a popular choice for metabolite analysis. This technique allows analysis of metabolites of more diverse chemical structure and size.^{4, 16, 22}

1.2. Mass spectrometry-Based Metabolomics

Although various analytical platforms have been used for metabolomic analyses, mass spectrometry-based metabolomics offers quantitative analyses with high

selectivity and sensitivity, and the potential to identify metabolites.^{1, 14} Mass spectrometry is often combined with separation techniques, such as LC. LC/MS provides metabolite separation by LC followed by ionization (e.g., electrospray ionization (ESI)). LC/MS differs from GC/MS in several distinct ways (e.g., lower analysis temperatures, and direct sample volatility not required), which simplify sample preparation.^{4, 16, 22}

A major challenge encountered in mass spectrometric metabolite analysis is the identification and structural characterization of the hundreds to thousands of detected metabolites.¹⁴ Currently, mass spectral libraries are not diverse enough to allow identification of all detected metabolites. Metabolite libraries directly compatible with GC/MS and LC/MS data are available (e.g. METLIN).^{16, 23} However, other databases, including Metacyc and KEGG, contain metabolite molecular weight information, but are not directly compatible with MS data^{13, 24-25} because the latter databases focus on biological pathways of known metabolites whereas mass spectrometry detects both known and unknown species. METLIN¹⁶ includes an annotated list of known metabolite structural information with tandem mass spectra and LC/MS data, however, the number of mass spectra in the latter database is still rather limited. Improved metabolite identification may be obtained through tandem mass

spectrometry (MS/MS), which can provide characteristic fragmentation patterns from collision induced dissociation (CID) of metabolite ions inside the mass spectrometer.^{15,}

24, 26-28

Fourier transform-ion cyclotron resonance (FT-ICR) mass spectrometry²⁹ can provide improved metabolite identification due to its accurate mass capabilities³⁰ and alternative MS/MS fragmentation techniques, including infrared multiphoton dissociation (IRMPD),³¹ and electron capture dissociation (ECD).³² These techniques can often provide complementary structural information compared to CID for various kinds of biomolecules.^{31, 33-46} However, alternative MS/MS techniques have seen very limited, if any, application to metabolite characterization and their utility for that type of analysis is explored in this thesis.

1.3. Fourier Transform-Ion Cyclotron Resonance Mass Spectrometry

Fourier transform-ion cyclotron resonance mass spectrometry (FT-ICR MS) is a very high resolution technique in that masses can be determined with very high accuracy.^{29, 47-48} This high resolution is useful in studying large macromolecules such as proteins with multiple charges which can be produced by ESI.¹⁵ In addition, the

high mass accuracy and resolution of FT-ICR mass spectrometry are highly useful for identifying various kinds of metabolites in a complex biological system, and crucial to the determination or confirmation of metabolite structure via a database search, or via interpretation of MS/MS spectra.¹⁴⁻¹⁶

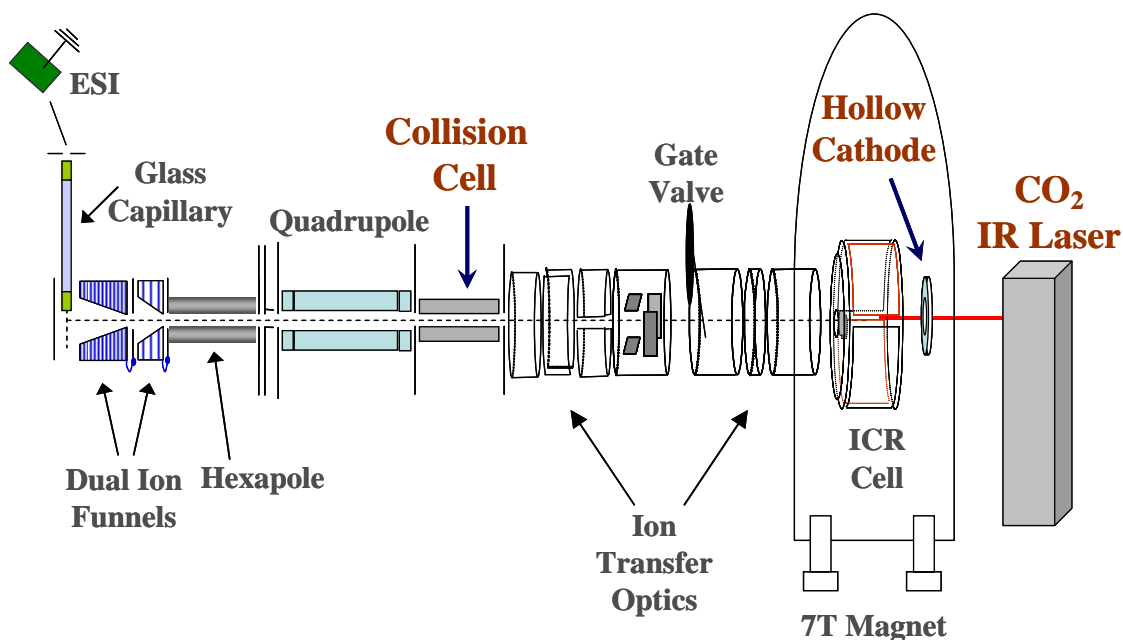


Figure 1.1. Schematic diagram of the 7 T Q-FT-ICR mass spectrometer used for the experiment presented in this thesis. The instrument is equipped with an ESI source, dual stage ion funnels, a quadrupole mass filter, high voltage ion transfer optics, and an ICR cell. A hexapole collision cell is used for CID. A hollow cathode and a 10.6 μm CO₂ laser located behind the ICR cell are used for ion-electron reactions and infrared multiphoton dissociation experiments, respectively.

The main components of the FT-ICR instrument I have used are an ESI source with a dual stage ion funnel, external quadrupole (Q) for precursor ion selection, high voltage ion transfer optics, and the ICR cell located in a strong, homogeneous, magnetic field (Figure 1.1). As the magnetic field strength increases, the performance

of the FT-ICR instrument improves, including increased mass resolving power, mass accuracy, dynamic range, and signal-to-noise ratio.²⁹

Ions are transferred from the ESI source and trapped in the ICR cell radially by the Lorenz force and axially by electrostatic trapping electrodes. After ions are formed and trapped in the ICR cell, they are excited coherently to larger detectable cyclotron radii by a sweep of RF voltages of varying frequencies. Ions orbiting at particular frequencies absorb energy and are coherently excited to higher kinetic energies so their cyclotron radii increase. All ions of the same mass to charge (m/q) ratio are excited coherently and undergo cyclotron motion as a packet. This coherently orbiting packet of ions moves alternately toward and away from the cell walls, generating an image current which is detected by two oppositely located detection electrodes. The image current is amplified and digitized to yield a time domain signal. The time domain signal contains the frequencies of all ions in the cell and is converted to the frequency domain by Fourier transformation. Figure 1.2 shows the time domain signal obtained after excitation and detection of the ions.

Cyclotron motion is characterized by the frequency with which the ions repeat their orbit, called the cyclotron frequency (f_c). The cyclotron frequency (in Hertz) is

given by equation (1), where the strength of the magnetic field (B) and the elementary charge (e) are constants.

$$f_c = zeB/2\pi m \quad (1)$$

The mass to charge ratio (m/z) of an ion is determined by measuring its cyclotron frequency. One important feature of this equation is that it is independent of ion kinetic energy and, therefore, ion kinetic energy has no influence on the accurate determination of the m/z ratio of ions. Furthermore, because the cyclotron frequency (f_c) can be measured very accurately, high mass accuracy can be achieved with FT-ICR MS instruments.

The experiments presented in this thesis were collected with a 7T ESI-Q-FT-ICR mass spectrometer as shown in Figure 1.2. The dual stage ion funnels in the front of the instrument provide improved ion transmission and increased sensitivity.⁴⁹⁻⁵⁰ A quadrupole mass filter (Q), located between the ion source and the ICR cell, allows mass selective external ion accumulation prior to the introduction of ions into the cell.⁵¹⁻⁵² This configuration improves the sensitivity and the dynamic range of the instrument.⁵¹⁻⁵³ A hexapole collision cell, located after the quadrupole, serves to fragment molecular ions via collisions with a neutral gas, usually argon. Ions are transferred to the ICR analyzer cell with high voltage ion transfer optics that allows

ions to overcome the magnetic mirror effect. An indirectly heated hollow dispenser cathode,⁵⁴ located behind the ICR cell, provides electrons for ion-electron reactions.

10.6 μm CO_2 IR laser beam photons are used for infrared multiphoton dissociation.

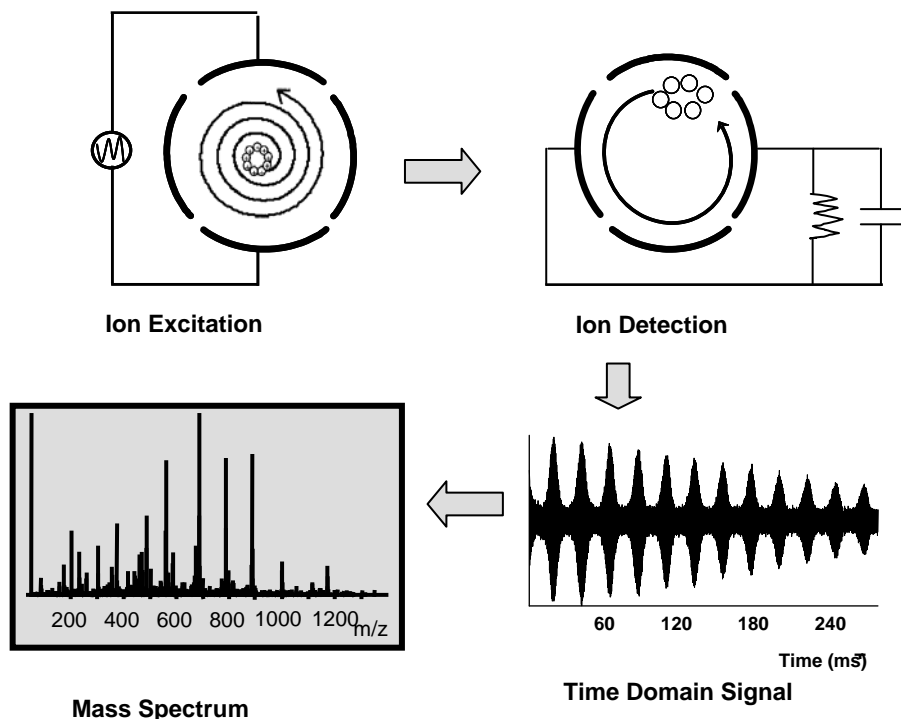


Figure 1.2. Excitation and detection events in an ICR cell, and generation of the time domain signal. Ions in resonance with the applied frequencies will be excited coherently to a larger ion cyclotron radius. The coherently orbiting ion packets induce an image current in a pair of detection electrodes.

1.4. Alternative MS/MS Strategies Available in FT-ICR MS

Tandem mass spectrometry, abbreviated MS/MS or MS^n , is any general method involving any number (n) of steps of mass analysis. In MS/MS, precursor

ions are mass selected from a mixture and subjected to gas-phase reactions, most commonly resulting in fragmentation, which provides structural information of the precursor ions. Additional MS/MS techniques available in FT-ICR MS include sustained off-resonance irradiation collision induced dissociation (SORI-CID),⁵⁵ blackbody infrared radiative dissociation (BIRD),⁵⁶⁻⁵⁷ IRMPD,^{31, 58} ECD,^{31-32, 46, 58-59} electron induced dissociation (EID),⁶⁰⁻⁶² and electron detachment dissociation (EDD).⁶³⁻⁶⁴ Fragmentation techniques used in my thesis work include mainly IRMPD, EID, ECD, and EDD, along with CID, which is the most commonly used MS/MS technique.

1.4.1. MS/MS via Vibrational Excitation

CID and IRMPD are vibrational excitation or slow heating-based dissociation techniques in which the product ions are formed via the lowest energy pathways.⁶⁵⁻⁶⁶ In CID, precursor ions are activated by collisions with a neutral target gas, such as argon or helium. These collisions between precursor ions and the neutral target gas result in conversion of the ion translational energy into internal energy. The internal energy is rapidly redistributed within the ion and, once it exceeds the threshold dissociation energy, fragmentation occurs. CID is the most widely used MS/MS fragmentation technique.

For MS/MS of metabolites, negative mode ionization is generally preferred due to the increased ionization efficiency of many acidic and neutral metabolites. However, negative mode CID often results in limited fragmentation, possibly due to the absence of a mobile proton.⁶⁷ Thus, alternative fragmentation strategies (e.g., IRMPD and EID) appear promising to overcome this issue. In IRMPD, precursor ions are excited and subsequently fragmented by the absorption of multiple photons. The absorption occurs by IR active groups present in the ion, followed by rapid redistribution of energy over all vibrational degrees of freedom. IRMPD has been shown to be an efficient fragmentation technique for nucleic acids and phosphopeptides, due to strong phosphate absorption at the 10.6 μm wavelength typically used.^{31, 33-37} Thus, IRMPD should be a valuable tandem mass spectrometric strategy for structural characterization of metabolites containing phosphate groups due to improved fragmentation efficiency or complementary fragmentation patterns compared to CID.

1.4.2. MS/MS via Electron Based Reactions

EID, which involves irradiation of singly charged analyte ions with electrons, was first shown in 1979 by Cody and Freiser for radical cations.⁶¹ This approach was

extended in 1990 by Wang and McLafferty to even-electron peptide cations.⁶⁸ The technique was initially termed electron impact excitation of ions from organics (EIEIO).⁶¹ More recently, approaches involving thermal electrons (electron capture dissociation)³² and medium energy electrons (10-20 eV, electron detachment dissociation)⁶³ have been introduced for analytically valuable fragmentation of even-electron biomolecular cations and anions, respectively. However, both ECD and EDD require precursor ions to carry at least two charges. Thus, they are not directly compatible with metabolite analysis because the smaller size of most metabolites renders formation of multiply charged ions difficult. Recently, EID has been applied to singly protonated precursor ions of aromatic amino acids, cystine, and small peptides and it was demonstrated that it yielded different and complementary fragmentation compared to that observed in CID.⁶²

In ECD, multiply charged precursor ions are irradiated with low energy (<1 eV) electrons, resulting in electron capture and formation of a radical species, $[M + nH]^{(n+1)+\bullet}$, called the charge reduced species (n = number of protons). This charge reduced species can undergo radical-driven fragmentation. One main advantage of ECD compared to slow heating, such as CID or IRMPD, is the retention of labile post-translational modifications (PTMs) of peptides.^{40, 69-71} However, its application to

metabolites has just recently started to emerge using divalent metal ions to increase charge states of metabolites.⁷²⁻⁷³ For example, Ca^{2+} was used to form adducts with acidic metabolites, which resulted in doubly positively charged metabolites. ECD of these metal complexes provided unique fragmentation compared to sustained off resonance irradiation-collision induced dissociation (SORI-CID).⁷³ EDD is applicable to negatively charged ions. In EDD, precursor ions are irradiated with higher energy electrons (> 10 eV), resulting in electron detachment and formation of a charge reduced species, $[\text{M} - n\text{H}]^{(n-1)-\cdot(*)}$. This charge reduced species undergoes radical-driven fragmentation from an excited state. Similar to ECD, EDD has been shown to result in retention of labile PTMs of peptides, such as sulfation⁶³ and phosphorylation.^{64, 74} EDD has also been applied to the characterization of oligonucleotides,⁷⁵⁻⁷⁶ and oligosaccharides.⁴⁰ One major drawback of EDD is that it exhibits even lower fragmentation efficiency than ECD.

1.5. Dissertation Overview

The thesis is composed of eight chapters and two appendices. The first (current) chapter introduces metabolomics, mass spectrometry-based metabolomics, and FT-ICR

MS and its MS/MS strategies for structural characterization of small organic molecules (e.g. metabolites and peptides). The last chapter contains a summary of all results in my thesis and suggestions for future directions.

Chapter 2 discusses metabolic profiling of a T-cell model of Lupus disease using LC/FT-ICR MS. This work was done in collaboration with Dr. Opiari's group in the University of Michigan Medical school and Dr. Glick in Chemistry. The developed LC/FT-ICR MS approach resulted in observation of T-cell metabolic changes following metabolic perturbation and, at the same time, this work demonstrates the necessity of alternative MS/MS strategies for identification and structural characterization of metabolites, because many of the observed metabolites could not be identified using currently available databases.

Each chapter from chapter 3 through 7 demonstrates new MS/MS strategies for the identification and structural characterization of small organic molecules. Chapter 3 shows that IRMPD and EID of phosphate-containing metabolites can provide complementary structural information to CID. This work was published in *Analytical Chemistry* in 2007.³⁷ In chapter 4, EID of Mn-adducted fatty acids was investigated to find double bond locations of fatty acids using charge-remote fragmentation. Chapters 5 and 6 explore various MS/MS strategies for the determination of

regiochemistry of phospholipids. In chapter 5, weak Lewis acidic mono-valent metal ions, such as Ag^+ ion, were used to form adducts with phospholipids, which resulted in unique fragmentation patterns in CID and IRMPD. In chapter 6, various divalent metal ions were explored to form adducts with phospholipids, and ECD was performed on these adducts. Among various divalent metal ions, Ni^{2+} - or Ba^{2+} -adducts provided phospholipid regiochemistry. Chapter 7 demonstrates that negatively charged peptide ions can capture electrons to form more highly charged radical species. In addition, extensive *c*- and *z*-type peptide backbone fragmentation was observed with complete retention of posttranslational modifications (PTMs). Further MS^n of these radical species was also investigated to provide peptide sequence information.

Finally, two appendices are included. The first appendix demonstrates use of high resolution FT-ICR MS and its alternative MS/MS strategies (such as IRMPD) for structural determination of bacterial cell surface lipopolysaccharide (LPS). This work was done in collaboration with Dr. DiRita's group in the University of Michigan Medical school. Part of this work is published in *Journal of Bacteriology* in 2010.⁷⁷ The second appendix shows that phosphate-containing metabolites can be enriched by TiO_2 to overcome ion suppression caused by highly abundant other polar metabolites.

1.6. References

1. Dettmer, K.; Aronov, P. A.; Hammock, B. D. *Mass Spectrom Rev* **2007**, *26*. 51-78.
2. Griffin, J. L.; Vidal-Puig, A. *Physiol Genomics* **2008**, *34*. 1-5.
3. Oliver, S. G.; Winson, M. K.; Kell, D. B.; Baganz, F. *Trends Biotechnol* **1998**, *16*. 373-378.
4. Dunn, W. B.; Ellis, D. I. *TrAC* **2005**, *24*. 285-294.
5. Want, E. J.; Cravatt, B. F.; Siuzdak, G. *Chembiochem* **2005**, *6*. 1941-1951.
6. Cascante, M.; Boros, L. G.; Comin-Anduix, B.; de Atauri, P.; Centelles, J. J.; Lee, P. W. *Nat Biotechnol* **2002**, *20*. 243-249.
7. Kell, D. B. *Curr Opin Microbiol* **2004**, *7*. 296-307.
8. Lindon, J. C.; Holmes, E.; Bollard, M. E.; Stanley, E. G.; Nicholson, J. K. *Biomarkers* **2004**, *9*. 1-31.
9. Rochfort, S. *J Nat Prod* **2005**, *68*. 1813-1820.
10. Wishart, D. S.; Tzur, D.; Knox, C.; Eisner, R.; Guo, A. C.; Young, N.; Cheng, D.; Jewell, K.; Arndt, D.; Sawhney, S.; Fung, C.; Nikolai, L.; Lewis, M.; Coutouly, M. A.; Forsythe, I.; Tang, P.; Shrivastava, S.; Jeroncic, K.; Stothard, P.; Amegbey, G.; Block, D.; Hau, D. D.; Wagner, J.; Miniaci, J.; Clements, M.; Gebremedhin, M.; Guo, N.; Zhang, Y.; Duggan, G. E.; Macinnis, G. D.; Weljie, A. M.; Dowlatabadi, R.; Bamforth, F.; Clive, D.; Greiner, R.; Li, L.; Marrie, T.; Sykes, B. D.; Vogel, H. J.; Querengesser, L. *Nucleic Acids Res* **2007**, *35*. D521-526.
11. Griffin, J. L.; Shockcor, J. P. *Nat Rev Cancer* **2004**, *4*. 551-561.
12. Pearson, H. *Nature* **2007**, *446*. 8.
13. Bino, R. J.; Hall, R. D.; Fiehn, O.; Kopka, J.; Saito, K.; Draper, J.; Nikolau, B. J.; Mendes, P.; Roessner-Tunali, U.; Beale, M. H.; Trethewey, R. N.; Lange, B. M.; Wurtele, E. S.; Sumner, L. W. *Trends Plant Sci* **2004**, *9*. 418-425.
14. Aharoni, A.; Ric de Vos, C. H.; Verhoeven, H. A.; Maliepaard, C. A.; Kruppa, G.; Bino, R.; Goodenowe, D. B. *Omics* **2002**, *6*. 217-234.
15. Brown, S. C.; Kruppa, G.; Dasseux, J. L. *Mass Spectrom Rev* **2005**, *24*. 223-231.
16. Smith, C. A.; O'Maille, G.; Want, E. J.; Qin, C.; Trauger, S. A.; Brandon, T. R.; Custodio, D. E.; Abagyan, R.; Siuzdak, G. *Ther Drug Monit* **2005**, *27*. 747-751.
17. Villas-Boas, S. G.; Mas, S.; Akesson, M.; Smedsgaard, J.; Nielsen, J. *Mass Spectrom Rev* **2005**, *24*. 613-646.

18. Boskey, A. L.; Mendelsohn, R. *Vib Spectrosc* **2005**, *38*. 107-114.
19. Defernez, M.; Colquhoun, I. J. *Phytochemistry* **2003**, *62*. 1009-1017.
20. Deleris, G.; Petibois, C. *Vib spectrosc* **2003**, *32*. 129-136.
21. Lenz, E. M.; Bright, J.; Knight, R.; Wilson, I. D.; Major, H. *J Pharm Biomed Anal* **2004**, *35*. 599-608.
22. Gika, H. G.; Theodoridis, G. A.; Wingate, J. E.; Wilson, I. D. *J Proteome Res* **2007**, *6*. 3291-3303.
23. Wagner, C.; Sefkow, M.; Kopka, J. *Phytochemistry* **2003**, *62*. 887-900, DOI: S0031942202007033 [pii].
24. Edwards, J. L.; Chisolm, C. N.; Shackman, J. G.; Kennedy, R. T. *J Chromatogr A* **2006**, *1106*. 80-88.
25. Krieger, C. J.; Zhang, P.; Mueller, L. A.; Wang, A.; Paley, S.; Arnaud, M.; Pick, J.; Rhee, S. Y.; Karp, P. D. *Nucleic Acids Res* **2004**, *32*. D438-442.
26. Buchholz, A.; Takors, R.; Wandrey, C. *Anal Biochem* **2001**, *295*. 129-137.
27. Byrd, G. D.; Ogden, M. W. *J Mass Spectrom* **2003**, *38*. 98-107.
28. Triolo, A.; Altamura, M.; Dimoulas, T.; Guidi, A.; Lecci, A.; Tramontana, M. *J Mass Spectrom* **2005**, *40*. 1572-1582.
29. Marshall, A. G.; Hendrickson, C. L.; Jackson, G. S. *Mass Spectrom Rev* **1998**, *17*. 1-35.
30. Sleno, L.; Volmer, D. A.; Marshall, A. G. *J Am Soc Mass Spectrom* **2005**, *16*. 183-198.
31. Little, D. P.; Speir, J. P.; Senko, M. W.; O'Connor, P. B.; McLafferty, F. W. *Anal Chem* **1994**, *66*. 2809-2815.
32. Zubarev, R. A.; Kellerher, N. L.; McLafferty, F. W. *J Am Chem Soc* **1998**, *120*. 3265-3266.
33. Crowe, M. C.; Brodbelt, J. S. *J Am Soc Mass Spectrom* **2004**, *15*. 1581-1592.
34. Flora, J. W.; Muddiman, D. C. *J Am Chem Soc* **2002**, *124*. 6546-6547.
35. Flora, J. W.; Muddiman, D. C. *J Am Soc Mass Spectrom* **2004**, *15*. 121-127.
36. Hofstadler, S. A.; Sannes-Lowery, K. A.; Griffey, R. H. *Anal Chem* **1999**, *71*. 2067-2070.
37. Yoo, H. J.; Liu, H.; Hakansson, K. *Anal Chem* **2007**, *20*. 7858-7866.
38. Adamson, J. T.; Hakansson, K. *J Proteome Res* **2006**, *5*. 493-501.
39. Adamson, J. T.; Hakansson, K. *Anal Chem* **2007**, *79*. 2901-2910.
40. Adamson, J. T.; Hakansson, K. *J Am Soc Mass Spectrom* **2007**, *18*. 2162-2172.

41. Cooper, H. J.; Hakansson, K.; Marshall, A. G. *Mass Spectrom Rev* **2005**, *24*, 201-222.
42. Hakansson, K.; Chalmers, M. J.; Quinn, J. P.; McFarland, M. A.; Hendrickson, C. L.; Marshall, A. G. *Anal Chem* **2003**, *75*, 3256-3262.
43. Hakansson, K.; Cooper, H. J.; Emmett, M. R.; Costello, C. E.; Marshall, A. G.; Nilsson, C. L. *Anal Chem* **2001**, *73*, 4530-4536.
44. Hakansson, K.; Hudgins, R. R.; Marshall, A. G.; O'Hair, R. A. *J Am Soc Mass Spectrom* **2003**, *14*, 23-41.
45. McLafferty, F. W.; Horn, D. M.; Breuker, K.; Ge, Y.; Lewis, M. A.; Cerda, B.; Zubarev, R. A.; Carpenter, B. K. *J Am Soc Mass Spectrom* **2001**, *12*, 245-249.
46. Zubarev, R. A. *Curr Opin Biotechnol* **2004**, *15*, 12-16.
47. Comisarow, M. B.; Marshall, A. G. *Chem. Phys. Lett* **1974**, *26*, 489.
48. Amster, I. J. *J. Mass Sepctrom.* **1996**, *31*, 1325.
49. Shaffer, S. A.; Prior, D. C.; Anderson, G. A.; Udseth, H. R.; Smith, R. D. *Anal Chem* **1998**, *70*, 4111-4119.
50. Shaffer, S. A.; Tolmachev, A.; Prior, D. C.; Anderson, G. A.; Udseth, H. R.; Smith, R. D. *Anal Chem* **1999**, *71*, 2957-2964.
51. Belov, M. E.; Nikolaev, E. N.; Anderson, G. A.; Udseth, H. R.; Conrads, T. P.; Veenstra, T. D.; Masselon, C. D.; Gorshkov, M. V.; Smith, R. D. *Anal Chem* **2001**, *73*, 253-261.
52. Hendrickson, C. L.; Quinn, J. P.; Emmett, M. R.; Marshall, A. G., in *49th ASMS Conference on Mass Spectrometry and Allied Topics*. Chicago, IL, 2001; CD-ROM.
53. He, F.; Hendrickson, C. L.; Marshall, A. G. *Anal Chem* **2001**, *73*, 647-650.
54. Tsybin, Y. O.; Hakansson, P.; Budnik, B. A.; Haselmann, K. F.; Kjeldsen, F.; Gorshkov, M.; Zubarev, R. A. *Rapid Commun Mass Spectrom* **2001**, *15*, 1849-1854.
55. Gauthier, J.; Trautman, T. R.; Jacobson, D. B. *Anal. Chim. Acta* **1991**, *246*, 211-225.
56. Dunbar, R. C. *Mass Spectrom Rev* **2004**, *23*, 127-158.
57. Schneider, B.; Budzikiewicz, H. *Rapid Commun Mass Spectrom* **1990**, *4*, 550-551.
58. Woodin, R. L.; Bomse, D. S.; Beauchamp, J. L. *J Am Chem Soc* **1978**, *100*, 3248-3250.

59. Zubarev, R. A.; Horn, D. M.; Fridriksson, E. K.; Kelleher, N. L.; Kruger, N. A.; Lewis, M. A.; Carpenter, B. K.; McLafferty, F. W. *Anal Chem* **2000**, *72*. 563-573.
60. Budnik, B. A.; Haselmann, K. F.; Elkin, Y. N.; Gorbach, V. I.; Zubarev, R. A. *Anal Chem* **2003**, *75*. 5994-6001.
61. Cody, R. B.; Freiser, B. S. *Anal Chem* **1979**, *51*. 541-551.
62. Lioe, H.; O'Hair, R. A. *Anal Bioanal Chem* **2007**, *389*. 1429-1437.
63. Budnik, B. A.; Haselmann, K. F.; Zubarev, R. A. *Chem Phys Lett* **2001**. 299-302.
64. Kjeldsen, F.; Silivra, O. A.; Ivonin, I. A.; Haselmann, K. F.; Gorshkov, M.; Zubarev, R. A. *Chemistry* **2005**, *11*. 1803-1812.
65. Hayes, R. N.; Gross, M. L. *Methods Enzymol* **1990**, *193*. 237-263.
66. McLuckey, S. A.; Goeringer, D. E.; Glish, G. L. *Anal Chem* **1992**, *64*. 1455-1460.
67. Wysocki, V. H.; Tsaprailis, G.; Smith, L. L.; Brechi, L. A. *J Mass Spectrom* **2000**, *35*. 1399-1406.
68. Wang, B. H.; McLafferty, F. W. *Org Mass Spectrom* **1990**, *25*. 554-556.
69. Coon, J. J.; Shabanowitz, J.; Hunt, D. F.; Syka, J. E. *J Am Soc Mass Spectrom* **2005**, *16*. 880-882.
70. Kjeldsen, F.; Haselmann, K. F.; Budnik, B. A.; Sorensen, E. S.; Zubarev, R. A. *Anal Chem* **2003**, *75*. 2355-2361.
71. Kweon, H. K.; Hakansson, K. *Anal Chem* **2006**, *78*. 1743-1749.
72. James, P. F.; Perugini, M. A.; O'Hair, R. A. *J Am Soc Mass Spectrom* **2008**, *19*. 978-986.
73. Liu, H.; Yoo, H. J.; Hakansson, K. *J Am Soc Mass Spectrom* **2008**, *19*. 799-808.
74. Kweon, H. K.; Hakansson, K. *J Proteome Res* **2008**, *7*. 749-755.
75. Mo, J.; Hakansson, K. *Anal Bioanal Chem* **2006**, *386*. 675-681.
76. Yang, J.; Mo, J.; Adamson, J. T.; Hakansson, K. *Anal Chem* **2005**, *77*. 1876-1882.
77. Matson, J. S.; Yoo, H. J.; Hakansson, K.; Dirita, V. J. *J Bacteriol* **2010**, *192*. 2044-2052.

Chapter 2

Metabolic Profiling of Jurkat T Cells by Hydrophilic Interaction Liquid Chromatography/Fourier Transform Ion Cyclotron Resonance Mass Spectrometry (HILIC FT-ICR MS)

2.1. Introduction

The metabolome consists of a large number of molecules exhibiting a high diversity of chemical structures and abundances, therefore requiring complementary analytical platforms for extensive coverage. The level of the metabolome represents integrative information of cellular function, and defines the phenotype of a cell or tissue in response to genetic or environmental changes. Because changes observed in the transcriptome or proteome do not always correspond to phenotypic alterations, measurement of the metabolome synthesized by a biological system is very important to assess genetic function and to complement proteomic data.¹⁻⁶ Metabolomics is the study of the complete set of endogenous small molecules in biological systems, with the end goal of identifying biomarkers and enzymatic pathways related to human disease.^{1,4,6}

Metabolomic measurements have been carried out for decades due to the fundamental regulatory importance of metabolites as components of biochemical pathways, the importance of certain metabolites in the human diet, and their use as

diagnostic markers for a wide range of biological conditions, including disease and response to chemical treatment.⁷⁻⁸ Historically, the measurement of metabolites has mostly been achieved by spectrophotometric assays that can detect single metabolites, or by simple chromatographic separation of mixtures of low complexity. Over the past decade, however, methods that offer both high accuracy and sensitivity for the measurement of highly complex mixtures of compounds have been established.⁷⁻⁸ Gas-chromatography/mass-spectrometry (GC/MS) and liquid chromatography/mass-spectrometry (LC/MS) are currently the principal mass spectrometry methods for metabolite analysis. Whereas gas chromatography-based approaches can only be used with volatile compounds or compounds that can be rendered volatile by derivatization, LC/MS can be adapted to a wider array of molecules, including a range of secondary metabolites such as alkaloids, flavonoids, glucosinolates, isoprenes, oxylipins, phenylpropanoids, pigments, and saponins.^{2, 7, 9-14}

A major challenge encountered in global mass spectrometric metabolite analysis is the identification and characterization of the hundreds to thousands of detected molecules. Fourier transform ion cyclotron resonance mass spectrometry (FT-ICR MS)¹⁵ can provide improved metabolite identification due to its accurate mass capabilities.¹⁶ Here, FT-ICR MS was coupled with HILIC separation for metabolic profiling of Jurkat T cells, which can serve as a model for autoimmunity in diseases such as lupus.

HILIC was chosen over other separation methods to observe a maximum number of water-soluble metabolites. An efficient way to retain very hydrophilic and uncharged compounds in LC is with a reversed “reverse phase (RP)” strategy in which a polar stationary phase is used and analytes are eluted with polar solvent. HILIC is such a

technique, where retention is believed to result from partitioning of the analyte between a water-enriched layer of stagnant eluent on a hydrophilic stationary phase and a relatively hydrophobic mobile phase, usually acetonitrile.¹⁷ The use of water as strongly eluting solvent gives HILIC a number of advantages over conventional normal phase (NP) chromatography. NP mobile phases are typically nonpolar (often based on hexane) and polar metabolites usually have low solubility in such solvents. The interfacing with electrospray ionization (ESI) MS is also a problem with NP, because analytes do not exist as ions in nonpolar solvents. The elution order in HILIC is more or less the opposite of that seen in RP separations, which means that HILIC works best for solutes that are problematic in RP chromatography.¹⁷⁻¹⁸

HILIC separation conditions (including mobile phase, gradient, and flow rate) and ESI conditions were optimized to separate polar metabolites and achieve stable ionization during LC/FT-ICR MS. The LC/FT-ICR MS reproducibility was tested with a standard metabolite mixture, and the biological reproducibility was explored using metabolite extractions from three sets of 40 million Jurkat T cells. The developed method was applied to metabolic profiling of drug (2-deoxyglucose, oligomycin, and Bz423)-treated vs. untreated (or chronically activated) Jurkat cells. 2-deoxyglucose and Bz423-treated cells showed significant metabolic changes compared to untreated cells.

2.2. Experimental Section

2.2.1. Sample Preparation

Standard metabolite mixture was composed of 2-4 μ M of nine metabolites (glycerol 3-phosphate (G3P), 3-phosphoglyceric acid (3PG), tryptophan, glyceraldehyde

3-phosphate (G3P), glucose 6-phosphate (G6P), fructose 1,6-bisphosphate (F1,6BP), adenosine diphosphate (ADP), adenosine 5'-triphosphate (ATP), and nicotinamide adenine dinucleotide (NADH)) purchased from Sigma-Aldrich (St. Louis, MO) and used without further purification. α -methyl phenylalanine (13 μ M) was added as an internal standard in the mixture.

40 million Jurkat T cells were prepared for each sample. First, Jurkat T cells were spun down (1000 \times g for 5 min) and washed with water as quickly as possible. The cell pellet was resuspended in 2 mL of water and transferred to a 2 mL eppendorf tube, then placed in a microcentrifuge and quickly spun for 20 seconds. Then, water was discarded immediately by pipetting. Cells were lysed by resuspending and vortexing in 1.4 mL of cold 80 % ethanol. 3.9 nmols of α -methyl phenylalanine was added to the sample. Cellular debris was removed after centrifugation at 14,000 rpm for 10 minutes at 4 °C. The supernatant was removed and placed in a 15 mL conical tube. 1.4 mL water and 0.75 mL chloroform were added to the sample, which was mixed briefly and centrifuged at 2000 \times g for 15 min to separate the layers. This extraction separates lipids from polar metabolites. The water (top) layer was removed and chloroform extraction was repeated once again. The collected water layers were dried overnight at room temperature. The dried lysate was stored at - 80 °C until use. Prior to LC/FT-ICR MS analysis, the sample was dissolved in 20 μ L of H₂O/acetonitrile (25/75, v/v) containing 7.5 mM ammonium acetate.

2.2.2. HILIC Separation.

LC/MS was performed with an Agilent 1100 HPLC system using a HILIC column (TSK GEL amide-80 column, 1 mm i.d. \times 25 cm, Tosoh Bioscience, Japan). First, the

LC separation conditions were optimized with standard metabolite mixture. The LC flow rate was 40 $\mu\text{L}/\text{min}$ and the LC solvents were Solvent A: 7.5 mM ammonium acetate in H_2O ; Solvent B: 7.5 mM ammonium acetate in acetonitrile. The gradients were as follows: $t = 0$, 75 % B; $t = 27$ min, 45 % B; $t = 32$ min, 30 % B; $t = 33$ min, 75% B; $t = 35$ min, 75% B. The LC column was kept at room temperature. 5 μL of sample was injected using manual sample injector valves (Rheodyne 7725i, IDEX Health & Science LLC, WA). At least 30 min passed between each sample injection.

2.2.3. Fourier Transform Ion Cyclotron Resonance Mass Spectrometry

Mass spectra were acquired with a 7 Tesla quadrupole- FT-ICR mass spectrometer (Bruker, Daltonics, MA) coupled with an Agilent 1100 HPLC system. All data were obtained in negative ion mode. For ESI, N_2 was used as both nebulizing gas (4 L/s) and drying gas (1.5 L/s). The drying gas temperature was set to 200 $^\circ\text{C}$. Briefly, ions produced by electrospray ionization were mass-selectively externally accumulated¹⁹⁻²⁰ in a hexapole for 1 s, transferred via high voltage ion optics, and captured in the ICR cell by dynamic trapping. This accumulation sequence was looped three times to improve precursor ion abundance. All LC/FT-ICR MS data were acquired with Hystar (version 3.1, Bruker Daltonics) and Apex control (version 1.0, Bruker Daltonics).

2.2.4. Data Analysis

Data processing was performed with Data Analysis software (version 3.4, Bruker Daltonics), MS Excel (Microsoft Office 2007), and MZmine (version 1.95).²¹ HILIC/FT-ICR MS of the standard metabolite mixture was performed prior to HILIC/FT-ICR MS of Jurkat T cells on each day. The m/z values of standard metabolites contained in standard

metabolite mixture were used to perform external calibration of all detected metabolites from HILIC/FT-ICR MS of Jurkat T cells using Data Analysis software.

ASCII and mzXML data formats were generated using Data Analysis software for 3D profiling and principal component analysis (PCA), respectively. 3D profile of HILIC/FT-ICR MS data was reconstructed using 3D surface function in a plot tool of MS Excel. MZmine was used to perform PCA of untreated and drug-treated Jurkat T cells, where 0.02 Da of m/z tolerance and 5 min of retention time tolerance were used with 90 % weight for m/z, because m/z was more reliable than retention time due to high mass accuracy of FT-ICR MS.

2.3. Results and Discussion

2.3.1. HILIC/FT-ICR MS Method Development and Reproducibility

The metabolic profiling in this study was focused on metabolites involved in glycolysis and the TCA cycle. Metabolites related to glycolysis and TCA cycle are often phosphorylated and highly polar. At first, a reverse phase column (C18) was used to separate standard metabolite mixture composed of phosphate-containing metabolites such as G6P and ATP. However, the resolution was poor even when very low percentage of organic solvent was used (data not shown). Thus, a HILIC column was chosen to improve separation for highly polar metabolites. The eluent from the HILIC column was directly connected to the FT-ICR mass spectrometer. LC/FT-ICR MS was optimized using a standard metabolite mixture. The optimized conditions are described in the Experimental Section.

Table 2.1 shows the retention time reproducibility of the developed method for intra- and interday analyses. While there was relatively large variation in retention time among interday analyses, the intraday variation was narrow; within 3% of relative standard deviation. Thus, the retention time should provide useful information for metabolite identification when standard metabolites were analyzed on the same day as a comparison. Even when the retention time varied among interday analyses, the elution order of analytes still remained the same.

For quantification, the unnatural amino acid α -methyl phenylalanine was added before metabolite extraction during sample preparation. Reproducibility of normalized peak area of extracted ion chromatogram (EIC) is shown in Table 2.2. There was no big difference between intra- and interday analyses, although intraday analysis was somewhat more reproducible compared to interday analysis. The relative standard deviations (RSD (%)) for nine metabolites were generally 30 %, which is comparable to RSD (%) for metabolites obtained by other research groups.²²⁻²⁴

(min)

(a)

Intraday	Trial 1	Trial 2	Trial 3	Average	STD	RSD (%)
Glycerol-3-phosphate	20.60	20.80	20.60	20.67	0.12	1
α -Methyl phenylalanine	13.00	12.70	12.50	12.73	0.26	2
3-Phosphoglyceric acid	22.40	22.20	22.10	22.23	0.15	1
Tryptophan	13.50	13.00	12.70	13.07	0.40	3
Glyceraldehyde-3-phosphate	16.9	16.90	17.00	16.93	0.06	0
Fructose-6-phosphate	21.60	21.50	21.50	21.53	0.06	0
Fructose-1,6-diphosphate	24.00	23.80	23.60	23.80	0.20	1
ADP	22.90	21.70	22.20	22.27	0.60	3
ATP	23.70	23.10	22.80	23.20	0.46	2
NADH	19.40	19.20	19.20	19.27	0.12	1

(min)

(b)

Interday	Day 1	Day 2	Day 3	Day 4	Average	STD	RSD (%)
Glycerol-3-phosphate	15.30	18.30	20.67	19.15	18.36	2.26	12
α -Methyl phenylalanine	10.50	12.07	12.73	12.00	11.83	0.94	8
3-Phosphoglyceric acid		20.65	22.23	21.40	21.43	0.79	4
Tryptophan	10.50	12.13	13.07	12.30	12.00	1.08	9
Glyceraldehyde-3-phosphate	10.70	12.13	16.93	12.50	13.07	2.69	21
Fructose-6-phosphate	16.7	19.73	21.53	20.50	19.62	2.08	11
Fructose-1,6-diphosphate	19.60	23.00	23.80	22.35	22.19	1.82	8
ADP	18.00	21.17	22.27	21.15	20.65	1.94	9
ATP	20.30	22.17	23.20	22.05	21.93	1.20	5
NADH	14.60	18.23	19.27	18.55	17.66	2.09	12

Table 2.1. Intra- and interday retention time reproducibility in HILIC/FT-ICR MS. For intraday reproducibility, three repetitive LC/FT-ICR MS runs, performed within the same day, were compared. For interday reproducibility, the same sample was subjected to HILIC/FT-ICR MS during four non-consecutive days. Std and RSD (%) indicate standard deviation and relative standard deviation, respectively.

(a)

Intraday	Trial 1	Trial 2	Trial 3	Average	STD	RSD (%)
Glycerol-3-phosphate	0.07	0.17	0.14	0.13	0.05	40
α -Methyl phenylalanine	1.00	1.00	1.00	1.00	0.00	0
3-Phosphoglyceric acid	0.01	0.02	0.01	0.01	0.01	98
Tryptophan	0.13	0.14	0.14	0.14	0.00	1
Glyceraldehyde-3-phosphate	0.71	0.92	0.70	0.77	0.12	16
Fructose 6 phosphate	0.12	0.38	0.29	0.26	0.13	50
Fructose-1,6-diphosphate	0.24	0.28	0.24	0.25	0.03	10
ACP	0.67	1.11	1.02	0.94	0.23	25
ATP	0.21	0.19	0.16	0.19	0.03	13
VADH	0.04	0.38	0.05	0.06	0.02	42

(b)

Interday	Day 1	Day 2	Day 3	Day 4	Average	STD	RSD (%)
Glycerol-3-phosphate	0.05	0.07	0.13	0.07	0.08	0.03	42
α -Methyl phenylalanine	1.00	1.00	1.00	1.00	1.00	0.00	0
3-Phosphoglyceric acid		0.04	0.01	0.02	0.03	0.02	60
Tryptophan	0.14	0.17	0.14	0.15	0.15	0.02	11
Glyceraldehyde-3-phosphate	1.34	1.20	0.77	0.66	0.99	0.33	33
Fructose-6-phosphate	0.20	0.15	0.26	0.24	0.21	0.05	24
Fructose-1,6-diphosphate	0.08	0.12	0.25	0.17	0.16	0.07	47
ACP	0.64	0.76	0.94	0.77	0.77	0.12	16
ATP	0.08	0.12	0.19	0.14	0.13	0.04	33
VADH	0.03	0.05	0.38	0.02	0.04	0.02	48

Table 2.2. Intra- and interday peak area reproducibility in HILIC/FT-ICR MS. For intraday reproducibility, three repetitive LC/FT-ICR MS runs, performed within the same day, were compared. For interday reproducibility, the same sample was subjected to HILIC/FT-ICR MS during four non-consecutive days. The peak area from EIC for each metabolite was normalized to that of an internal standard (α -methyl phenylalanine). Std and RSD (%) indicate standard deviation and relative standard deviation, respectively.

2.3.2. Evaluation of Cell Washing Conditions

Jurkat cells were washed with water before cell lysis to get rid of unwanted salts, which cause ion suppression during electrospray. However, it has been reported that water-rich conditions can cause decomposition of nucleotides and result in artifacts in mass spectrometric data.²⁵ Thus, several buffer solutions were tested to ensure that our sample preparation does not cause metabolite decomposition during sample preparation. In addition, the remaining buffer content should not negatively affect electrospray ionization.

First, to test whether remaining buffer content affects the electrospray process and causes detrimental effects on LC/FT-ICR MS, standard metabolite solution prepared in 10-50 mM Tris, phosphate, or HEPES buffer, where pH was adjusted to 7.5 with either formic acid or ammonium hydroxide, were injected for LC/MS analysis. When metabolites were dissolved in HEPES buffer, most of the metabolites were not observed in LC/FT-ICR MS spectra regardless of the concentration of HEPES buffer. However, metabolites in 10 mM phosphate or Tris buffer were observed in similar abundance as when they were dissolved in the HILIC mobile phase. Thus, it was assumed that cell washing with 10 mM phosphate or Tris buffer would not affect LC/MS analysis, because preparation of the cell lysate involves additional steps after the cell wash and lower amount of buffer would remain in the sample.

Based on the observation above, 100 million Jurkat cells were washed with water, 10 mM Tris buffer, or 10 mM phosphate buffer, respectively. The remaining sample preparation followed the procedure described in the Experimental Section. Each sample was subjected to HILIC/FT-ICR MS, and absolute signal abundances of selected metabolites were compared as shown in Table 2.3 and Figure 2.1. Normalized signal

[M - H] ⁻	H ₂ O		10 mM Tris buffer		10 mM Phosphate buffer	
	average	% RSD	average	% RSD	average	% RSD
135.045	22,411,198	16.3	42,394,288	4.3	14,348,785	5.7
171.089	6,198,944	52.7	7,794,510	6.5	8,371,222	28.0
174.945	57,582,341	55.9	67,595,808	27.8	50,500,519	62.7
178.880	1,528,842	98.9	2,207,488	19.2	2,709,221	28.4
191.027	116,131,117	30.7	112,057,353	6.0	109,058,240	42.7
214.057	258,509,990	58.9	48,854,090	16.4	240,898,714	59.1
259.029	30,894,618	20.1	22,295,353	33.7	29,435,302	6.4
308.043	7,708,593,538	17.1	9,543,774,213	25.5	7,750,807,634	8.9
348.069	230,614,631	31.6	352,624,826	5.6	161,213,452	16.9
355.009	609,665,678	32.8	205,450,241	26.3	1,170,581,857	55.3
428.037	1,708,224,788	25.7	1,197,453,830	6.3	1,489,287,545	22.0
508.003	872,362,793	41.3	571,192,728	59.0	455,741,274	51.3
565.054	78,310,963	58.6	61,735,340	12.5	60,345,822	39.3
579.430	48,705,967	12.3	45,729,821	1.3	34,695,538	28.3
608.095	4,702,520,783	9.2	4,357,154,533	1.4	5,504,475,536	30.4
611.157	1,305,641,114	27.7	285,118,747	14.2	1,567,273,970	42.9
664.114	11,278,852	112.8	9,604,510	94.9	17,758,570	43.5

Table 2.3. Comparison of metabolite signal abundances from Jurkat cells after washing with water, 10 mM Tris buffer, or 10 mM phosphate buffer, respectively.

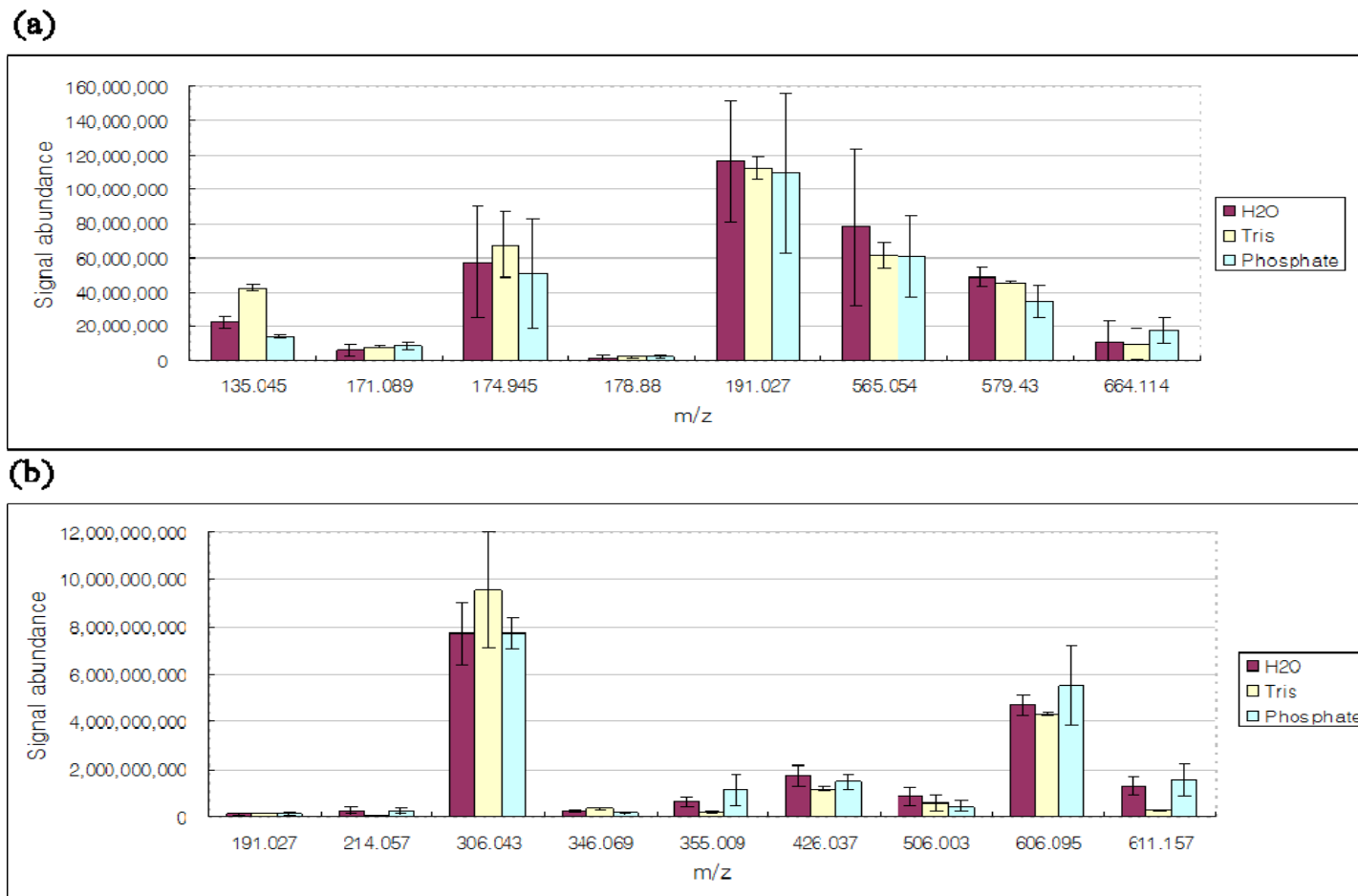


Figure 2.1. Comparison of metabolite signal abundances from Jurkat cells washed with water, 10 mM phosphate buffer, or 10 mM tris buffer, respectively. Metabolites with lower signal abundances are shown in (a), and metabolites with higher abundances are shown in (b) for better visualization.

abundances were not available due to lack of internal standard (α -methyl phenylalanine) in LC/FT-ICR MS data (very low amount of α -methyl phenylalanine was accidentally added during sample preparation and its signal was therefore not observed in the spectra). Jurkat cells washed with 10 mM Tris buffer generally provided similar signal abundances as compared to the water wash for most metabolites, except m/z 355.009 and 611.167 where the former is unknown and the latter matches the mass of oxidized glutathione. However, metabolites from Jurkat cells washed with 10 mM phosphate buffer did not show any deviation from water washed samples.

2.3.3. LC/FT-ICR MS for Untreated and Drug-treated Jurkat Cells

40 million Jurkat cells were treated with small molecules and compared with untreated Jurkat cells. Oligomycin²⁶⁻²⁷, 2-deoxyglucose^{26, 28} and Bz-423²⁹⁻³⁰ were used to treat Jurkat cells by our collaborator (Dr. Opipari's group, Medical school, University of Michigan). Oligomycin inhibits ATP synthesis, thus significant decrease of ATP is expected from oligomycin-treated cells.³¹ 2-deoxyglucose blocks further glycolysis, and metabolites related to glycolysis are expected to decrease in 2-deoxyglucose-treated cells.^{26, 28} Metabolic changes for Bz-423-treated cells have not previously been investigated, although it is known that Bz-423 induces cell death via increased levels of reactive oxygen species.^{29-30, 32} 500 nM of oligomycin or 2-deoxyglucose was added to 40 million Jurkat cells for 2 hrs, whereas 16 μ M Bz-423 was added to 40 million cells for 2 hrs. After treatment with small molecules, cell washing, lysis, and liquid-liquid extraction were performed as described in the Experimental Section.

HILIC/FT-ICR MS data were compared between each small molecule-treated and untreated Jurkat cells. Figure 2.2 shows total ion chromatogram (TIC) and extracted ion

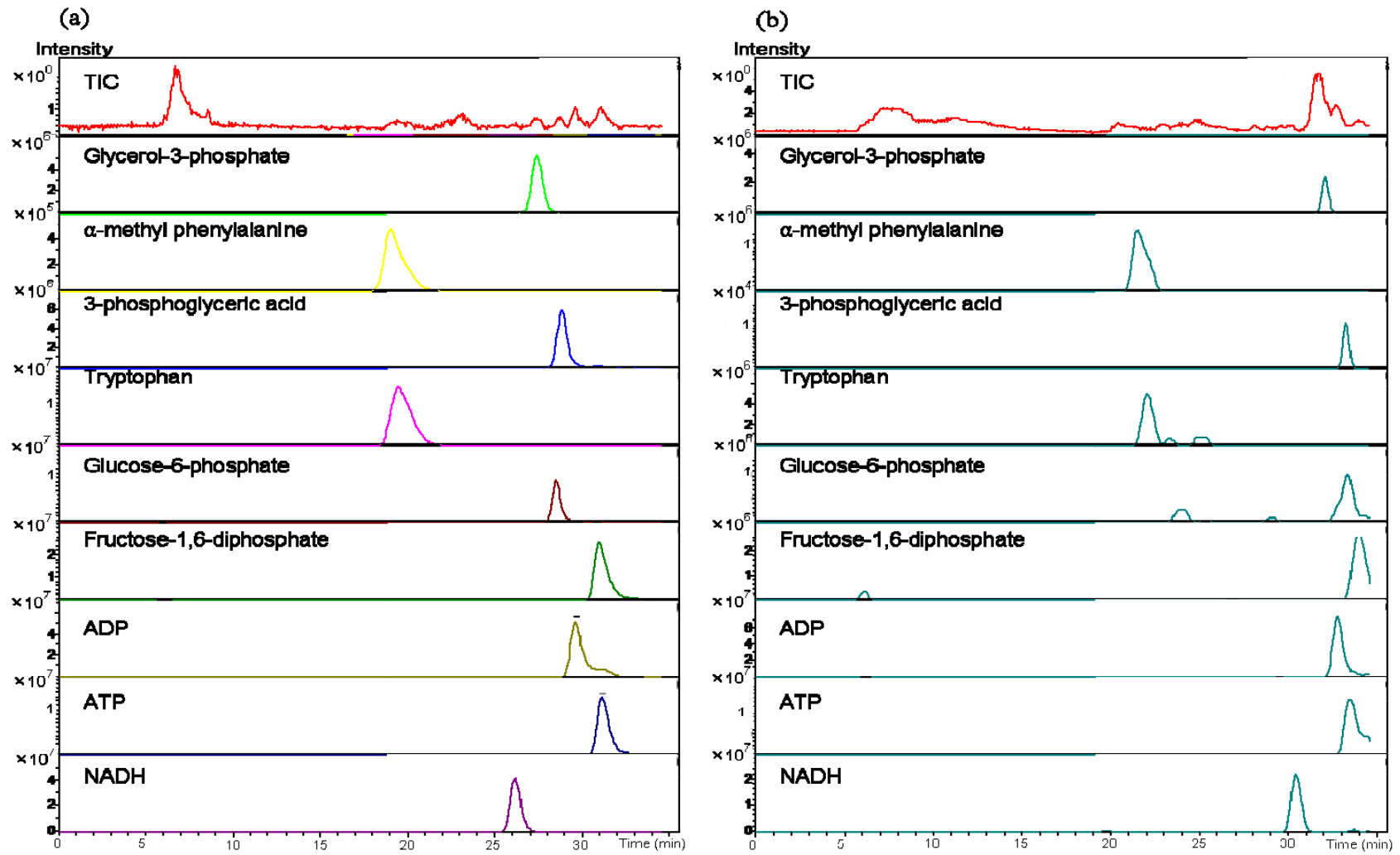


Figure 2.2. TIC and EICs for metabolites in standard metabolite mixture (a) and 40 million Jurkat cells (b).

chromatogram (EIC) for metabolites present in a standard metabolite mixture (a) and 40 million Jurkat cells (b). As shown in this Figure, retention time for each metabolite varied as explained in section I, however, the elution order among metabolites did not change. Thus, retention time can be used for tentative metabolite identification. Also retention time alignment could be done using several strategies available from various sources.^{21, 33-34} To generate EIC for each metabolite, the mass range for each metabolite was generally +/- 0.01 Da for the exact mass of the metabolite, however, sometimes narrower mass range was chosen to eliminate adjacent unwanted peaks.

Figure 2.3 shows 3D profiles, reconstructed with MS Excel, for overall comparisons of the differently treated and untreated cells. Oligomycin-treated Jurkat cells (b) did not show any significant difference compared to untreated Jurkat cells (a). However, 2-deoxyglucose-treated Jurkat cells (c) showed obvious changes compared to untreated Jurkat cells (a). The same conclusion could be drawn from PCA analysis with MZmine,²¹ shown in Figure 2.4 (a). Oligomycin-treated cells could not be differentiated from untreated cells, however, 2-deoxyglucose treated cells formed a separate group, which is clearly differentiated from untreated cells.

Bz-423-treated and untreated Jurkat cells were also compared with/without stimulation. Jurkat cells were activated via stimulation with anti-human CD3 (1 µg/ml) and further treated with Bz-423 by our collaborator. As shown in Figure 2.4, Bz-423-treated Jurkat cells clearly showed metabolic changes compared to untreated Jurkat cells. Bz-423 treatment caused metabolic changes even for stimulated Jurkat cells.

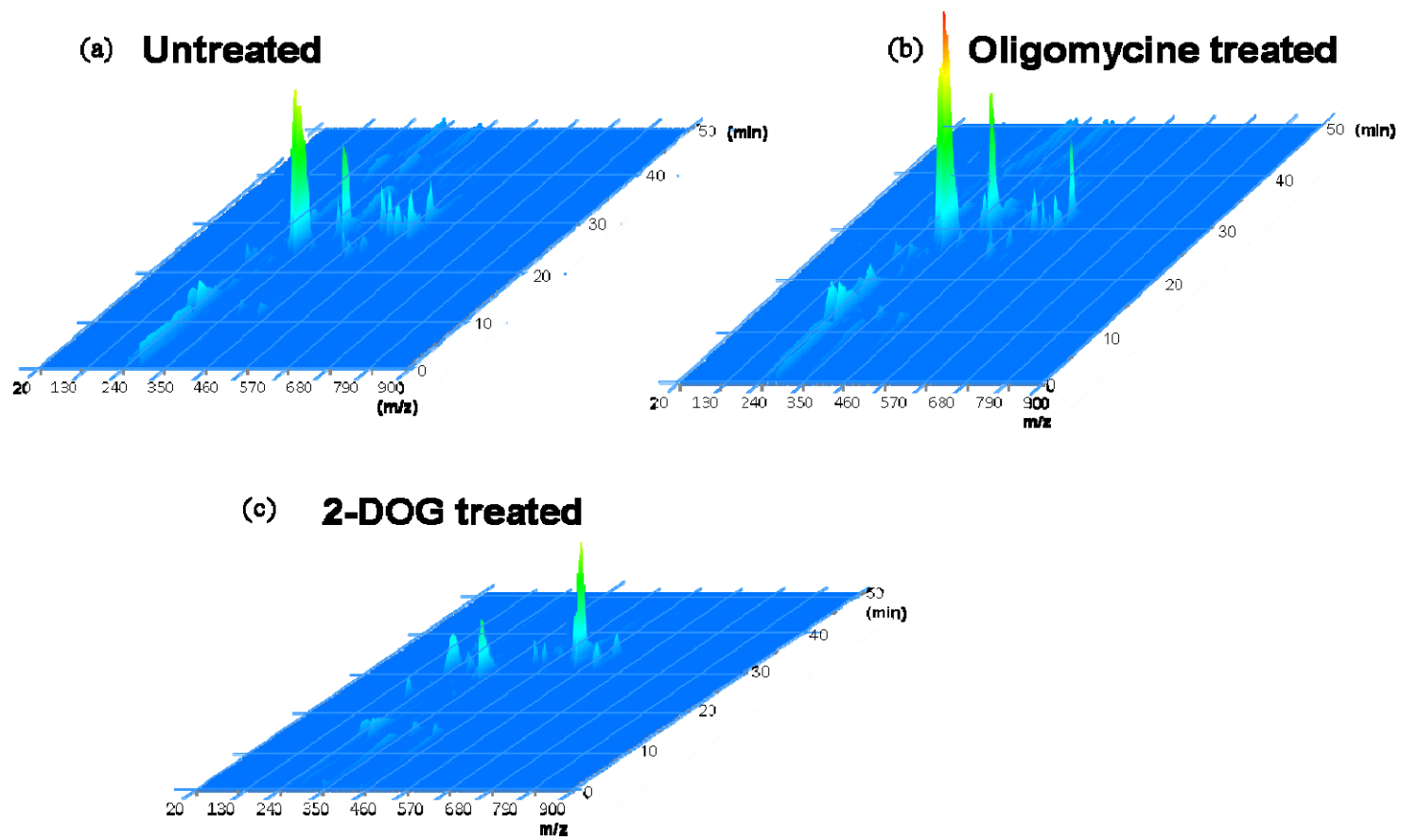


Figure 2.3. 3D profiles, reconstructed with MS Excel, for untreated, oligomycin-treated, and 2-deoxyglucose-treated Jurkat cells.

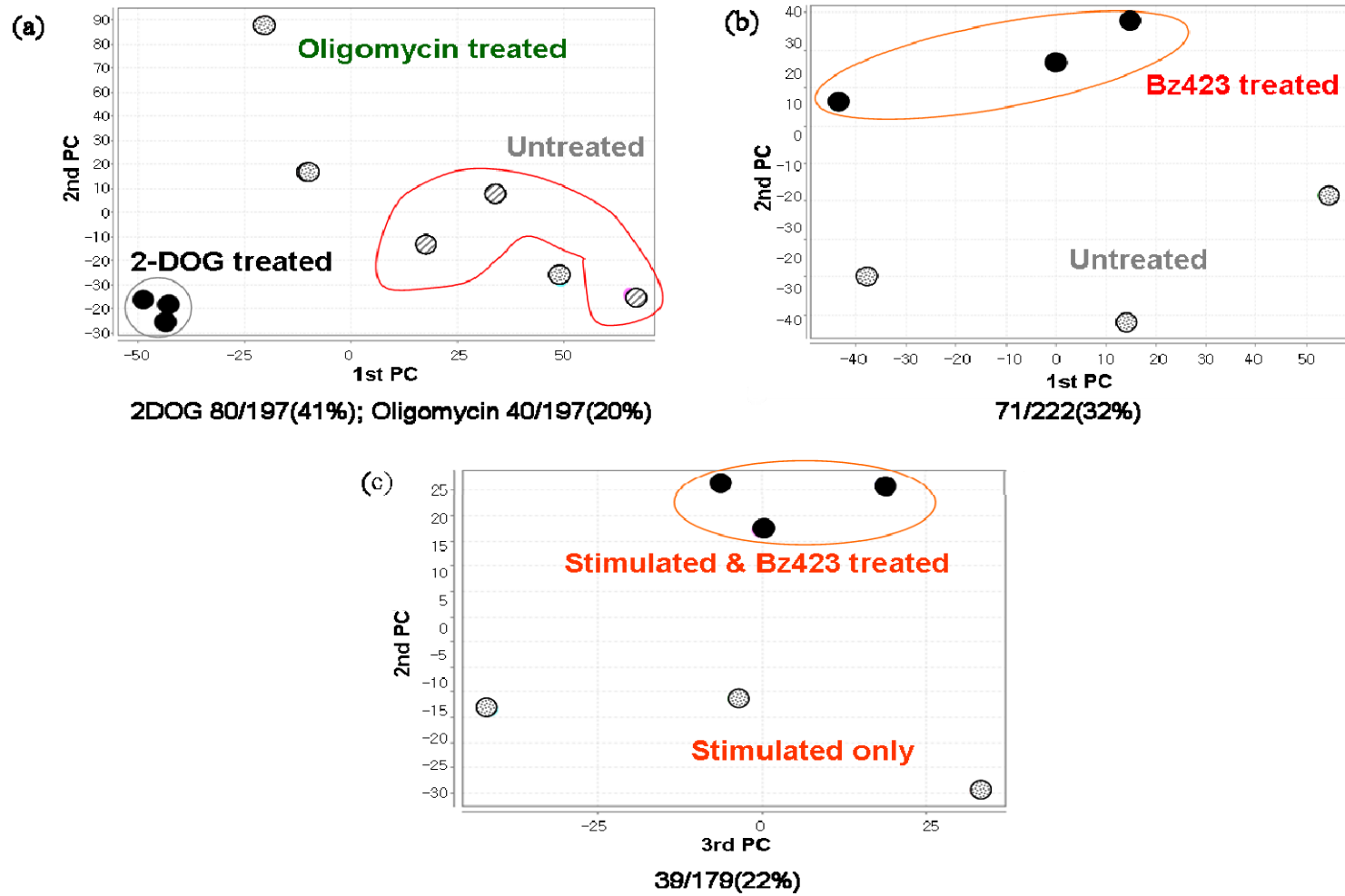


Figure 2.4. PCA analysis for (a) untreated vs. oligomycin-treated or 2-deoxyglucose-treated Jurkat cells; (b) untreated vs. Bz-423-treated Jurkat cells; (c) stimulated vs. stimulated and Bz-423-treated Jurkat cells.

2.3.4. Comparison between Untreated Jurkat cells and 2-deoxyglucose-Treated Jurkat cells

2-deoxyglucose-treated Jurkat cells provided the most obvious metabolic changes compared to untreated Jurkat cells and more detail is provided in this section. Hirayama et al. compared metabolic changes related to glycolysis and TCA cycle between normal and tumor samples.³⁵ Most metabolites involved in glycolysis and TCA cycle were increased in tumor samples, although many of the metabolic changes were not statistically significant. Lactate, citrate, malate, fumarate, and sedoheptulose 7-phosphate (S7P) showed statistically significant increase in tumor cells based on t-test. It is known that most cancer cells predominantly produce energy via glycolysis, which was also observed in their study.³⁵ When Jurkat cells were treated with 2-deoxyglucose, metabolites involved in glycolysis were expected to be decreased.^{26, 28} Small molecules (≤ 100 Da), including lactate, could not be observed with the utilized FT-ICR MS instrument, however, G6P in 2-deoxyglucose-treated Jurkat cells was significantly increased (based on t-test ($P = 0.025$)). F1,6BP, G3P, and 3PG were decreased after 2-deoxyglucose treatment. Hirayama et al. observed that F1,6BP and 3PG were increased in tumor tissues, compared to non-cancerous tissue.³⁵

Other groups compared metabolic changes after treating human epithelial cells with 2-deoxyglucose.^{26, 36} They observed 2-deoxyglucose 6-phosphate accumulation, which was also observed in my study. 2-deoxyglucose is a stable glucose analogue that is actively taken up by hexose transporters and phosphorylated to 2-deoxyglucose 6-phosphate, which cannot be fully metabolized and therefore inhibits glycolytic enzymes.^{26, 36} Another group observed metabolic changes in cancerous HeLa cells with 2-deoxyglucose treatment. Glutathion and nucleotides (dGMP, AMP, ADP, UMP, and

UDP) were decreased in their study.³⁷ My study also showed decrease of the same metabolites: all the details are summarized in Table 2.4.

2.4. Conclusions

HILIC/FT-ICR MS was developed to monitor metabolic changes in untreated and small molecule (drug)-treated Jurkat cells. HILIC column was used to separate highly polar metabolites involved in glycolysis and TCA cycle. Jurkat cells treated with 500 nM oligomycin did not show any changes compared to untreated cells. Higher amount of oligomycin may be needed to detect statistically significant metabolic changes. However, 500 nM of 2-deoxyglucose caused significant metabolic changes, and some of these changes have also been observed by other groups for other biological systems. Bz-423 treatment also resulted in metabolic changes (e.g. glutathione and ADP). Several groups have reported that autoimmune diseases are associated with altered cellular metabolism (such as ATP and glucose levels).^{29-30, 38} However, metabolic changes caused by Bz-423 treatment have not previously been measured, thus it would be interesting to apply the developed HILIC/FT-ICR MS method to investigate the effect of Bz-423 on metabolism of autoimmune diseases such as Lupus.

This study clearly showed that the developed HILIC/FT-ICR MS could be applied to monitor metabolic changes in a biological system, with potential for further improvement such as extension of the mass range to observe very small metabolites, e.g., lactate (≤ 100 Da).

Table 2.4. Metabolic changes after 2-deoxyglucose treatment of Jurkat cells. Normalized peak area was used and the number shown corresponds to the difference between EIC normalized area for a metabolite from untreated and treated Jurkat cells. For example, a negative number indicates that a metabolite was decreased after 2-deoxyglucose treatment, and a positive number indicates an increase of a metabolite after treatment. Higher numbers imply larger metabolic changes. P-values are also shown for each metabolite. Metabolic changes with P-value ≤ 0.025 mean that the change is statistically significant with 95 % confidence interval. Metabolite identification was performed with the METLIN database³⁹ based on exact mass.

m/z	Metabolites	Calc. m/z	Error (ppm)	day1	day2	day3	average	STD	p-value
189.035				-3.51	-4.44	-2.86	-3.60	0.80	0.0043
197.022				3.93	3.08	4.24	3.75	0.60	0.0017
201.028				0.12	0.24	0.36	0.25	0.13	0.0484
202.042				-0.56	-1.13	-0.57	-0.76	0.32	0.0269
203.727				-0.92	-1.25	-0.66	-0.94	0.29	0.0117
213.011				-1.18	-1.30	-1.18	-1.22	0.07	0.0001
216.034				9.48	12.36	17.19	12.67	4.37	0.0162
218.104	Pantothenic acid	218.103	2.751	-8.16	-7.22	-3.25	-6.21	2.61	0.0258
220.038				21.43	25.41	21.96	22.93	2.16	0.0004
223.021	Cys Cys	223.022	-4.484	2.61	3.91	5.19	3.67	1.29	0.0139
225.018				25.08	32.02	49.02	35.37	12.32	0.0156
228.065	FENAMISAL	228.067	-8.331	1.69	0.97	1.51	1.36	0.43	0.0118
241.010	Inositol cyclic phosphate	241.012	-9.299	2.54	4.51	4.71	3.92	1.20	0.0110
243.028	Fucose 1-phosphate, 2-DOG 6-phosphate,	243.027	5.349	35.33	36.41	50.99	40.91	8.75	0.0031
253.145				-8.34	-11.17	-5.19	-8.23	2.99	0.0175
255.235	2-hexyldecanoic acid, isopalmitic acid	255.233	7.839	38.93	64.96	29.48	54.26	35.29	0.0793
259.019	Glucose 6-phosphate, Fructose 6-phosphate	259.022	-11.592	7.93	8.84	15.98	10.85	4.46	0.0243
263.477				1.34	1.04	1.83	1.44	0.46	0.0120
267.073	3-Deoxy-D-glycero-D-galacto-2-nonulosonic acid	267.072	3.744	-1.42	-1.97	-1.28	-1.56	0.37	0.0052

m/z	Metabolites	Calc. m/z	Error(ppm)	day1	day2	day3	average	STD	p-value
269.251	6-methyl-hexadecanoic acid, Margoric acid, (+)-14-methyl palmitic acid, 2-methyl-hexadecanoic acid	269.249	7.799	1.94	3.99	5.12	3.84	1.90	0.0291
270.067	p-Hydroxyketorolac, Mefenamic acid Metabolite (Benzoic acid, 3-[(2-carboxyphenyl)amino]-2-methyl-)	270.067	0.000	0.96	1.04	1.69	1.23	0.40	0.0132
272.093	Hydroxytolmetin, L-Thyronine	272.093	-0.368	0.93	0.81	1.29	0.94	0.33	0.0163
274.095	Ethenodeoxyadenosine	274.095	0.730	1.80	1.95	4.18	2.84	1.33	0.0415
280.038				1.90	1.45	2.99	2.09	0.90	0.2061
283.267	Stearic acid, 11,15-dimethyl-hexadecanoic acid, lambda isostearic acid	283.264	10.591	51.48	80.08	35.97	49.14	12.27	0.0061
285.075	Ethylphenthiazine-2-carbamate, Gummiferol, 3-Hydroxy-N-methylpyridinium glucuronide, Hydroxytolbutamide, Salicin	285.070	17.540	6.49	9.77	9.35	8.54	1.79	0.0037
286.988				2.17	2.76	4.45	3.12	1.19	0.0195
288.068				-2.21	-3.70	-1.01	-2.30	1.34	0.0591
293.974				1.37	1.99	2.90	2.05	0.78	0.0200
296.083	5'-Methylthioadenosine	296.083	1.351	-1.48	-2.13	-0.92	-1.48	0.66	0.0287
299.141	Asn Ala Pro, Gln Pro Gly	299.136	16.715	3.42	3.09	3.69	3.40	0.30	0.0003
300.051	N-Acetylglucosamine-1-phosphate, N-Acetyl-D-mannosamine 6-phosphate, 4-Aminophenyl 1-thio-beta-D-glucuronide, 2-Chloroadenosine, Dehydrochlorambucil	300.049	6.996	1.24	2.15	2.84	2.09	0.90	0.0206
302.055				1.94	-8.02	-1.17	-2.42	5.09	0.4723
305.026	Pelargonidin	305.023	11.475	1.52	1.94	3.99	2.41	1.29	0.0471
306.079	Glutathione, Cys Glu Gly, Asp Ala Cys	306.076	9.901	-17.11	102.30	39.53	-52.99	44.16	0.1290
313.048	5'-Phosphoribosyl-N-formylglycinamide (FGAR)	313.044	12.778	-0.99	-3.43	-1.12	-1.91	1.40	0.1120
314.005				1.03	1.14	1.44	1.20	0.21	0.0023
318.078				-2.58	-1.70	-1.67	-1.99	0.52	0.0069

m/z	Metabolites	Calc. m/z	Error(ppm)	day1	day2	day3	average	STD	p-value
321.001	Chloramphenicol	321.005	-13.395	0.24	0.31	0.32	0.29	0.04	0.0012
323.030	Uridine monophosphate (UMP), Arabinose-uridinemonophosphate	323.029	6.191	-6.03	-29.47	4.76	-9.91	16.9 5	0.3969
332.062	bromodiphenhydramine	332.066	-11.444	3.08	3.50	6.83	4.47	2.06	0.0327
333.062				2.01	1.92	3.47	2.47	0.67	0.1609
334.060	Dihydroneopterin phosphate	334.056	11.675	-2.23	-1.55	-2.04	-1.94	0.35	0.0024
335.095				-1.29	-0.87	-1.08	-1.08	0.21	0.0031
337.965				2.07	2.69	1.36	2.03	0.66	0.0131
338.992	Fructose1,6-bisphosphate, D-Glucose 1,6-bisphosphate, D-myo-Inositol 1,4-bisphosphate	338.999	11.800	-1.17	-4.59	-1.31	-2.36	1.94	0.1254
338.997				0.49	0.53	0.93	0.82	0.19	0.0101
344.035	3',5'-Cyclic GMP	344.040	-15.696	0.43	0.14	0.33	0.30	0.15	0.0403
345.028				1.05	1.28	0.97	1.09	0.15	0.0011
346.059	deoxyguanosine 5'-monophosphate (dGMP), Adenylic acid (adenosine monophosphate, AMP)	346.055	10.869	-24.69	120.11	-42.35	-62.39	50.7 7	0.1230
350.034				0.79	0.91	1.33	1.01	0.29	0.0099
354.074				-2.28	-4.82	-2.74	-3.27	1.36	0.0253
357.071	Furo[3,4-b]pyridine-3-carboxylic acid, 5,7-dihydro-2-methyl-4-(3-nitrophenyl)-5-oxo-, 2-hydroxyethyl	357.073	-5.881	2.81	2.47	2.29	2.46	0.16	0.0001
359.108				1.21	1.34	1.84	1.46	0.34	0.0049
360.955				1.75	1.91	2.02	1.89	0.14	0.0002
362.054	Guanidylic acid (guanosine monophosphate)	362.051	8.296	1.43	1.05	1.91	1.43	0.39	0.0073
364.083	Asp Cys Glu	364.082	2.747	2.15	2.35	4.14	2.89	1.10	0.0199

m/z	Metabolites	Calc. m/z	Error(ppm)	day1	day2	day3	average	STD	p-value
364.137	Cys Phe Pro	364.134	8.239	-3.42	-3.89	-2.41	-3.24	0.76	0.0051
371.077	Sulindac sulfone	371.076	2.695	2.19	2.76	3.69	2.69	0.75	0.0069
376.128	Gln Cys Gln, Asn Met Asn	376.130	-5.051	-0.92	-1.58	-0.74	-1.08	0.44	0.0243
380.091	Glu Cys Met	380.096	-12.628	7.82	6.82	9.82	8.16	1.53	0.0027
382.552				-1.51	-3.05	-1.73	-2.10	0.83	0.0223
389.298				0.27	0.87	1.55	0.89	0.64	0.0942
393.283	25-hydroxy-16,17,23,23,24,24-hexadehydrovitamin D3 / 25-hydroxy-16,17,23,23,24,24-hexadehydrocholeca	393.280	7.628	-2.45	-2.24	-2.27	-2.32	0.11	0.0001
403.001	Uridine diphosphate (UDP)	402.895	14.392	-6.72	-24.66	-6.72	-12.80	10.5 3	0.1254
413.157	Diltiazem	413.154	6.535	-1.25	-1.52	-0.89	-1.15	0.42	0.0180
422.094				-2.41	-8.87	-5.07	-5.45	3.25	0.0620
423.143				-0.35	-1.38	-0.66	-0.80	0.53	0.0797
426.027	Adenosine diphosphate (ADP), Deoxyguanosine diphosphate (dGDP), 5'-Adenylyl sulfate (APS)	426.022	11.736	-15.77	-55.28	-18.43	-28.16	22.6 2	0.1120
431.120				-0.41	-0.60	-0.51	-0.51	0.10	0.0028
432.190	Thr Gln Trp,	432.189	2.092	-0.09	-0.13	-0.10	-0.10	0.02	0.0036
442.022	Guanosine 5'-diphosphate (GDP)	442.016	13.574	1.22	-6.97	1.81	-1.31	4.91	0.6932
445.075				0.84	0.91	1.42	1.06	0.32	0.0108
445.200				-4.35	-2.79	-2.08	-3.08	1.16	0.0183
447.138				-5.05	-7.32	6.16	-2.07	7.22	0.6514
449.164				-4.80	-4.86	-2.49	-4.02	1.34	0.0137
452.143				4.10	2.71	7.73	4.95	2.59	0.0479
453.135				-1.44	-0.84	-0.98	-1.11	0.29	0.0065

m/z	Metabolites	Calc. m/z	Error(ppm)	day1	day2	day3	average	STD	p-value
463.985	Acyclovir triphosphate	463.978	15.087	1.38	1.00	0.97	1.08	0.26	0.0057
470.105				8.97	2.65	1.82	4.48	3.91	0.1421
470.165				0.66	0.43	2.48	1.18	1.12	0.1630
471.073				-1.08	-5.45	-3.05	-3.18	2.18	0.0854
473.223	Methylprednisolone succinate	473.218	9.721	-1.18	-0.89	-0.84	-0.97	0.18	0.0027
478.300	GPEtn(18:1(8Z)/0:0)	478.284	12.128	-1.80	-2.38	-0.77	-1.65	0.82	0.0395
482.112	Nicergoline	482.109	6.638	-1.02	-1.48	-0.86	-1.08	0.41	0.0215
482.967	Uridine triphosphate (UTP)	482.962	10.353	-0.64	-4.43	-0.70	-1.92	2.17	0.2212
499.057				-1.03	-3.82	-1.80	-2.18	1.53	0.0883
500.286	Fexofenadine	500.281	10.184	-1.83	-2.48	-1.00	-1.77	0.74	0.0258
505.994	ATP, Deoxyguanosine triphosphate (dGTP), Inosine triphosphate (ITP)	505.988	11.858	-2.52	-11.41	-0.88	-4.93	5.86	0.2282
508.125				-0.89	-1.86	-1.40	-1.32	0.38	0.0100
514.095				6.22	8.55	10.50	8.42	2.14	0.0085
518.074				-0.35	-3.42	-1.32	-1.70	1.57	0.1583
520.055				0.18	0.14	0.28	0.20	0.08	0.0188
521.992	GTP	521.983	17.242	-0.52	-1.48	-0.01	-0.67	0.75	0.2188
523.058				0.28	0.18	0.58	0.35	0.21	0.0873
525.028				0.67	0.88	1.43	0.88	0.40	0.0230
527.980				0.23	0.28	0.28	0.27	0.03	0.0008
528.304				-0.93	-1.27	-0.54	-0.91	0.36	0.0222
530.308				-0.89	-0.92	-0.54	-0.78	0.21	0.0072
532.103	Indomethacin glucuronide	532.102	2.087	18.54	18.80	31.21	22.18	7.90	0.0188
540.058	Cyclic adenosine diphosphate ribose	540.054	7.407	-2.14	-5.54	-0.08	-2.58	2.77	0.2037

m/z	Metabolites	Calc. m/z	Error(ppm)	day1	day2	day3	average	STD	p-value
549.060				4.34	4.90	8.56	5.93	2.30	0.0209
554.082				0.69	0.63	0.80	0.71	0.09	0.0007
556.323				-0.77	-0.93	-0.56	-0.75	0.19	0.0063
565.053	UDP-glucose, UDP-D-galactose	565.047	10.619	-1.47	-6.23	-0.40	-2.70	3.10	0.2282
567.032				3.44	2.36	4.38	3.39	1.01	0.0101
575.008				0.01	0.02	0.03	0.02	0.01	0.0464
579.030	Uridine diphosphate glucuronic acid	579.026	6.908	-0.74	-3.17	-0.41	-1.44	1.51	0.1975
588.081	Guanosine diphosphofucose	588.075	10.203	4.03	4.01	7.95	5.33	2.27	0.0268
606.081	UDP-GlcNac, UDP-N-acetyl-D-galactosamine	606.074	11.550	-2.60	-7.07	2.65	-2.34	4.87	0.4674
611.147	Glutathione, oxidized	611.147	0.000	-6.73	-9.23	-0.54	-5.50	4.47	0.1230
620.026				-0.04	-0.39	0.07	-0.12	0.24	0.4483
626.018				0.25	0.10	0.34	0.23	0.12	0.0454
633.055				0.13	0.07	0.09	0.10	0.03	0.0121
638.032				-0.19	-0.31	-0.31	-0.27	0.07	0.0061
640.181				-0.12	-0.31	-0.14	-0.19	0.10	0.0497
641.906				-0.07	-0.07	-0.02	-0.05	0.03	0.0501
644.036				0.36	0.09	0.33	0.26	0.15	0.0563
649.080				0.41	0.19	0.47	0.35	0.15	0.0259
652.048				0.18	0.12	6.32	2.21	3.56	0.3631
664.116	NADH	664.117	-1.506	0.20	-0.08	0.18	0.10	0.16	0.3631
685.209				-0.11	-0.15	-0.10	-0.12	0.03	0.0054

2.5. References

1. Cascante, M.; Boros, L. G.; Comin-Anduix, B.; de Atauri, P.; Centelles, J. J.; Lee, P. W. *Nat Biotechnol* **2002**, *20*. 243-249.
2. Kell, D. B. *Curr Opin Microbiol* **2004**, *7*. 296-307.
3. Lindon, J. C.; Holmes, E.; Bollard, M. E.; Stanley, E. G.; Nicholson, J. K. *Biomarkers* **2004**, *9*. 1-31.
4. Rochfort, S. *J Nat Prod* **2005**, *68*. 1813-1820.
5. van der Greef, J.; Stroobant, P.; van der Heijden, R. *Curr Opin Chem Biol* **2004**, *8*. 559-565.
6. Villas-Boas, S. G.; Mas, S.; Akesson, M.; Smedsgaard, J.; Nielsen, J. *Mass Spectrom Rev* **2005**, *24*. 613-646.
7. Fernie, A. R.; Trethewey, R. N.; Krotzky, A. J.; Willmitzer, L. *Nat Rev Mol Cell Biol* **2004**, *5*. 763-769.
8. Werner, E.; Heilier, J. F.; Ducruix, C.; Ezan, E.; Junot, C.; Tabet, J. C. *J Chromatogr B Analyt Technol Biomed Life Sci* **2008**, *871*. 143-163.
9. Aharoni, A.; Giri, A. P.; Deuerlein, S.; Griepink, F.; de Kogel, W. J.; Verstappen, F. W.; Verhoeven, H. A.; Jongsma, M. A.; Schwab, W.; Bouwmeester, H. J. *Plant Cell* **2003**, *15*. 2866-2884.
10. Brown, S. C.; Kruppa, G.; Dasseux, J. L. *Mass Spectrom Rev* **2005**, *24*. 223-231.
11. Dettmer, K.; Aronov, P. A.; Hammock, B. D. *Mass Spectrom Rev* **2007**, *26*. 51-78.
12. Dunn, W. B.; Ellis, D. I. *TrAC* **2005**, *24*. 285-294.
13. Matuszewski, B. K.; Constanzer, M. L.; Chavez-Eng, C. M. *Anal Chem* **2003**, *75*. 3019-3030.
14. Yang, J.; Schmelzer, K.; Georgi, K.; Hammock, B. D. *Anal Chem* **2009**, *81*. 8085-8093.
15. Marshall, A. G.; Hendrickson, C. L.; Jackson, G. S. *Mass Spectrom Rev* **1998**, *17*. 1-35.
16. Aharoni, A.; Ric de Vos, C. H.; Verhoeven, H. A.; Maliepaard, C. A.; Kruppa, G.; Bino, R.; Goodenowe, D. B. *OmicS* **2002**, *6*. 217-234.
17. Hemstrom, P.; Irgum, K. *J Sep Sci* **2006**, *29*. 1784-1821.
18. Bajad, S. U.; Lu, W.; Kimball, E. H.; Yuan, J.; Peterson, C.; Rabinowitz, J. D. *J Chromatogr A* **2006**, *1125*. 76-88.
19. Belov, M. E.; Nikolaev, E. N.; Anderson, G. A.; Udseth, H. R.; Conrads, T. P.; Veenstra, T. D.; Masselon, C. D.; Gorshkov, M. V.; Smith, R. D. *Anal Chem* **2001**, *73*. 253-261.
20. Hendrickson, C. L.; Quinn, J. P.; Emmett, M. R.; Marshall, A. G., in *49th ASMS Conference on Mass Spectrometry and Allied Topics*. Chicago, IL, 2001; CD-ROM.
21. Katajamaa, M.; Miettinen, J.; Oresic, M. *Bioinformatics* **2006**, *22*. 634-636.
22. Soga, T.; Ohashi, Y.; Ueno, Y.; Naraoka, H.; Tomita, M.; Nishioka, T. *J Proteome Res* **2003**, *2*. 488-494.
23. Uehara, T.; Yokoi, A.; Aoshima, K.; Tanaka, S.; Kadowaki, T.; Tanaka, M.; Oda, Y. *Anal Chem* **2009**, *81*. 3836-3842.
24. Wikoff, W. R.; Gangoiti, J. A.; Barshop, B. A.; Siuzdak, G. *Clin Chem* **2007**, *53*. 2169-2176.

25. Kimball, E.; Rabinowitz, J. D. *Anal Biochem* **2006**, *358*. 273-280.
26. Ramanathan, A.; Wang, C.; Schreiber, S. L. *Proc Natl Acad Sci U S A* **2005**, *102*. 5992-5997.
27. Shepina, L. A.; Pletjushkina, O. Y.; Avetisyan, A. V.; Bakeeva, L. E.; Fetisova, E. K.; Izyumov, D. S.; Saprunova, V. B.; Vyssokikh, M. Y.; Chernyak, B. V.; Skulachev, V. P. *Oncogene* **2002**, *21*. 8149-8157.
28. Soller, M.; Drose, S.; Brandt, U.; Brune, B.; von Knethen, A. *Mol Pharmacol* **2007**, *71*. 1535-1544.
29. Boitano, A.; Ellman, J. A.; Glick, G. D.; Opipari, A. W., Jr. *Cancer Res* **2003**, *63*. 6870-6876.
30. Boitano, A.; Emal, C. D.; Leonetti, F.; Blatt, N. B.; Dineen, T. A.; Ellman, J. A.; Roush, W. R.; Opipari, A. W.; Glick, G. D. *Bioorg Med Chem Lett* **2003**, *13*. 3327-3330.
31. Otero, M. J.; Carrasco, L. *Mol Cell Biochem* **1984**, *61*. 183-191.
32. Blatt, N. B.; Boitano, A. E.; Lyssiotis, C. A.; Opipari, A. W., Jr.; Glick, G. D. *Biochem Pharmacol* **2009**, *78*. 966-973.
33. Benton, H. P.; Wong, D. M.; Trauger, S. A.; Siuzdak, G. *Anal Chem* **2008**, *80*. 6382-6389.
34. Katajamaa, M.; Oresic, M. *J Chromatogr A* **2007**, *1158*. 318-328.
35. Hirayama, A.; Kami, K.; Sugimoto, M.; Sugawara, M.; Toki, N.; Onozuka, H.; Kinoshita, T.; Saito, N.; Ochiai, A.; Tomita, M.; Esumi, H.; Soga, T. *Cancer Res* **2009**, *69*. 4918-4925.
36. Ralser, M.; Wamelink, M. M.; Struys, E. A.; Joppich, C.; Krobitsch, S.; Jakobs, C.; Lehrach, H. *Proc Natl Acad Sci U S A* **2008**, *105*. 17807-17811.
37. Lin, X.; Zhang, F.; Bradbury, C. M.; Kaushal, A.; Li, L.; Spitz, D. R.; Aft, R. L.; Gius, D. *Cancer Res* **2003**, *63*. 3413-3417.
38. Bian, X.; Giordano, T. D.; Lin, H. J.; Solomon, G.; Castle, V. P.; Opipari, A. W., Jr. *J Biol Chem* **2004**, *279*. 4663-4669.
39. Smith, C. A.; O'Maille, G.; Want, E. J.; Qin, C.; Trauger, S. A.; Brandon, T. R.; Custodio, D. E.; Abagyan, R.; Siuzdak, G. *Ther Drug Monit* **2005**, *27*. 747-751.

Chapter 3

Infrared Multiphoton Dissociation and Electron Induced Dissociation as Alternative MS/MS Strategies for Metabolite Identification

3.1. Introduction

Metabolites play multiple key roles in living cells and their levels represent integrative information on cellular function, and define the phenotype of a cell or tissue in response to genetic or environmental changes. mRNA levels do not always correlate with protein levels, and translated protein may or may not be enzymatically active. Therefore, changes observed in the transcriptome or proteome do not always directly correspond to phenotypic alterations. Thus, measurement of the metabolites synthesized by a biological system is often crucial to completely assess genetic function.¹⁻⁶

Metabolite analysis includes identification and quantification of all intracellular and extracellular metabolites by different analytical techniques. Metabolites have wide variations in chemical (molecular weight, polarity, acidity) and physical (e.g., volatility) properties, rendering it difficult to analyze various metabolites simultaneously. Mass spectrometry (MS), and nuclear magnetic resonance (NMR), Fourier transform infrared

(FT-IR), and Raman spectroscopy are all used for metabolite analysis^{2, 7-12} FT-IR and Raman spectroscopy allow rapid, nondestructive, and high-throughput analyses of a diverse range of sample types. These two techniques are typically used for metabolic profiling due to its holistic nature, although absorptions at specific wavelengths can be used for identification of unknown metabolites. However, the sensitivity and selectivity of FT-IR and Raman spectroscopy are not as high as for other methods.¹¹ NMR spectroscopy also constitutes a rapid and non-destructive, high-throughput method that requires minimal sample preparation. Furthermore, chemical shifts can be assigned to specific metabolites. However, NMR requires millimolar to high micromolar concentration of samples, and, thus, its sensitivity is not as high as that of mass spectrometry. Another major weakness of NMR is its poor dynamic range (10^3), which results in detection of only the most abundant components.^{11, 13} Mass spectrometry remains the most suitable technology for measurement of metabolites because of its wide dynamic range (10^4 - 10^6), good sensitivity (nM) and ability to detect a diverse number of molecular species.⁸ Gas chromatography/mass spectrometry (GC/MS) has been the most commonly used MS method for small molecule analysis. However, this technique often involves sample derivatization to improve volatility, and is limited in terms of molecule size and type due to volatility and polarity constraints. Therefore, liquid chromatography/mass spectrometry (LC/MS) has become a popular alternative choice for metabolite analysis. This technique has advantages over GC/MS in that sample derivatization is generally not required, although it can be beneficial to improve chromatographic resolution and sensitivity, and more diverse chemical structures and increased molecular sizes can be observed.^{8, 11, 14}

One major challenge encountered in MS-based metabolite research is the identification and characterization of the hundreds to thousands of detected metabolites. Currently, mass spectral libraries are not complete enough to allow identification of all unknown metabolites. For example, the Golm metabolome database (<http://csbdb.mpimp-golm.mpg.de/csbdb/gmd/gmd.html>) includes mostly plant metabolites and is limited to GC/MS data,¹⁵ and the National Institute of Standards and Technology (NIST) database (<http://www.nist.gov/srd/nist1.htm>) includes only electron ionization (EI)/MS data.¹⁶ The METLIN (METabolite LINK) database (<http://metlin.scripps.edu/>) includes an annotated list of known metabolite structural information with tandem mass spectra, and LC/MS data, but the number of mass spectra is still not sufficient to cover the large number of metabolites typically detected.¹⁶ Nevertheless, successful metabolite identification has been reported by utilizing molecular weight matching with the MetaCyc, NIST, and the Kyoto Encyclopedia of Genes and Genomes (KEGG) databases.^{15, 17-18} However, the existence of compounds with similar or identical molecular weights, i.e., isobars and isomers, can result in misidentification. In such cases, tandem mass spectrometry (MS/MS) involving collision induced dissociation (CID) has been used to obtain structural information about metabolites, thereby aiding their identification.^{7, 17, 19-21}

Fourier transform ion cyclotron resonance (FT-ICR) mass spectrometry provides several advantages for metabolite analysis. First, the accurate mass capabilities of FT-ICR MS can reduce the number of possible metabolite candidates at a given nominal mass.²² Second, the ultrahigh resolution of FT-ICR MS allows analysis of highly complex metabolite mixtures.⁷ Third, an FT-ICR mass analyzer coupled with mass

selective external ion accumulation provides improved dynamic range.²³⁻²⁴ Furthermore, FT-ICR MS offers MS/MS techniques other than CID, such as electron-induced dissociation (EID)²⁵⁻²⁶ and infrared multiphoton dissociation (IRMPD),^{27,28} that can provide additional structural information, sometimes crucial to the determination or confirmation of metabolite structure.⁸ To identify and characterize an unknown metabolite, it is desirable to obtain as many bond cleavages as possible for increased confidence. For MS/MS of metabolites, negative mode ionization is generally preferred due to the increased ionization efficiency of many acidic and neutral metabolites. However, negative mode CID often results in limited fragmentation, possibly due to the absence of a mobile proton.²⁹ Thus, alternative fragmentation strategies (e.g., IRMPD and EID) appear promising to overcome this issue. Electron-induced dissociation, which involves irradiation of analyte ions with electrons, was first shown in 1979 by Cody and Freiser for radical cations.²⁶ This approach was extended in 1990 by Wang and McLafferty to even-electron peptide cations.³⁰ The former experiments utilized a range of electron energies whereas the latter involved 70 eV electrons. In both cases, similar fragmentation patterns were observed as in CID of the same species. More recently, approaches involving thermal electrons (electron capture dissociation (ECD))³¹ and medium energy electrons (10-20 eV, electron detachment dissociation (EDD))³² have been introduced for analytically valuable fragmentation of even-electron biomolecular cations and anions, respectively. However, both ECD and EDD require precursor ions to carry at least two charges. Thus, they are not directly compatible with metabolite analysis because the smaller size of most metabolites renders formation of multiply

charged ions difficult. Zubarev and co-workers have demonstrated EID experiments involving 10-13 eV electron irradiation of singly charged even-electron cations.²⁵

Phosphate-containing metabolites are important in life processes, such as phosphate metabolism and energy conversion. Phosphates are most commonly found in the form of nucleotides, cofactors, and phosphorylated carbohydrates. Phosphate-containing metabolites have been identified by accurate mass and/or CID-based MS/MS, which provides limited structural information because it mainly results in cleavages at phosphate groups, or charge-directed fragmentation.^{17, 19, 33-34} IRMPD has been shown to be an efficient technique for fragmentation of nucleic acids and phosphopeptides due to strong phosphate absorption at the 10.6 μm wavelength typically used.^{27, 35-38} However, IRMPD of phosphate-containing metabolites has, to our knowledge, not previously been described. Here, we report the utility of both IRMPD and EID FT-ICR MS for characterization of phosphate-containing metabolites, including phosphorylated carbohydrates and nucleotides. These fragmentation techniques are also compared to CID of the same species.

3.2. Experimental Section

3.2.1. Sample Preparation

Phosphate-containing metabolites investigated in this work were purchased from Sigma-Aldrich (St. Louis, MO) and used without further purification. Negative mode electrospray solvent consisted of 1:1 (v/v) isopropanol:water (Fisher, Fair Lawn, NJ) with 10 mM ammonium acetate (Fisher). The final metabolite concentration was 1 to 20 μM .

3.2.2. Fourier Transform Ion Cyclotron Resonance Mass Spectrometry

All experiments were performed with a 7 Tesla quadrupole (Q)-FT-ICR mass spectrometer³⁹ (Bruker Daltonics, Billerica, MA) operating in negative ion mode. Samples were infused via an external Apollo electrospray ion source at a flow rate of 60 to 70 $\mu\text{L}/\text{h}$, mass selectively externally accumulated²³⁻²⁴ (6 m/z isolation window) for 1-3 s, and captured in the ICR cell by dynamic trapping. The accumulation, ion transfer, and capture events were looped 2-3 times to improve precursor ion abundance.

CID was performed in the external hexapole at a collision cell DC offset of 4-20 V with Ar as collision gas. IRMPD was performed inside the ICR cell with a vertically mounted 25 W, 10.6 μm , CO_2 laser (Synrad, Mukilteo, WA). The laser beam was deflected by two mirrors for alignment through a hollow dispenser cathode to the center of the ICR cell. The beam entered the vacuum system through a BaF_2 window. Photon irradiation was performed for 50-100 ms at 8.75-10 W laser power. An indirectly heated hollow dispenser cathode was used for electron generation.⁴⁰ A heating current of 1.8 A was applied to a heater element located behind the cathode. For EID, performed inside the ICR cell, the cathode bias voltage was pulsed to 15-20 V for 6-8 s.

All mass spectra were acquired with XMASS software (version 6.1, Bruker Daltonics) in broadband mode from m/z 21 to 1000 with 512k data points and summed over 10-15 scans. Data processing was performed with the MIDAS analysis software.⁴¹ Calculated masses of precursor ions, $[\text{M} - \text{H}]^-$, and product ions corresponding to either loss of the phosphate moiety, or adenine, were used for internal calibration. Following calibration, assigned product ions were within 10 ppm with only a few exceptions. H_2O losses were considered if 18 Da differences between adjacent peaks could not be explained by direct fragmentation of metabolites.

3.3. Results

3.3.1. CID, IRMPD, and EID of Phosphorylated Carbohydrates Involved in Glycolysis

Glucose-6-phosphate (G6P) is a glucose molecule phosphorylated at carbon number 6. Such phosphorylation occurs immediately following glucose entry into a cell. G6P participates in two important metabolic pathways: glycolysis and the pentose phosphate pathway. Other carbohydrates, such as fructose 1,6-bisphosphate (F1,6BP), phosphoenolpyruvate (PEP), and phosphoglycerate (PG), participating in glycolysis are also phosphorylated. Figure 3.1 shows CID, IRMPD, and EID MS/MS spectra from deprotonated G6P and observed bond cleavages are summarized in Scheme 3.1. From Fig. 3.1 and Scheme 3.1, it is evident that sugar cross-ring cleavages are generated for this carbohydrate with all three fragmentation methods although they are most prevalent in CID, which produced three cross-ring fragments (at m/z 139, 169, and 199) differing by 30 amu (i.e., CH_2O). IRMPD resulted in similar product ions as CID although cross-ring cleavage was less prominent, and the most abundant product ions were instead from cleavage at the phosphate group (m/z 97). The latter product ions are likely abundant in external CID as well, however, due to the time-of-flight effect when transferring ions to the ICR cell, they are likely not trapped as efficiently as in IRMPD in which product ions are generated inside the ICR cell. By contrast, EID showed only limited fragmentation (two cross-ring fragments were detected) compared to the other two dissociation methods, and phosphate group cleavages were not observed. Other phosphorylated carbohydrates, including F1,6BP, PEP, and PG involved in glycolysis were also investigated, and the only observed product ions in MS/MS (sustained off-resonance irradiation collision induced dissociation (SORI)-CID,⁴² IRMPD and EID) spectra

corresponded to phosphate group cleavages (data not shown). Only limited fragmentation was observed in IRMPD and EID of F1,6BP, PEP and PG, likely due to low precursor ion abundances and the necessity to use in-cell precursor ion isolation due to interfering species with similar m/z values. The latter approach affects the position of the ion cloud in the cell and, consequently, can reduce the overlap between precursor ions with photons or electrons. For phosphorylated carbohydrates, CID appears to be the most suitable MS/MS strategy although phosphate group cleavages are more apparent in IRMPD. Similar CID fragmentation of small phosphorylated carbohydrates has been reported by Ferule et al.³³

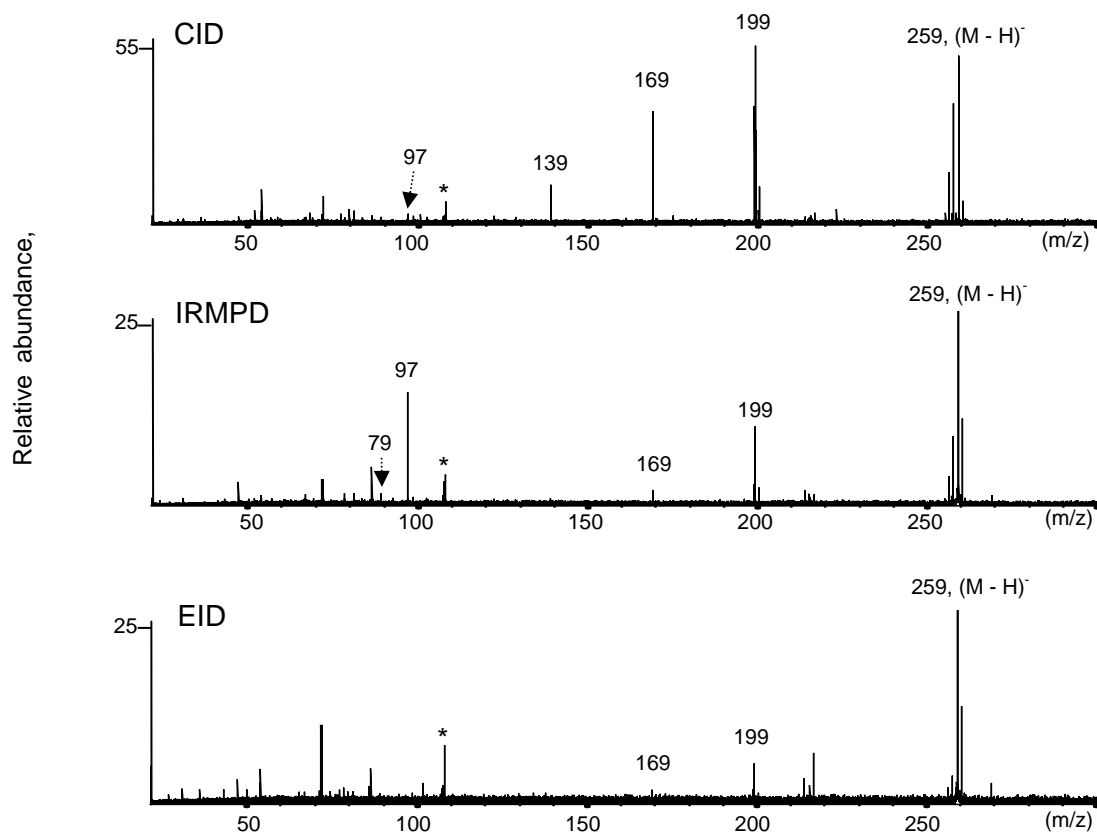
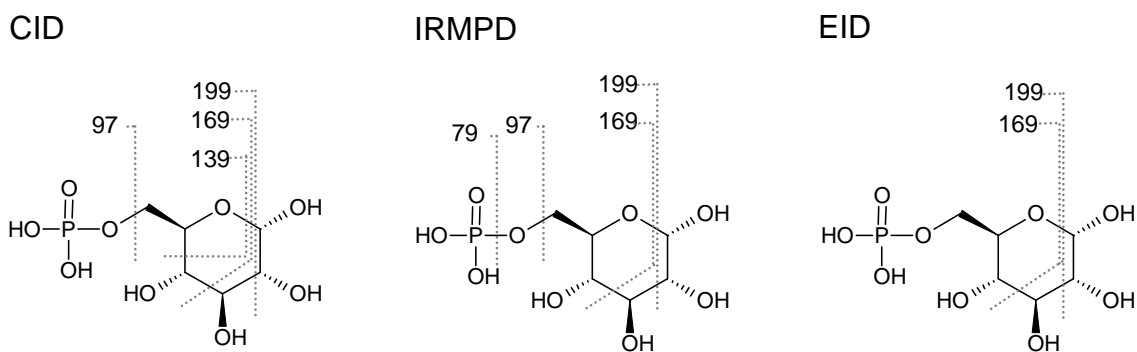


Figure 3.1. CID (7 V collision cell DC offset, 15 scans, top), IRMPD (10 W, 100 ms, 15 scans, middle), and EID (20 eV, 8 s, 15 scans, bottom) MS/MS spectra of glucose 6-phosphate. Electronic noise peaks are marked with asterisks.



Scheme 3.1. Structure and observed MS/MS fragmentation of glucose 6-phosphate.

3.3.2. CID, IRMPD, and EID of Adenosine 5'-triphosphate (ATP)

ATP is a multifunctional nucleotide with several biochemical roles. This molecule transports chemical energy within cells and is produced during photosynthesis and cellular respiration. ATP is also one of four nucleotides required for the synthesis of ribonucleic acids. The structure of this molecule consists of a purine base (adenine) attached to the 1' carbon atom of a pentose (ribose), which also has three phosphate groups attached at its 5' carbon (see Scheme 3.2).

CID, IRMPD, and EID of deprotonated ATP were explored and the results are shown in Figure 3.2 and in Scheme 3.2. From these data, it is evident that CID and EID of ATP provide complementary structural information. Product ions at m/z 328, 371, and 426, originating from neutral loss of the two terminal phosphates (178 Da), adenine (135 Da), and terminal phosphite (80 Da), respectively, were observed only in CID. Furthermore, the carbon-oxygen ester bond of adenosine was only cleaved in EID (resulting in the product ion at m/z 257) and H₂O losses from secondary fragmentation (m/z 310 and 353 in CID, and m/z 390 in EID) were only observed in CID and EID. Neutral loss of the terminal phosphate group (98 Da) was the dominant fragmentation channel in both CID and IRMPD, whereas no fragmentation channel was particularly dominant in EID, which resulted in product ions of relatively even abundance. In summary, CID provided most structural information for ATP although EID resulted in the additional carbon-oxygen bond cleavage of adenosine. However, the fragmentation efficiency of EID was much lower than that of CID.

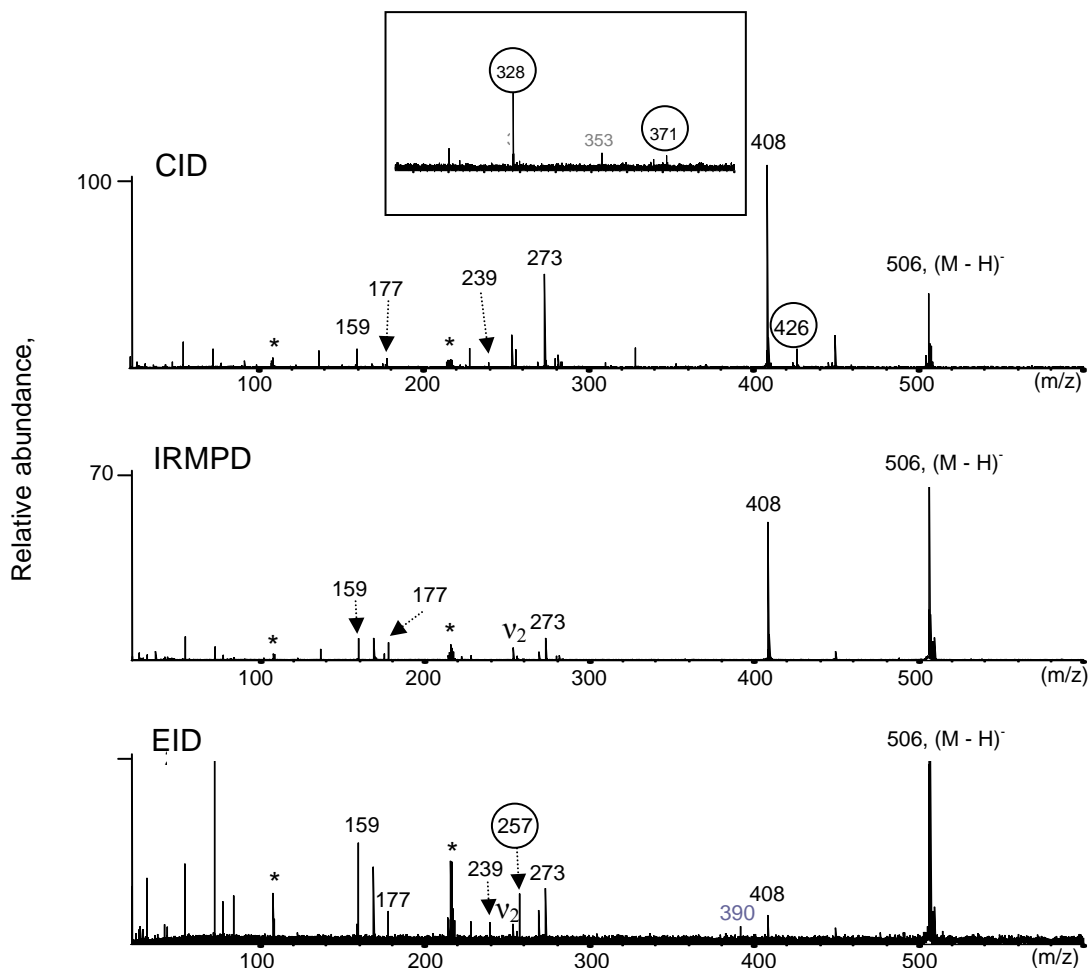
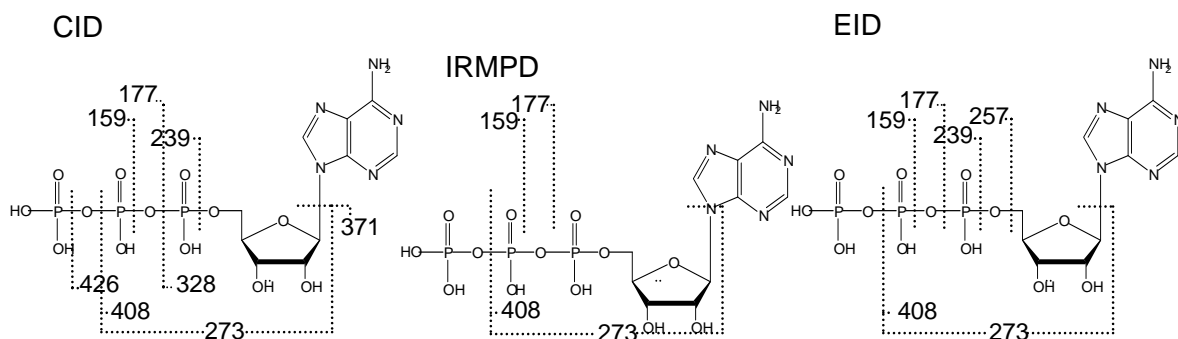


Figure 3.2. CID (20 V collision cell DC offset, 9 scans, top), IRMPD (10 W, 50 ms, 9 scans, middle), and EID (19 eV, 6 s, 9 scans, bottom) MS/MS spectra of adenosine 5'-triphosphate. Open circles indicate product ions providing complementary information compared to other fragmentation strategies. Product ions with gray labels correspond to secondary H₂O losses. v₂ and v₃ indicate harmonic peaks. Electronic noise peaks are marked with asterisks.



Scheme 3.2. Structure and observed MS/MS fragmentation of adenosine 5'-triphosphate.

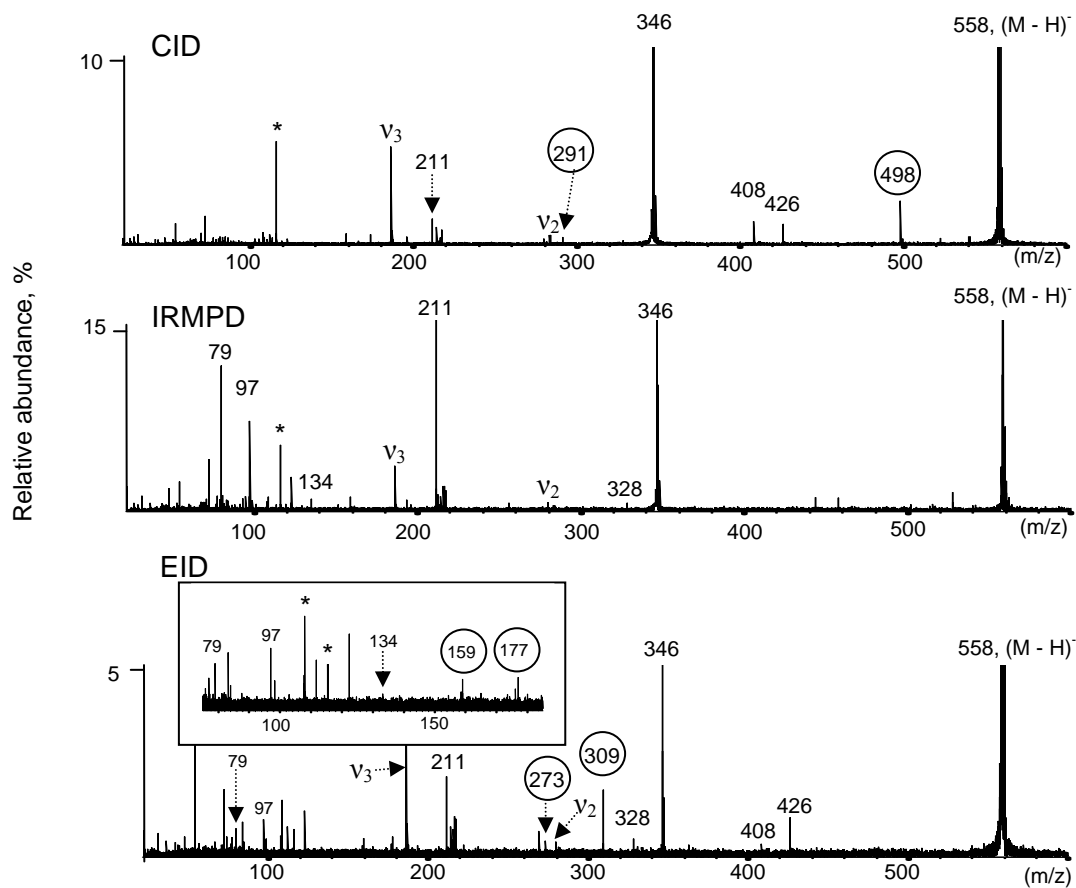
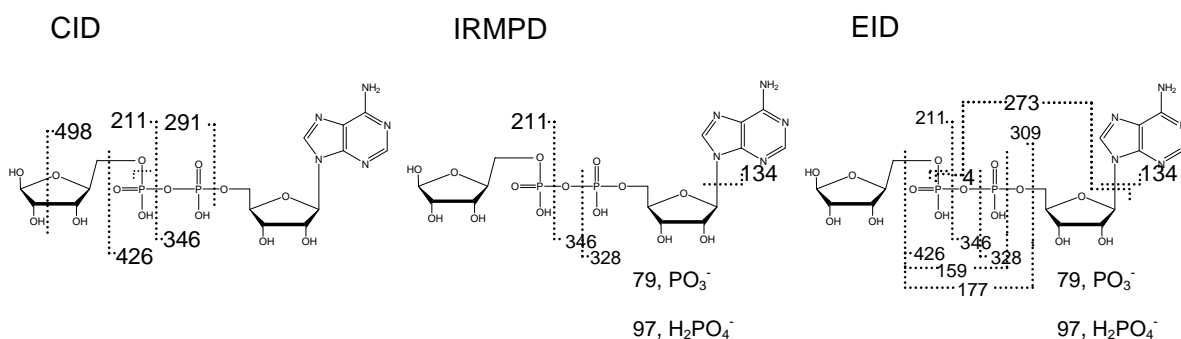


Figure 3.3. CID (15 V collision cell DC offset, 5 scans, top), IRMPD (10 W, 70 ms, 5 scans, middle), and EID (16 eV, 6 s, 5 scans, bottom) MS/MS spectra of adenosine diphosphate-ribose. Open circles indicate product ions providing complementary information compared to other fragmentation strategies. v_2 and v_3 indicate harmonic peaks. Electronic noise peaks are marked with asterisks.



Scheme 3.3. Structure and observed MS/MS fragmentation of adenosine diphosphate-ribose.

3.3.3. CID, IRMPD, and EID of Adenosine 5'-diphosphate-ribose (ADP-ribose)

ADP-ribose has a structure similar to ATP, except that the terminal phosphate is replaced with ribose (see Scheme 3.3). This molecule has been proposed to be involved in cellular signaling leading to necrosis or apoptosis.⁴³ Figure 3.3 shows CID, IRMPD, and EID spectra of deprotonated ADP-ribose. Product ions at $m/z = 291$ and 498 , corresponding to cleavage of one phosphoester bond to lose diphosphate-ribose and ribose cross-ring cleavage, respectively, were only observed in CID. The carbon-oxygen ester bond of adenosine was only fragmented (resulting in $m/z 309$) in EID, similar to the case of ATP (Figure 3.2 and Scheme 3.2). Neutral ribose ring loss, corresponding to $m/z 426$, was observed in CID and EID but not in IRMPD, whereas deprotonated adenine ($m/z 134$) was observed in IRMPD and EID but not in CID. Product ions from secondary fragmentation were observed in EID and IRMPD but not in CID. EID generated more extensive secondary fragments than IRMPD, including $m/z 159$, 177 , and 273 , which were all unique to EID. In IRMPD, phosphoanhydride bond cleavage and phosphate loss dominated. Overall, for ADP-ribose, EID showed the most extensive fragmentation although relative product ion abundances were weak.

3.3.4. CID, IRMPD, and EID of Nicotinamide Adenine Dinucleotide (NAD)

Nicotinamide adenine dinucleotide (NAD) is an important cofactor found in cells. NAD, which is the oxidized form of NADH, is extensively used in glycolysis and the citric acid cycle of cellular respiration. The reducing potential stored in NADH can be converted to ATP through the electron transport chain, or used for anabolic metabolism. In NAD, nicotinamide is attached at the 1' carbon of ribose (see Scheme 3.4).

In CID of deprotonated NAD (Figure 3.4), only neutral nicotinamide loss (resulting in m/z 540) was observed, independently of the collision energy. By contrast, extensive fragmentation of NAD occurred in both IRMPD and EID. Phosphoanhydride bond cleavages (to yield m/z 328 and 346) and loss of deprotonated adenine (m/z 134) dominated in IRMPD along with neutral nicotinamide loss (m/z 540). The same fragments were observed in EID but, once again, the latter technique showed relatively evenly abundant product ions although the fragmentation efficiency was lower than that of IRMPD.

3.3.5. CAD, IRMPD, and EID of Nicotinic Acid-Adenine Dinucleotide Phosphate (NAADP)

Recent work suggests that NAADP constitutes one of the Ca^{2+} signaling messengers.^{33,44-45} The structure of NAADP is similar to NAD, but it contains nicotinic acid instead of nicotinamide, and a phosphate group is attached to the 2' carbon of the adenosine ribose (Scheme 3.5).

CID of deprotonated NAADP (Figure 3.5) showed dominant neutral nicotinic acid loss (m/z 620) (independently of the collision energy), but IRMPD and EID both resulted in rich fragmentation patterns, similar to NAD. In IRMPD, secondary fragmentation was extensive: dominant product ions resulting from phosphate loss, cleavages of a phosphoester bond (m/z 159, 255, and 488), and cleavages of phosphoanhydride bonds (m/z 193, 291, 328, 408, and 426) were observed, along with combined loss of the nicotinic acid nucleoside and the adenine 2' nucleotide (m/z 177). The EID spectrum was quite similar to IRMPD although fragmentation was not as efficient and more product ions were observed in IRMPD.

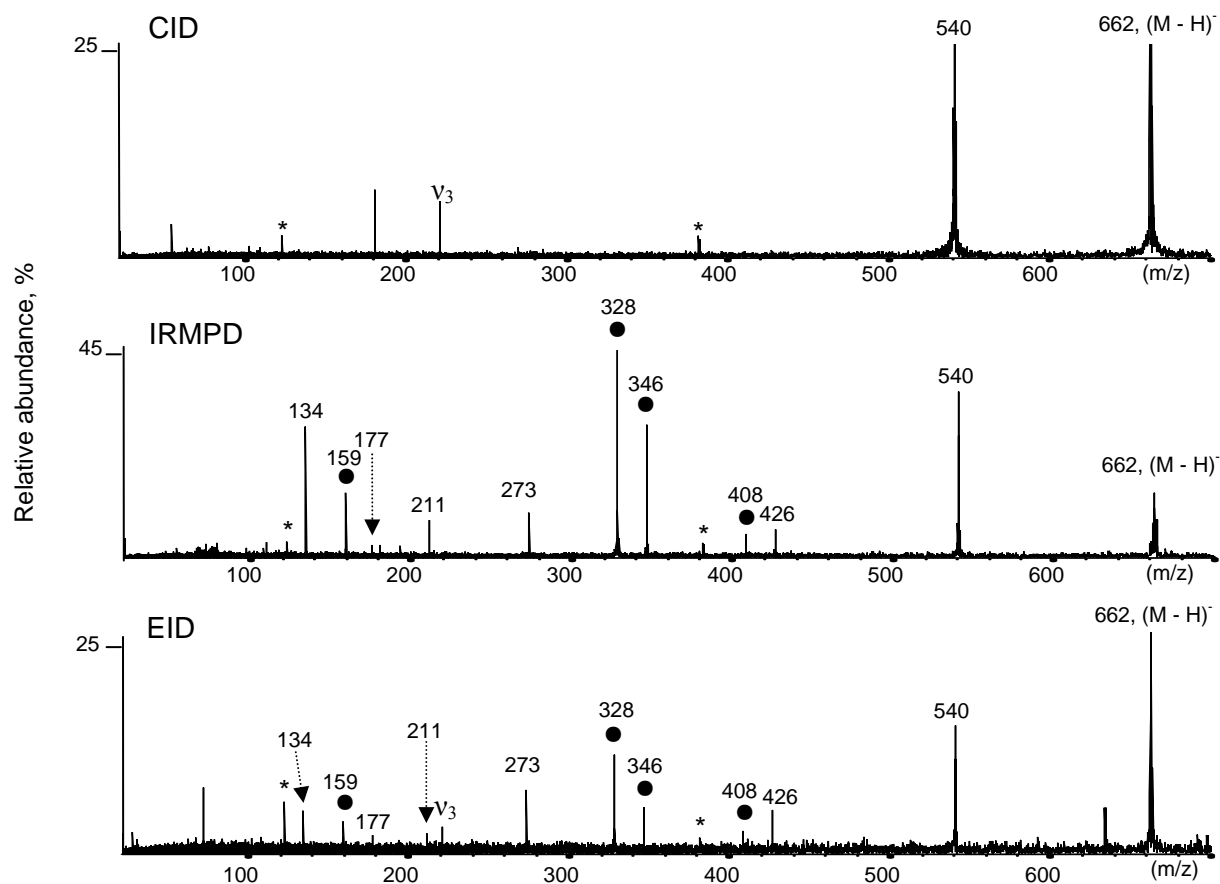


Figure 3.4. CID (4 V collision cell DC offset, 3 scans, top), IRMPD (8.75 W, 70 ms, 3 scans, middle), and EID (15 eV, 7 s, 3 scans, bottom) MS/MS spectra of nicotinamide adenine dinucleotide. Product ions labeled with filled circles result from phosphoester and phosphoanhydride bond cleavages, and are more abundant in IRMPD than in EID. v₃ indicates a harmonic peak. Electronic noise peaks are marked with asterisks.

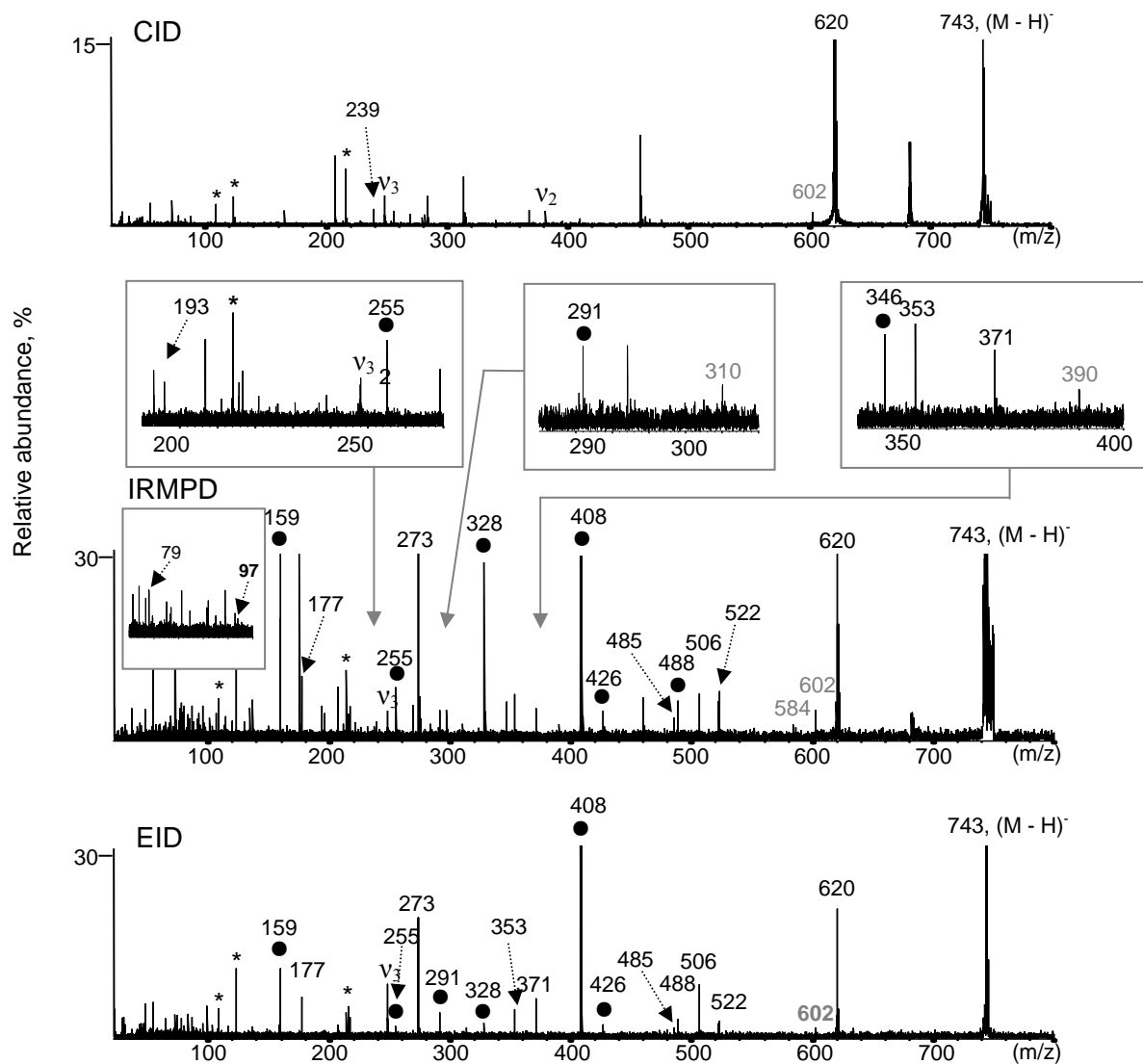


Figure 3.5. CID (7 V collision cell DC offset, 15 scans, top), IRMPD (10 W, 70 ms, 15 scans, middle), and EID (16 eV, 6 s, 15 scans, bottom) MS/MS spectra of nicotinic acid adenine dinucleotide phosphate. Product ions labeled with filled circles result from phosphoester and phosphoanhydride bond cleavages, and are more abundant in IRMPD than in EID. v_2 and v_3 indicate harmonic peaks. Product ions with gray labels correspond to secondary H_2O losses. Electronic noise peaks are marked with asterisks.

3.4. Discussion

The MS/MS spectra shown above represent experimental conditions that provided the highest fragmentation efficiency. In CID, the collision energy was chosen to reduce the precursor ion abundance by ~50%. For NAD and NAADP, higher collision energy provided no further fragmentation, i.e., only nicotinic acid or nicotinamide neutral loss was observed independent of the energy chosen. In IRMPD, abundances of lower m/z product ions increase with increased irradiation time or laser power due to increased secondary fragmentation. Irradiation conditions were chosen to yield similarly abundant product ions at lower and higher m/z values. In EID, electron energy plays an important role for the fragmentation outcome. The utilized cathode bias voltage range of – (15-20) V yielded similar EID spectra at the same irradiation time. Lower quality EID data were obtained within 2 V outside this range. However, lower electron energy generated no fragmentation, and higher electron energy resulted in significant depletion of precursor ions without detection of product ions. The detrimental effects of too high or low electron energy could be somewhat compensated for by adjusting the irradiation time (longer time for lower energy electrons and shorter time for high energy electrons).

In the experiments reported above, CID showed very limited fragmentation for NAD and NAADP with dominant nicotinic acid or nicotinamide neutral loss. By contrast, CID provided more extensive fragmentation than IRMPD and EID for smaller molecules, including G6P, ATP, and ADP-ribose. However, EID provided quite extensive fragmentation for all metabolites, including structural information complementary to that obtained from CID for smaller molecules. For smaller molecules, IRMPD provided somewhat less information than CID, except for the phosphate loss

(due to secondary fragmentation) observed for ADP-ribose. By contrast, IRMPD resulted in extensive fragmentation, similar to EID, for larger molecules, although the IRMPD fragmentation efficiency was higher than that in EID. The product ions being dominant in CID were also dominant in IRMPD along with product ions generated by phosphate loss, phosphoester and/or phosphoanhydride bond cleavages. For the larger phosphate-containing metabolites, EID and IRMPD both showed extensive secondary fragmentation.

From these results, it appears that CID is the best MS/MS strategy for small phosphorylated carbohydrates involved in glycolysis although EID can provide complementary structural information that can aid the identification of such metabolites. IRMPD appears superior to both CID and EID for larger phosphate-containing metabolites due to its higher extent of fragmentation and higher fragmentation efficiency. Furthermore, characteristic product ions at m/z 79, 97, 159, and 177 are indicative of phosphate moieties. Such ions, along with product ions generated by phosphoester and phosphoanhydride bond cleavages, are most prominent in IRMPD.

In CID, precursor ions collide inelastically with inert gases and are vibrationally excited by the resulting energy transfer.⁴⁶ However, this process does not always provide sufficient internal energy deposition to dissociate larger biomolecules, and it is known that the collisional activation efficiency decreases in a manner inversely proportional to the precursor ion mass.⁴⁷ Thus, it is not surprising that CID provided extensive structural information (including cross-ring cleavage) for smaller metabolites, such as G6P. The limited fragmentation observed in CID of larger metabolites, such as NAD and NAADP,

may also be explained through charge-directed fragmentation⁴⁸ (both NAD and NAADP contain a fixed charge at the preferred cleavage site).

IRMPD generally showed similar fragmentation as CID for smaller metabolites, however, IRMPD of NAD and NAADP was quite different from CID. The efficiency of IRMPD is not diminished with ion mass because excitation by IR absorption is characterized as a slow heating method in which many excitation steps are involved.⁴⁹⁻⁵⁰ As stated in the introduction, phosphate-containing compounds can efficiently dissociate when they are activated by IR irradiation because the P-O stretch (9.6-11 μm) is in direct resonance with the CO₂ IR laser (10.57-10.63 μm). In addition, the presence of aromatic phosphates (e.g., phosphotyrosine) results in a significantly greater dissociation rate than for aliphatic species, which is attributed to their higher absorptivity of IR photons.³⁵ G6P contains only one phosphate group while the other metabolites investigated in this work contain at least two. NAD has one phosphate group whereas NAADP has three. Consequently, as the number of phosphate groups increased, more extensive fragmentation was observed in IRMPD. In addition, the aromaticity of NAADP and NAD may contribute to more extensive fragmentation although this effect should be smaller than for phosphotyrosine³⁵ due to the larger distance between aromatic rings and phosphate groups in NAADP and NAD.

EID of phosphate-containing metabolites generally showed extensive fragmentation and provided complementary structural information compared to the other dissociation methods. Reilly and co-workers showed that 157 nm photons, corresponding to 8 eV, can deposit 3-4 eV more than required to cleave a peptide backbone, thereby generating secondary fragmentation.⁵¹ Thus, we speculate that the electron energy (15-20 eV) used

in EID is sufficient to generate secondary fragmentation of metabolites. Furthermore, the relatively long irradiation time (6-8 s) may also promote secondary fragmentation, although the precise fragmentation mechanism is unknown. However, the fragmentation efficiency of EID is lower than that of other fragmentation strategies. Efforts to increase EID fragmentation efficiency should be undertaken because it is apparent that EID can provide unique metabolite structural information, which could be crucial for metabolite identification.

3.5. Conclusions

CID, IRMPD, and EID spectra of phosphate-containing metabolites provided valuable complementary structural information, which can aid in the identification of such compounds. In our experiments, CID showed most extensive structural information for smaller phosphate-containing metabolites such as G6P and ATP. For larger phosphate-containing metabolites, CID resulted in more limited fragmentation. However, IRMPD showed extensive fragmentation for larger phosphate-containing metabolites, including NAD and NAADP. The increased number of bond cleavages could be attributed to an increased number of phosphate groups and, possibly, to their aromatic character. EID generally provided extensive fragmentation regardless of metabolite size, although fragmentation efficiency is lower than those of other MS/MS strategies. Thus, CID should be the preferred MS/MS strategy for smaller phosphate-containing metabolites. However, for larger phosphate-containing metabolites, particularly for species containing multiple phosphate groups, IRMPD is an advantageous strategy for metabolite structural identification. EID generally showed extensive fragmentation for

all phosphate-containing metabolites, and provided complementary structural information. Thus, EID could be used as a complementary MS/MS strategy to CID and IRMPD to yield further structural confirmation.

3.6. References

1. Rochfort, S. *J Nat Prod* **2005**, *68*. 1813-1820.
2. Villas-Boas, S. G.; Mas, S.; Akesson, M.; Smedsgaard, J.; Nielsen, J. *Mass spectrometry reviews* **2005**, *24*. 613-646.
3. Cascante, M.; Boros, L. G.; Comin-Anduix, B.; de Atauri, P.; Centelles, J. J.; Lee, P. W. *Nat Biotechnol* **2002**, *20*. 243-249.
4. Kell, D. B. *Current opinion in microbiology* **2004**, *7*. 296-307.
5. Lindon, J. C.; Holmes, E.; Bollard, M. E.; Stanley, E. G.; Nicholson, J. K. *Biomarkers* **2004**, *9*. 1-31.
6. van der Greef, J.; Stroobant, P.; van der Heijden, R. *Curr Opin Chem Biol* **2004**, *8*. 559-565.
7. Brown, S. C.; Kruppa, G.; Dasseux, J. L. *Mass spectrometry reviews* **2005**, *24*. 223-231.
8. Want, E. J.; Cravatt, B. F.; Siuzdak, G. *Chembiochem* **2005**, *6*. 1941-1951.
9. Boskey, A. L.; Mendelsohn, R. *Vib Spectrosc* **2005**, *38*. 107-114.
10. Defernez, M.; Colquhoun, I. J. *Phytochemistry* **2003**, *62*. 1009-1017.
11. Dunn, W. B.; Ellis, D. I. *TrAC* **2005**, *24*. 285-294.
12. Deleris, G.; Petibois, C. *Vib spectrosc* **2003**, *32*. 129-136.
13. Lenz, E. M.; Bright, J.; Knight, R.; Wilson, I. D.; Major, H. *J Pharm Biomed Anal* **2004**, *35*. 599-608.
14. Metz, T. D.; Zhang, L.; Page, J. S.; Shen, Y.; Callister, S. J.; Jacobs, J. M.; Smith, R. D. *Biomarkers in medicine* **2007**, *1*. 159-185.
15. Bino, R. J.; Hall, R. D.; Fiehn, O.; Kopka, J.; Saito, K.; Draper, J.; Nikolau, B. J.; Mendes, P.; Roessner-Tunali, U.; Beale, M. H.; Trethewey, R. N.; Lange, B. M.; Wurtele, E. S.; Sumner, L. W. *Trends Plant Sci* **2004**, *9*. 418-425.
16. Smith, C. A.; O'Maille, G.; Want, E. J.; Qin, C.; Trauger, S. A.; Brandon, T. R.; Custodio, D. E.; Abagyan, R.; Siuzdak, G. *Ther Drug Monit* **2005**, *27*. 747-751.
17. Edwards, J. L.; Chisolm, C. N.; Shackman, J. G.; Kennedy, R. T. *J Chromatogr A* **2006**, *1106*. 80-88.
18. Krieger, C. J.; Zhang, P.; Mueller, L. A.; Wang, A.; Paley, S.; Arnaud, M.; Pick, J.; Rhee, S. Y.; Karp, P. D. *Nucleic acids research* **2004**, *32*. D438-442.
19. Buchholz, A.; Takors, R.; Wandrey, C. *Analytical biochemistry* **2001**, *295*. 129-137.
20. Byrd, G. D.; Ogden, M. W. *J Mass Spectrom* **2003**, *38*. 98-107.
21. Triolo, A.; Altamura, M.; Dimoulas, T.; Guidi, A.; Lecci, A.; Tramontana, M. *J Mass Spectrom* **2005**, *40*. 1572-1582.

22. Aharoni, A.; Ric de Vos, C. H.; Verhoeven, H. A.; Maliepaard, C. A.; Kruppa, G.; Bino, R.; Goodenowe, D. B. *Omic* **2002**, *6*. 217-234.
23. Belov, M. E.; Nikolaev, E. N.; Anderson, G. A.; Udseth, H. R.; Conrads, T. P.; Veenstra, T. D.; Masselon, C. D.; Gorshkov, M. V.; Smith, R. D. *Analytical chemistry* **2001**, *73*. 253-261.
24. Hendrickson, C. L.; Quinn, J. P.; Emmett, M. R.; Marshall, A. G., in *49th ASMS Conference on Mass Spectrometry and Allied Topics*. Chicago, IL, 2001; CD-ROM.
25. Budnik, B. A.; Haselmann, K. F.; Elkin, Y. N.; Gorbach, V. I.; Zubarev, R. A. *Analytical chemistry* **2003**, *75*. 5994-6001.
26. Cody, R. B.; Freiser, B. S. *Analytical chemistry* **1979**, *51*. 541-551.
27. Little, D. P.; Speir, J. P.; Senko, M. W.; O'Connor, P. B.; McLafferty, F. W. *Analytical chemistry* **1994**, *66*. 2809-2815.
28. Woodin, R. L.; Bomse, D. S.; Beauchamp, J. L. *Journal of the American Chemical Society* **1978**, *100*. 3248-3250.
29. Wysocki, V. H.; Tsaprailis, G.; Smith, L. L.; Brei, L. A. *J Mass Spectrom* **2000**, *35*. 1399-1406.
30. Wang, B. H.; McLafferty, F. W. *Org Mass Spectrom* **1990**, *25*. 554-556.
31. Zubarev, R. A.; Kellerher, N. L.; McLafferty, F. W. *Journal of the American Chemical Society* **1998**, *120*. 3265-3266.
32. Budnik, B. A.; Haselmann, K. F.; Zubarev, R. A. *Chem Phys Lett* **2001**. 299-302.
33. Feurle, J.; Jomaa, H.; Wilhelm, M.; Gutsche, B.; Herderich, M. *J Chromatogr A* **1998**, *803*. 111-119.
34. Sekiguchi, Y.; Mitsuhashi, N.; Kokaji, Y.; Miyakoda, H.; Mimura, T. *J Chromatogr A* **2005**, *1085*. 131-136.
35. Flora, J. W.; Muddiman, D. C. *Journal of the American Society for Mass Spectrometry* **2004**, *15*. 121-127.
36. Crowe, M. C.; Brodbelt, J. S. *Journal of the American Society for Mass Spectrometry* **2004**, *15*. 1581-1592.
37. Flora, J. W.; Muddiman, D. C. *Journal of the American Chemical Society* **2002**, *124*. 6546-6547.
38. Hofstadler, S. A.; Sannes-Lowery, K. A.; Griffey, R. H. *Analytical chemistry* **1999**, *71*. 2067-2070.
39. Adamson, J. T.; Hakansson, K., in *Lectins: Analytical Technologies*, ed. Nisson, C. L. Elsevier: Amsterdam, 2007; in press.
40. Tsybin, Y. O.; Hakansson, P.; Budnik, B. A.; Haselmann, K. F.; Kjeldsen, F.; Gorshkov, M.; Zubarev, R. A. *Rapid Commun Mass Spectrom* **2001**, *15*. 1849-1854.
41. Senko, M. W.; Canterbury, J. D.; Guan, S.; Marshall, A. G. *Rapid Commun Mass Spectrom* **1996**, *10*. 1839-1844.
42. Gauthier, J.; Trautman, T. R.; Jacobson, D. B. *Anal. Chim. Acta* **1991**, *246*. 211-225.
43. Kun, E.; Kirsten, E.; Bauer, P. I.; Ordahl, C. P. *Int J Mol Med* **2006**, *17*. 293-300.
44. Rutter, G. A. *Biochem J* **2003**, *373*. e3-4.
45. Churchill, G. C.; Galione, A. *EMBO J* **2001**, *20*. 2666-2671.

46. Goeringer, D. E.; McLuckey, S. A. *Rapid Commun Mass Spectrom* **1996**, *10*. 328-334.
47. Hayes, R. N.; Gross, M. L. *Methods Enzymol* **1990**, *193*. 237-263.
48. Wheelan, P.; Zirrolli, J. A.; Murphy, R. C. *Biol Mass Spectrom* **1993**, *22*. 465-473.
49. Raspopov, S. A.; El-Faramawy, A.; Thomson, B. A.; Siu, K. W. *Anal Chem* **2006**, *78*. 4572-4577.
50. Hoffmann, E. d.; Charette, J.; Stroobant, V. *Mass spectrometry : principles and applications*. 2nd ed.; Chichester ; New York : Wiley ; Paris : Masson, c1996: **1996**.
51. Zhang, L.; Cui, W.; Thompson, M. S.; Reilly, J. P. *Journal of the American Society for Mass Spectrometry* **2006**, *17*. 1315-1321.

Chapter 4

Determination of Double Bond Location in Fatty Acids by Manganese Adduction and Electron Induced Dissociation

4.1. Introduction

When an oil or fat becomes oxidized, health concern is due to the potential production of free radicals, which can be highly carcinogenic.¹⁻⁴ Double bond sites in unsaturated fatty acids and lipids are plausibly oxidized and form free radicals, which can cause tissue damage and alterations in cell membranes.^{1-2, 5-7} Thus, the identification of double bond locations in fatty acids is beneficial for understanding disease states and possibly for early diagnosis of diseases such as Alzheimer's.^{6, 8}

Double bond locations in aliphatic compounds, including fatty acids, can be obtained from mass spectrometry (MS).⁹⁻¹⁴ Such information can be determined by charge-remote fragmentation processes of alkali metal-adducted fatty acids in high energy collisional activation with fast atom bombardment (FAB) ionization.^{9, 15} However, FAB desorption of fatty acid mixtures can result in preferential desorption of some ions, chemical noise, and low sensitivity.¹⁶⁻¹⁷ In addition, sector type instruments

for high energy CAD are not universally available and high energy CAD involves a high degree of scattering, causing product ion loss.¹⁸ Double bond migration and hydrogen scrambling in fatty acids and fatty acid esters were observed in electron ionization (EI)-MS, and chemical ionization (CI)-MS with conventional proton-transfer reagents such as methane, precluding unambiguous assignment of double bond locations.^{13, 19} Thus, such ionization methods must be combined with derivatization methods for determination of double bond positions in unsaturated fatty acids.²⁰ Dimethyl disulfide derivatization has been used to identify double bond positions in mono-unsaturated fatty acid methyl esters and mono-unsaturated acetates using EI-MS analysis.²¹ Various reactant gases such as acetonitrile were used to characterize fatty acid methyl esters with CI-MS.^{11, 22}

Chemical derivatization has been used to generate characteristic fragments during tandem mass spectrometric processes. Several derivatization methods,^{15, 23-24} including expoxidation,²⁵ hydroxylation,²⁶⁻²⁹ and ozonide derivatives³⁰⁻³¹ have been employed to determine double bond positions. The major disadvantage of chemical derivatization methods is that they often require a specialized wet chemical reaction step, additional equipment, and more labor and effort prior to MS analysis. Recently, low energy CAD of Cu(II)-adducted fatty acids in an ion trap instrument was used to provide diagnostic product ions to aid the identification of double bond locations in unsaturated fatty acids,³² however, double bond localization remains challenging for monounsaturated fatty acids.

Charge remote fragmentation occurs remote from a charge site and appears to readily occur in high energy collision activated dissociation (CAD) of fatty acids, lipids, steroids, and other compounds containing long alkyl chains.^{15, 17, 33} Charge remote fragmentation has been used to provide double bond positions of fatty acids from FAB-

MS/MS (high energy CAD) of lithiated fatty acids using sector-type mass spectrometry by Gross and others.^{17, 33-34} More recently, tandem time-of-flight (TOF/TOF) MS was applied to determine double bond locations of lithiated fatty acids by McEwen and co-workers using solvent-free matrix-assisted laser desorption ionization (MALDI).¹⁰ Charge-remote bond cleavages in fatty acids are reduced in the vicinity of double bonds, thus providing information on double bond locations.³³ Fixed charge sites are important for predominant charge-remote fragmentation processes because charge-driven processes compete with charge-remote processes. In charge-driven fragmentation, charge migration results in rearrangement of chemical structure, making identification of double bond positions difficult.¹⁵ High energy CAD is known to involve electronic excitation as a dominant process for generating charge-remote product ions and vibrational/rotational excitation is considerably less efficient.³³

Fourier transform ion cyclotron resonance (FT-ICR) mass spectrometry can provide unique structural information due to its accurate mass capabilities,³⁵ ultrahigh resolution,³⁶ wide dynamic range,³⁷⁻³⁸ and additional tandem mass spectrometric fragmentation techniques, including infrared multiphoton dissociation (IRMPD)³⁹⁻⁴⁰ and electron induced dissociation (EID).⁴¹⁻⁴⁴ EID involves interactions between singly charged analyte ions and free electrons and was first shown in 1979 by Cody and Freiser for radical cations.⁴² Electron capture dissociation (ECD)⁴⁵⁻⁴⁸ and electron detachment dissociation (EDD)⁴⁹⁻⁵¹ were introduced more recently and provide radical-driven fragmentation and analytically valuable structural information for biomolecular cations and anions, respectively. However, both ECD and EDD require precursor ions to carry at least two charges because these processes involve charge-reduction, either through

electron capture or detachment. Thus, ECD and EDD are not directly compatible with smaller biomolecule (such as fatty acid) analysis because formation of gas-phase multiply charged ions is energetically unfavorable. Zubarev and co-workers applied EID (10-13 eV electron irradiation) to singly charged oligosaccharide cations⁴¹ and we have applied EID for structural characterization of phosphate-containing metabolites.⁴⁴ EID of phosphate-containing metabolites provided complementary structural information compared to CAD and IRMPD, and generally generated more extensive fragmentation than the latter two techniques.⁴⁴ O'Hair and co-workers have proposed that EID occurs via electronic and vibrational excitation, based on similarities between the types of product ions observed from EID, ultraviolet photodissociation, and EI.⁴³ Thus, EID may be an alternative technique to high-energy CAD for revealing information on double bond locations in fatty acids. To our knowledge, EID has not previously been applied towards fatty acid analysis. We used several metals (Li, Zn, Co, Ag, Ni, Mg, Ca, Fe, and Mn) to fix a positive charge at the end of fatty acids and generated charge-remote fragmentation via EID. The charge-remote product ion abundances at each carbon location were compared to deduce double bond positions. EID of Mn(II)-adducted fatty acids was compared with IRMPD of the same species.

4.2. Experimental Section

4.2.1. Sample Preparation

Fatty acids used in this work include stearic acid, oleic acid, linolenic acid, and arachidonic acid. Fatty acids and metal salts, including MnCl₂, CoBr₂, and NiBr₂, were purchased from Sigma-Aldrich (St. Louis, MO). 70–200 μM fatty acid was mixed with

200-600 μ M metal salt in methanol/water. Sample solutions of metal (Met)-adducted fatty acids were freshly made 10-30 min prior to MS analysis.

4.2.2. Fourier Transform Ion Cyclotron Resonance Mass Spectrometry

Singly charged metal-adducted fatty acids, $(M + \text{Met} - \text{H})^+$, were generated by external electrospray ionization (ESI) at 70 μ L/h (Apollo II dual stage ion funnel ion source, Bruker Daltonics, Billerica, MA). All experiments were performed with a 7 Tesla quadrupole (Q)-FT-ICR mass spectrometer (APEX-Q, Bruker Daltonics) as previously described.⁵¹ All data were obtained in positive ion mode. Briefly, ions produced by ESI were mass-selectively externally accumulated³⁷⁻³⁸ in a hexapole for 0.1-2 s, transferred via high voltage ion optics, and captured in the ICR cell by dynamic trapping. This accumulation sequence was looped three times to improve precursor ion abundance. In MS/MS experiments, mass selective external accumulation of $[M + \text{Met} - \text{H}]^+$ was employed. In some cases, mass selective external accumulation was followed by further isolation via correlated harmonic excitation fields (CHEF)⁵² inside the ICR cell to eliminate unwanted peaks caused by impurities and byproducts from adduct forming reactions. An indirectly heated hollow dispenser cathode was used for electron generation.⁵³ A heating current of 1.8 A was applied to a heater element located behind the cathode. For EID, performed inside the ICR cell, the cathode bias voltage was pulsed to 25-50 eV for 50-500 ms. IRMPD was performed inside the ICR cell with a 25 W, 10.6 μ m, CO₂ laser (Synrad, Mukilteo, WA). The laser beam was deflected by two mirrors for alignment through the hollow dispenser cathode to the center of the ICR cell. The beam entered the vacuum system through a BaF₂ window. Photon irradiation was performed for 300-600 ms at 8.75-10 W laser power. All mass spectra were acquired with XMASS

software (version 6.1, Bruker Daltonics) in broadband mode from m/z 21 to 1000 with 256K data points and summed over 10-30 scans. Data processing was performed with the MIDAS analysis software.⁵⁴ Calculated masses of precursor ions, $[M + \text{Met} - \text{H}]^+$, and one of the most abundant product ions were used for internal calibration.

4.3. Results and Discussion

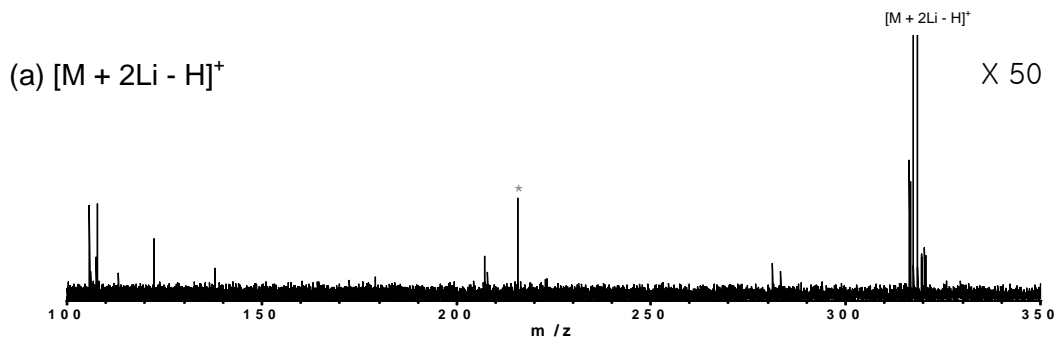
4.3.1. EID of Metal-adducted Arachidonic Acid

In order to elucidate whether metal-adducted fatty acids can undergo charge-remote fragmentation in EID, complexes between arachidonic acid and Li, Zn, Co, Ag, Ni, Mg, Ca, Fe, and Mn were investigated. Lithium was our first metal of choice because doubly Li-adducted fatty acids, $[M + 2\text{Li} - \text{H}]^+$, have been shown to yield charge-remote fragmentation in high energy CAD.^{9-10, 33-34} However, electron irradiation (26 eV electrons) of the $[M + 2\text{Li} - \text{H}]^+$ form of arachidonic acid did not yield any product ions, as shown in Figure 4.1 (a). Fragmentation was also absent following electron irradiation of the $[M + \text{Li}]^+$ and $[M + \text{H}]^+$ forms of arachidonic acid (data not shown). EID (20 eV electrons) of Zn(II)-adducted arachidonic acid yielded mostly alkylcarbocations without the metal adduct and charge-remote fragmentation was rare (Figure 4.1 (b); Zn-adducted charge-remote fragments are indicated in black). This result implies that the interaction between Zn cations and arachidonic acid is rather weak because Zn cations were readily released from arachidonic acid during the EID process.

EID of Co(II)-adducted arachidonic acid provided limited fragmentation, mainly yielding low m/z fragments. These fragments are mainly Co(II)-adducted alkylcarbocations (Figure 4.1 (c)) but several cobalt-adducted charge remote fragments were also observed. In EID of Ag(I)-adducted arachidonic acid, charge-remote

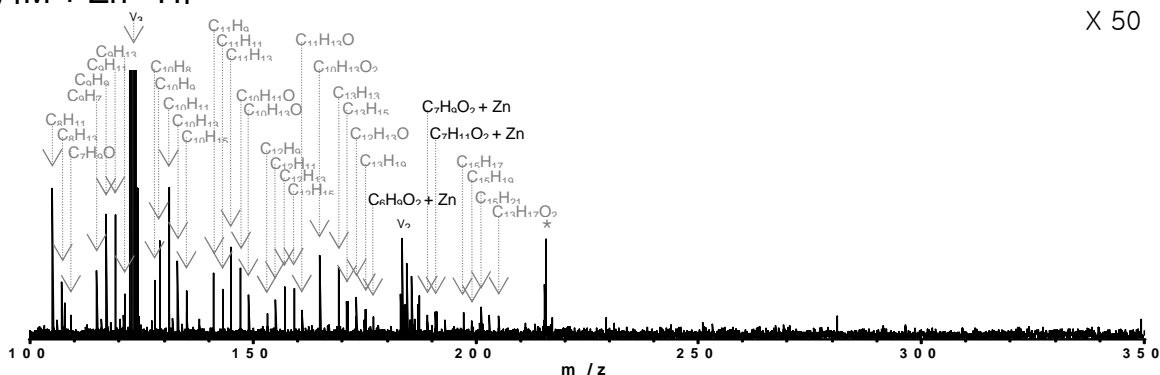
fragmentation occurred mainly at alkyl chain bonds between the C₆ and C₁₃ positions, whereas charge-driven fragmentation was preferred at lower carbon positions (<C₆). However, peak identification for Ag(I)-adducted arachidonic acid was complicated by the broad silver isotope patterns. Thus, Ag(I) adduction does not appear practical for generation of charge-remote fatty acid fragmentation and, thus, the corresponding data are not shown. Similar to the EID results reported here, limited charge-remote fragmentation was observed in high energy CAD of Co(II) and Ag(I)-adducted fatty acids.⁹ The low abundance of charge-remote product ions is due to the competitive release of metal cations.⁹ Thus, the interactions between Co(II)/Ag(I) and arachidonic acid do not appear strong enough to fix a charge on the fatty acid carboxylate end.

Figure 4.1 (d) shows that Ni(II) was retained to a large extent in EID of nickel-adducted arachidonic acid. Thus, such adducts appear more stable than the metals discussed above. Extensive fragmentation, caused by both charge-remote and charge-driven processes were observed in EID of Ni(II)-adducted arachidonic acid. Similar results were obtained from EID of Mg, Ca, Fe, and Mn-adducted arachidonic acid. Thus, all the latter, more stable, metal adducts were further investigated for generation of fatty acid double bond location information.



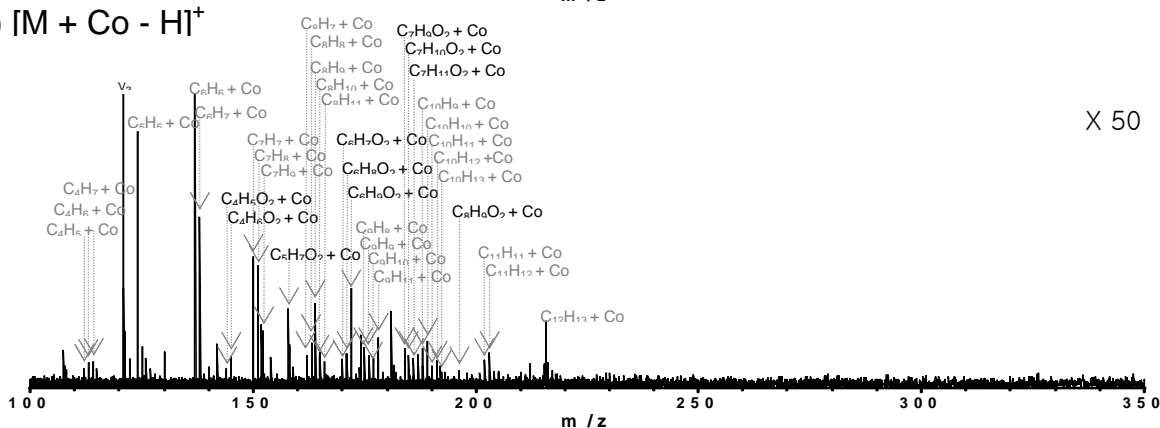
(b) $[M + Zn - H]^+$

X 50



(c) $[M + Co - H]^+$

X 50



(d) $[M + Ni - H]^+$

X 200

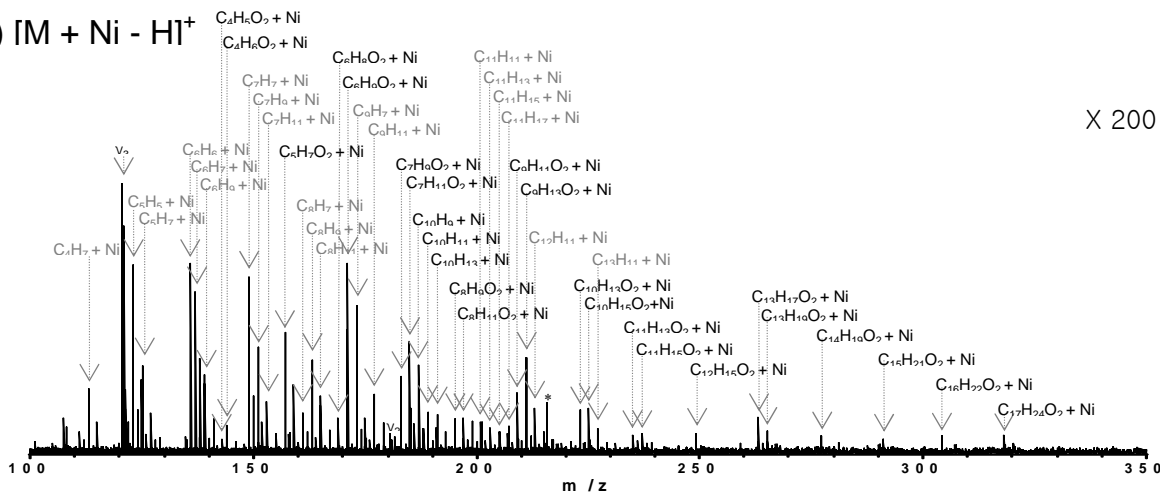


Figure 4.1. EID of metal-adducted arachidonic acid: (a) Li adducts, (b) Zn(II) adduct, (c) Co(II) adduct, and (d) Ni(II) adduct. Asterisks indicate electronic noise peaks. v_2 and v_3 denote the second and third harmonic peaks. Charge-remote product ion peaks, $[C_xH_yO_2 + Met]^+$, are labeled in black whereas other labels are in gray. Precursor ion peaks, $[M + Zn - H]^+$ (m/z 367), $[M + Co - H]^+$ (m/z 362), and $[M + Ni - H]^+$ (m/z 361), are outside the displayed m/z region.

Several product ion types were observed in EID spectra of such metal-adducted fatty acids: $[C_xH_yO_2 + Met]^+$ and $[C_xH_y + Met]^+$ ion series are representative of charge-remote and charge-driven fragmentation processes, respectively. Product ion series of the types $[C_xH_yO + Met]^+$, $[C_xH_yO_2]^+$, and $[C_xH_yO]^+$ may be produced by a charge-remote fragmentation process combined with water or metal loss, or a combination of both types of losses. However, such product ion types were not used for determination of double bond locations because they were rarely observed compared to $[C_xH_yO_2 + Met]^+$. Thus, the latter product ion type was used as representing characteristic charge-remote fragmentation.

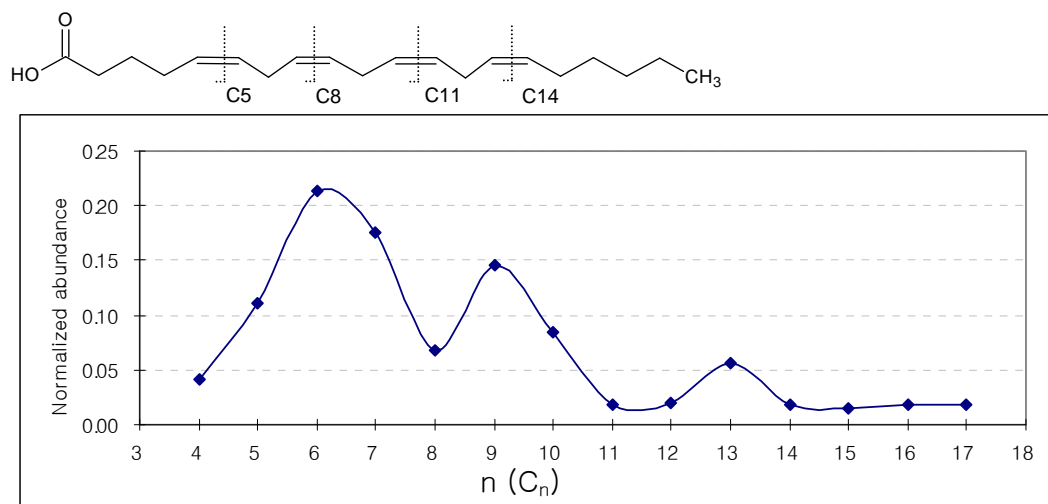
4.3.2. Charge-Remote Fragmentation in EID of Ni(II), Mg(II), Ca(II), Fe(II), and Mn(II)-adducted Arachidonic Acid

Heterolytic (resulting in product ions of, e.g., the types $[C_nH_{2n-1}O_2 + Met]$, $[C_nH_{2n-3}O_2 + Met]$, and $[C_nH_{2n-5}O_2 + Met]$) as well as homolytic bond cleavages (producing, e.g., $[C_nH_{2n-2}O_2 + Met]^-$, $[C_nH_{2n-4}O_2 + Met]^-$, and $[C_nH_{2n-6}O_2 + Met]^-$ -type product ions) were observed in EID of Ni, Mg, Ca, Fe, and Mn-adducted fatty acids. Similar behavior was noted in high energy CAD of ESI-generated precursor ions while mostly heterolytic bond cleavages were observed in FAB-high energy CAD.⁵⁵

Figure 4.2 shows charge-remote product ion abundances as function of alkyl chain carbon position from EID spectra of Ni(II) and Mg(II)-adducted arachidonic acid. As mentioned above, $[C_xH_yO_2 + Met]^+$ -type product ions were used to generate this plot. Charge-remote product ion abundances at each carbon-carbon cleavage site were calculated by adding all of the $[C_xH_yO_2 + Met]^+$ -type ion abundances at each carbon position, and normalizing to the total $[C_xH_yO_2 + Met]^+$ -type ion abundances in the EID

spectrum. EID of Ca(II) and Fe(II)-adducted arachidonic acid provided very similar results, thus the corresponding data are not shown. In high energy CAD, reduced charge

(a) $[M + Ni - H]^+$



(b) $[M + Mg - H]^+$

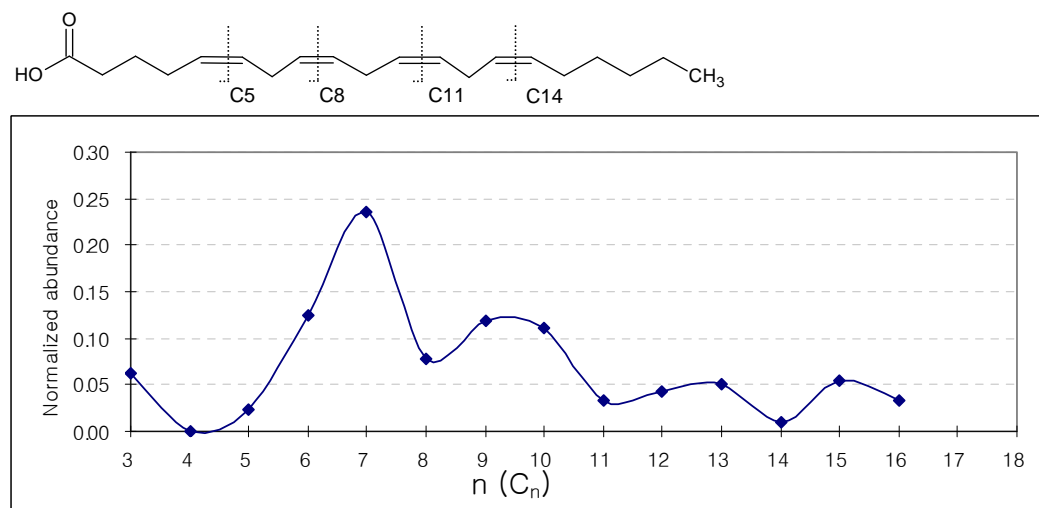


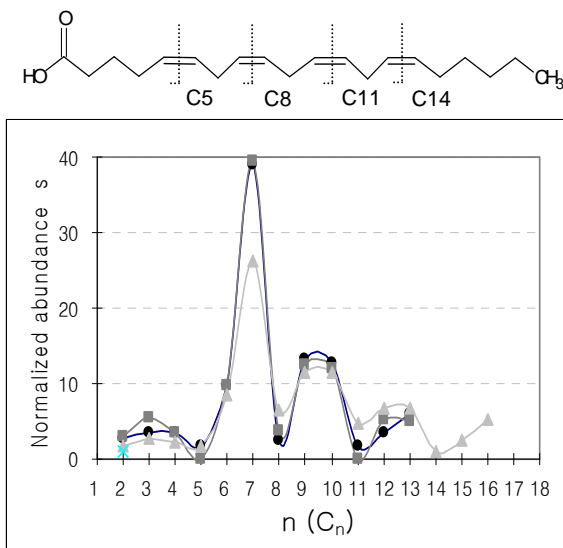
Figure 4.2. Normalized product ion abundances of $[C_xH_yO_2 + Met]^+$ vs. C_n (n denotes carbon position from the carboxylate end of a fatty acid) in EID of Ni(II) and Mg(II)-adducted arachidonic acid. The structure of arachidonic acid is shown with double bond locations.

-remote fragmentation near/at double bonds provide information on fatty acid double bond locations for Li-adducted species.³³ For arachidonic acid, reduced charge-remote cleavages at the C₅, C₈, C₁₁, and C₁₄ positions are expected due to carbon-carbon double bonds existing between C₅-C₆, C₈-C₉, C₁₁-C₁₂, and C₁₄-C₁₅, respectively. However, EID of Ni, Mg, Ca, and Fe-adducted arachidonic acid did not provide characteristic ion abundance patterns at all double bond positions. The double bond (C₁₄-C₁₅) far from the carboxylate end could not be identified from EID of Ni(II)-adducted arachidonic acid (Figure 4.2 (a)). Further, the double bond (C₅-C₆) close to the carboxylate end could not be determined from EID of Ni(II) nor Mg(II)-adducted arachidonic acid (Figures 4.2 (a) and (b)). On the other hand, EID of Mn(II)-adducted arachidonic acid provided characteristic product ion abundances at all double bond locations, as shown in Figure 4.3. Thus, EID of Mn(II)-adducted fatty acids was further explored as discussed below.

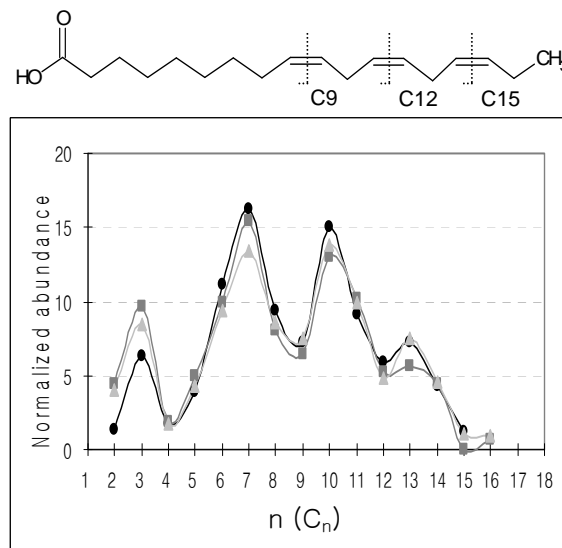
Among the metals that promoted extensive charge-remote fragmentation in EID, Mn(II) is expected to bind tightly with the carboxylate anion end of fatty acids because both Mn(II) and the carboxylate anion have hard Lewis acid and base properties, respectively. By contrast, Ni(II) and Fe(II) may bind less tightly due to their weaker Lewis acidities. In addition, the carbon-carbon double bond, which is a weak Lewis base, may be involved in adduct formation with weaker Lewis acids such as Ni(II) and Fe(II), and therefore prevent formation of a fixed charge at the carboxylate end of fatty acids. Binding energies of divalent metal ions and H₂O/OH⁻ increase sharply at the transition between d⁰ (Ca(II)) - dⁿ (Sc(II)) due to electron occupation in d orbitals.⁵⁶ These chemical properties may explain why Mn(II) appears to be more efficient than the other metals examined for “fixing” a charge at the carboxylate end of fatty acids.

EID of Ni(II), Mg(II), Ca(II), and Fe(II)-adducted arachidonic acid showed reduced product ion abundances at the C₄ position instead of the expected C₅ position (see Figure 4.2 for the two former metals). Gas-phase ion fragmentation reactions are charge-remote when there is no important interaction between the charge and the cleavage sites. However, hydrocarbon chains are flexible and such interactions can therefore occur even in the presence of a terminal fixed charge, particularly at less remote sites.¹⁵ Gross and co-workers have reported that some product ions formed by cleavage near the charge are stabilized by a cyclic conformation.¹⁵ For example, C₄-C₅ bond cleavage in deprotonated palmitic acid was enhanced due to formation of a cyclic structure.³⁴ Similarly, enhanced cleavage at the C₃ position occurred in EID of Mg(II)-adducted arachidonic acid (Figure 4.2 (b)), possibly due to ring formation. Because cleavage at C₅ did not show reduced abundance in EID of Ni(II), Ca(II), Mg(II), and Fe(II)-adducted arachidonic acid, double bond location information close to the carboxylate terminus could not be obtained for these metal-adducted species. However, different behavior was observed in EID of Mn(II)-adducted fatty acids. Here, the lowest abundance product ions were from cleavage at C₄ when there was no double bond at C₅-C₆, such as in linolenic acid, oleic acid, and stearic acid (Figure 4.3). However, for arachidonic acid, which has a double bond at C₅-C₆, cleavage at C₅ showed even lower abundance than at C₄ (Figure 4.3). Thus, all double bond locations could be obtained from EID of Mn(II)-adducted fatty acids.

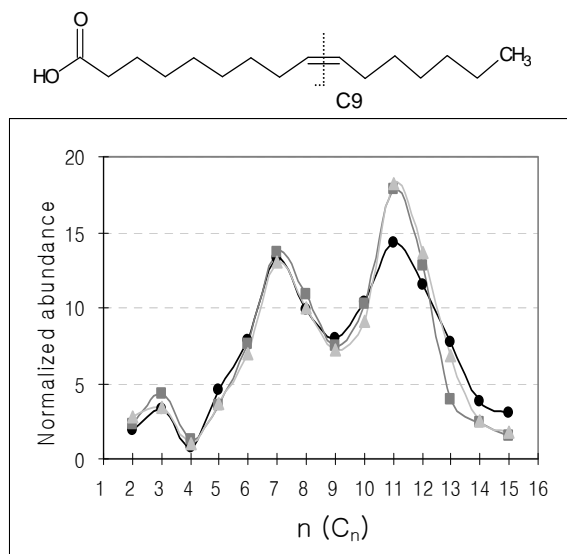
(a) Arachidonic acid



(b) Linolenic acid



(c) Oleic acid



(d) Stearic acid

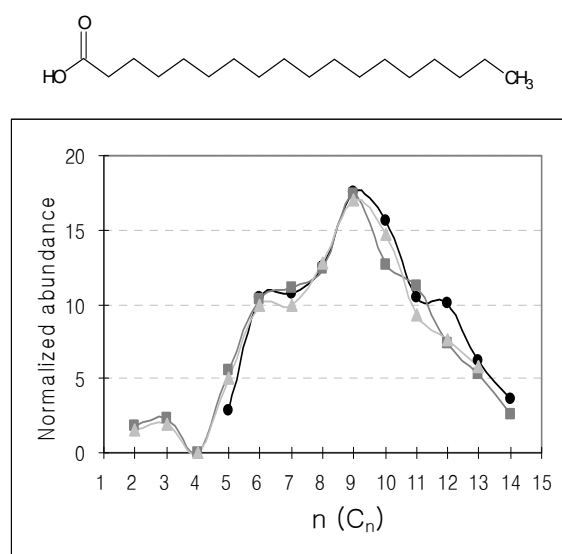


Figure 4.3. Normalized product ion abundances of $[C_xH_yO_2 + Met]^+$ vs. C_n (n denotes carbon position from the carboxylate end of a fatty acid) in EID of Mn(II)-adducted fatty acids: (a) arachidonic acid ($d = 4$), (b) linolenic acid ($d = 3$), (c) oleic acid ($d = 1$), and (d) stearic acid ($d = 0$), where d indicates the number of double bonds in each fatty acid. Three observations were made for each Mn(II)-adducted fatty acid.

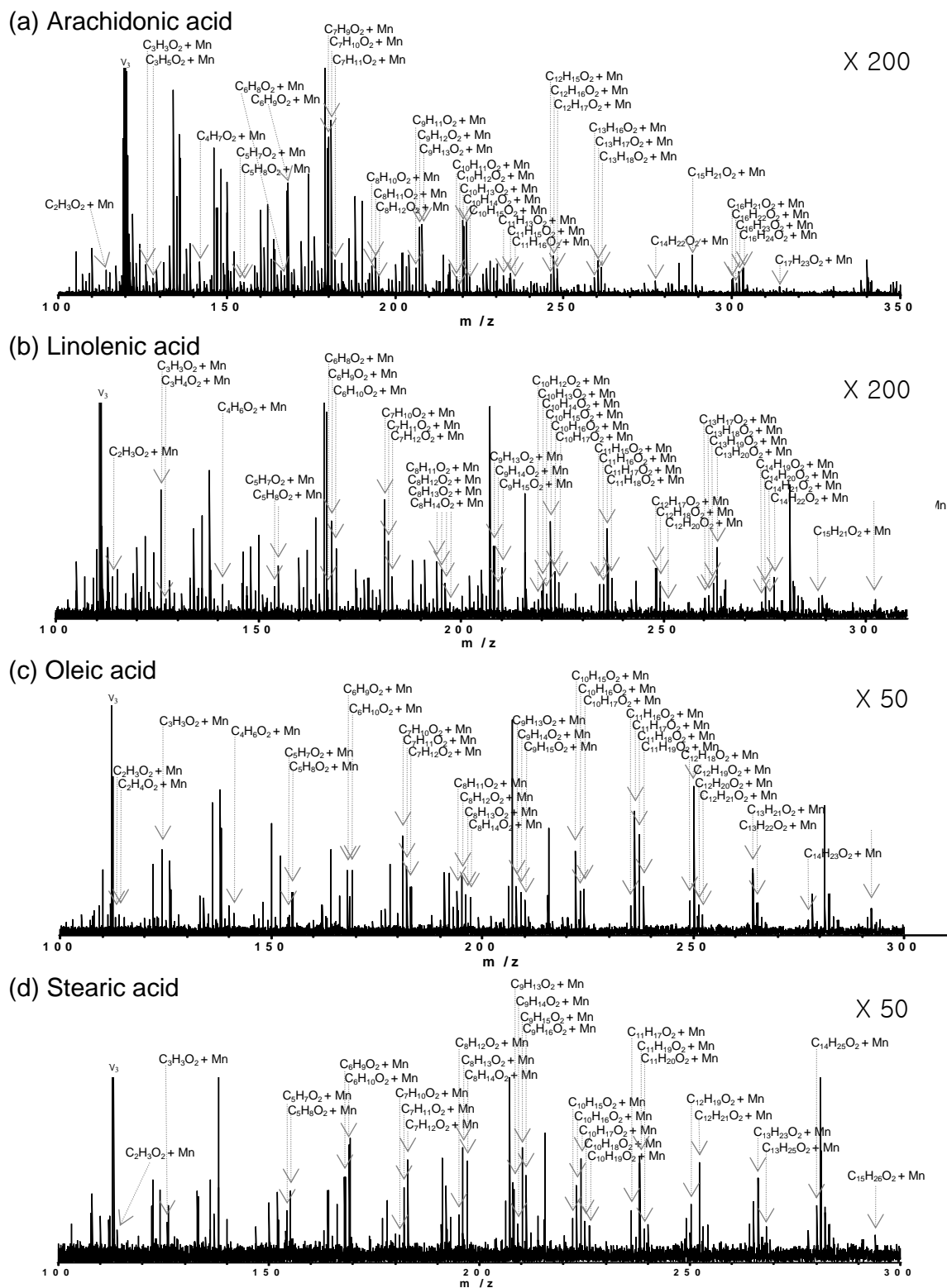


Figure 4.4. EID of Mn(II)-adducted fatty acids: (a) arachidonic acid ($d = 4$), (b) linolenic acid ($d = 3$), (c) oleic acid ($d = 1$), and (d) stearic acid ($d = 0$), where d indicates the number of double bonds in each fatty acid. Only charge-remote product ion peaks, $[C_xH_yO_2 + Mn]^+$, are labeled. The precursor ion peaks, $[M + Mn - H]^+$, are outside the displayed m/z range.

4.3.3. Charge-Remote Fragmentation in EID of Mn(II)-Adducted Fatty Acids

Figure 4.4 shows EID spectra of Mn(II)-adducted arachidonic acid, linolenic acid, oleic acid, and stearic acid, where each fatty acid has 4, 3, 1, and 0 double bonds, respectively. In this Figure, only characteristic charge-remote fragments, $[C_xH_yO_2 + Mn]^+$, are labeled whereas unlabeled peaks are mostly due to charge-driven fragmentation, including $[C_xH_y + Mn]^+$. Figure 4.3 shows normalized charge-remote product ion abundances at each carbon position of the same four fatty acids.

In EID of Mn(II)-adducted fatty acids, even or odd electron species, generated by heterolytic and homolytic bond cleavages respectively, were observed. Double bond locations can be identified from normalized product ion abundances at each carbon site, as shown in Figure 4.3. EID experiments for each fatty acid were repeated three times on three different days to verify the reliability of EID as a method for double bond localization in fatty acids. As shown in Figure 4.3, EID spectra of Mn(II)-adducted fatty acids provided highly reproducible structural information regarding double bond positions for each fatty acid. Lower product ion abundances at the C_4 position, observed in EID of Mn(II)-adducted linolenic acid, oleic acid, and stearic acid indicated that those fatty acids do not have double bonds between C_5 and C_6 . In contrast, the lower product ion abundance at C_5 compared to C_4 was indicative of the existence of a double bond between C_5 and C_6 in arachidonic acid. Other double bond locations in each fatty acid could be obtained from valley positions in the graph of normalized charge-remote product ion abundances vs. carbon position (C_n), as shown in Figure 4.3.

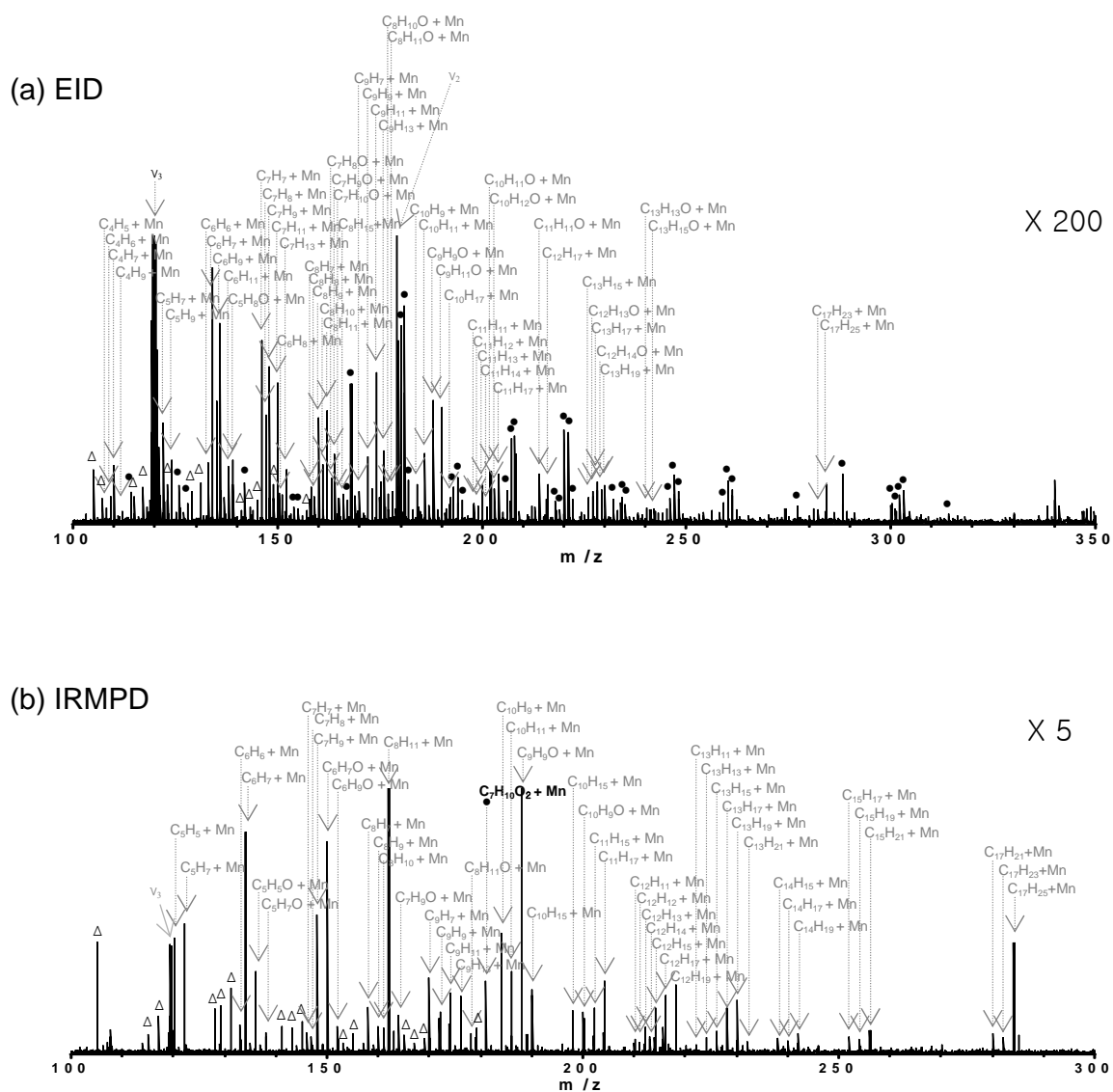


Figure 4.5. EID (a) and IRMPD (b) of Mn(II)O adducted arachidonic acid. v_2 and v_3 denote the second and third harmonic peaks. $[C_xH_yO_2 + Mn]^+$ product ion peaks are labeled with “•”, and $[C_xH_y]^+$ -type peaks are labeled with “ Δ ”. Figure 4.5a shows the same spectrum as in Figure 4.3a but here all peaks are labeled for comparison with the IRMPD spectrum.

4.3.4. EID vs. IRMPD of Mn-adducted Fatty Acids

Figure 4.5 shows EID and IRMPD spectra of Mn(II)-adducted arachidonic acid. The mixture of mostly $[C_xH_y + Mn]^+$ and $[C_xH_yO_2 + Mn]^+$ species observed in EID implies competition between charge-remote and charge-driven processes. However, IRMPD of the same precursor ions mainly yielded product ions from charge-driven fragmentation, $[C_xH_y + Mn]^+$, as expected from vibrational activation. Only one potential charge-remote product ion (based on mass), $[C_7H_{10}O_2 + Mn]^+$, was observed. The internal energy required for charge-remote fragmentation is estimated to be $\sim 1.4\text{-}2.9$ eV for protonated fatty acids.⁵⁷ In 70 eV EI, molecular ions of small alkenes were found to be completely isomerized to a mixture of interconverting structures.¹⁹ We propose that the 25-50 eV electron energies used in EID are sufficient to promote charge-remote fragmentation, but not high enough to cause isomerization of Mn(II)-adducted fatty acids, which would result in double bond migration.

4.4. Conclusions

Metal-adducted fatty acids were analyzed to investigate the utility of EID for determining double bond locations. Various metals (Li, Zn, Co, Ag, Ni, Mg, Ca, Fe, and Mn) were used for fixing one charge at the carboxylate end of fatty acids to promote charge-remote fragmentation. Protonated, $[M + H]^+$, and Li-adducted, $[M + 2Li - H]^+$ and $[M + Li]^+$, fatty acids did not yield any product ions from electron irradiation. Alkylcarbocations without metal ions were mainly observed in EID of Zn(II)-adducted fatty acids whereas limited charge-remote fragmentation was observed in EID of Co(II) and Ag(I)-adducted fatty acids. In contrast, extensive charge-remote fragmentation was

observed in EID of other metal-adducted fatty acids. Charge-remote product ion abundances of $[C_xH_yO_2 + Met]^+$ -type fragments are significantly reduced at double bond positions. Analysis of $[C_xH_yO_2 + Mn]^+$ -type product ion abundances from EID of Mn(II)-adducted fatty acids allowed determination of all double bond positions. However, other metal adducts did not generally provide characteristic product ion abundances at all double bond locations. The resulting structural information on double bond locations for Mn(II)-adducted fatty acids may be explained by dominant electronic excitation processes in EID, and efficient generation of a fixed charge at the carboxylate end due to strong interaction between Mn(II) cation and carboxylate anion. EID of Mn(II)-adducted fatty acids was compared with IRMPD of the same species. In the latter type of fragmentation, mostly charge-driven fragmentation, including alkylcarbocation formation, was observed and double bond information could not be deduced, as expected from vibrational activation.

4.5. References

1. Yao, D.; Shi, W.; Gou, Y.; Zhou, X.; Yee Aw, T.; Zhou, Y.; Liu, Z. *Free Radic Biol Med* 2005, 39. 1385-1398.
2. North, J. A.; Spector, A. A.; Buettner, G. R. *Am J Physiol* 1994, 267. C177-188.
3. Pandey, M.; Sharma, L. B.; Singh, S.; Shukla, V. K. *World J Surg Oncol* 2003, 1. 5.
4. Black, H. S. *Integr Cancer Ther* 2004, 3. 279-293.
5. de Kok, T. M.; ten Vaarwerk, F.; Zwingman, I.; van Maanen, J. M.; Kleinjans, J. C. *Carcinogenesis* 1994, 15. 1399-1404.
6. Farooqui, A. A.; Horrocks, L. A. *Cell Mol Neurobiol* 1998, 18. 599-608.
7. Montine, T. J.; Morrow, J. D. *Am J Pathol* 2005, 166. 1283-1289.
8. Adams, J.; Gross, M. L. *Analytical chemistry* 1987, 59. 1576-1582.
9. Trimpin, S.; Clemmer, D. E.; McEwen, C. N. *Journal of the American Society for Mass Spectrometry* 2007, 18. 1967-1972.
10. Van Pelt, C. K.; Brenna, J. T. *Analytical chemistry* 1999, 71. 1981-1989.
11. Buser, H. R.; Arn, H.; Cuerin, P.; Rauscher, S. *Analytical chemistry* 1983, 55. 818-822.
12. Schneider, B.; Budzikiewicz, H. *Rapid Commun Mass Spectrom* 1990, 4. 550-551.

13. Malosse, C.; Kerhoas, L.; Einhorn, J. J of Chromatogr 1998, 803. 203-209.
14. Cheng, C.; Gross, M. L. Mass spectrometry reviews 2000, 19. 398-420.
15. Adams, J.; Gross, M. L. Org. Mass Spectrom. 1988, 23. 307-316.
16. Adams, J. Mass spectrometry reviews 1990, 9. 141-186.
17. Fallick, A. E. Intemationul Journal of Mlass Spectrometry and Ion Physics 1983, 46. 59-62.
18. Borchers, F.; Levsen, K.; Schwartz, H.; Wesdemiotis, C.; Winkler, H. C. Journal of the American Chemical Society 1977, 99. 6359-6365.
19. Rontani, J. F. Rapid Commun Mass Spectrom 1998, 12. 961-967.
20. Dunkelblum, E.; Tan, S. H.; Silk, P. J. J Chem Ecol 1985, 11. 265-277.
21. Doolittle, R. E.; Tumilinson, J. H.; Proveaux, A. Analytical chemistry 1985, 57. 1625-1630.
22. Fay, L.; Richli, U. J of Chromatogr 1991, 541. 89-98.
23. Lankelma, J.; Ayanoglu, E.; Djerassi, C. Lipids 1983, 18. 853-858.
24. Grabovskiy, S. A.; Kabal'nova, N. N.; Chatgialiloglu, C.; Ferreri, C. Helvetica Chimica Acta 2006, 89. 2243-2253.
25. Moe, M. K.; Anderssen, T.; Strom, M. B.; Jensen, E. Rapid Commun Mass Spectrom 2004, 18. 2121-2130.
26. Moe, M. K.; Anderssen, T.; Strom, M. B.; Jensen, E. Journal of the American Chemical Society 2004, 16. 46-59.
27. Moe, M. K.; Jensen, E. Eur J Mass Spectrom (Chichester, Eng) 2004, 10. 47-55.
28. Moe, M. K.; Anderssen, T.; Strom, M. B.; Jensen, E. Journal of the American Society for Mass Spectrometry 2005, 16. 46-59.
29. Harrison, K. A.; Murphy, R. C. Analytical chemistry 1996, 68. 3224-3230.
30. Thomas, M. C.; Mitchell, T. W.; Blanksby, S. J. Journal of the American Chemical Society 2006, 128. 58-59.
31. Afonso, C.; Riu, A.; Xu, Y.; Fournier, F.; Tabet, J. C. J Mass Spectrom 2005, 40. 342-349.
32. Hayes, R. N.; Gross, M. L. Methods Enzymol 1990, 193. 237-263.
33. Jensen, N. J.; Tomer, K. B.; Gross, M. L. Journal of the American Chemical Society 1985, 107. 1863-1868.
34. Aharoni, A.; Ric de Vos, C. H.; Verhoeven, H. A.; Maliepaard, C. A.; Kruppa, G.; Bino, R.; Goodenowe, D. B. Omics 2002, 6. 217-234.
35. Brown, S. C.; Kruppa, G.; Dasseux, J. L. Mass spectrometry reviews 2005, 24. 223-231.
36. Belov, M. E.; Nikolaev, E. N.; Anderson, G. A.; Udseth, H. R.; Conrads, T. P.; Veenstra, T. D.; Masselon, C. D.; Gorshkov, M. V.; Smith, R. D. Analytical chemistry 2001, 73. 253-261.
37. Hendrickson, C. L.; Quinn, J. P.; Emmett, M. R.; Marshall, A. G., in 49th ASMS Conference on Mass Spectrometry and Allied Topics. Chicago, IL, 2001; CD-ROM.
38. Little, D. P.; Speir, J. P.; Senko, M. W.; O'Connor, P. B.; McLafferty, F. W. Analytical chemistry 1994, 66. 2809-2815.
39. Woodin, R. L.; Bomse, D. S.; Beauchamp, J. L. Journal of the American Chemical Society 1978, 100. 3248-3250.

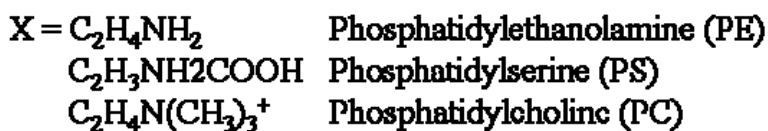
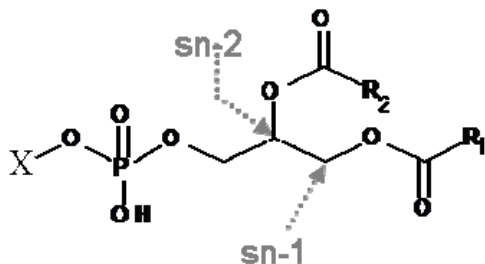
40. Budnik, B. A.; Haselmann, K. F.; Elkin, Y. N.; Gorbach, V. I.; Zubarev, R. A. *Analytical chemistry* 2003, 75. 5994-6001.
41. Cody, R. B.; Freiser, B. S. *Analytical chemistry* 1979, 51. 541-551.
42. Lioe, H.; O'Hair, R. A. *Analytical and bioanalytical chemistry* 2007, 389. 1429-1437.
43. Yoo, H. J.; Liu, H.; Hakansson, K. *Analytical chemistry* 2007, 20. 7858-7866.
44. Zubarev, R. A.; Horn, D. M.; Fridriksson, E. K.; Kelleher, N. L.; Kruger, N. A.; Lewis, M. A.; Carpenter, B. K.; McLafferty, F. W. *Analytical chemistry* 2000, 72. 563-573.
45. Zubarev, R. A.; Kelleher, N. L.; McLafferty, F. W. *Journal of the American Chemical Society* 1998, 120. 3265-3266.
46. Zubarev, R. A. *Current opinion in biotechnology* 2004, 15. 12-16.
47. Cooper, H. J.; Hakansson, K.; Marshall, A. G. *Mass spectrometry reviews* 2005, 24. 201-222.
48. Budnik, B. A.; Haselmann, K. F.; Zubarev, R. A. *Chem Phys Lett* 2001. 299-302.
49. Adamson, J. T.; Hakansson, K. *Journal of the American Society for Mass Spectrometry* 2007, 18. 2162-2172.
50. Yang, J.; Mo, J.; Adamson, J. T.; Hakansson, K. *Analytical chemistry* 2005, 77. 1876-1882.
51. de Koning, L. J.; Nibbering, N. M. M.; van Orden, S. L.; Laukien, F. H. *Int. J. Mass Spectrom.* 1997, 165. 209-219.
52. Tsybin, Y. O.; Witt, M.; Baykut, G.; Kjeldsen, F.; Hakansson, P. *Rapid Commun Mass Spectrom* 2003, 17. 1759-1768.
53. Senko, M. W.; Canterbury, J. D.; Guan, S.; Marshall, A. G. *Rapid Commun Mass Spectrom* 1996, 10. 1839-1844.
54. Cheng, C.; Pittenauer, E.; Gross, M. L. *Journal of the American Society for Mass Spectrometry* 1998, 9. 840-844.
55. Magnusson, E.; Moriarty, N. W. *Inorg Chem* 1996, 35. 5711-5719.
56. Deterding, L.; Gross, M. L. *Org. Mass. Spectrom.* 1988, 23. 169-177.

Chapter 5

Determination of Phospholipid Regiochemistry by Ag(I) Adduction and Tandem Mass Spectrometry

5.1. Introduction

Phospholipids, present in all organisms, are the building blocks for cellular membranes, and are involved in a diverse number of other functions, from compartmentalization of cytoplasm to cell signaling.¹⁻⁷ Differentiation between the sn-1 and sn-2 positions of phospholipids (their structure is shown in Scheme 5.1) is important from both a biochemical and nutritional viewpoint because cell signaling through phospholipids and absorption of polyunsaturated fatty acids into the body are related to the position of the acyl chains on the glycerol backbone.⁸⁻¹¹



Scheme 5.1. Structure of phospholipids.

Classical methods for phospholipid analysis heavily rely on thin-layer chromatography (TLC) to separate and identify the various phospholipid classes with relatively nonspecific detection techniques, such as visualization of phosphorous by spray reagents (e.g., primuline, which fluoresces under a UV lamp).¹² Analysis of the fatty acyl substituents typically involves scraping of the TLC spots, followed by extraction and hydrolysis of the fatty-acyl group, and derivatization for gas chromatography (GC) or GC/mass spectrometry (MS) to identify specific fatty acids in each phospholipid class. Fast atom bombardment (FAB)-MS and electrospray ionization (ESI)-MS can directly analyze phospholipids as intact molecules and preserve the information inherent in their chemical structures.^{3, 13-16} It has been shown that determination of the acyl chains at sn-1 versus sn-2 can be made from the ratio of R_1COO/R_2COO in negative ion mode

collision induced dissociation (CID) tandem mass spectrometry but the observed ion ratio is dependent on the extent of saturation of the fatty acyl group at sn-2, the total chain length, the collision energy, and the nature of the polar headgroup.^{14, 16-18} ESI-MS is superior to FAB-MS because the former technique does not suffer from some of the problems associated with the latter, including complication of spectra due to matrix ions and decomposition of molecular ions during the ionization event.^{3, 19} Alkali metals, alkaline earth metals, and divalent metal ions have been used to form metal-phospholipid complexes for structural determination of phospholipids.²⁰⁻²¹ Positive ion mode CID of alkali metal-adducted phosphatidylserine resulted in greater abundance product ions from cleavage at the sn-2 position compared to the sn-1 position.²⁰ Alkaline earth metals and divalent metal ions were also used to form adducts with phospholipids for structural characterization.²¹ However, it was reported that CID product ion abundances from cleavage at the sn-1 and sn-2 esterification sites may change depending on the types of metals and phospholipids.²¹

Fourier transform ion cyclotron resonance (FT-ICR) mass spectrometry²² can provide improved molecular identification due to its accurate mass capabilities²³ and additional MS/MS fragmentation techniques, including infrared multiphoton dissociation (IRMPD),²⁴⁻²⁵ electron induced dissociation (EID),²⁶⁻²⁹ and electron capture dissociation

(ECD)³⁰⁻³³. These techniques can often provide complementary structural information compared to CID for the characterization of various kinds of biomolecules.^{26, 30-32, 34-37} However, there has been very limited application of alternative MS/MS fragmentation techniques available in FT-ICR mass spectrometry to phospholipids.³⁸ James et al. applied ECD to complexes of the form $[\text{Metal}^{\text{II}}(\text{L})_n]^{2+}$ where L corresponds to diacylglycerophosphocholine. In these experiments, the ratio of sn-1/sn-2 acyl chain loss was dependent on the number (n) of lipids complexed with metal ions.³⁸ IRMPD has been shown to be an efficient fragmentation technique for nucleic acids, phosphopeptides, and phosphate-containing metabolites due to strong phosphate absorption at the 10.6 μm wavelength typically used.^{24, 26, 39-42} Thus, IRMPD may also have advantages over CID for structural characterization of phospholipids.

Silver-high performance liquid chromatography (Ag-HPLC) has been utilized to separate various fatty acid methyl esters, triacylglycerols, and lipids based on number, geometry, and position of double bonds.^{9, 43-45} In addition to Ag-HPLC, various kinds of silver ion chromatography have been widely applied to all lipid classes. For many years, Ag-TLC has been one of the key separation techniques used in lipid analysis.⁴³⁻⁴⁴ Furthermore, atmospheric pressure column chromatography, HPLC, and supercritical fluid chromatography (SFC) have also been used in silver ion mode for lipid analysis.⁴³⁻⁴⁴

In most cases, silver ion chromatography involves column support materials to which silver ions can bind, typically silica gel.⁴³⁻⁴⁴ The retention mechanism in silver ion chromatography is based on the interaction between Ag^+ ions and olefinic π electrons of unsaturated organic molecules.⁴³⁻⁴⁵ We hypothesized that such interactions may be utilized to reveal esterification site information in tandem mass spectrometry of Ag-adducted phospholipids.

The relative ion abundance changes with types of headgroup, the extent of unsaturation, and types of metals in tandem mass spectrometry of alkali, alkaline earth, or divalent metal-adducted phospholipids may cause confusion when characterizing the regiochemistry of phospholipids.²⁰⁻²¹ Thus, a more consistent method is desired for straightforward determination of phospholipid acyl chains. To our knowledge, the present work represents the first application of Ag-adduction to determine esterification site information for phospholipids by tandem mass spectrometry. Both IRMPD and CID were used for fragmentation of Ag-adducted phospholipids. Because Ag (I) and Cu(I) have similar Lewis acid properties, Cu(I)-adducted phospholipids were also analyzed for comparison.

5.2. Experimental Section

5.2.1. Sample Preparation

Phospholipids used in this work include phosphatidylethanolamine (C18:0/C18:2-PE and C18:0/C20:4-PE), phosphatidylserine (C16:0/C18:2-PS and C18:0/C18:1-PS) and phosphatidylcholine (C16:0/C18:1-PC, C18:1/C16:0-PC and C16:0/C18:2-PC). Phospholipids are designated as follows: $C_1:d_1/C_2:d_2$ -PL, where C_1 and C_2 are the number of carbon atoms in the fatty acyl chains of the sn-1 and sn-2 positions, respectively; d_1 and d_2 are the number of double bonds of the sn-1 and sn-2 fatty acyl chains, respectively; and PL is the abbreviation of each type of phospholipid.⁴⁶ Phospholipids were purchased from Avanti Polar lipid (Alabaster, Al). Silver acetate and copper acetate used for formation of phospholipid adducts were purchased from Sigma-Aldrich (St. Louis, MO). 130–140 μ M phospholipids were mixed with 2 mM silver acetate (or copper acetate) in water/methanol (20:80) with 1% chloroform. Ag-adducted phosphatidylserine solutions were made with methanol containing 0.1% formic acid, due to the acidity of phosphatidylserines. All sample solutions were freshly made at least 30 min prior to MS analysis.

5.2.2. Fourier Transform Ion Cyclotron Resonance Mass Spectrometry

Singly charged Ag-adducted phospholipids, $[M + Ag]^+$ (or $[M - H + Ag]^+$ for PC, which contains a fixed positive charge), were generated by external ESI at 70 $\mu\text{L/h}$ (Apollo II ion source, Bruker Daltonics, Billerica, MA). All experiments were performed with a 7 Tesla quadrupole (Q)-FT-ICR mass spectrometer (APEX-Q, Bruker Daltonics) as previously described⁴⁷. All data were obtained in positive ion mode.

Briefly, ions produced by ESI were mass-selectively externally accumulated in a hexapole for 0.2-2 s⁴⁸⁻⁴⁹ transferred via high voltage ion optics, and captured in the ICR cell by dynamic trapping. This accumulation sequence was looped three times to improve precursor ion abundance. In MS/MS experiments, mass selective external accumulation of $[M + Ag]^+$ (or $[M - H + Ag]^+$ for PC) was accomplished. CID was performed at a collision cell DC offset of 20-35 V with Ar as collision gas. IRMPD was performed inside the ICR cell with a 25 W, 10.6 μm , CO₂ laser (Synrad, Mukilteo, WA). The laser beam was deflected by two mirrors for alignment through a hollow dispenser cathode to the center of the ICR cell. The beam entered the vacuum system through a BaF₂ window. Photon irradiation was performed for 300-750 ms at 5-7.5 W laser power. All mass spectra were acquired with XMASS software (version 6.1, Bruker Daltonics) in broadband mode from m/z 21 to 1000 with 256K data points and summed over 5-10 scans, except for Cu(I)-adducted phospholipids, where 20-30 scans were

summed. Data processing was performed with MIDAS analysis software⁵⁰. Internal calibration was performed with $[M - \text{headgroup} + \text{Ag}]^+$ and $[\text{R}_2\text{COOH} - \text{H}_2\text{O} + \text{Ag}]^+$ as calibrants. All product ions were assigned within 10 ppm mass accuracy. The numerical mass value (e.g., 141 and 185) used in product ion labels denotes the mass of a fragment resulting from heterolytic cleavage, unless otherwise stated.

5.3. Results and Discussion

5.3.1. CID of Protonated Phospholipids

CID of protonated/non silver-adducted phospholipids generally resulted in head group loss, as shown in Figure 5.1. Singly protonated phosphatidylethanolamine and phosphatidylserine provided head group losses with or without the combined loss of R_2COOH where R_2 is the sn-2 acyl chain. Similar results from CID of protonated phosphatidylserine have been reported by others.²⁰ Product ions were rarely observed for phosphatidylcholine, even at higher collision energy where precursor ion abundance was depleted by more than 90 %. However, the different behavior for PC may be explained by the absence of a mobile proton due to the fixed charge on the PC headgroup. Thus, esterification site information could not be deduced from CID of protonated

phospholipids, although the phospholipid type could be deduced from the headgroup losses.

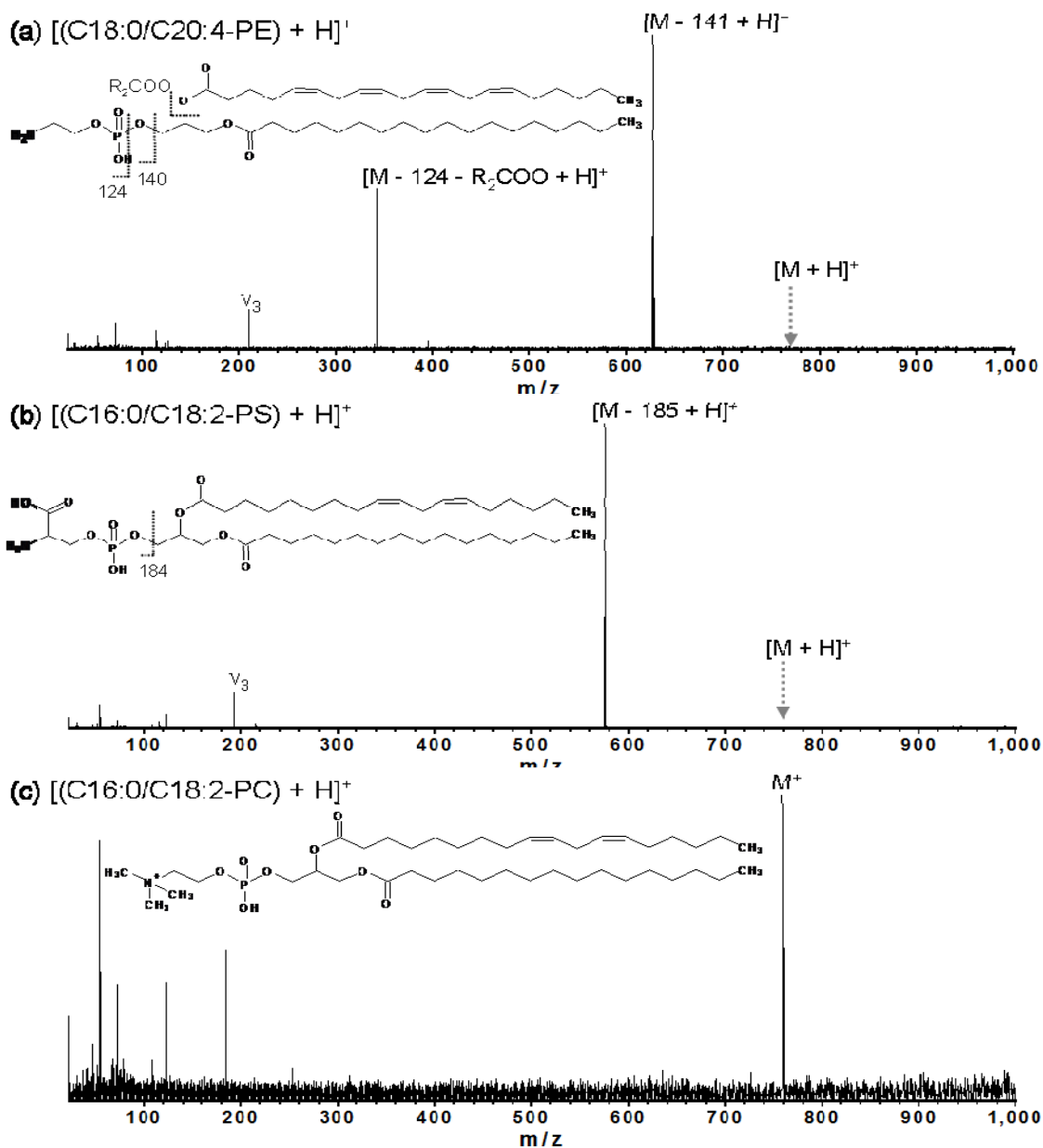


Figure 5.1. CID of protonated phospholipids: (a) CID of $[(C18:0/C20:4-PE) + H]^+$ (collision voltage: -20 V), where loss of 124 and R_2COO are homolytic cleavages, (b) CID of $[(C16:0/C18:2-PS) + H]^+$ (collision voltage: -25 V), (c) CID of $[(C16:0/C18:2-PC) + H]^+$ (collision voltage: -20 V).

5.3.2. CID and IRMPD of Ag-adducted Phospholipids

Figure 5.2 shows CID and IRMPD of Ag-adducted phosphatidylethanolamine, [(C18:0/C18:2-PE) + Ag]⁺. Headgroup loss, [M - 141 + Ag]⁺, from precursor ions was the most dominant fragmentation pathway in both CID and IRMPD. [R₂COOH + Ag]⁺ was also observed along with accompanying water loss, [R₂COOH - H₂O + Ag]⁺. In addition, [R₂COOH - CO₂ - H₂ + Ag]⁺ was observed, even though this product ion was not as abundant as [R₂COOH + Ag]⁺ and [R₂COOH - H₂O + Ag]⁺. Neutral losses from [R₂COOH + Ag]⁺ were only observed for the sn-2 acyl chain of Ag-adducted phosphatidylethanolamine, [(C18:0/C18:2-PE) + Ag]⁺. [R₁COOH + Ag]⁺ was also observed, both in IRMPD and CID but with very low abundance. In addition, no neutral losses were observed from [R₁COOH + Ag]⁺. Another phosphatidylethanolamine lipid, [C18:0/C20:4-PE] + Ag]⁺, with different fatty acyl group attached to the sn-2 position was also investigated and showed similar behavior as [(C18:0/C18:2-PE) + Ag]⁺ in both CID and IRMPD (the IRMPD spectrum is shown in Figure 5.5a).

We believe that silver adducts form in ESI of Ag(I)-containing phospholipid solutions. Thus, Ag⁺ should be interacting with the sn-2 acyl chain (which contains double bonds),^{9, 43-45} consistent with the observation of the [R₂COOH + Ag]⁺ product ion.

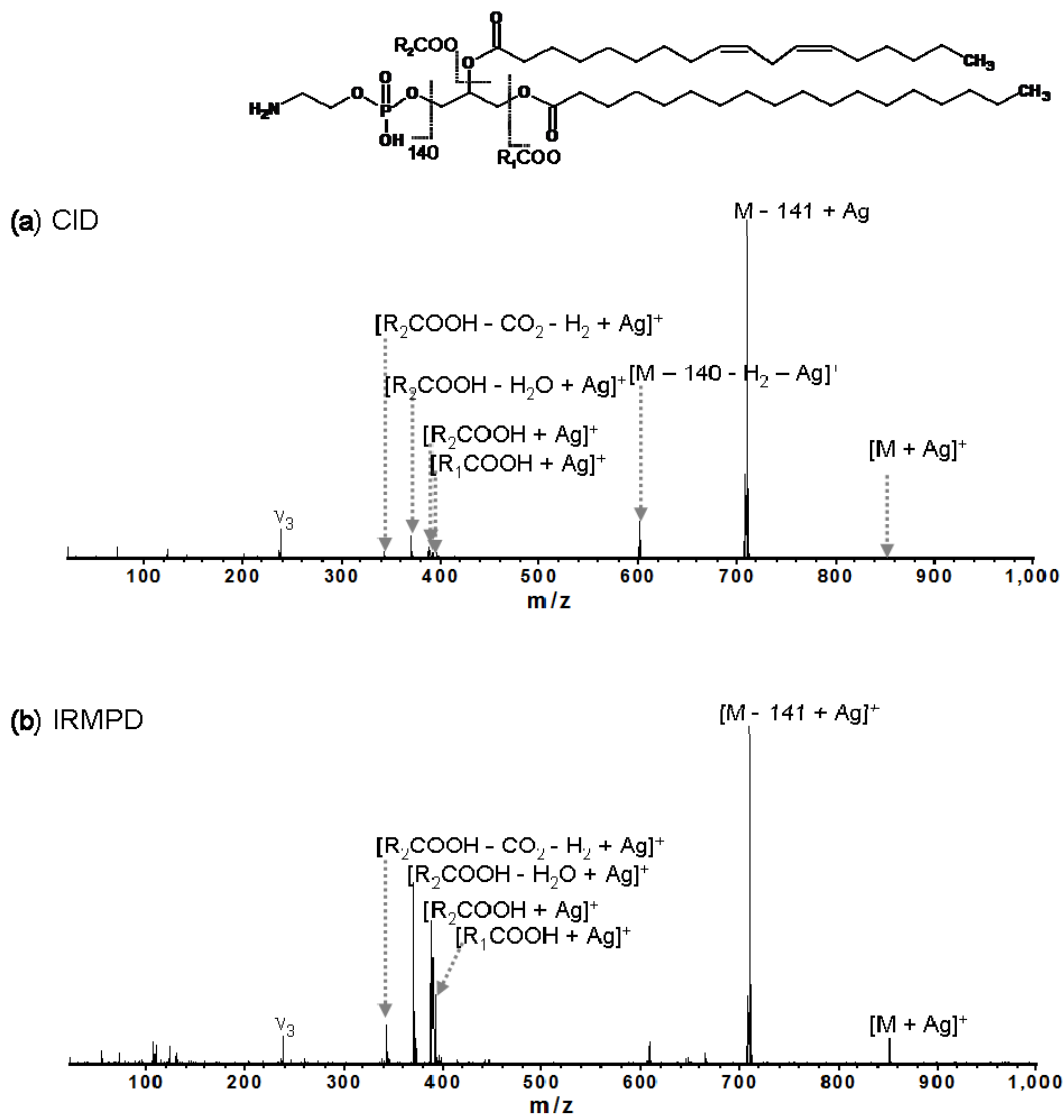


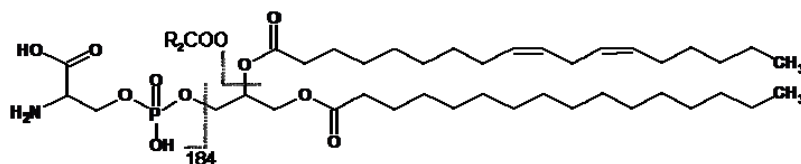
Figure 5.2. CID (collision voltage: -35 V) and IRMPD (laser power: 7.5 W, irradiation time: 750 ms) of Ag-adducted phosphatidylethanolamine, [(C18:0/C18:2-PE) + Ag]⁺.

By contrast, the sn-1 acyl chain does not contain double bonds and [R₁COOH + Ag]⁺ was not always observed. Even when [R₁COOH + Ag]⁺ was observed, its abundance was much lower than other product ions. Generally, [R₁COOH + Ag]⁺ was observed when a less unsaturated fatty acyl chain was present at the sn-2 esterification site as shown in Figures 5.2 and 5.5. For example, [R₁COOH + Ag]⁺ was observed for C18:0/C18:2-PE

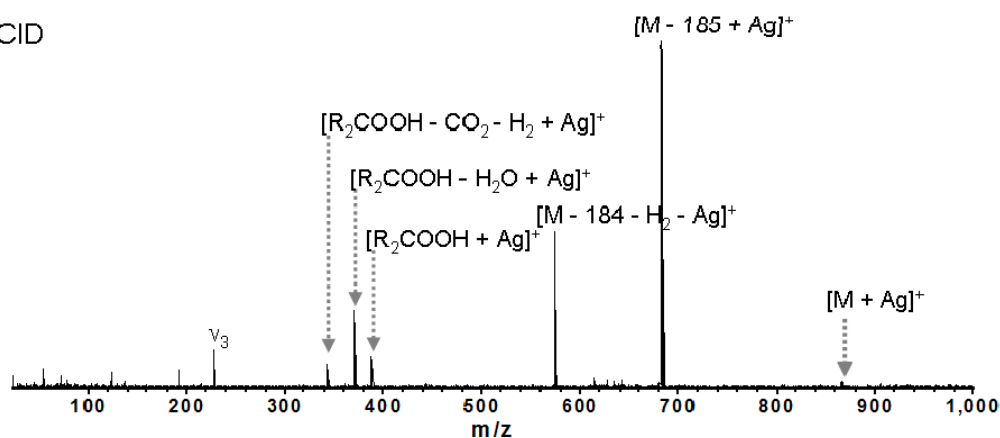
(Figure 5.2), but not for C18:0/C20:4-PE. The interaction between Ag^+ ions and organic molecules increases with the number of double bonds.⁴⁴ Thus, observation of $[\text{R}_1\text{COOH} + \text{Ag}]^+$ could be explained by relatively weak interaction between Ag^+ ions and less unsaturated R_2COOH acyl chains, compared to stronger interaction between Ag^+ and more unsaturated sn-2 fatty acyl groups. In some cases, other minor neutral losses, such as $[\text{R}_2\text{COOH} - \text{H}_2 + \text{Ag}]^+$ were also observed with relatively low abundances. Based on the tandem mass spectra shown in Figure 5.2, $[\text{R}_2\text{COOH} + \text{Ag}]^+$ and related neutral losses could be used as characteristic product ions to characterize phospholipid structures. More phospholipids were examined to further verify this hypothesis.

CID and IRMPD spectra of Ag-adducted phosphatidylserine, $[(\text{C16:0/C18:2-PS}) + \text{Ag}]^+$, are shown in Figure 5.3. Similar results were observed as in CID and IRMPD of Ag-adducted phosphatidylethanolamine (Figure 5.2). Headgroup losses, with or without Ag adduction, from precursor ions were very abundant in both CID and IRMPD of $[(\text{C16:0/C18:2-PS}) + \text{Ag}]^+$. Again, $[\text{R}_2\text{COOH} + \text{Ag}]^+$, $[\text{R}_2\text{COOH} - \text{H}_2\text{O} + \text{Ag}]^+$, and $[\text{R}_2\text{COOH} - \text{CO}_2 - \text{H}_2 + \text{Ag}]^+$ were observed with very similar relative abundances as observed in CID and IRMPD of phosphatidylethanolamine. CID and IRMPD of phosphatidylcholine, $[(\text{C16:0/C18:2-PC}) - \text{H} + \text{Ag}]^+$ followed the same trend as the other types of phospholipids investigated. As shown in Figure 5.4, characteristic product ions

containing the sn-2 acyl chain ($[\text{R}_2\text{COOH} + \text{Ag}]^+$, $[\text{R}_2\text{COOH} - \text{H}_2\text{O} + \text{Ag}]^+$, and $[\text{R}_2\text{COOH} - \text{CO}_2 - \text{H}_2 + \text{Ag}]^+$) were observed along with abundant headgroup losses, with or without Ag adduction, from precursor ions.



(a) CID



(b) IRMPD

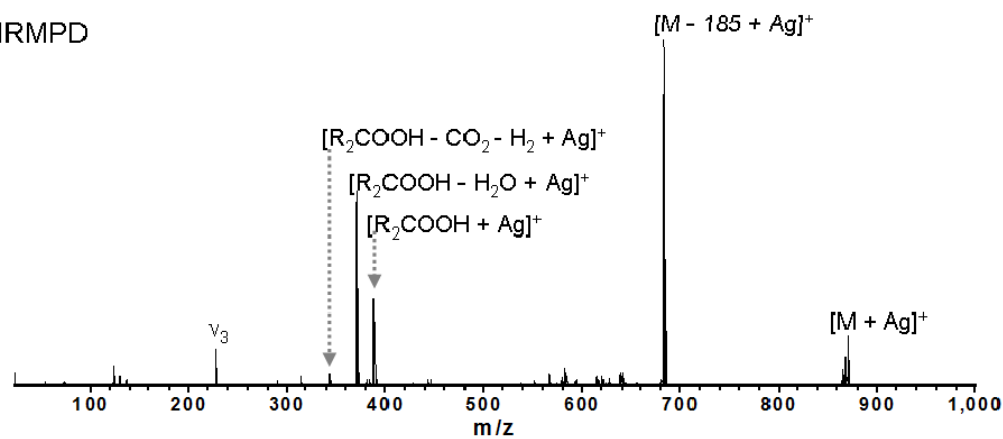
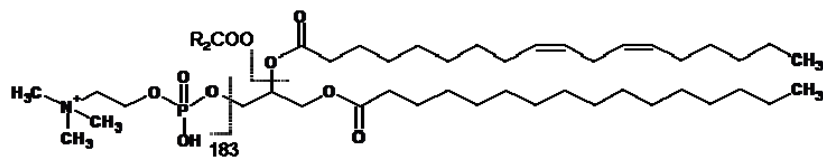
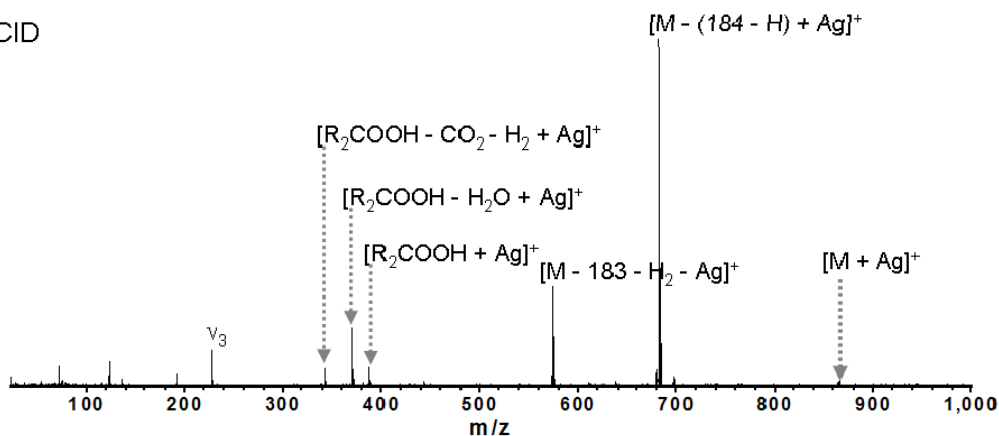


Figure 5.3. CID (collision voltage: -35 V) and IRMPD (laser power: 7.5 W, irradiation time: 300 ms) of Ag-adducted phosphatidylserine, $[(\text{C16:0}/\text{C18:2-PS}) + \text{Ag}]^+$.



(a) CID



(b) IRMPD

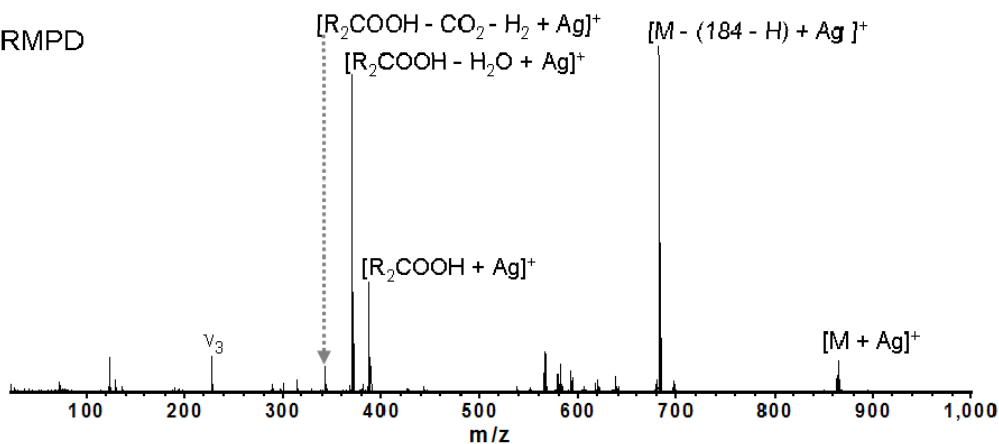


Figure 5.4. CID (collision energy: -35 V) and IRMPD (laser power: 7.5 W, irradiation time: 450 ms) of Ag-adducted phosphatidylcholine, [(C16:0/C18:2-PC) + Ag]⁺

Further examination of Figures 5.2 to 5.4 reveals that low m/z regions, where characteristic product ions are observed such as $[R_2COOH + Ag]^+$, are more abundant in IRMPD spectra compared to CID. Precursor ion activation may be more efficient in IRMPD than CID, due to high IR absorption by phosphate groups and the longer

interaction time between molecular ions and IR photons.^{26, 39, 41} Thus, IRMPD may be preferred over CID to ensure observation of all characteristic product ions, including $[R_2COOH + Ag]^+$ and related neutral losses, for characterization of phospholipid esterification sites. Additional IRMPD spectra of other Ag-adducted phospholipids are shown in Figure 5.5. Characteristic product ions observed in IRMPD can be used to identify the sn-1 and sn-2 acyl chains of each phospholipid. Other product ions such as $[R_1COOH + Ag]^+$ were also observed. However these species were not dominant and not consistently observed for all phospholipids. Thus, such product ions may not be useful for phospholipid structural characterization. On the other hand, $[R_2COOH + Ag]^+$ and related neutral losses were observed for all investigated phospholipids with unsaturated acyl chains at the sn-2 esterification site. Potential low abundance $[R_1COOH + Ag]^+$ product ions should not cause confusion when determining unsaturated phospholipid sn-2 acyl chains, because no neutral losses were observed from $[R_1COOH + Ag]^+$. Figure 5.6 shows IRMPD of Ag-adducted phosphatidylcholine (C18:1/C16:0-PC) which has an unsaturated acyl chain at the sn-1 position. As expected, $[R_1COOH + Ag]^+$, $[R_1COOH - H_2O + Ag]^+$, and $[R_1COOH - CO_2 - H_2 + Ag]^+$ were observed, presumably due to interaction between Ag^+ and the double bond in the sn-1 acyl chain.

However, the water loss peak, $[R_1COOH - H_2O - H + Ag]^+$, is much less abundant than $[R_1COOH + Ag]^+$.

Hsu et. al used Li^+ and Na^+ to form adducts with phosphatidylserine.²⁰ CID of Li^+ or Na^+ -adducted phosphatidylserine yielded mainly headgroup loss and R_xCOOH ($x = 1, 2$) losses, where greater relative ion abundances of R_2COOH loss over R_1COOH loss allowed identification of the fatty acyl group attached at the sn-2 site of phosphatidylserine.²⁰ However, the abundance ratios of product ions formed via loss of R_2COOH and R_1COOH , respectively, in CID of alkali metal-adducted phospholipids change depending on types of phospholipid and types of alkali metal adduct for the same type of phospholipid..²¹ In addition to alkali metals, alkaline earth and divalent metals (Met) such as Co^{2+} have been applied for phospholipid structural characterization via characteristic $[M - R_2COOH + Met]^+$ and $[M - R_1COOH + Met]^+$ product ion abundances in CID.²¹ However, the ratios of $[M - R_2COOH + Met]^+ / [M - R_1COOH + Met]^+$ were still dependent on phospholipid and metal type. By contrast, fragmentation patterns reported here from tandem mass spectrometry of Ag-adducted phospholipids were not dependent on types of phospholipid. In CID and IRMPD of Ag-adducted phospholipids, the activation energy did not appear to affect characteristic fragmentation patterns: lower activation energy only had an influence on fragmentation efficiency.

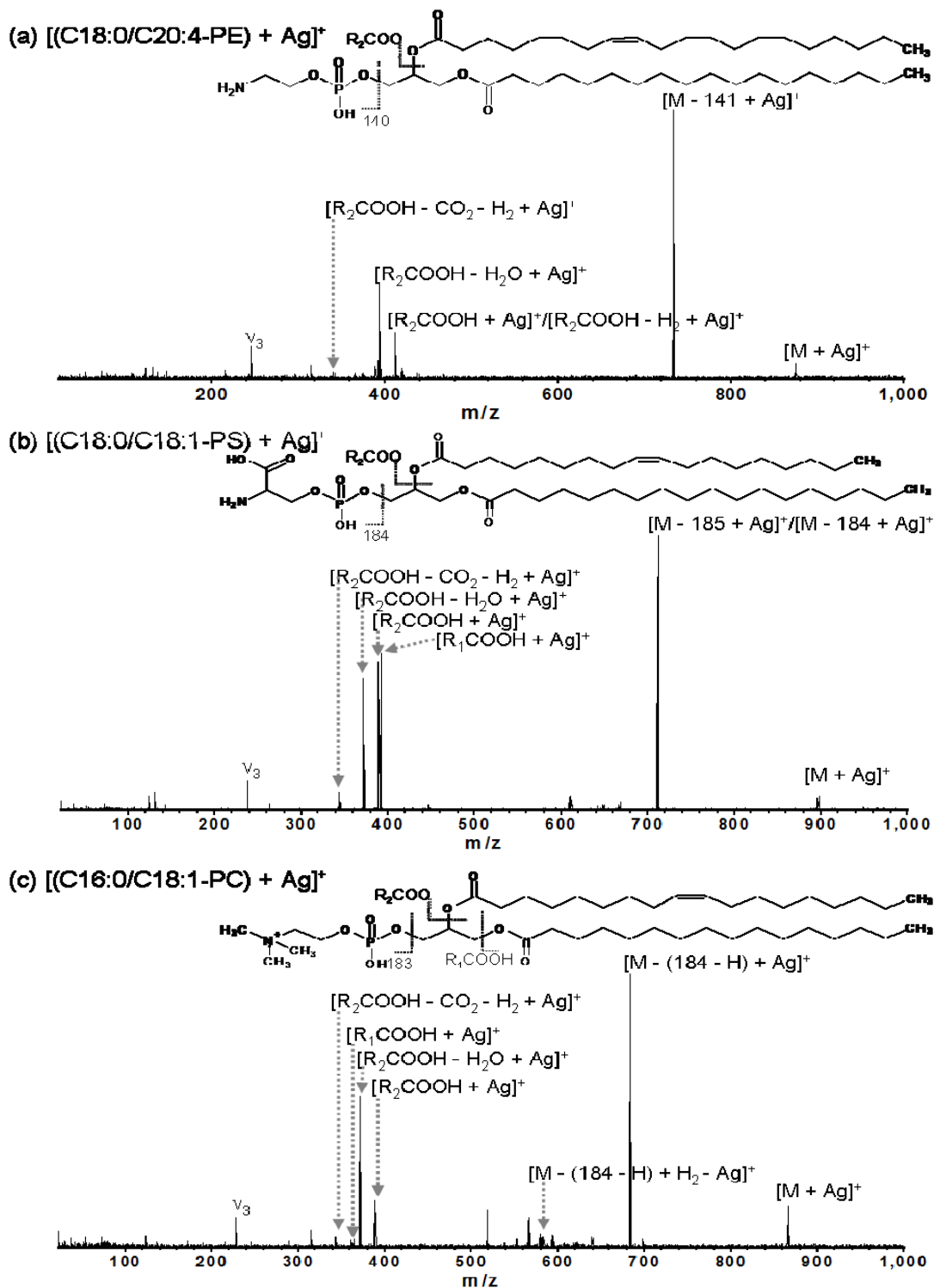


Figure 5.5. IRMPD of Ag-adducted phospholipids: (a) $[(18:0/C20:4-PE) + Ag]^+$ (laser power: 5 W, irradiation time: 300 ms), (b) $[(C16:0/C18:1-PS) + Ag]^+$ (laser power: 7.5 W, irradiation time: 600 ms), (c) $[(C16:0/C18:1-PC) + Ag]^+$ (laser power: 7.5 W, irradiation time: 450 ms, where 87 is homolytic cleavage).

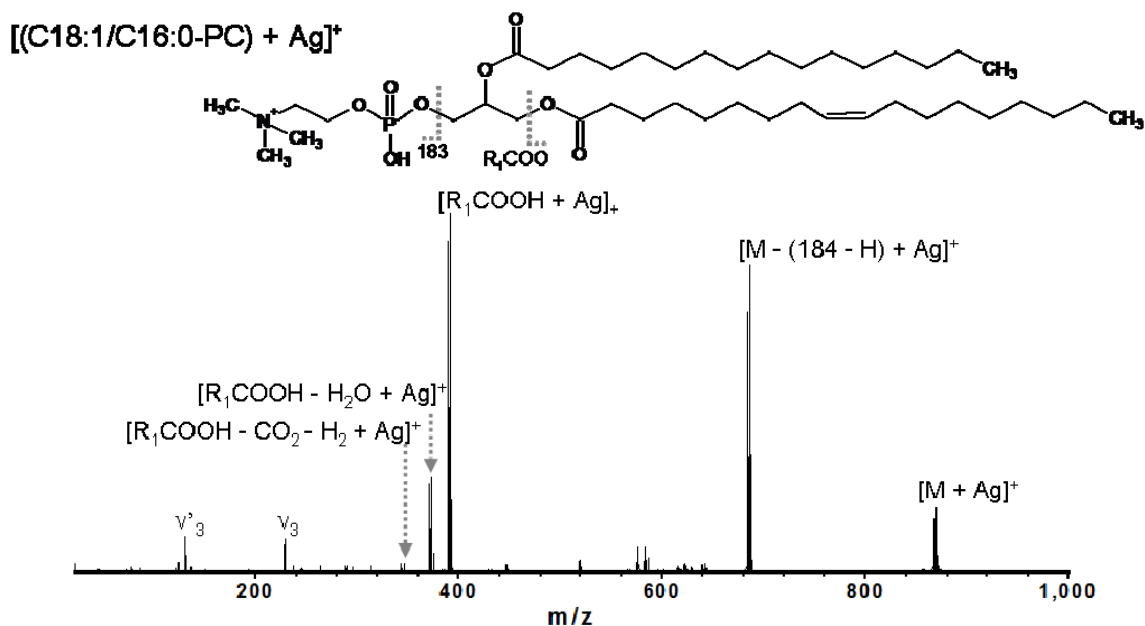


Figure 5.6. IRMPD of Ag-adducted $[(C18:1/C16:0-PC) + Ag]^+$ (laser power:7.5 W, irradiation time: 300 ms).

The most abundant characteristic product ion ($[R_2COOH - H_2O + Ag]^+$), where R_2COOH is unsaturated, was observed at lower activation energy than other characteristic fragments such as $[R_2COOH + Ag]^+$, which started to appear as the CID and IRMPD activation energy increased. The relative abundances of characteristic product ions did not change with activation energy. Thus, CID and IRMPD of Ag-adducted phospholipids could be very useful for determination of esterification sites. The characteristic product ions, $[R_xCOOH + Ag]^+$, $[R_xCOOH - H_2O + Ag]^+$, and $[R_xCOOH - CO_2 - H_2 + Ag]^+$ could be used to determine esterification sites of phospholipids in which R_xCOOH is unsaturated. IRMPD appeared more beneficial for phospholipid structural characterization due to increased ion abundances at the lower m/z

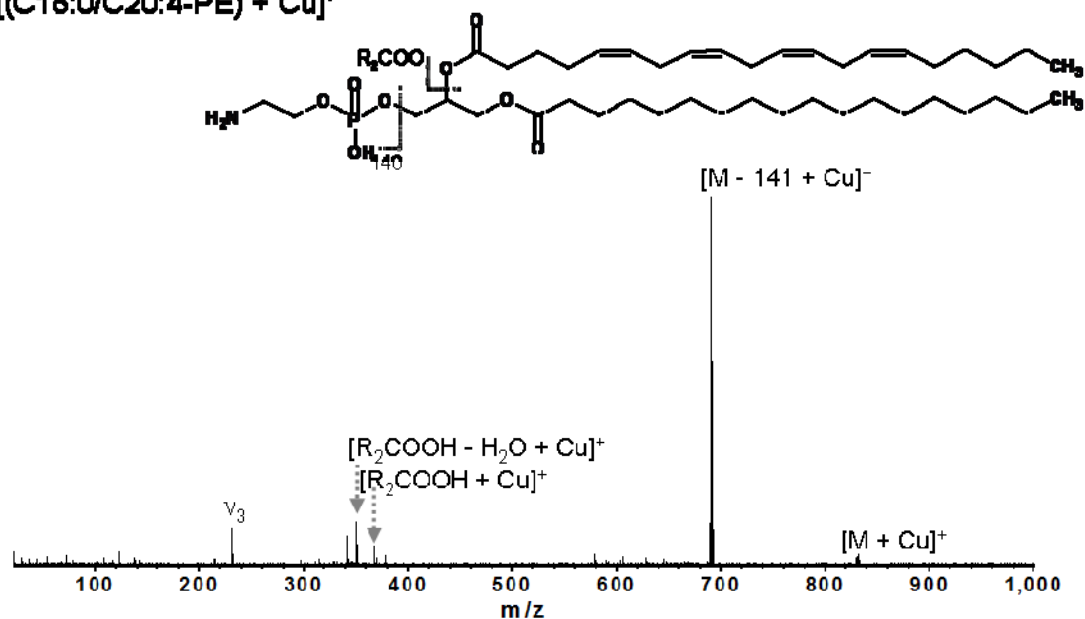
region where characteristic product ions are located. In addition to these characteristic product ions, abundant headgroup loss enabled us to identify the types of phospholipid, and other fatty acid fragments provided further confirmation about the fatty acyl groups attached at each esterification site. As a result, complete structural characterization of phospholipids appears possible from CID and IRMPD of Ag-adducted species.

5.3.3. CID and IRMPD of Cu-adducted Phospholipids

Ag⁺ ion has soft acid property based on the hard and soft acid and base (HSAB) principle, and Ag⁺ interacts well with olefinic π electrons of double bonds, which have soft basic property.^{9, 43-45} Thus, metals such as Cu⁺, which also has soft acid property,⁵¹ are expected to provide similar results as Ag-adducted phospholipids in MS/MS.

CID and IRMPD of Cu-adducted phospholipids were examined. Overall, similar results were observed as those of Ag-adducted phospholipids, as anticipated. Figure 5.7 shows IRMPD of two phospholipids (phosphatidylethanolamine, [(C18:0/20:4-PE) + Ag]⁺, and phosphatidylcholine, [(C18:0/C18:1) - H + Ag]⁺). CID yielded similar fragmentation patterns but with poorer fragmentation efficiencies than IRMPD, particularly in the lower m/z region (data not shown). No Cu⁺ complex was observed for phosphatidylserine. Thus, Ag⁺ appears more suitable for phospholipid characterization due to its higher ability to form complexes with phospholipids.

(a) $[(C18:0/C20:4-PE) + Cu]^+$



(b) $[(C16:0/C18:1-PC) + Cu]^+$

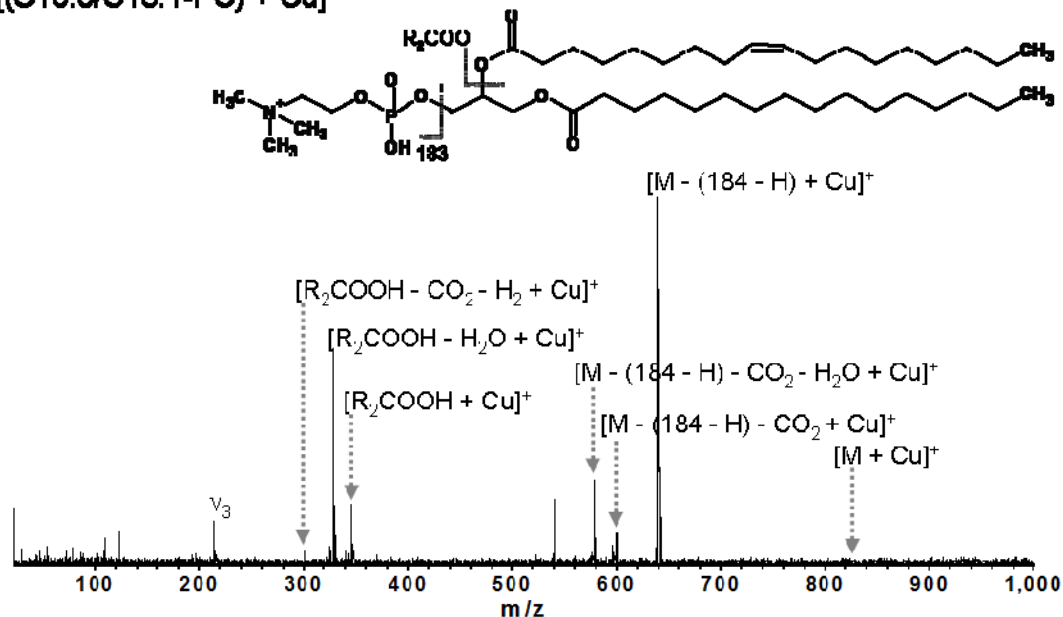


Figure 5.7. IRMPD of Cu-adducted phospholipids: (a) $[(C18:0/C20:4-PE) + Cu]^+$ (laser power:7.5 W, irradiation time: 300 ms) (b) $[(C16:0/C18:1-PC) + Cu]^+$ (laser power:7.5 W, irradiation time: 300 ms)

5.4. Conclusions

CID and IRMPD of Ag-adducted phospholipids were used to determine fatty acyl groups attached to the sn-1 and sn-2 esterification sites. CID and IRMPD of Ag-adducted phosphatidylethanolamine mostly provided abundant headgroup loss, $[M - 141 + Ag]^+$. In addition to headgroup loss, $[R_xCOOH + Ag]^+$ was observed along with accompanying neutral losses, $[R_xCOOH - H_2O + Ag]^+$ and $[R_xCOOH - CO_2 - H_2 + Ag]^+$, where R_xCOOH is unsaturated. Other types of phospholipids, including phosphatidylserine and phosphatidylcholine were also examined, and their CID and IRMPD spectra showed similar fragmentation patterns. Thus, $[R_xCOOH + Ag]^+$ and its related neutral loss peaks obtained from CID or IRMPD of Ag-adducted phospholipids may be used as characteristic product ions to determine sn-1 and sn-2 esterification sites of phospholipids. Interaction between Ag^+ ion and olefinic π bonds of fatty acyl groups of phospholipids are believed to be crucial for revealing esterification sites of phospholipids. This explanation may be supported by IRMPD of Cu-adducted phospholipids, where similar fragmentation patterns were observed but with lower fragmentation efficiencies. Headgroup losses were always observed along with $[R_xCOOH + Ag]^+$ and its neutral losses. Thus, complete structural characterization of phospholipids is possible with CID and/or IRMPD of Ag-adducted phospholipids.

5.5. References

1. Anderson, H. A.; Maylock, C. A.; Williams, J. A.; Paweletz, C. P.; Shu, H.; Shacter, E. *Nat Immunol* **2003**, *4*. 87-91.
2. Irvine, R. F. *Nat Rev Mol Cell Biol* **2003**, *4*. 349-360.
3. Wenk, M. R.; Lucast, L.; Di Paolo, G.; Romanelli, A. J.; Suchy, S. F.; Nussbaum, R. L.; Cline, G. W.; Shulman, G. I.; McMurray, W.; De Camilli, P. *Nat Biotechnol* **2003**, *21*. 813-817.
4. Mills, G. B.; Moolenaar, W. H. *Nat Rev Cancer* **2003**, *3*. 582-591.
5. Zegzouti, H.; Anthony, R. G.; Jahchan, N.; Bogre, L.; Christensen, S. K. *Proc Natl ACID Sci U S A* **2006**, *103*. 6404-6409.
6. Esmon, N. L.; Smirnov, M. D.; Esmon, C. T. *Haematologica* **1997**, *82*. 474-477.
7. Meijer, H. J.; Munnik, T. *Annu Rev Plant Biol* **2003**, *54*. 265-306.
8. Prestwich, G. D. *Prostaglandins Other Lipid Mediat* **2005**, *77*. 168-178.
9. Dugo, P.; Favoino, O.; Tranchida, P. Q.; Dugo, G.; Mondello, L. *J Chromatogr A* **2004**, *1041*. 135-142.
10. Han, J. J.; Yamane, T. *Lipids* **1999**, *34*. 989-995.
11. Xu, X.; Fomuso, L. B.; Akoh, C. C. *J Agric Food Chem* **2000**, *48*. 3-10.
12. Mitoma, J.; Kasama, T.; Furuya, S.; Hirabayashi, Y. *J Biol Chem* **1998**, *273*. 19363-19366.
13. Cheng, C.; Gross, M. L. *Mass Spectrom Rev* **2000**, *19*. 398-420.
14. Han, X.; Gross, R. W. *J Am Soc Mass Spectrom* **1995**, *6*. 1202-1210.
15. Huang, Z. H.; Gage, D. A.; C., S. C. *J Am Soc Mass Spectrom* **1992**, *3*. 71-78.
16. Clay, K. L. M., R. C. *Biomed Mass Spectrom* **1983**, *10*. 489-494.
17. Hvattum, E.; Hagelin, G.; Larsen, A. *Rapid Commun Mass Spectrom* **1998**, *12*. 1405-1409.
18. Pulfer, M.; Murphy, R. C. *Mass Spectrom Rev* **2003**, *22*. 332-364.
19. Han, X.; Gross, R. W. *Proc Natl ACID Sci U S A* **1994**, *91*. 10635-10639.
20. Hsu, F. F.; Turk, J. *J Am Soc Mass Spectrom* **2005**, *16*. 1510-1522.
21. Ho, Y. P.; Huang, P. C.; Deng, K. H. *Rapid Commun Mass Spectrom* **2003**, *17*. 114-121.
22. Marshall, A. G.; Hendrickson, C. L.; Jackson, G. S. *Mass Spectrom Rev* **1998**, *17*. 1-35.
23. Aharoni, A.; Ric de Vos, C. H.; Verhoeven, H. A.; Maliepaard, C. A.; Kruppa, G.; Bino, R.; Goodenowe, D. B. *Omic* **2002**, *6*. 217-234.

24. Little, D. P.; Speir, J. P.; Senko, M. W.; O'Connor, P. B.; McLafferty, F. W. *Anal Chem* **1994**, *66*. 2809-2815.
25. Woodin, R. L.; Bomse, D. S.; Beauchamp, J. L. *J Am Chem Soc* **1978**, *100*. 3248-3250.
26. Yoo, H. J.; Liu, H.; Hakansson, K. *Anal Chem* **2007**, *20*. 7858-7866.
27. Budnik, B. A.; Haselmann, K. F.; Elkin, Y. N.; Gorbach, V. I.; Zubarev, R. A. *Anal Chem* **2003**, *75*. 5994-6001.
28. Cody, R. B.; Freiser, B. S. *Anal Chem* **1979**, *51*. 541-551.
29. Lioe, H.; O'Hair, R. A. *Anal Bioanal Chem* **2007**, *389*. 1429-1437.
30. McLafferty, F. W.; Horn, D. M.; Breuker, K.; Ge, Y.; Lewis, M. A.; Cerda, B.; Zubarev, R. A.; Carpenter, B. K. *J Am Soc Mass Spectrom* **2001**, *12*. 245-249.
31. Cooper, H. J.; Hakansson, K.; Marshall, A. G. *Mass Spectrom Rev* **2005**, *24*. 201-222.
32. Zubarev, R. A. *Curr Opin Biotechnol* **2004**, *15*. 12-16.
33. Zubarev, R. A.; Horn, D. M.; Fridriksson, E. K.; Kelleher, N. L.; Kruger, N. A.; Lewis, M. A.; Carpenter, B. K.; McLafferty, F. W. *Anal Chem* **2000**, *72*. 563-573.
34. Adamson, J. T.; Hakansson, K. *J Proteome Res* **2006**, *5*. 493-501.
35. Adamson, J. T.; Hakansson, K. *Anal Chem* **2007**, *79*. 2901-2910.
36. Hakansson, K.; Chalmers, M. J.; Quinn, J. P.; McFarland, M. A.; Hendrickson, C. L.; Marshall, A. G. *Anal Chem* **2003**, *75*. 3256-3262.
37. Hakansson, K.; Cooper, H. J.; Emmett, M. R.; Costello, C. E.; Marshall, A. G.; Nilsson, C. L. *Anal Chem* **2001**, *73*. 4530-4536.
38. James, P. F.; Perugini, M. A.; O'Hair, R. A. *J Am Soc Mass Spectrom* **2008**, *19*. 978-986.
39. Crowe, M. C.; Brodbelt, J. S. *J Am Soc Mass Spectrom* **2004**, *15*. 1581-1592.
40. Flora, J. W.; Muddiman, D. C. *J Am Chem Soc* **2002**, *124*. 6546-6547.
41. Flora, J. W.; Muddiman, D. C. *J Am Soc Mass Spectrom* **2004**, *15*. 121-127.
42. Hofstadler, S. A.; Sannes-Lowery, K. A.; Griffey, R. H. *Anal Chem* **1999**, *71*. 2067-2070.
43. Dobson, G.; Christie, W. W.; Nikolova-Damyanova, B. *J Chromatogr B Biomed Appl* **1995**, *671*. 197-222.
44. Momchilova, S.; Nikolova-Damyanova, B. *J Sep Sci* **2003**, *26*. 261-270.
45. Adlof, R.; List, G. *J Chromatogr A* **2004**, *1046*. 109-113.
46. Fang, J.; Barcelona, M. J. *J Microbio Methods* **1998**, *33*. 23-35.
47. Yang, J.; Mo, J.; Adamson, J. T.; Hakansson, K. *Anal Chem* **2005**, *77*. 1876-1882.

48. Belov, M. E.; Nikolaev, E. N.; Anderson, G. A.; Udseth, H. R.; Conrads, T. P.; Veenstra, T. D.; Masselon, C. D.; Gorshkov, M. V.; Smith, R. D. *Anal Chem* **2001**, *73*. 253-261.
49. Hendrickson, C. L.; Quinn, J. P.; Emmett, M. R.; Marshall, A. G., in *49th ASMS Conference on Mass Spectrometry and Allied Topics*. Chicago, IL, 2001; CD-ROM.
50. Senko, M. W.; Canterbury, J. D.; Guan, S.; Marshall, A. G. *Rapid Commun Mass Spectrom* **1996**, *10*. 1839-1844.
51. Deng, H.; Kebarle, P. *J. Am. Chem. Soc.* **1998**, *120*. 2925-2931.

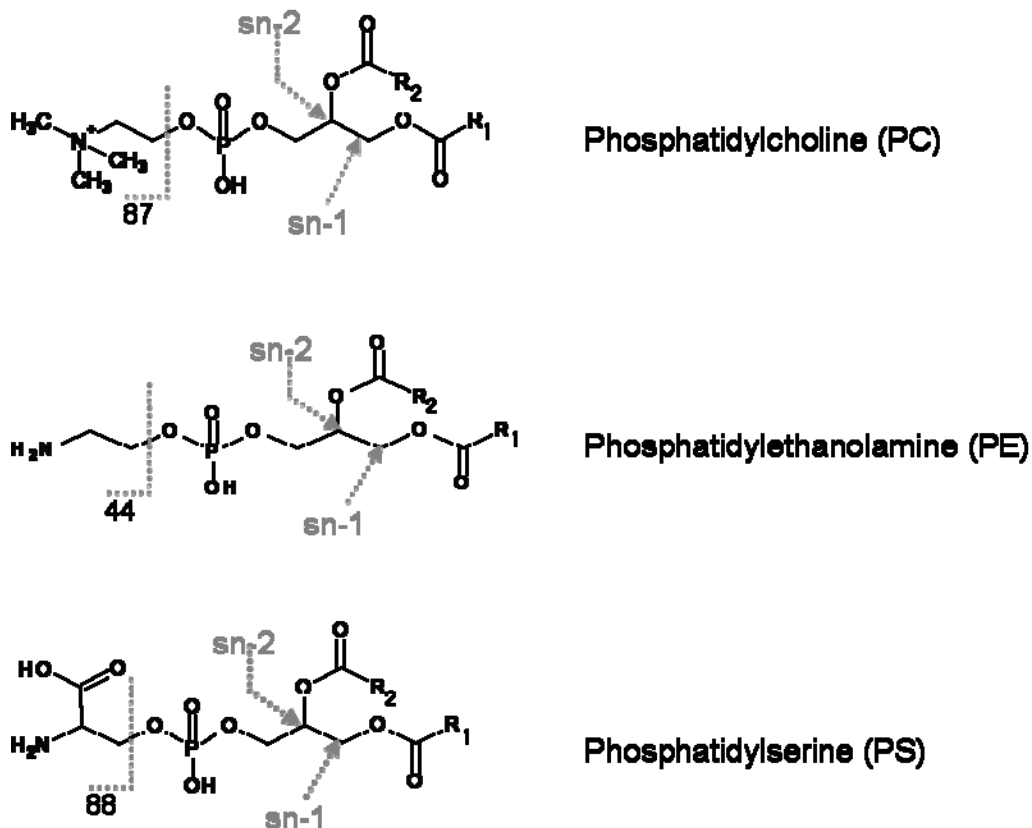
Chapter 6

Electron Capture Dissociation of Divalent Metal-Adducted Phospholipids

6.1. Introduction

Phospholipids, present in all organisms, are the building blocks for cellular membranes, and are involved in a diverse number of other functions, from compartmentalization of cytoplasm to cell signaling.¹⁻⁷ Phospholipids consist of a hydrophilic headgroup and hydrophobic tails which are long fatty acid carbon chains attached at two different esterification sites (sn-1 or sn-2), as shown in Scheme 6.1. Differentiation between the sn-1 and sn-2 positions of phospholipids is important from both a biochemical and nutritional viewpoint because cell signaling through phospholipids and absorption of polyunsaturated fatty acids into the body are related to the position of the acyl chains on the glycerol backbone.⁸⁻¹¹

Fast atom bombardment-mass spectrometry (FAB-MS) and electrospray ionization (ESI)-MS can directly analyze phospholipids as intact molecules and preserve the information inherent in their chemical structures.^{3, 12-15} It has been shown that



Scheme 6.1. Structure of phospholipids.

determination of the fatty acyl chains at the sn-1 versus sn-2 esterification sites can be performed by analysis of the ratio of $[R_1\text{COOH} - \text{H}]^-/[R_2\text{COOH} - \text{H}]^-$ product ions in negative ion mode collision induced dissociation (CID) spectra, however, the observed ion ratio is dependent on the extent of unsaturation of the sn-2 fatty acyl group as well as on the total chain length, collisional activation energy, and the type of phospholipid polar headgroup.^{13, 15-17} ESI-MS has become a popular tool for phospholipid analysis because it does not suffer from some of the problems associated with FAB-MS, including complication of spectra due to matrix ions and decomposition of molecular ions during the ionization event.^{3, 18} Alkali, alkaline earth, and divalent metal ions have been used

to form metal adducts for structural determination of phospholipids.¹⁹⁻²⁰ CID of alkali metal-adducted phosphatidylserine resulted in a greater abundance of product ions from bond cleavage at the sn-2 position compared to the sn-1 position.¹⁹ Alkaline earth metals and divalent metal ions have also been used to form complexes with phospholipids for phospholipid structural characterization.²⁰ However, product ion abundances from bond cleavage at the sn-1 and sn-2 esterification sites in CID spectra changed depending on the types of metals and phospholipids.²⁰

FT-ICR mass spectrometry²¹ has accurate mass capabilities²² and additional MS/MS fragmentation techniques, including infrared multiphoton dissociation (IRMPD),²³⁻²⁴ electron induced dissociation (EID),²⁵⁻²⁷ and electron capture dissociation (ECD)²⁸⁻³⁰. These techniques can often provide complementary structural information compared to CID for the characterization of various kinds of biomolecules.^{29, 31-37} However, there has been very limited application of additional MS/MS fragmentation techniques available in FT-ICR mass spectrometry to phospholipids.³⁸ Recently, our group showed that regiochemical information of phospholipids could be unambiguously obtained from characteristic product ions observed in CID or IRMPD of phospholipids adducted with weak Lewis acidic metal ions such as Ag^+ and Cu^+ .³⁹ In contrast, ECD is challenging to apply towards phospholipid structural characterization due to the requirement for at least doubly positively charged precursor ions. James et al. applied ECD to complexes ($[\text{Met-PC}_n - n\text{H}]^{2+}$, $n \geq 2$) of phosphatidylcholine (PC) and divalent metals (Met) and found that the product ion ratio from losses of the sn-1/sn-2 acyl chains was dependent on the number (n) of phospholipids complexed with metal ions.³⁸ The dominant fragmentation pathway in ECD of $[\text{Met-PC}_n - n\text{H}]^{2+}$ ($n \geq 2$) was ligand (PC) loss

but product ions resulting from cleavage at the sn-1 or sn-2 esterification site were also observed at lower abundance. However, unambiguous determination of phosphatidylcholine regiochemistry was unsuccessful due to lack of consistency of the product ion ratio from bond cleavage at the sn-1 and sn-2 esterification sites.

To our knowledge, the present work represents the first application of ECD to monomeric divalent metal-adducted phospholipids, $[\text{PL} + \text{Met}]^{2+}$ or $[\text{PC} - \text{H} + \text{Met}]^{2+}$ for PC, which contains a fixed positive charge, for determination of fatty acyl chains at the sn-1 and sn-2 esterification sites. ECD of metal-adducted phosphatidylcholine provided the most extensive fragmentation, possibly because electrons can be captured by either the electron deficient trimethylamine, $\text{N}(\text{CH}_3)_3^+$, headgroup, or by divalent metal ions. The positions (sn-1 and sn-2) of phospholipid acyl chains could be determined through either characteristic product ions, $[\text{R}_2\text{COOH} - \text{H} + \text{Met}]^+$ (and $[\text{M} - \text{R}_2\text{COOH}]^+$ for PC), in ECD of Ni^{2+} -adducted phospholipids, or from the product ion ratio of the sum of all product ion abundances involving sn-2 bond cleavage to that of all product ion abundances involving sn-1 bond cleavage in ECD of Ba^{2+} -adducted phospholipids.

6.2. Experimental Section

6.2.1. Sample Preparation

Phospholipids used in this work include phosphatidylethanolamine (C18:0/C18:2-PE and C18:0/C20:4-PE), phosphatidylserine (C16:0/C18:2-PS and C18:0/C18:1-PS) and phosphatidylcholine (C16:0/C18:1-PC, C16:0/C18:2-PC, and C18:1/16:0-PC). Phospholipids are designated as follows: $\text{C}_1:\text{d}_1/\text{C}_2:\text{d}_2\text{-PL}$, where C_1 and C_2 are the number

of carbon atoms in the fatty acyl chains attached to the sn-1 and sn-2 positions, respectively; d_1 and d_2 are the numbers of double bonds of the sn-1 and sn-2 fatty acyl chains, respectively; PE, PS, and PC is the abbreviation of each phospholipid type.⁴⁰ Phospholipids were purchased from Avanti Polar lipids (Alabaster, Al). Barium chloride, calcium acetate, magnesium acetate, nickel bromide, cobalt bromide, zinc acetate, and manganese chloride used for the formation of divalent metal-adducted phospholipids were purchased from Sigma-Aldrich (St. Louis, MO). 200–300 μ M phospholipids were mixed with 2 mM divalent metal solutions in methanol/water/chloroform (82/16/2, v/v/v). For phosphatidylserine, 0.8 % formic acid was added to the reaction solution to aid complex formation with divalent metal ions, due to the additional acidic carboxylate group of the phosphatidylserine headgroup. All sample solutions were freshly made at least 20 min prior to MS/MS analysis.

6.2.2. Fourier Transform Ion Cyclotron Resonance Mass Spectrometry

Divalent metal-adducted phospholipids, $[\text{PL} + \text{Met}]^{2+}$ or $[\text{PC} - \text{H} + \text{Met}]^{2+}$, were generated by external ESI at 70 μ L/h (Apollo II ion source, Bruker Daltonics, Billerica, MA). All experiments were performed with a 7 Tesla quadrupole (Q)-FT-ICR mass spectrometer (APEX-Q, Bruker Daltonics) as previously described⁴¹. All data were obtained in positive ion mode. For ESI, N_2 was used as both nebulizing gas (4 L/s) and drying gas (2 L/s). The drying gas temperature was set to 200 °C. Briefly, ions produced by electrospray ionization were mass-selectively externally accumulated⁴²⁻⁴³ in a hexapole for 0.2-3 s, transferred via high voltage ion optics, and captured in the ICR cell by dynamic trapping. This accumulation sequence was looped three times to improve precursor ion abundance. For MS/MS experiments, mass selective external accumulation

of divalent metal ion-adducted phospholipids, $[\text{PL} + \text{Met}]^{2+}$ or $[\text{PC} - \text{H} + \text{Met}]^{2+}$, was followed by further isolation via correlated harmonic excitation fields (CHEF)⁴⁴ inside the ICR cell. For ECD, divalent metal ion-adducted phospholipids, $[\text{PL} + \text{Met}]^{2+}$ or $[\text{PC} - \text{H} + \text{Met}]^{2+}$, were irradiated for 3-5 s with low-energy electrons provided by an indirectly heated hollow dispenser cathode⁴⁵ at - 0.01 V bias voltage. A lens electrode located in front of the hollow cathode was kept at 1.0 V.

All mass spectra were acquired with XMASS software (version 6.1, Bruker Daltonics) in broadband mode from m/z 21 to 1000 with 256K data points and summed over 4-30 scans. Data processing was performed with the MIDAS analysis software⁴⁶. Internal calibration was performed with $[\text{PL} + \text{Met}]^{2+}$ or $[\text{PC} - \text{H} + \text{Met}]^{2+}$ and one product ion peak generated by headgroup loss (or the charge-reduced peak, $[\text{PL} + \text{Met}]^{+}$ or $[\text{PC} - \text{H} + \text{Met}]^{+}$, if applicable) as calibrants. All ECD product ion peak assignments were performed within 10 ppm mass accuracy.

6.3. Results and Discussion

6.3.1. ESI of Divalent Metal Ion-adducted Phospholipids

Divalent metal ion-adducted phospholipids, $[\text{PL} + \text{Met}]^{2+}$ or $[\text{PC} - \text{H} + \text{Met}]^{2+}$, were formed simply by mixing divalent metal ions (Ca^{2+} , Mg^{2+} , Co^{2+} , Zn^{2+} , Ba^{2+} , Ni^{2+} , and Mn^{2+}) and phospholipid solutions (phosphatidylethanolamine, phosphatidylserine, and phosphatidylcholine) as described in the Experimental Section. Scheme 6.1 shows the structure of phospholipids used in these experiments. Note that PC contains a fixed positive charge at the head group. $[\text{PC} - \text{H} + \text{Met}]^{2+}$ was observed at higher abundance

compared to non metal-adducted phospholipid, PC^+ , for phosphatidylcholine. $[PE + Met]^{2+}$ was observed at higher abundance than protonated phospholipid for phosphatidylethanolamine. As an example, Figure 6.1 shows Ca^{2+} , Mg^{2+} , and Co^{2+} -adducted phosphatidylcholine observed in ESI-MS of mixtures of divalent metal ions and phosphatidylcholine. For phosphatidylserine, two types of adducts, $[PL + Met]^{2+}$ and $[PL - 2H + 2Met]^{2+}$, were observed (data not shown). In most cases, ECD was performed on $[PL - 2H + 2Met]^{2+}$, which was typically more abundant than $[PL + Met]^{2+}$.

6.3.2. ECD of Divalent Metal Ion-adducted Phospholipids

Figure 6.2 shows ECD spectra of Ca^{2+} -adducted phospholipids. ECD of Ca^{2+} -adducted phosphatidylcholine provided the most extensive fragmentation. Electrons may be captured by either the electron deficient trimethylamine ($-N(CH_3)_3^+$) headgroup, or by divalent metal ions, which may result in multiple ECD fragmentation pathways. For all three types of phospholipids investigated, product ions involving either sn-1 or sn-2 acyl chain loss were most abundant. In addition, headgroup losses were often observed along with one of the acyl chain losses. For phosphatidylcholine, the product ion $[R_2COOH - H + Ca]^+$ was observed along with its complementary fragment, $[M - R_2COOH]^+$ (the positive charge in this fragment is due to the fixed charge on the trimethylamine headgroup). However, such product ions were not observed in ECD of Ca^{2+} -adducted phosphatidylethanolamine or phosphatidylserine (which do not contain fixed charges). ECD of Mg^{2+} -adducted phospholipids is shown in Figure 6.3. Similar to the calcium adducts, Mg^{2+} -adducted phosphatidylcholine provided the most extensive fragmentation in ECD, compared to Mg^{2+} adducts of other phospholipids. $[R_2COOH - H + Mg]^+$ and/or $[M - R_2COOH]^+$ (for PC)/ $[M - R_2COO + Mg]^+$ (for PE) were obtained in ECD of phosphatidylcholine and phosphatidylethanolamine. However, $[R_2COOH - H + Mg]^+$

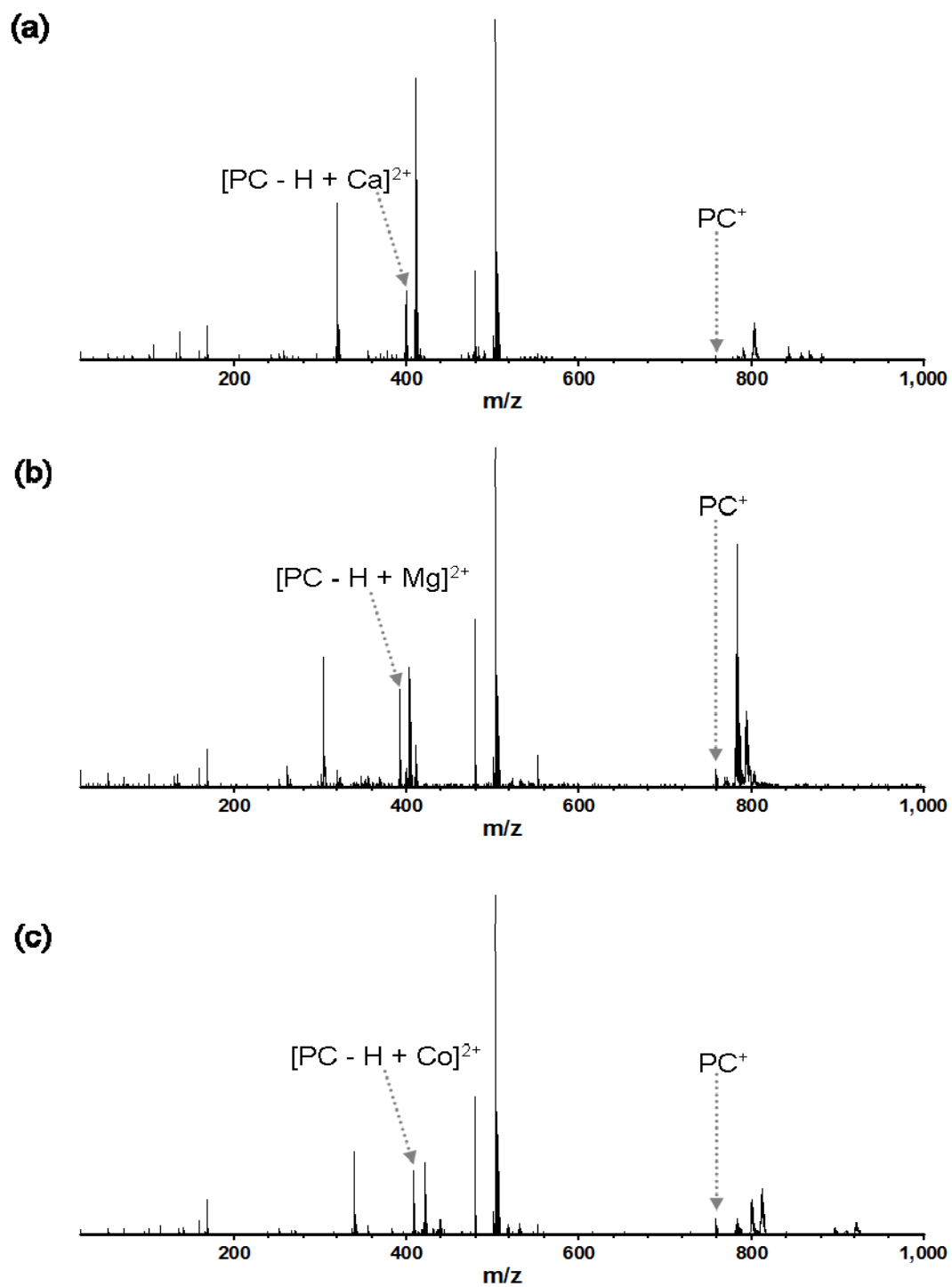


Figure 6.1. ESI mass spectra of phosphatidylcholine from divalent metal-containing solutions; (a) Ca^{2+} solution, (b) Mg^{2+} solution, and (c) Co^{2+} solution. Abundant unassigned peaks are presumably due to sample degradation because these peaks become more abundant with time.

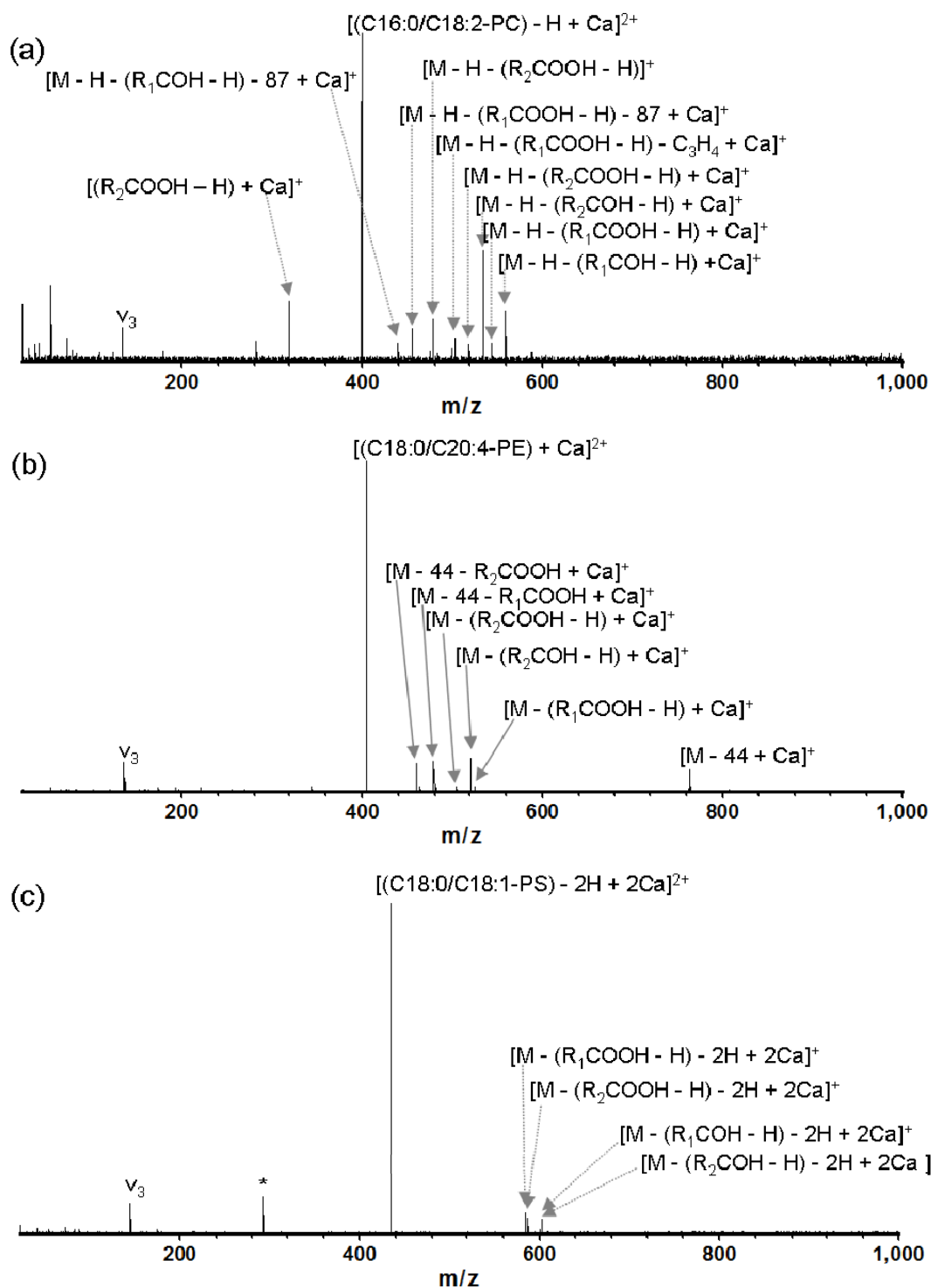


Figure 6.2. ECD of Ca^{2+} -adducted phospholipids; (a) ECD of $[(C16:0/C18:2-PC) - H + Ca]^{2+}$ (b) ECD of $[(C18:0/C20:4-PE) + Ca]^{2+}$ (c) ECD of $[(C18:0/C18:1-PS) - 2H + 2Ca]^{2+}$. Headgroup losses of 87 (for PC) and 44 (for PE) are indicated in Scheme 6.1.

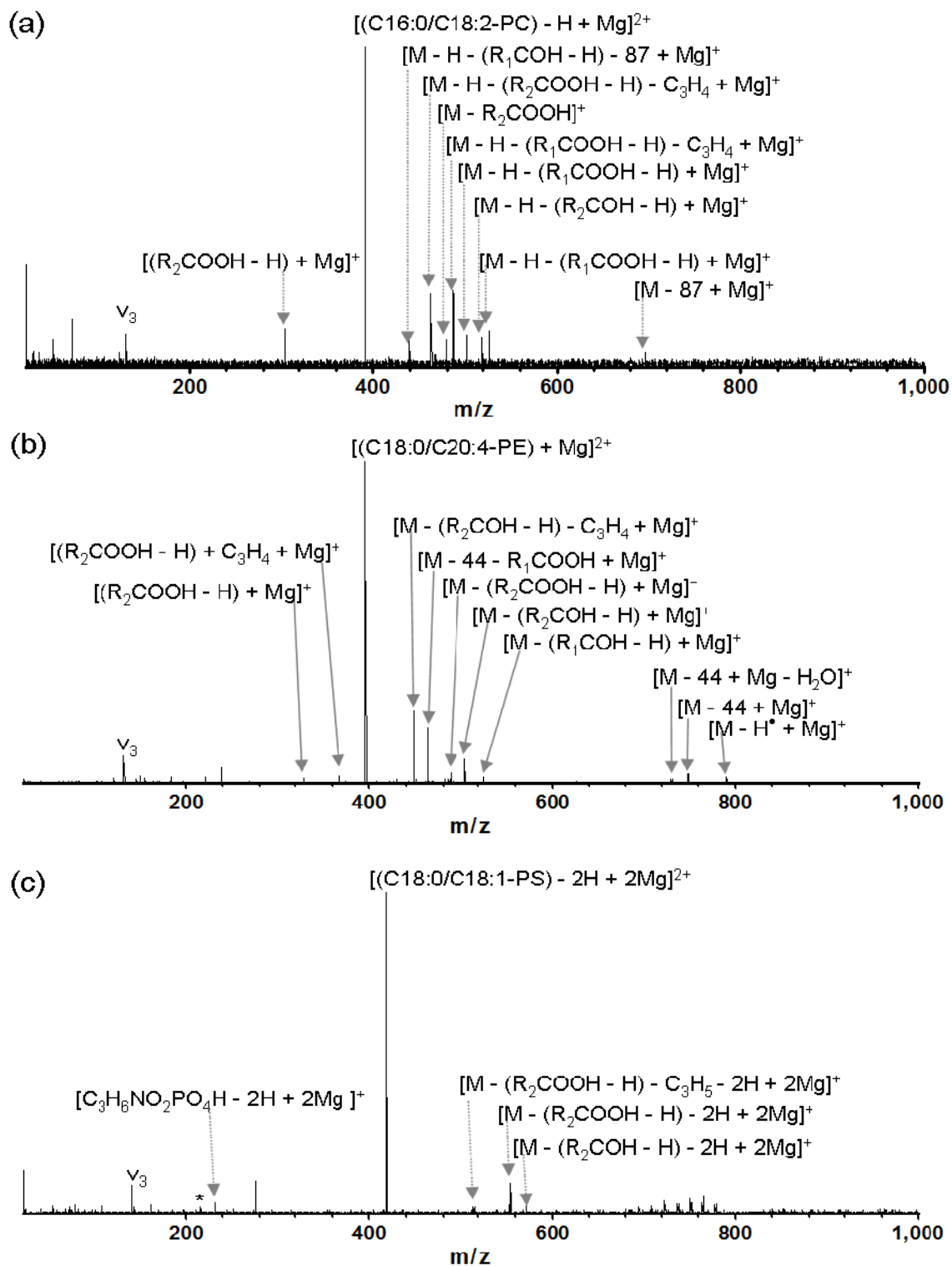


Figure 6.3. ECD of Mg^{2+} -adducted phospholipids; (a) ECD of $[(C16:0/C18:2-PC) - H + Mg]^{2+}$ (b) ECD of $[(C18:0/C20:4-PE) + Mg]^{2+}$ (c) ECD of $[(C18:0/C18:1-PS) - 2H + 2Mg]^{2+}$.

was not observed for phosphatidylserine. Hydrogen radical loss from the charge reduced peak was observed in ECD of Mg^{2+} -adducted phosphatidylethanolamine. Headgroup losses were also observed in ECD of Mg^{2+} -adducted phosphatidylcholine and phosphatidylethanolamine. Product ions involving either sn-1 or sn-2 acyl chain loss constituted major peaks in ECD spectra.

Electrons may be captured by divalent metal ions for divalent metal-adducted phospholipids. Divalent metal ions are likely located near the phosphate group due to Columbic interactions. Thus, the sn-2 esterification site should be more facile to cleave than the sn-1 site, due to its closer proximity to the phosphate group. $[R_2COOH - H + Met]^+$ and $[M - R_2COOH]^+$ for PC ($[M - R_2COO + Met]^+$ for PE) were frequently observed in ECD of Ca^{2+} - or Mg^{2+} -adducted phosphatidylcholine and phosphatidylethanolamine. On the other hand, $[M - R_2COO - 2H + Met]^+$ was observed in ECD of Ca^{2+} - or Mg^{2+} -adducted phosphatidylserine. Based on the argument above, the total product ion abundance involving bond cleavage at the sn-2 acyl chain would be expected to be larger than the total ion abundance involving cleavage at the sn-1 acyl chain. However, this ratio was not always larger than 1 for Mg^{2+} - or Ca^{2+} -adducted phospholipids.

ECD of Co^{2+} - and Zn^{2+} -adducted phospholipids is shown in Figures 6.4 and 6.5. Generally, less extensive fragmentation was observed compared to ECD of Ca^{2+} - or Mg^{2+} -adducted phospholipids. $[R_2COOH - H + Met]^+$ and/or its complementary fragment, $[M - R_2COOH]^+$, were observed in ECD of phosphatidylcholine. The ratio of product ion abundances involving cleavage at the sn-2 vs. sn-1 esterification site is larger

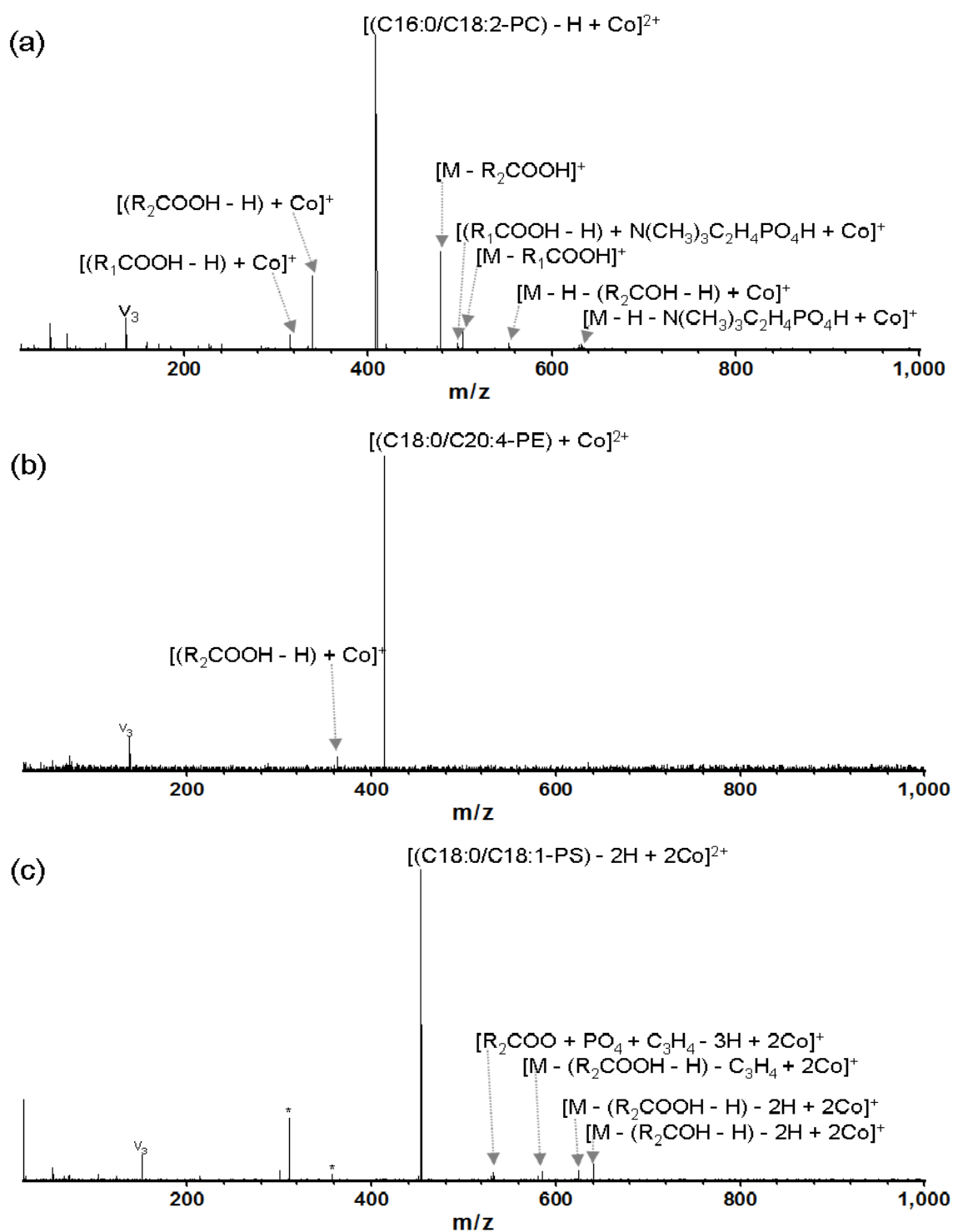


Figure 6.4. ECD of Co^{2+} -adducted phospholipids; (a) ECD of $[(C16:0/C18:2-PC) - H + Co]^{2+}$ (b) ECD of $[(C18:0/C20:4-PE) + Co]^{2+}$ (c) ECD of $[(C18:0/C18:1-PS) - 2H + 2Co]^{2+}$.

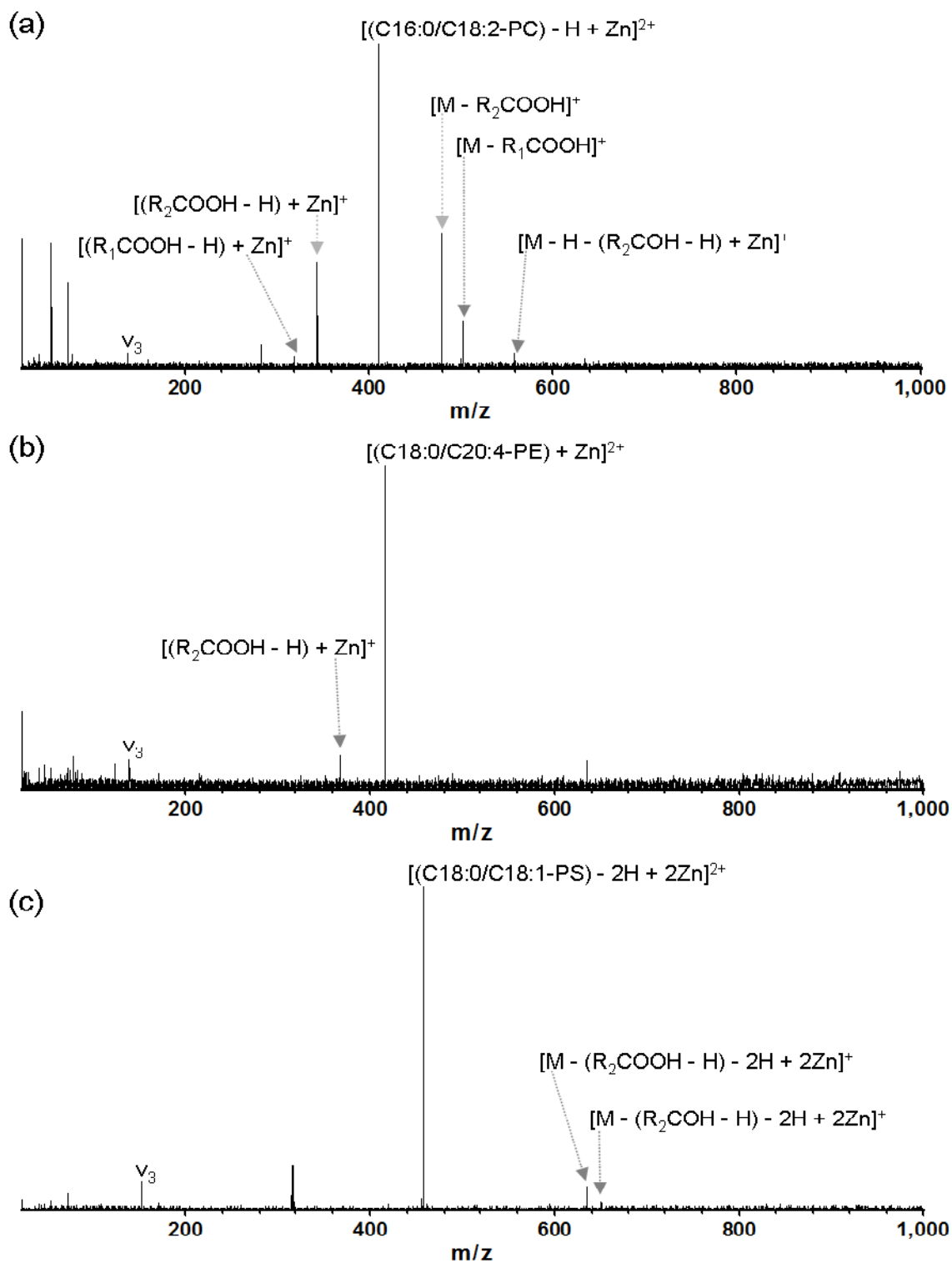


Figure 6.5. ECD of Zn^{2+} -adducted phospholipids; (a) ECD of $[(C16:0/C18:2-PC) - H + Zn]^{2+}$ (b) ECD of $[(C18:0/C20:4-PE) + Zn]^{2+}$ (c) ECD of $[(C18:0/C18:1-PS) - 2H + 2Zn]^{2+}$.

than 1, and no product ions involving bond cleavage at the sn-1 esterification site were observed for phosphatidylserine.

Figure 6.6 shows ECD spectra of Ni²⁺-adducted phospholipids. [R₂COOH - H + Met]⁺ ([R₂COOH - 3H + 2Met]⁺ for PS) were observed in ECD spectra of all phospholipids. However, [M - R₂COOH]⁺, complementary to [R₂COOH - H + Met]⁺ was observed only for phosphatidylcholine. The product ion abundance ratio for cleavage at the sn-2 vs. sn-1 esterification site does not always imply preferred cleavage at the sn-2 position. For Mn²⁺-adducted phospholipids (data not shown), [R₂COOH - H + Met]⁺ and/or the complementary fragment, [M - R₂COO]⁺ were observed only for phosphatidylcholine. The product ion abundance ratio for cleavage at the sn-2 vs. sn-1 esterification site did not always indicate preferred sn-2 site cleavages, similar to ECD of Ni²⁺-adducted phospholipids.

Phospholipid regiochemistry could be deduced from characteristic product ions, such as [R₂COOH - H + Met]⁺ (and [M - R₂COOH]⁺ for PC) observed in ECD of divalent metal ion-adducted phospholipids (as summarized in Table 6.1). In particular, Ni²⁺-adducted phospholipids provided these characteristic product ions in all cases studied. For phosphatidylcholine, divalent metal ion adducts provided characteristic product ions regardless of the type of metal, possibly because the electron deficient headgroup offered another electron capture site, which may result in more extensive ECD fragmentation.

The observed ECD fragmentation patterns are related to the second ionization energy of metal ions. Co²⁺, Zn²⁺, and Ni²⁺, which are weak Lewis acidic metal ions, have

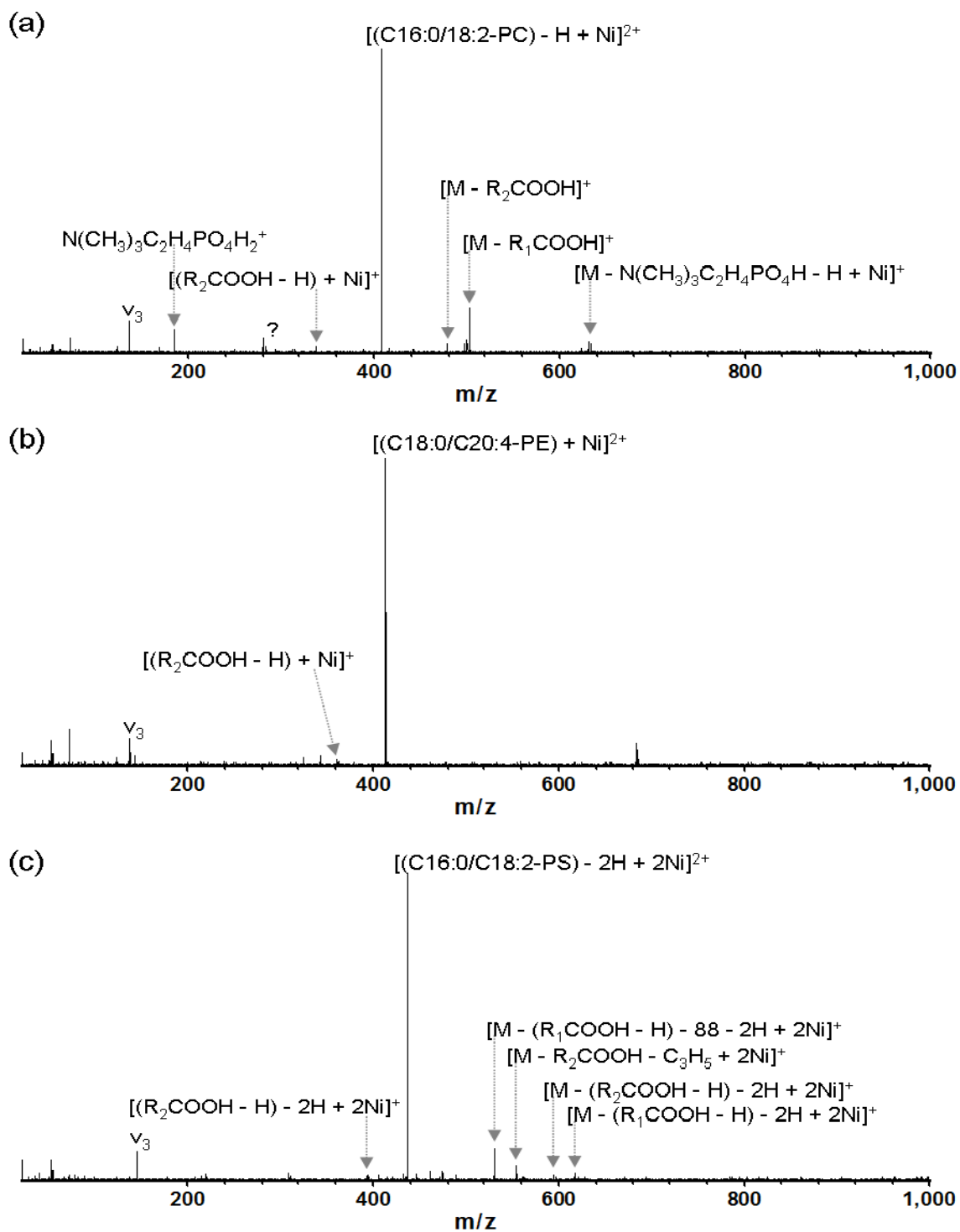


Figure 6.6. ECD of Ni^{2+} -adducted phospholipids; (a) ECD of $[(C16:0/C18:2-PC) - H + Ni]^{2+}$ (b) ECD of $[(C18:0/C20:4-PE) + Ni]^{2+}$ (c) ECD of $[(C16:0/C18:2-PS) - 2H + 2Ni]^{2+}$.

	C18:0/20:4-PE	C18:0/C18:2-PE	C18:0/18:1-PS	C16:0/C18:2-PS	C16:0/C18:1-PC	C16:0/C18:2-PC	C18:1/C16:0-PC	Ionic radii (Å)	IE2 (eV)
Ni	R ₂ COOH - H + Ni (1.34)	R ₂ COOH - H + Ni (2.94)	R ₂ COOH - H + Ni (0.45)	R ₂ COOH - 3H + 2Ni (0.74)	R ₂ COOH - H + Ni M - R ₂ COOH (0.56)	R ₂ COOH - H + Ni (0.31)	R ₂ COOH - H + Ni M - R ₂ COOH (only sn-2)	0.83	18.2
Zn	R ₂ COOH - H + Zn (only sn-2)	R ₂ COOH - H + Zn M - R ₂ COOH (only sn-2)	(only sn-2)	(4.68)	R ₂ COOH - H + Zn (6.25)	R ₂ COOH - H + Zn M - R ₂ COOH (3.05)	R ₂ COOH - H + Zn M - R ₂ COOH (2.28)	0.88	18
Co	R ₂ COOH - H + Co (only sn-2)	R ₂ COOH - H + Co (3.26)	(only sn-2)	(3.09)	R ₂ COOH - H + Co M - R ₂ COOH (7.48)	R ₂ COOH - H + Co M - R ₂ COOH (4.18)	R ₂ COOH - H + Co M - R ₂ COOH (4.24)	0.75/0.88 ^c	17.1
Mn	(3.39)	(0.48)	(3.27)	R ₂ COOH - H + Mn (0.94)	R ₂ COOH - H + Mn + H ₂ (6.35)	R ₂ COOH - H + Mn M - R ₂ COOH (4.18)	M - R ₂ COOH (1.51)	0.81/0.97 ^c	16.2
Mg	R ₂ COOH - H + Mg (1.92)	(0.38)	(5.39)	(4.19)	R ₂ COOH - H + Mg M - R ₂ COOH (0.33)	R ₂ COOH - H + Mg M - R ₂ COOH (1.90)	(4.81)	0.86	15
Ca	(1.90)	(1.16)	(1.15)	(0.30)	R ₂ COOH - H + Ca M - R ₂ COOH (1.91)	R ₂ COOH - H + Ca M - R ₂ COOH (1.59)	R ₂ COOH - H + Ca M - R ₂ COOH (4.10)	1.14	11.9
Ba	(1.92)	(1.13)	(5.69)	(1.59)	R ₂ COOH - H + Ba M - R ₂ COOH (1.62)	R ₂ COOH - H + Ba (1.66)	R ₂ COOH - H + Ba M - R ₂ COOH (2.25)	1.49	10

Table 6.1. Observation of [R₂COOH - H + Met]⁺ and [M - R₂COOH]⁺ (for PC), and the ratio of the sum of total product ion abundances involving bond cleavage at the sn-2 to that of total product ion abundances involving bond cleavage at the sn-1 esterification site in ECD spectra of divalent metal-adducted phospholipids. The ratio of product ion abundances involving cleavage at the sn-2 and sn-1 sites is shown in parenthesis. ‘Only sn-2’ means no product ions were observed from cleavage at the sn-1 position.

second ionization energies (IE2) of 17.1 eV, 18.0 eV, and 18.2 eV respectively. Divalent metal ions, which are plausible electron capture sites on metal adducted-phospholipids, are expected to be located near the phosphate group due to Coulombic interactions. Thus, product ions involving cleavage of the sn-2 esterification site would be expected to be dominant due to closer proximity to phosphate group. In addition, these metal ions may interact with the acyl chains, because the latter are weak Lewis bases. In that case, R_2COOH fragments would have higher affinity for weaker Lewis acidic metal ions, and should be observed as $[R_2COOH - H + Met]^+$ in ECD spectra. Also, the metal ion with highest IE2 should capture electrons more preferentially and with higher energy release, thereby potentially resulting in more efficient ECD fragmentation. The lowest IE2 of Ni^{2+} among the metals investigated may explain why $[R_2COOH - H + Met]^+$ was only consistently observed in ECD of Ni^{2+} -adducted phospholipids. On the other hand, $[R_2COOH - H + Met]^+$ was observed only for phosphatidylethanolamine and phosphatidylcholine in ECD of Co^{2+} - and Zn^{2+} -adducted phospholipids. IE2s of Co^{2+} and Zn^{2+} are lower than that of Ni^{2+} , correlating with the observed less efficient ECD fragmentation and possibly explaining why $[R_2COOH - H + Met]^+$ was not consistently observed in ECD of Co^{2+} - or Zn^{2+} -adducted phospholipids.

The divalent metal ions with lowest IE2s are Ca^{2+} (11.9 eV) and Ba^{2+} (10.0 eV). These ions should prefer to exist as divalent rather than monovalent metal ions and therefore not capture electrons as efficiently as divalent metal ions with higher IE2s, such as Ni^{2+} . Thus, these metal-adducted phospholipids may result in poor ECD efficiency. Only phosphatidylcholine, which has an additional electron capture site, ($-N^+(CH_3)_3$), provided $[R_2COOH - H + Met]^+$ product ions in ECD. The additional electron capture

site in phosphatidylcholine may enhance ECD efficiency, and consistently provide $[\text{R}_2\text{COOH} - \text{H} + \text{Met}]^+$ in ECD spectra. In addition, positively charged $\text{N}^+(\text{CH}_3)_3$ may promote divalent metal ion binding closer to the sn-2 acyl chain due to Coulombic repulsion and therefore more easily generate $[\text{R}_2\text{COOH} - \text{H} + \text{Met}]^+$ ions. Mg^{2+} and Mn^{2+} have IE2s of 15.0 eV and 16.2 eV, respectively. Phosphatidylcholine consistently provided $[\text{R}_2\text{COOH} - \text{H} + \text{Met}]^+$ product ions for these two metal ions. However, $[\text{R}_2\text{COOH} - \text{H} + \text{Met}]^+$ was not always observed in ECD of phosphatidylethanolamine and phosphatidylserine, presumably because their second ionization energies are not as high as those of Ni^{2+} , Co^{2+} , and Zn^{2+} , and are therefore not expected to capture electrons as efficiently as other divalent metal ions. In addition, Ca^{2+} and Ba^{2+} are expected to form less stable adducts with phospholipids, because they are known to yield less stable adducts with acetylphosphate, acetylphosphonate,⁴⁷ and carboxylate,⁴⁸ compared to transition metal ions with the same charge states. Thus, the ECD fragmentation of Ca^{2+} - and Ba^{2+} -adducted phospholipids may not be as informative as that of Co^{2+} -, Zn^{2+} -, and Ni^{2+} -adducted phospholipids.

The ionic radius of divalent metal ions may also play a role in product ion abundances in ECD spectra. Figure 6.7 shows ECD spectra of Ba^{2+} -adducted phospholipids. Ba^{2+} would not be expected to provide $[\text{R}_2\text{COOH} - \text{H} + \text{Met}]^+$ product ions due to its hard Lewis acidic property and low IE2. The ionic radius (1.49 Å) of Ba^{2+} is the largest among the divalent metal ions studied. The larger size of the metal ion provides a greater inductive effect when neutral oxygen donors, such as fatty acyl groups in phospholipids, are nearby.⁴⁹ Ba^{2+} interacts mainly with the phosphate group due to electrostatic interaction, however, its greater inductive effect may also provide effective

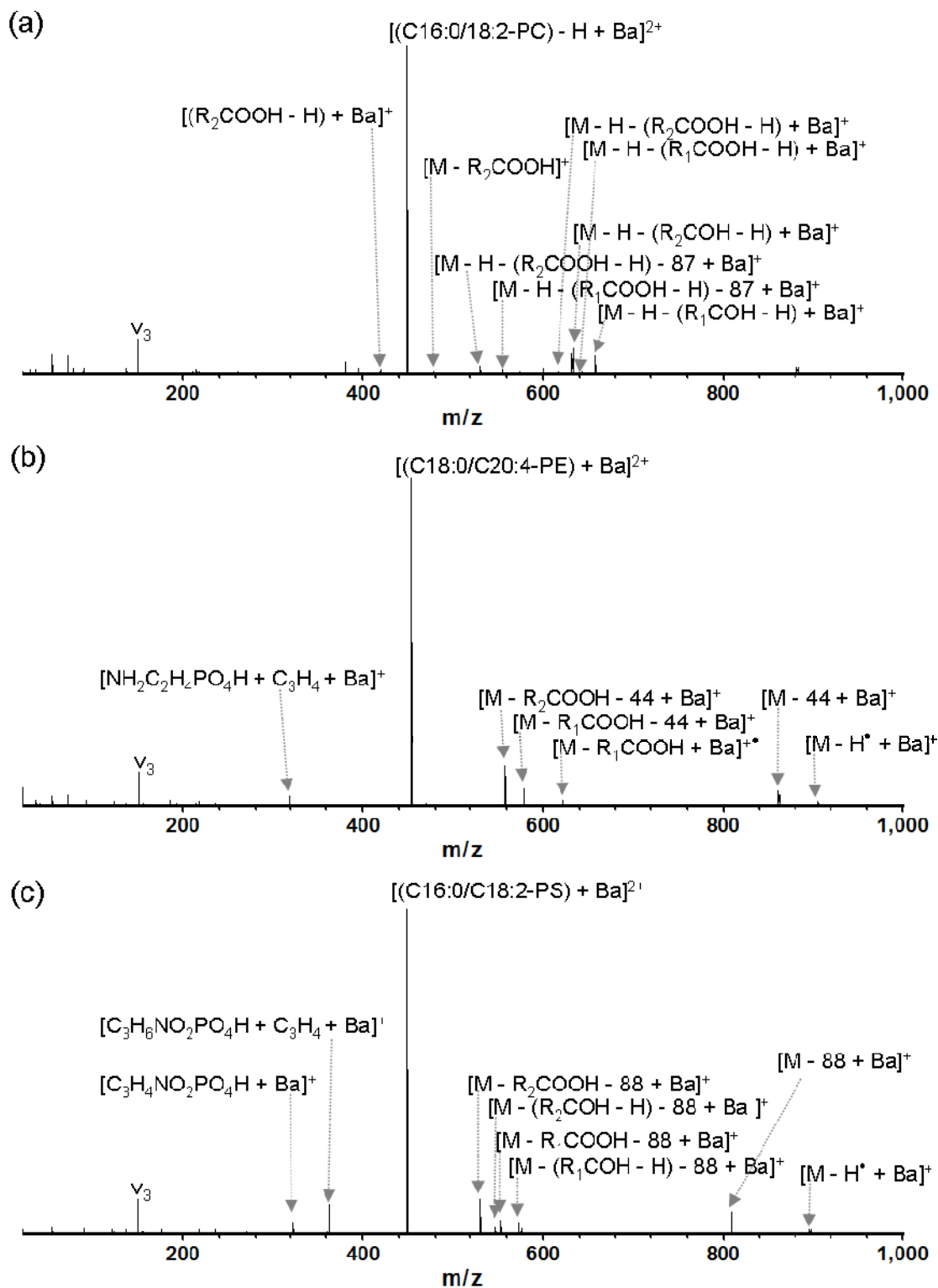


Figure 6.7. ECD of Ba^{2+} -adducted phospholipids; (a) ECD of $[(C16:0/C18:2-PC) - H + Ba]^{2+}$ (b) ECD of $[(C18:0/C20:4-PE) + Ba]^{2+}$ (c) ECD of $[(C16:0/C18:2-PS) + Ba]^{2+}$.

interaction between the metal ion and oxygens in fatty acids. Consistently, more abundant product ions involving bond cleavage at the sn-2 esterification site compared to the sn-1 site were observed for Ba²⁺-adducted phospholipids. However, [R₂COOH - H + Met]⁺ fragments are still not observed because hard Lewis acidic Ba²⁺ may hinder interactions with weak Lewis basic fatty acids. On the other hand, for the smaller size divalent metal ions such as Ni²⁺ (0.83 Å), the product ions involving cleavage at the sn-2 site were not favored either, even when [R₂COOH - H + Met]⁺ was consistently observed. For Co²⁺- or Zn²⁺-adducted phospholipids, sn-2 site cleavages were consistently preferred over sn-1 site cleavages, although the sizes of these ions are not as large as Ba²⁺. The lower IE₂ of these ions may play a role because, in many cases, only sn-2 cleavages are observed in ECD spectra.

Unambiguous regiochemical information of phospholipids could be deduced from the characteristic product ions ([R₂COOH - H + Met]⁺ (and [M - R₂COOH]⁺ for PC) for weak Lewis acid metal ions such as Ni²⁺, or more abundant product ions involving sn-2 cleavages compared to sn-1 cleavages for hard Lewis acid metal ions with larger ionic radius such as Ba²⁺.

6.4. Conclusions

In the research presented here, ECD of divalent metal-adducted phospholipids, [PL + Met]²⁺ or [PC - H + Met]²⁺, was explored. Ni²⁺, the weakest Lewis acidic metal among the divalent metal ions investigated, should capture electrons most efficiently and the presence of nickel resulted in efficient ECD fragmentation. In addition, Ni²⁺ is likely to

reside near acyl chains due to their weak Lewis base character and the weak Lewis acid character of Ni^{2+} . In correlation with this hypothesis, $[\text{R}_2\text{COOH} - \text{H} + \text{Ni}]^+$ (and $[\text{M} - \text{R}_2\text{COOH}]^+$ for PC) were consistently observed in ECD of Ni^{2+} -adducted phospholipids. Thus phospholipid regiochemistry could be determined from the observation of nickel-adducted acyl chain, $[\text{R}_x\text{COOH} - \text{H} + \text{Ni}]^+$, which should originate from the sn-2 position. Ba^{2+} may reside near the phosphate group due to its hard Lewis acidic property, and its large ionic radius, which may result in effective interaction between the metal ion and oxygens in the sn-2 fatty acyl chains. Thus, the ratio of the sum of total product ion abundances involving bond cleavage at the sn-2 to that of total product ion abundances involving bond cleavage at the sn-1 esterification site should be larger than 1, however, $[\text{R}_2\text{COOH} - \text{H} + \text{Ba}]^+$ ions was not always observed for all phospholipids.

6.5. References

1. Anderson, H. A.; Maylock, C. A.; Williams, J. A.; Paweletz, C. P.; Shu, H.; Shacter, E. *Nat Immunol* **2003**, *4*, 87-91.
2. Irvine, R. F. *Nat Rev Mol Cell Biol* **2003**, *4*, 349-360.
3. Wenk, M. R.; Lucast, L.; Di Paolo, G.; Romanelli, A. J.; Suchy, S. F.; Nussbaum, R. L.; Cline, G. W.; Shulman, G. I.; McMurray, W.; De Camilli, P. *Nat Biotechnol* **2003**, *21*, 813-817.
4. Mills, G. B.; Moolenaar, W. H. *Nat Rev Cancer* **2003**, *3*, 582-591.
5. Zegzouti, H.; Anthony, R. G.; Jahchan, N.; Bogre, L.; Christensen, S. K. *Proc Natl Acad Sci U S A* **2006**, *103*, 6404-6409.
6. Esmon, N. L.; Smirnov, M. D.; Esmon, C. T. *Haematologica* **1997**, *82*, 474-477.
7. Meijer, H. J.; Munnik, T. *Annu Rev Plant Biol* **2003**, *54*, 265-306.
8. Prestwich, G. D. *Prostaglandins Other Lipid Mediat* **2005**, *77*, 168-178.
9. Dugo, P.; Favoino, O.; Tranchida, P. Q.; Dugo, G.; Mondello, L. *J Chromatogr A* **2004**, *1041*, 135-142.
10. Han, J. J.; Yamane, T. *Lipids* **1999**, *34*, 989-995.
11. Xu, X.; Fomuso, L. B.; Akoh, C. C. *J Agric Food Chem* **2000**, *48*, 3-10.
12. Cheng, C.; Gross, M. L. *Mass Spectrom Rev* **2000**, *19*, 398-420.
13. Han, X.; Gross, R. W. *J Am Soc Mass Spectrom* **1995**, *6*, 1202-1210.
14. Huang, Z. H.; Gage, D. A.; C., S. C. *J Am Soc Mass Spectrom* **1992**, *3*, 71-78.

15. Clay, K. L. M., R. C. *Biomed Mass Spectrom* **1983**, *10*. 489-494.
16. Hvattum, E.; Hagelin, G.; Larsen, A. *Rapid Commun Mass Spectrom* **1998**, *12*. 1405-1409.
17. Pulfer, M.; Murphy, R. C. *Mass Spectrom Rev* **2003**, *22*. 332-364.
18. Han, X.; Gross, R. W. *Proc Natl Acad Sci U S A* **1994**, *91*. 10635-10639.
19. Hsu, F. F.; Turk, J. *J Am Soc Mass Spectrom* **2005**, *16*. 1510-1522.
20. Ho, Y. P.; Huang, P. C.; Deng, K. H. *Rapid Commun Mass Spectrom* **2003**, *17*. 114-121.
21. Marshall, A. G.; Hendrickson, C. L.; Jackson, G. S. *Mass Spectrom Rev* **1998**, *17*. 1-35.
22. Aharoni, A.; Ric de Vos, C. H.; Verhoeven, H. A.; Maliepaard, C. A.; Kruppa, G.; Bino, R.; Goodenowe, D. B. *Omic* **2002**, *6*. 217-234.
23. Little, D. P.; Speir, J. P.; Senko, M. W.; O'Connor, P. B.; McLafferty, F. W. *Anal Chem* **1994**, *66*. 2809-2815.
24. Woodin, R. L.; Bomse, D. S.; Beauchamp, J. L. *J Am Chem Soc* **1978**, *100*. 3248-3250.
25. Budnik, B. A.; Haselmann, K. F.; Elkin, Y. N.; Gorbach, V. I.; Zubarev, R. A. *Anal Chem* **2003**, *75*. 5994-6001.
26. Cody, R. B.; Freiser, B. S. *Anal Chem* **1979**, *51*. 541-551.
27. Lioe, H.; O'Hair, R. A. *Anal Bioanal Chem* **2007**, *389*. 1429-1437.
28. Zubarev, R. A.; Kellerher, N. L.; McLafferty, F. W. *J Am Chem Soc* **1998**, *120*. 3265-3266.
29. Zubarev, R. A. *Curr Opin Biotechnol* **2004**, *15*. 12-16.
30. Zubarev, R. A.; Horn, D. M.; Fridriksson, E. K.; Kelleher, N. L.; Kruger, N. A.; Lewis, M. A.; Carpenter, B. K.; McLafferty, F. W. *Anal Chem* **2000**, *72*. 563-573.
31. Yoo, H. J.; Liu, H.; Hakansson, K. *Anal Chem* **2007**, *20*. 7858-7866.
32. Adamson, J. T.; Hakansson, K. *J Proteome Res* **2006**, *5*. 493-501.
33. Adamson, J. T.; Hakansson, K. *Anal Chem* **2007**, *79*. 2901-2910.
34. Cooper, H. J.; Hakansson, K.; Marshall, A. G. *Mass Spectrom Rev* **2005**, *24*. 201-222.
35. Hakansson, K.; Chalmers, M. J.; Quinn, J. P.; McFarland, M. A.; Hendrickson, C. L.; Marshall, A. G. *Anal Chem* **2003**, *75*. 3256-3262.
36. Hakansson, K.; Cooper, H. J.; Emmett, M. R.; Costello, C. E.; Marshall, A. G.; Nilsson, C. L. *Anal Chem* **2001**, *73*. 4530-4536.
37. McLafferty, F. W.; Horn, D. M.; Breuker, K.; Ge, Y.; Lewis, M. A.; Cerda, B.; Zubarev, R. A.; Carpenter, B. K. *J Am Soc Mass Spectrom* **2001**, *12*. 245-249.
38. James, P. F.; Perugini, M. A.; O'Hair, R. A. *J Am Soc Mass Spectrom* **2008**, *19*. 978-986.
39. Yoo, H. J. H., K. in *Pittcon 2009*. Philadelphia, **2009**.
40. Fang, J.; Barcelona, M. J. *J Microbio Methods* **1998**, *33*. 23-35.
41. Yang, J.; Mo, J.; Adamson, J. T.; Hakansson, K. *Anal Chem* **2005**, *77*. 1876-1882.
42. Belov, M. E.; Nikolaev, E. N.; Anderson, G. A.; Udseth, H. R.; Conrads, T. P.; Veenstra, T. D.; Masselon, C. D.; Gorshkov, M. V.; Smith, R. D. *Anal Chem* **2001**, *73*. 253-261.

43. Hendrickson, C. L.; Quinn, J. P.; Emmett, M. R.; Marshall, A. G., in *49th ASMS Conference on Mass Spectrometry and Allied Topics*. Chicago, IL, 2001; CD-ROM.
44. de Koning, L. J. N., N. M. M.; van Orden, S. L.; Laukien, F. H. *Int. J. Mass Spectrom.* **1997**, *165*. 209-219.
45. Tsybin, Y. O.; Witt, M.; Baykut, G.; Kjeldsen, F.; Hakansson, P. *Rapid Commun Mass Spectrom* **2003**, *17*. 1759-1768.
46. Senko, M. W.; Canterbury, J. D.; Guan, S.; Marshall, A. G. *Rapid Commun Mass Spectrom* **1996**, *10*. 1839-1844.
47. Sigel, H. C., C. P.; Song, B.; Carloni, P.; Gregan, F. *J. Am. Chem. Soc.* **1999**, *121*. 6248-6257.
48. Bunting, J. W. T., K. M. *Can. J. of Chem.* **1969**, *48*. 1654.
49. Hancock, R. D. *Pure & Appl. Chem.* **1986**, *58*. 1445-1452.

Chapter 7

Electron Capture by Peptide Anions: Direct Dissociation and Radical-Driven MS³

7.1. Introduction

Gas-phase ion-electron reactions are growing in popularity for ion activation in tandem mass spectrometry. Examples include electron capture dissociation (ECD),¹⁻⁴ hot electron capture dissociation (HECD),⁵ electron ionization dissociation,⁶ electron detachment dissociation (EDD),⁷⁻¹⁰ and electron induced dissociation (EID).¹¹⁻¹³ These tandem mass spectrometric strategies are used for structural analyses of various kinds of biomolecules, including peptides,^{1-2, 4} oligonucleotides,⁸ oligosaccharides,^{1-2, 4, 9, 14-16} and smaller organic molecules.^{13, 17-18}

The fragmentation patterns observed in electron-mediated MS/MS are different from those observed in vibrational excitation techniques, such as collision induced dissociation (CID) and, therefore, electron-based activation provides complementary information compared to traditional MS/MS. Many post-translational modifications (PTMs), such as phosphorylation and glycosylation, are labile in the gas phase and

information on their position is therefore lost during CID.¹⁹ The mechanism of ECD, the most widely used electron-based MS/MS technique, is still under debate. There are two main hypotheses: first, ECD is believed to be a nonergodic process, thus not necessarily favoring cleavage of the most labile bonds, which results in retention of PTMs.^{4, 20} Therefore, a major attraction of ECD is the possibility to localize PTMs.^{3,21} The second proposed explanation to this behavior is that peptide backbone N-C_α bonds are weakened following electron capture into an amide π* orbital.²² In either mechanism, a charge-reduced radical intermediate is generated, which dissociates into N-terminal *c'* fragments and C-terminal *z'* fragments from backbone N-C_α bond cleavage.⁴ In contrast, vibrational excitation techniques provide amide (C(O)-N) backbone bond cleavage that produces N-terminal *b* and C-terminal *y'* ions.

Maximum fragmentation efficiency in ECD occurs at ~ 0 eV electrons, however a second maximum, ~7 eV, has also been observed and the resulting fragmentation process is termed hot electron capture dissociation (HECD). In HECD, a hot electron is proposed to lose kinetic energy from collisions with molecular cations and decelerated electrons are then captured by the excited molecular ions.⁵ Similar to ECD, N-C_α bond cleavages are observed in HECD, however, in addition, secondary fragmentation of amino acid side chains in *z'* fragments results in *w* ions, which allow differentiation between the isomeric amino acids leucine and isoleucine.^{5, 23-24} More recently, electron ionization and subsequent extensive dissociation has been reported following irradiation of [M + nH]ⁿ⁺ (n ≥ 1) cations with fast electrons (at least 10 eV higher than the ionization energy of the cations, i.e., electron energies above 20 eV). Such irradiation causes double ionization to [M + nH]⁽ⁿ⁺²⁾⁺ followed by electron capture to form electronically excited [M + nH]⁽ⁿ⁺

^{1)++*} ions. Dissociation of such ions yields both side-chain losses and backbone fragmentation. Both N-C_α bond cleavage, resulting in *c*-/*z*-type fragments and C-C bond cleavage, yielding *a*-/*x*-type fragments are observed in electron ionization dissociation.⁶
²⁵ Unfortunately, the acronym introduced for this process is “EID” (the same as for electron induced dissociation). Here, we will refer to electron ionization dissociation as “Zubarev EID”.

In contrast to positively charged peptide ions, capture of low energy electrons by negatively charged peptide ions appears unlikely due to Coulombic repulsion. Instead, EDD was introduced for multiply negatively charged ions. In EDD, relatively high energy electrons (> 10 eV) are used to ionize negative ions via electron detachment, resulting in hydrogen-deficient radical anions. Neutral loss of CO₂ (and SO₃ for sulfopeptides) are prominent in EDD but *a*-, *c*-, and *z*-type product ions from peptide backbone cleavage are also observed.⁷

Electron induced dissociation (EID) was first shown in 1979 by Cody and Freiser for radical cations.¹² Precursor and product ions have the same charge state in EID, i.e., no oxidation or reduction occurs but electronic excitation can provide complementary fragmentation compared to CID. One attraction of EID is that it is compatible with singly charged precursor ions, whereas ECD, HECD, and EDD require precursor ions to carry at least two charges. By contrast, Zubarev EID is compatible with singly charged cations but not with anions. Thus, ECD, HECD, and EDD are not directly compatible with small biomolecule analysis (such as metabolomics) because the smaller size of such molecules makes multiple charging energetically unfavorable in the gas phase. EID has been explored for structural analysis of, e.g., metabolites and oligosaccharides.^{13, 15}

It has been proposed that ECD involves radical migration and that radicals may propagate intramolecularly to induce a cascade of bond cleavages throughout a peptide ion.²⁶ O'Connor and co-workers used coumarin tags as radical traps to test the hypothesis that ECD involves long-lived radical intermediates and that radical migration is necessary for efficient fragmentation.²⁷ The large sp^2 conjugated system of coumarin can efficiently trap radicals and addition of coumarin tags to peptides resulted in dramatic reduction of backbone bond fragmentation due to the decreased mobility of the radicals.²⁸

Here, we hypothesized that coumarin tags may aid electron capture by anions and we also explored a wide electron energy range for maximum electron capture efficiency. We found that peptide anions can capture electrons within a rather narrow energy range. Coumarin-tagged peptides provided higher electron capture efficiency than non-derivatized peptides, however, infrared multiphoton dissociation (IRMPD) MS^3 of the more highly charged radical species produced from electron capture did not result in structurally informative fragments. By contrast, electron irradiation, within a similarly narrow energy range, of many underivatized peptide anions resulted in extensive backbone fragmentation, strikingly similar to ECD in positive ion mode. We refer to this novel technique as negative ion electron capture dissociation (niECD). Negatively charged, distonic radical species generated by electron capture of peptide anions were also isolated and subjected to IRMPD MS^3 .

7.2. Experimental Section

7.2.1. Sample Preparation

The following peptides were used: GNLWATGHFM (neuromedin B), DMHDFVGLM (neurokinin B), EHWSYGLRPG, YPISL (exorphin C), RRREEEpSEEEAA, KRSpYEEHIP, DRVYIHPFHL (angiotensin I), RRApSVA, TSTEPQpYQPGENL-NH₂, PPGFSPFR, RPKPQQFFGLM (substance P), and DsYMGWMDf-NH₂ (CCKS). Most peptides were purchased from Sigma-Aldrich (St. Louis, MO), except TSTEPQpYQPGENL-NH₂ (which was from Millipore, Billerica, MA) and DsYMGWMDf-NH₂ (from Advanced Chemtech, Louisville, NY). Bovine milk α - and β -casein were from Sigma-Aldrich. Coumarin tag (7-methoxycoumarin-3-carboxylic acid succinimidyl ester) was from Sigma-Aldrich. The above chemicals were used without further purification. Coumarin tagging reaction was performed according to a published procedure,²⁷ except for using longer reaction time (~ 1 h). Trypsin (Promega, Madison, WI) digestion of α -/ β -casein was performed for 12 h at 37 °C at an enzyme/substrate ratio of 1:50. The tryptic peptides FQpSEEQQQTEDELQDK (β -casein 48-63), YLGYLEQLLR (α -casein 106-115), and VPQLEIVPNpSAEER (α -casein 121-134) were subjected to MS/MS. Phosphopeptide enrichment was performed with ZrO₂ microtips (Glygen, Columbia, MD), when necessary.²⁹ 5-10 μ M peptide solutions were prepared in 50/50 (v/v, H₂O/isopropanol) with 0.1 % triethylamine.

7.2.2. Fourier Transform Ion Cyclotron Resonance Mass Spectrometry

Negatively charged peptide ions were generated by external ESI at 70 μ L/h (Apollo II ion source, Bruker Daltonics, Billerica, MA). All experiments were performed with a 7 Tesla quadrupole (Q)-FT-ICR mass spectrometer (APEX-Q, Bruker Daltonics) as

previously described.⁸ All data were obtained in negative ion mode. For ESI, N₂ was used as both nebulizing gas (5 L/s) and drying gas (2.5 L/s). The drying gas temperature was set to 200°C. Briefly, ions produced by ESI were mass-selectively externally accumulated in a hexapole for 0.2-3 s, transferred via high voltage ion optics, and captured in the ICR cell by dynamic trapping. This accumulation sequence was looped three times to improve precursor ion abundance. For MS/MS experiments, mass-selective external accumulation of negatively charged peptide ions was performed. For niECD, mass selectively accumulated peptide ions were irradiated for 10-20 s with ~ 6-7 eV electrons provided by an indirectly heated hollow dispenser cathode.³⁰ A lens electrode located in front of the hollow cathode was kept ~ 1.5 V lower than bias voltage. For isolation of radical species produced from electron capture by negatively charged peptide ions, correlated harmonic excitation fields (CHEF) was performed inside the ICR cell.³¹ For MS³, IRMPD was performed inside the ICR cell with a 25 W, 10.6 μm, CO₂ laser (Synrad, Mukilteo, WA). The laser beam was deflected by two mirrors for alignment through a hollow dispenser cathode to the center of the ICR cell. The beam entered the vacuum system through a BaF₂ window. Photon irradiation was performed for 300-700 ms at 7.5-10 W laser power. CID was performed in an external hexapole at a collision cell DC offset of 20-40 V with argon as collision gas. For EDD, doubly deprotonated precursor ions were irradiated with ~20 eV electrons for 1-2 s.

All mass spectra were acquired with XMASS software (version 6.1, Bruker Daltonics) in broadband mode from m/z 200 to 3000 with 256K data points and summed over 10-32 scans. Data processing was performed with the MIDAS analysis software.³² Peaks in MSⁿ were assigned within 10 ppm error after internal calibration. For example,

internal calibration was performed with precursor ions and their electron-capture species as calibrants.

7.3. Results and Discussion

7.3.1. Electron Capture by Negatively Charged Peptides

Figure 7.1a shows an electrospray ionization Fourier transform ion cyclotron resonance (ESI-FT-ICR) mass spectrum following coumarin-tagging of the peptide angiotensin I. Angiotensin I with and without coumarin was observed in singly and doubly deprotonated forms. Electron irradiation (~ 6 eV electrons, 20 s) of quadrupole-isolated singly deprotonated coumarin-tagged angiotensin I, $[M + \text{tag} - H]^-$, provided very abundant radical species, $[M + \text{tag} - H]^{2-\bullet}$, generated from electron capture by the coumarin-tagged peptide, as shown in Figure 7.1b. This radical species was further isolated inside the ICR cell and subjected to IRMPD MS^3 , which resulted in electron loss to reform $[M + \text{tag} - H]^-$, and loss of NH^\bullet with and without H_2O loss from the $[M + \text{tag} - H]^{2-\bullet}$ radical precursor (Figure 7.1c). Similar to the observations by O'Connor and co-workers,²⁷ product ions mainly involving small radical loss were obtained in IRMPD MS^3 of the radical species, $[M + \text{tag} - H]^{2-\bullet}$, presumably due to the low mobility of the radicals. Similar experiments with other peptides, including substance P, also revealed that the presence of a coumarin tag enhances electron capture by peptide anions and produces abundant radical species following electron irradiation. However, IRMPD MS^3 of these more highly charged radical species resulted in small radical losses and very limited backbone bond fragmentation (data not shown).

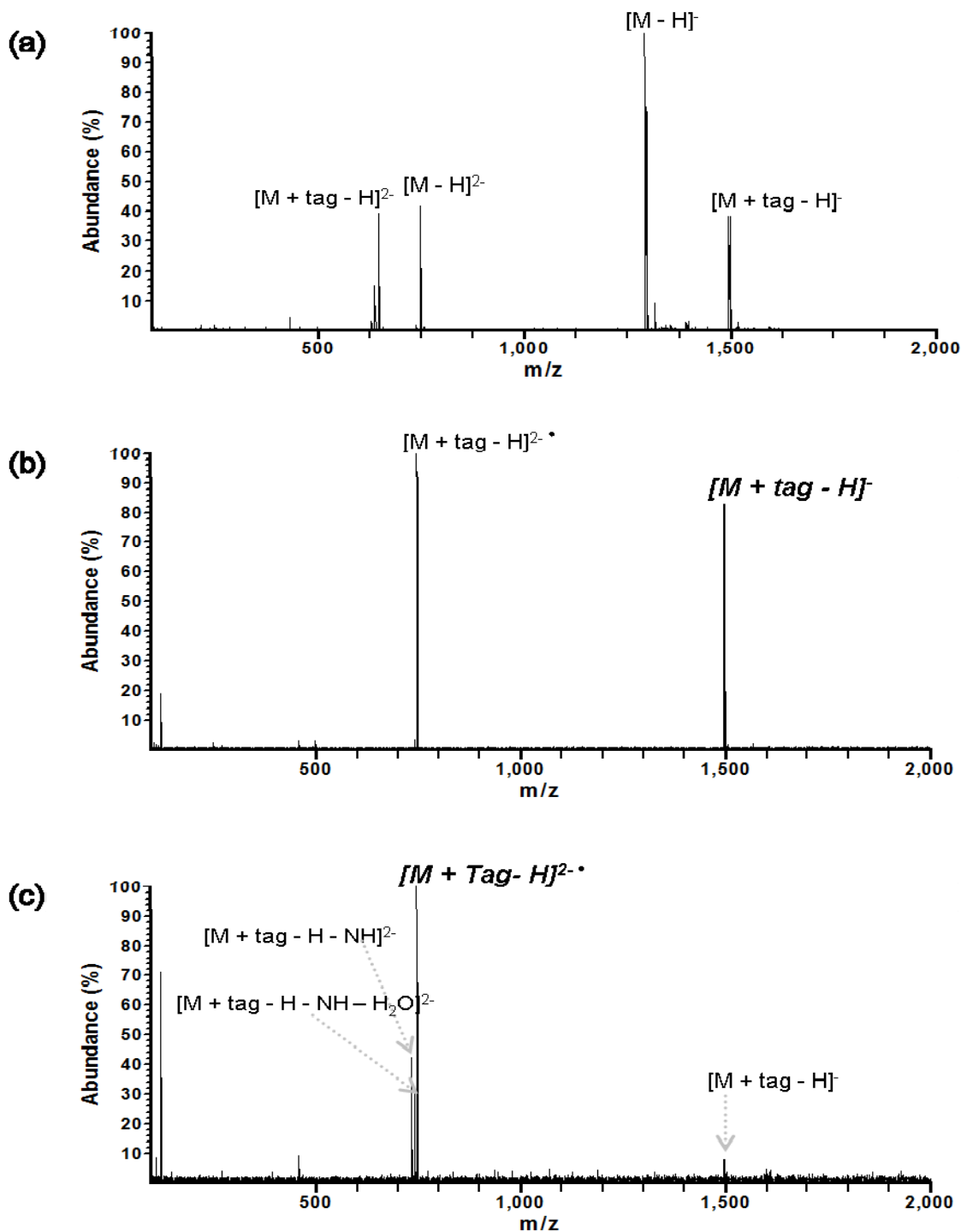


Figure 7.1. Activation and dissociation of coumarin-tagged angiotensin I: (a) ESI FT-ICR mass spectrum of the reaction mixture of coumarin and angiotensin I. (b) electron irradiation (~6 eV electrons for 20s) of singly-tagged angiotensin I, $[M + tag - H]^-$ to form $[M + tag - H]^{2\bullet-}$, (c) IRMPD MS^3 of $[M + tag - H]^{2\bullet-}$ (7.5 W laser power for 500 ms). Peak labels in bold and italics indicate precursor ions used for activation/fragmentation.

Figure 7.2a shows electron irradiation of singly deprotonated angiotensin I without coumarin tag, $[M - H]^-$. Here, the electron capture efficiency is lower compared to coumarin-tagged angiotensin I. IRMPD MS³ of the radical species, $[M - H]^{2\bullet}$, provided backbone bond fragmentation (c'_3 and z'_7 product ions) as shown in Figure 7.2b, however, small molecule and/or electron loss (e.g., $[M - CO_2 - H]^-$ and $[M - H_2O - H]^{2\bullet}$) were more dominant. Despite the dearth of structural information in the data shown in Figures 7.1 and 7.2, we were encouraged to observe electron capture by peptide anions.

7.3.2. Effect of Electron Energy on Electron Capture Efficiency

The optimum electron energy for electron capture by peptide anions with and without coumarin tags was determined. We observed that electron capture occurred within a rather narrow energy range. Figure 7.3 shows that the optimum energy was ~6 eV, which is clearly higher than the optimum (0 – 1 eV) in positive ion mode ECD, however, it is similar to the optimum energy in HECD (~7 eV). One can argue that 6 eV electrons would be decelerated by anionic peptide ions and then may be captured due to a local favorable environment, such as electron deficient groups or delocalized groups. Recent work by Vasilev et al. showing resonance capture of 1-2 eV electrons by neutral gaseous peptides supports this idea.³³ Another explanation may be that gas-phase zwitterions are required to promote electron capture at positively charged sites.

The optimum electron irradiation time for coumarin-tagged angiotensin I was also determined as shown in Figure 7.3c. There was no significant difference in optimum electron irradiation time between tagged and untagged peptides. Generally, 10 s was necessary to observe abundant electron capture species.

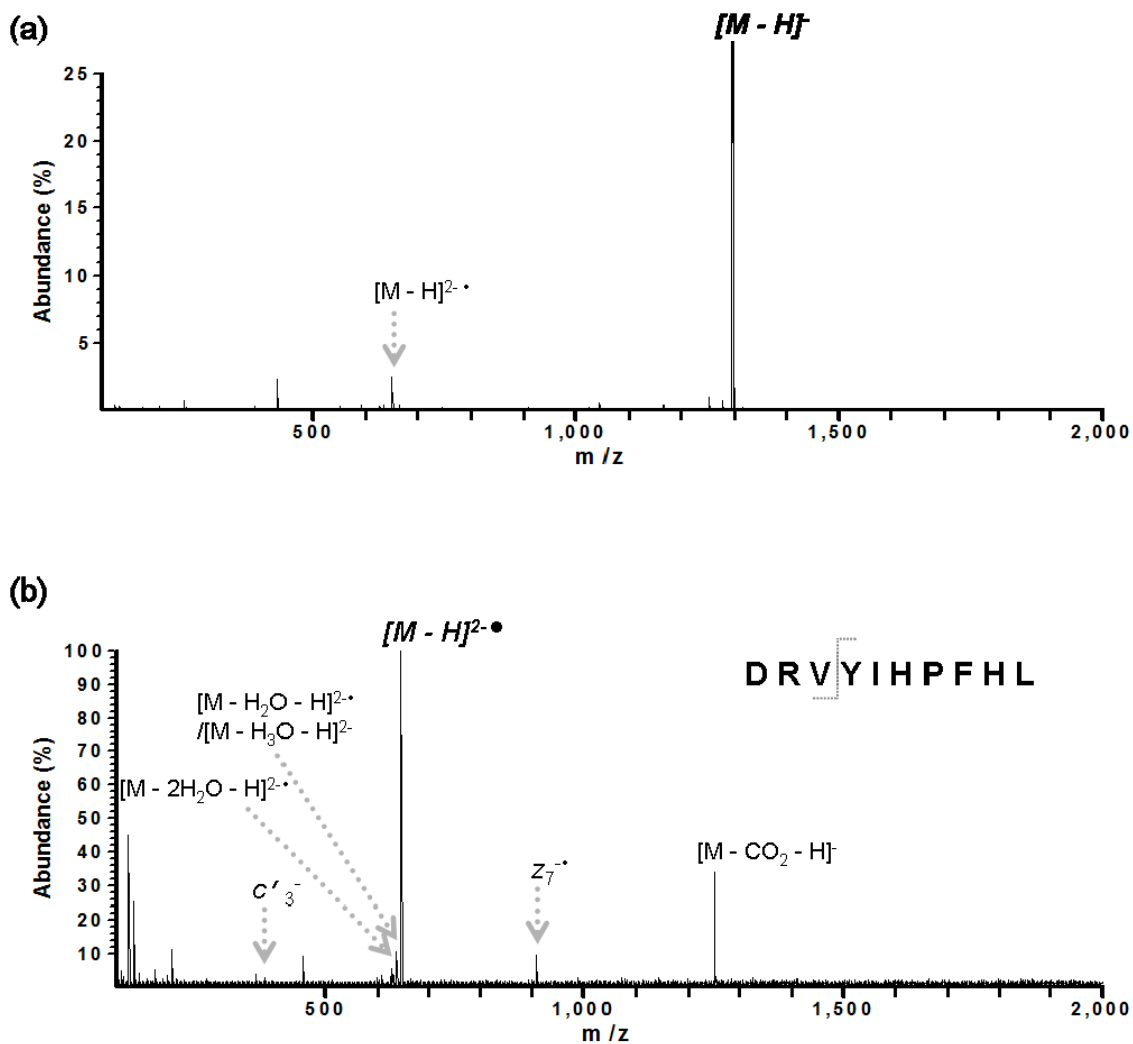


Figure 7.2. Activation and dissociation of untagged angiotensin I: (a) electron irradiation (~ 6 eV electrons for 20 s) of singly deprotonated angiotensin I, $[M - H]^-$. (b) IRMPD MS^3 of the radical species, $[M - H]^{2\bullet}$, generated by electron capture (7.5 W laser power for 300 ms). Peak labels in bold and italics indicate precursor ions used for activation/fragmentation.

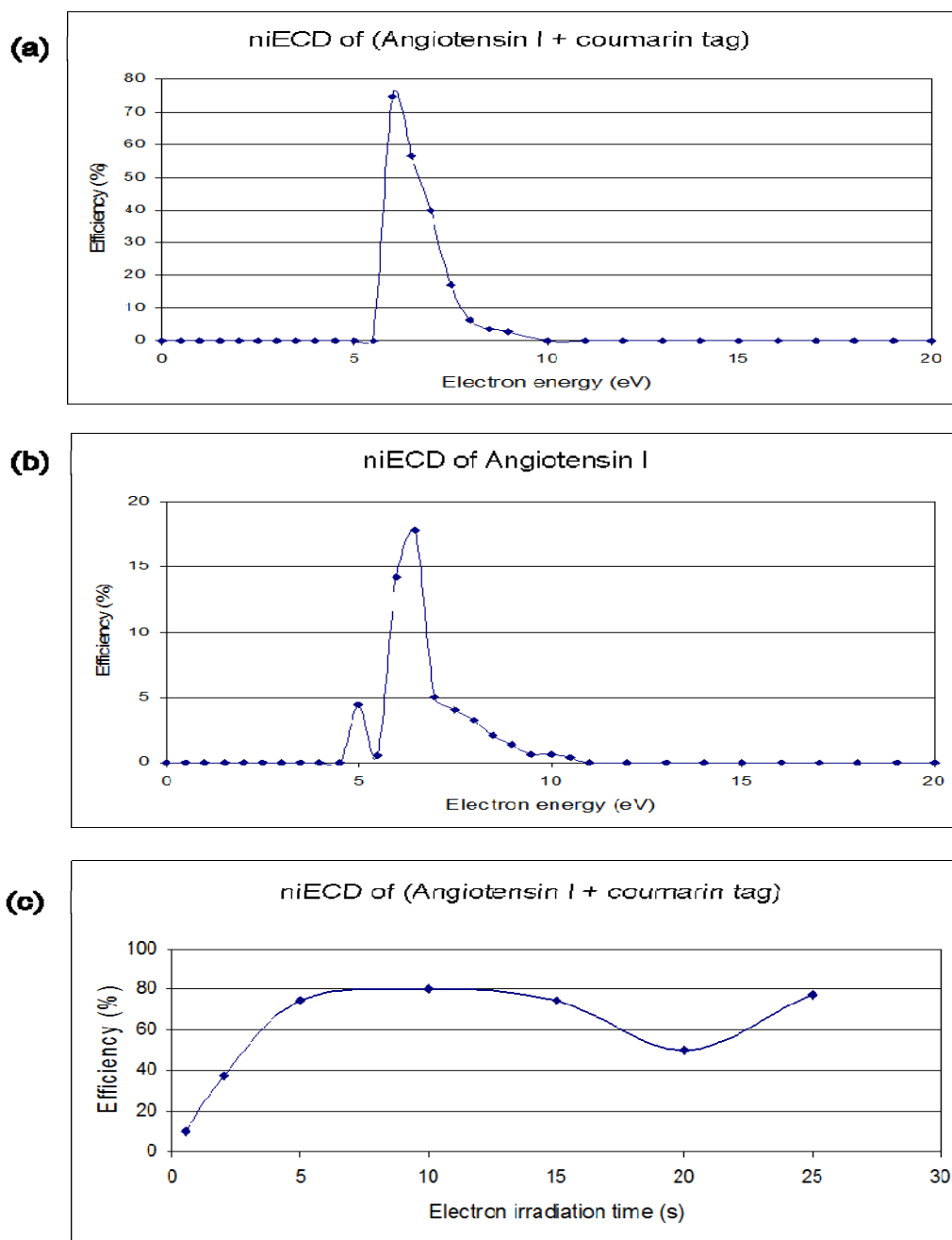


Figure 7.3. Electron capture efficiency as function of electron energy and electron irradiation time: (a) electron capture efficiency for coumarin-tagged angiotensin I (20 s irradiation) as function of electron energy. (b) electron capture efficiency for untagged angiotensin I (10 s irradiation) as function of electron energy. (c) electron capture efficiency for coumarin-tagged angiotensin I as function of electron irradiation time (~6 eV electrons). Electron capture efficiencies were calculated from the ion abundance ratios of radical species, $[M - H]^{2-}$, in MS/MS spectra to ion abundances of precursor ions, $[M - H]$, in isolation spectra. The y-axes are shown in percent (% efficiency = ratio \times 100).

Table 7.1 summarizes the observation of electron capture by 13 singly and doubly deprotonated standard and tryptic peptides with and without phosphorylation. No electron capture was observed for smaller peptides (≤ 1000 Da). Smaller peptide size may hinder delocalization of the extra electron over the peptide. For peptides that did capture electrons in negative ion mode, zwitterionic gas-phase structures appear likely: several sequences contain both acidic and basic residues (e.g., RRREEEpSEEEAA). Another recurring property appears to be the presence of tyrosine, which has an aromatic side chain that could facilitate electron capture. However, in some cases, a peptide (e.g., GNLWATGHFM) including an aromatic side chain (here tryptophan) did not capture an electron. On the other hand, this peptide sequence does not contain strongly basic residues (lysine or arginine), which may favor the zwitterion idea over the presence of aromatic side chains. However, the two complementary backbone fragments (c'_3 and z'_7) observed in IRMPD MS³ of the $[M - H]^{2-\bullet}$ radical form of angiotensin I (Figure 7.2b) originate from N-C bond cleavage next to tyrosine.

7.3.3. IRMPD MS³ of Distonic Radical Anions generated by Electron Capture vs. MS/MS of Even-electron Peptide Anions of the Same Charge State

Activation/dissociation of a singly deprotonated tyrosine-phosphorylated peptide (KRSpYEEHIP) was explored. The radical species, $[M - H]^{2-\bullet}$, generated by electron capture, was isolated and further dissociated with IRMPD MS³, see Figure 7.4a. Backbone fragmentation mainly occurred near the phosphotyrosine residue, again implying that this aromatic side chain may constitute a possible electron capture site. In addition, several z-type product ions were observed with or without phosphate loss although sequence coverage from IRMPD MS³ was rather low. IRMPD and EDD of the corresponding even-electron peptide ions, $[M - 2H]^{2-}$, were compared to IRMPD MS³ of

z	m/z	Peptide sequence (Peptide name if available)	$[M - H]^{2-}$ or $[M - 2H]^{3-}$ radical species present?
-1	1131.504	GNLWATGHFM (Neuromedin B)	No
-1	1209.507	DMHDFVGLM (Neurokinin B)	No
-1	1199.559	EHWSYGLRPG	Yes
-1	590.318	YPISL (Exorphin C)	No
-1	1568.634	RRREEE pSEEEAA	Yes
-1	1236.541	KRS pYEEHIP	Yes
-1	1294.669	DRV YIHPHL (Angiotensin I)	Yes
-1	737.345	RRA pSVA	No
-1	1540.632	TST EPQpYQPGENL-NH ₂	Yes
-2	1029.403	FQ pSEEQQQTEDELQDK (β -casein 48-63)	Yes
-1	902.452	PPGFSPFR	No
-1	1346.704	RPKPQQFFGLM (Substance P)	No
-1	1265.6	YLGYLEQLLR (α -casein 106-115)	Yes

Table 7.1. Observation of radical species, $[M - H]^{2-}$ or $[M - 2H]^{3-}$, generated from electron capture by negatively charged peptides. Lines indicate backbone fragmentation observed in IRMPD MS³ of such radical species.

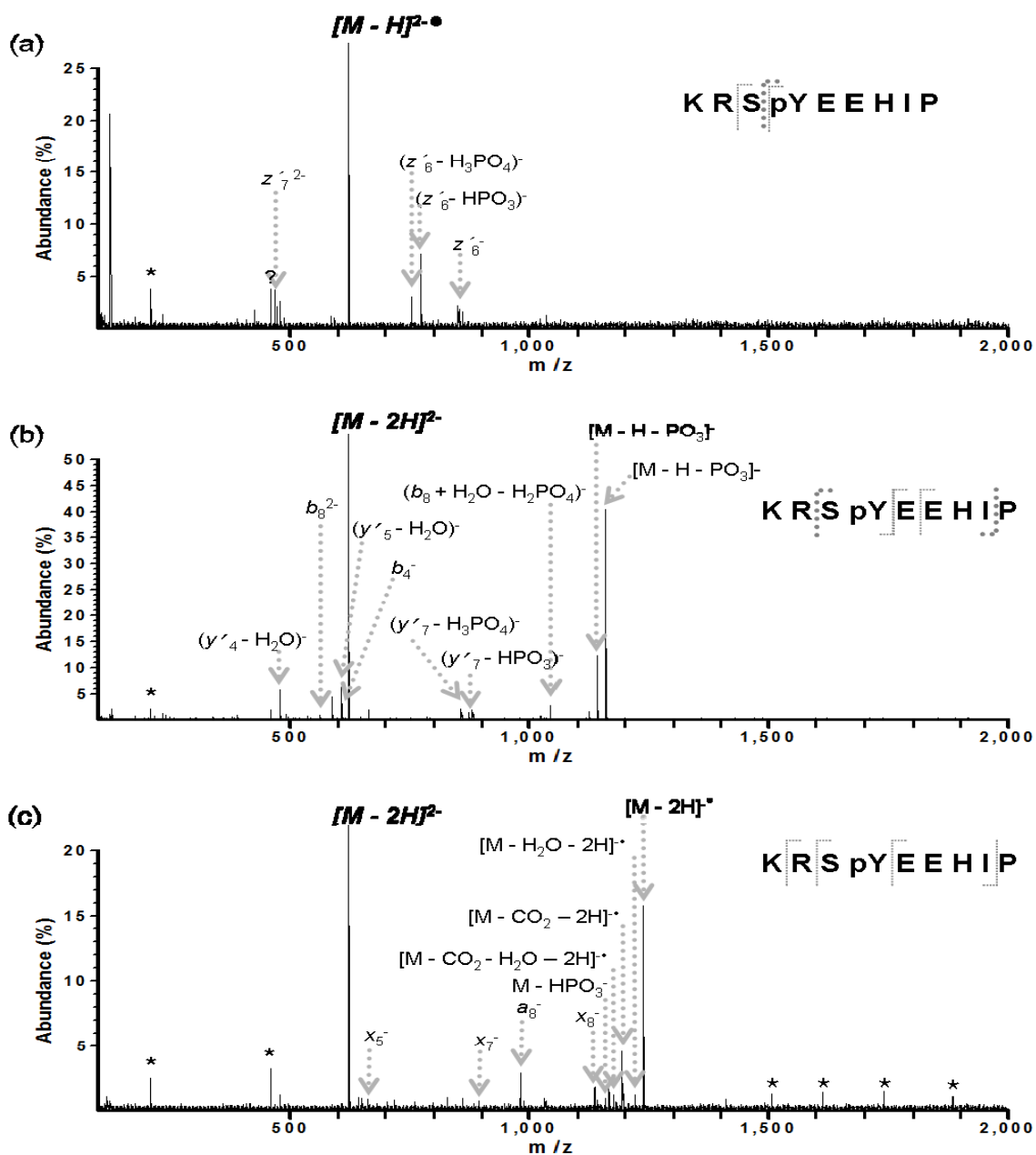


Figure 7.4. Comparison of IRMPD MS³ of the radical species, $[M - H]^{2\bullet-}$, with MS/MS of the doubly deprotonated form of a tyrosine-phosphorylated peptide. (a) IRMPD MS³ of the radical species, $[M - H]^{2\bullet-}$, generated from electron capture by singly deprotonated peptide, $[M - H]^-$ (7.5 W laser power for 300 ms). (b) IRMPD of doubly deprotonated peptide, $[M - 2H]^{2-}$, (7.5 W laser power for 700 ms). (c) EDD of doubly deprotonated peptide, $[M - 2H]^{2-}$ (21 eV electrons for 2 s). Peak labels in bold and italics indicate precursor ions used for fragmentation. “▲” indicates H₂O loss from an adjacent peak. “*” indicates an electronic noise peak. Thin lines on peptide sequences indicate backbone fragmentation. Thick dotted line indicates backbone bond fragmentation involving phosphate loss.

the radical species, $[M - H]^{2-\bullet}$, (Figures 7.4b and c, respectively). IRMPD and EDD of the even-electron peptide ions provided typical fragmentation patterns observed in these MS/MS techniques: IRMPD resulted in *b*- and *y*-type backbone fragmentation along with abundant neutral losses, including H₂O and H₃PO₄ losses. EDD of the same peptide ions provided charged-reduced radical species and *a* and *x*-type backbone fragments along with neutral losses such as H₂O and CO₂. Product ion abundances were much lower in EDD compared to IRMPD of the same peptide ions, as expected. Thus, a unique dissociation process, more similar to ECD in positive ion mode, is clearly occurring in IRMPD of radical anions.

7.3.4. niECD of Peptide Anions

Following careful optimization of electron irradiation conditions, we noted a plentitude of product ions in addition to the electron capture species (see Figure 7.5a for singly deprotonated angiotensin I). These product ions are *c*- and *z*-type ions, analogous to ECD in positive ion mode. Notably, a doubly negatively-charged $c'_9{}^{2-}$ ion is observed that must originate from the $[M - H]^{2-\bullet}$ electron capture species. By contrast, irradiation of the same singly deprotonated species with higher energy electrons (>10 eV, i.e, EID-type activation) resulted in completely different backbone product ions (*a*, *b*, and *y*-type fragment) along with abundant neutral losses (Figure 7.5b). No electron capture was observed at these electron energies. Our group has previously shown that EID (10-12 eV electrons) of singly deprotonated peptide ions frequently results in more extensive fragmentation compared to CID with a higher degree of PTM retention³⁴. CID of singly deprotonated angiotensin I anions is shown in Figure 7.5c. Consistent with our previous findings, fewer backbone products are observed compared to EID and, again, no *c*- or *z*-type ions are generated.

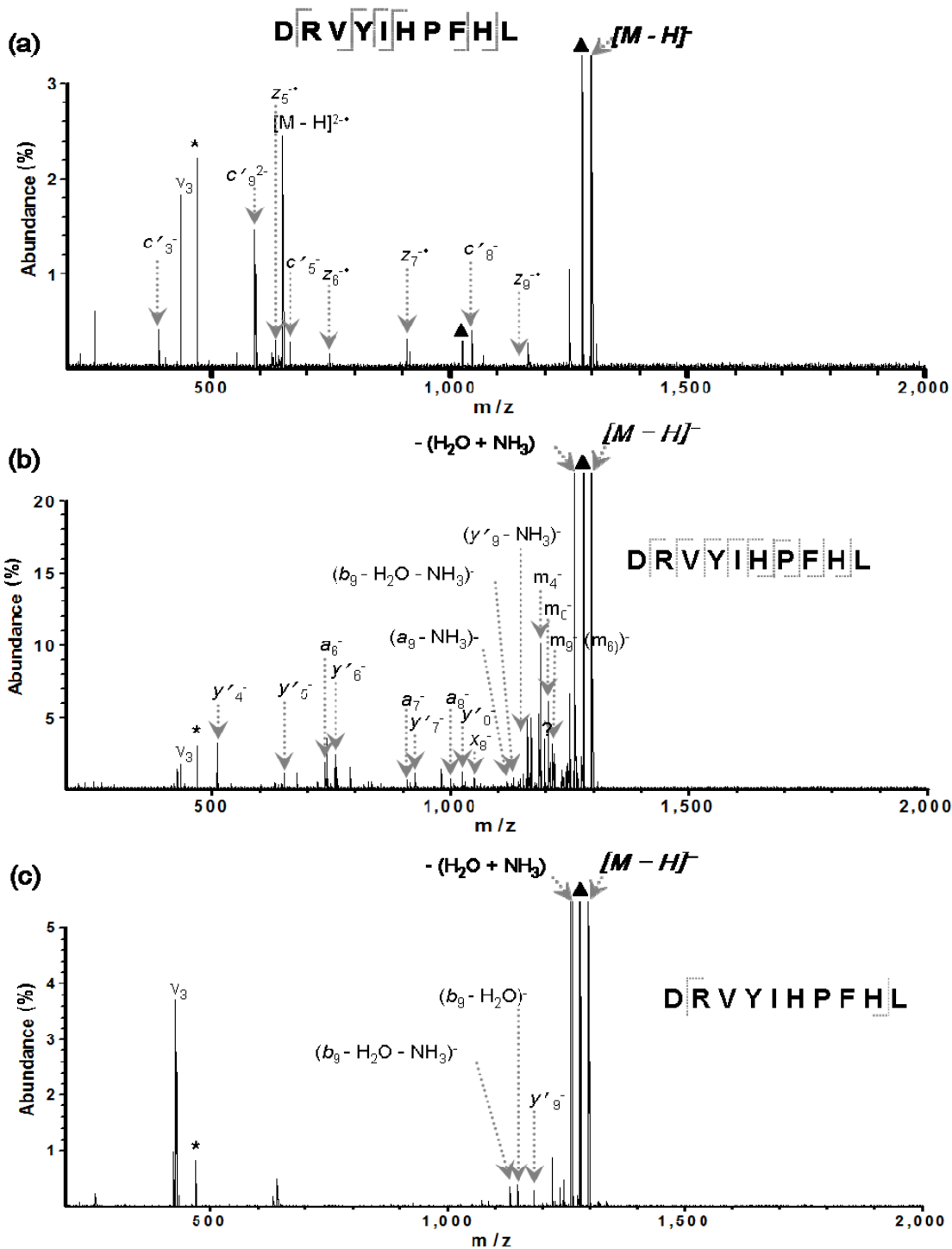


Figure 7.5. niECD, EID, and CID spectra of singly deprotonated angiotensin I. (a) niECD of angiotensin I (7 eV electrons for 20 s). (b) EID of angiotensin I (11 eV electrons for 20 s). (c) CID of angiotensin I (30 V collision voltage). Peak labels in bold and italics indicate precursor ions used for MS/MS. “▲” indicates H₂O loss from an adjacent peak and “*” indicates an electronic noise peak. Lines on peptide sequences indicate backbone fragmentation.

Figure 7.6 shows niECD and CID spectra of a singly deprotonated tyrosine-phosphorylated peptide (KRSpYEEHIP). niECD of this peptide yielded many *c*- and *z*-type product ions with complete retention of the phosphate group. Notably, four of these product ions are doubly charged. Increasing the charge state is highly significant in FT-ICR mass analysis because generated image current is proportional to the charge state.⁶ The *c/z* product ion pattern clearly allows the phosphate location to be determined. In contrast, CID provided *b* and *y*-type product ions along with abundant neutral losses such as H₂O and H₃PO₄. Even though some product ions, e.g., *b*₅⁻, retained the phosphate, the precise phosphate location could not be deduced due to the consecutive two possible phosphorylation sites (serine and tyrosine). EID (~12 eV electrons) was also performed to generate backbone fragmentation of this peptide. Overall, the product ions observed in EID were similar to those in CID with two additional fragments (*a*₅⁻ and *a*₇⁻) (data not shown). However, backbone fragmentation (e.g., *z*'₆²⁻ and *z*'₇²⁻) crucial to assign the PTM site was only obtained only in niECD of this peptide. This result is significant because phosphopeptides are frequently rather acidic and therefore ionize better in negative ion mode compared to positive ion mode. Similar results (summarized in Table 7.2) were obtained for a singly deprotonated sulfopeptide (CCKS) in niECD with 6 eV electrons: extensive *c*- and *z*-type product ions were obtained and all these backbone fragments preserved the highly labile sulfate modification.

Figure 7.7 shows niECD and CID spectra of doubly deprotonated β-casein 48-63 tryptic peptide (FQpSEEQQTEDELQDK). Here, electron capture by the doubly charged precursor ions forms triply charged radical anions, [M – 2H]^{3•-} and extensive *c*- and *z*-type product ions, typical of positive ion mode ECD. Notably, three of these

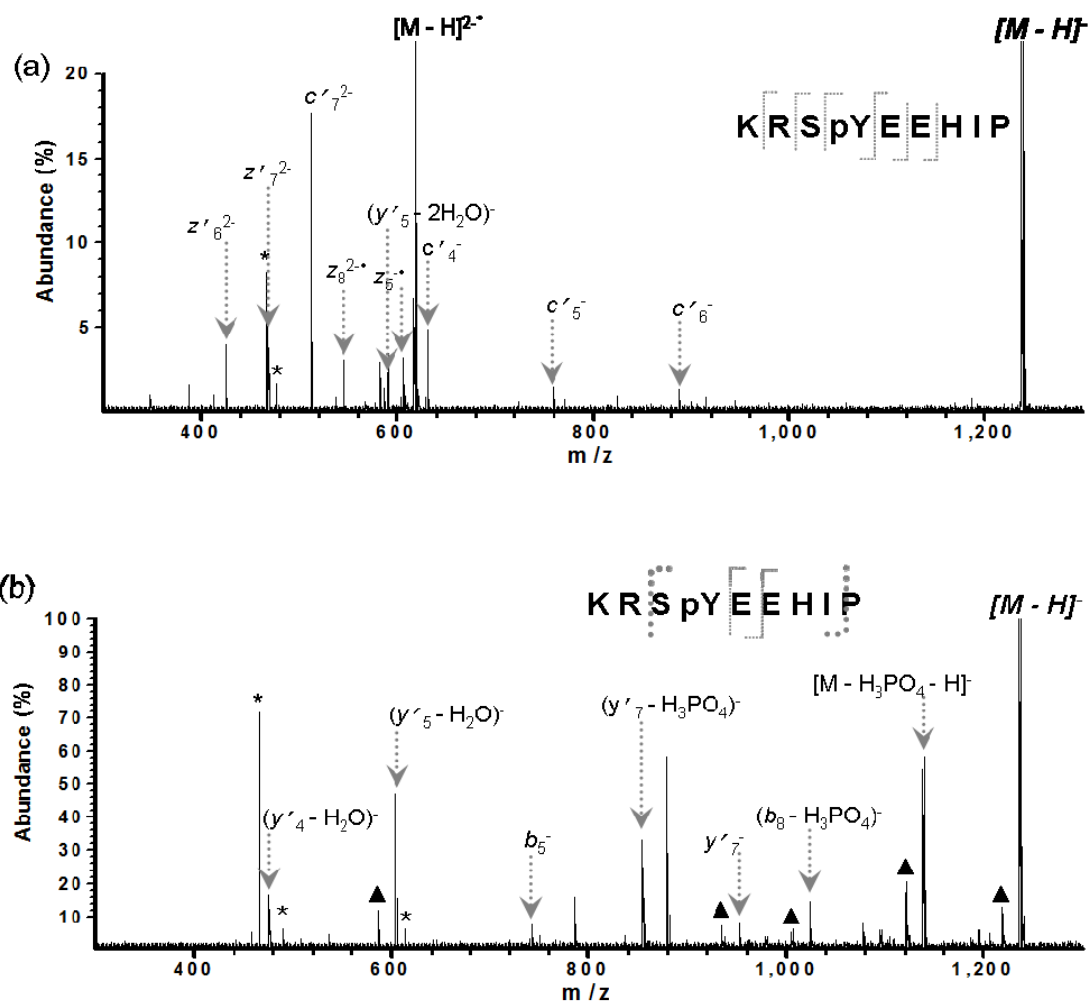


Figure 7.6. niECD and CID of tyrosine-phosphorylated peptide. (a) niECD of singly deprotonated peptide, $[M - H]^-$ (7 eV electrons for 20 s). (b) CID of singly deprotonated peptide, $[M - H]^-$ (40 V collision voltage). Peak labels in bold and italics indicate precursor ions used for MS/MS. “▲” indicates H_2O loss from an adjacent peak and “*” indicates an electronic noise peak. Thin lines on peptide sequences indicate backbone fragmentation whereas thick dotted line indicate backbone bond fragmentation involving phosphate loss.

z	m/z	MS/MS	Peptide sequence
-1	1568.634	niECD	RRREEE [pS] [E] [E] [E] [A] [A]
		CID	RRREEE pS EEEAA
-1	1236.541	niECD	K [R] [S] [pY] [E] [E] [H] [I] [P]
		CID	K R S pY E E H I P
-1	1540.632	niECD	T [S] [T] [E] [P] [Q] [pY] [Q] [P] [G] [E] [N] [L]-NH ₂
		CID	T S T E P Q pY Q P G E N L-NH ₂
-2	1029.403 (β -casein 48-63)	niECD	F [Q] [pS] [E] [E] [Q] [Q] [T] [E] [D] [E] [L] [Q] [D] [K]
		CID	F Q pS E E Q Q T E D E L Q D K
-1	1658.779 (α -casein 121-134)	niECD	V [P] [Q] [L] [E] [I] [V] [P] [N] [pS] [A] [E] [E] [R]
		CID	V P Q L E I V P N pS A E E R
-1	1141.342 (CCKS)	niECD	D [sY] [M] [G] [W] [M] [D] [F]-NH ₂
		CID	D sY M G W M D F-NH ₂

Table 7.2. Backbone bond fragmentation observed in niECD and CID of phosphorylated and sulfated peptides. Thin lines on peptide sequences indicate backbone fragmentation whereas thick dotted lines indicate backbone bond cleavage accompanied by phosphate loss.

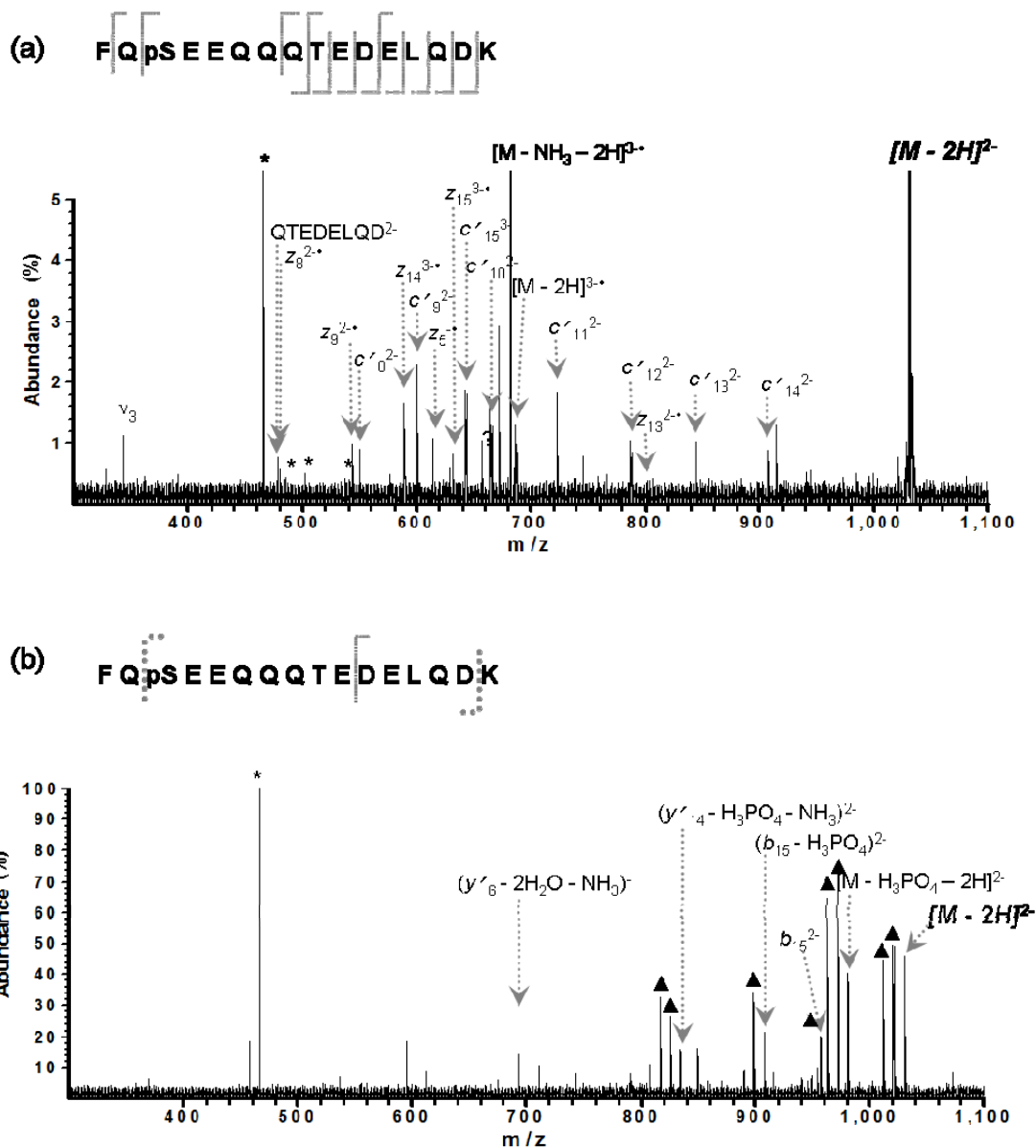


Figure 7.7. niECD and CID of a serine-phosphorylated β -casein tryptic peptide (residues 48-63). (a) niECD of the doubly deprotonated peptide, $[M - 2H]^{2-}$ (7 eV electrons for 10 s). (b) CID of doubly deprotonated peptide, $[M - 2H]^{2-}$ (25 V collision voltage). Peak labels in bold and italics indicate precursor ions used for MS/MS. “▲” indicates H_2O loss from an adjacent peak and “*” indicates an electronic noise peak. Thin lines on peptide sequences indicate backbone fragmentation whereas thick dotted lines indicate backbone bond fragmentation involving phosphate loss.

backbone product ions are triply charged and must therefore originate from the $[M - 2H]^{3-}$ species. Similar to the tyrosine-phosphopeptide shown in Figure 7.6, all backbone fragments containing the phosphoserine residue retained the phosphate group, which allows PTM site localization. On the contrary, CID resulted in *b*- and *y*-type product ions along with neutral losses. None of the product ions obtained from CID retained the phosphate group, thereby precluding PTM site determination

Table 7.2 summarizes backbone bond fragmentation observed in niECD (*c*- and *z*-type ions) and CID (*b*- and *y*-type ions, for comparison) of phosphorylated and sulfated peptides. Overall, the sequence coverage in niECD is much higher than that in CID, which also frequently results in neutral PTM loss. Product ion abundances in niECD of a doubly deprotonated peptide (Figure 7.7a) were lower compared to those in niECD of singly deprotonated peptides (e.g., Figure 7.6a). Higher peptide charge state may decrease electron capture efficiency due to higher Coulombic repulsion. In summary, niECD provided backbone bond fragments which retained labile acidic PTMs. In addition, niECD yielded higher sequence coverage than CID of the same precursor ions. Thus, niECD appears promising for phosphate and sulfate site determination as well as for *de novo* sequencing.

7.4. Conclusions

In this paper, we have shown that negatively charged peptides can capture 6-7 eV electrons, resulting in radical species with higher charge state, and yielding peptide backbone bond fragmentation analogous to that observed in positive ion mode ECD. The presence of a coumarin radical trap improved electron capture efficiency, however,

IRMPD MS³ of [M - nH]^{(n+1)•} species resulting from electron capture resulted in limited peptide backbone fragmentation, presumably due to decreased radical mobility. Without coumarin tag, singly deprotonated peptides were still able to capture electrons to yield radical species, [M - H]^{2•}, although the yield of this radical was lower than for coumarin-tagged peptides. IRMPD MS³ of [M - H]^{2•} species from untagged peptides provided backbone fragmentation, including *c*- and *z*-type product ions, as well as neutral and/or hydrogen radical losses.

After further optimization of the experimental conditions, extensive backbone fragmentation was observed, along with generation of a [M - nH]^{(n+1)•} radical species, a process we call niECD. niECD of singly or doubly deprotonated peptides provided extensive *c*- and *z*-type product ions retaining PTMs. In addition, niECD showed higher sequence coverage than CID of the same peptide precursor ions. Thus, niECD shows high promise for localization of PTMs, and for *de novo* sequencing, particularly for acidic peptides that ionize better in negative ion mode compared to positive ion mode, i.e., phospho- and sulfopeptides. Further, niECD is compatible with singly-charged peptides, which renders this technique compatible with MALDI.

7.5. References

1. Cooper, H. J.; Hakansson, K.; Marshall, A. G. *Mass Spectrom Rev* **2005**, *24*. 201-222.
2. McLafferty, F. W.; Horn, D. M.; Breuker, K.; Ge, Y.; Lewis, M. A.; Cerda, B.; Zubarev, R. A.; Carpenter, B. K. *J Am Soc Mass Spectrom* **2001**, *12*. 245-249.
3. Zubarev, R. A. *Mass Spectrom Rev* **2003**, *22*. 57-77.
4. Zubarev, R. A. *Curr Opin Biotechnol* **2004**, *15*. 12-16.
5. Kjeldsen, F.; Haselmann, K. F.; Budnik, B. A.; Jensen, F.; Zubarev, R. A. *Chem. Phys. Lett* **2002**, *356*. 201-206.
6. Fung, Y. M.; Adams, C. M.; Zubarev, R. A. *J Am Chem Soc* **2009**, *131*. 9977-9985.

7. Budnik, B. A.; Haselmann, K. F.; Zubarev, R. A. *Chem Phys Lett* **2001**, 299-302.
8. Yang, J.; Mo, J.; Adamson, J. T.; Hakansson, K. *Anal Chem* **2005**, 77. 1876-1882.
9. Wolff, J. J.; Chi, L.; Linhardt, R. J.; Amster, I. J. *Anal Chem* **2007**, 79. 2015-2022.
10. Wolff, J. J.; Amster, I. J.; Chi, L.; Linhardt, R. J. *J Am Soc Mass Spectrom* **2007**, 18. 234-244.
11. Lioe, H.; O'Hair, R. A. *Anal Bioanal Chem* **2007**, 389. 1429-1437.
12. Cody, R. B.; Freiser, B. S. *Anal Chem* **1979**, 51. 541-551.
13. Yoo, H. J.; Liu, H.; Hakansson, K. *Anal Chem* **2007**, 20. 7858-7866.
14. Adamson, J. T.; Hakansson, K. *J Am Soc Mass Spectrom* **2007**, 18. 2162-2172.
15. Wolff, J. J.; Laremore, T. N.; Aslam, H.; Linhardt, R. J.; Amster, I. J. *J Am Soc Mass Spectrom* **2008**, 19. 1449-1458.
16. Budnik, B. A.; Haselmann, K. F.; Elkin, Y. N.; Gorbach, V. I.; Zubarev, R. A. *Anal Chem* **2003**, 75. 5994-6001, DOI: 10.1021/ac034477f.
17. James, P. F.; Perugini, M. A.; O'Hair, R. A. *J Am Soc Mass Spectrom* **2008**, 19. 978-986.
18. Liu, H.; Yoo, H. J.; Hakansson, K. *J Am Soc Mass Spectrom* **2008**, 19. 799-808.
19. Witze, E. S.; Old, W. M.; Resing, K. A.; Ahn, N. G. *Nat Methods* **2007**, 4. 798-806.
20. Zubarev, R. A.; Kellerher, N. L.; McLafferty, F. W. *J Am Chem Soc* **1998**, 120. 3265-3266.
21. Kelleher, N. L.; Zubarev, R. A.; Bush, K.; Furie, B.; Furie, B. C.; McLafferty, F. W.; Walsh, C. T. *Anal Chem* **1999**, 71. 4250-4253.
22. Turecek, F.; Syrstad, E. A. *J Am Chem Soc* **2003**, 125. 3353-3369.
23. Kjeldsen, F.; Haselmann, K. F.; Budnik, B. A.; Sorensen, E. S.; Zubarev, R. A. *Anal Chem* **2003**, 75. 2355-2361.
24. Williams, J. P.; Creese, A. J.; Roper, D. R.; Green, B. N.; Cooper, H. J. *J Am Soc Mass Spectrom* **2009**, 20. 1707-1713.
25. Budnik, B. A.; Zubarev, R. A. *Chem. Phys. Lett* **2000**, 316. 19-23.
26. Leymarie, N.; Costello, C. E.; O'Connor, P. B. *J Am Chem Soc* **2003**, 125. 8949-8958.
27. Belyayev, M. A.; Cournoyer, J. J.; Lin, C.; O'Connor, P. B. *J Am Soc Mass Spectrom* **2006**, 17. 1428-1436.
28. Sohn, C. H.; Chung, C. K.; Yin, S.; Ramachandran, P.; Loo, J. A.; Beauchamp, J. L. *J Am Chem Soc* **2009**, 131. 5444-5459.
29. Kweon, H. K.; Hakansson, K. *Anal Chem* **2006**, 78. 1743-1749.
30. Tsybin, Y. O.; Witt, M.; Baykut, G.; Kjeldsen, F.; Hakansson, P. *Rapid Commun Mass Spectrom* **2003**, 17. 1759-1768.
31. de Koning, L. J. N., N. M. M.; van Orden, S. L.; Laukien, F. H. *Int. J. Mass Spectrom.* **1997**, 165. 209-219.
32. Senko, M. W.; Canterbury, J. D.; Guan, S.; Marshall, A. G. *Rapid Commun Mass Spectrom* **1996**, 10. 1839-1844.
33. Vasil'ev, Y. V.; Figard, B. J.; Morre, J.; Deinzer, M. L. *J Chem Phys* **2009**, 131. 044317.
34. Kalli, A.; Grigorean, G.; Hakansson, K. **2010**, *Submitted*.

Chapter 8

Conclusions and Future Directions

8.1. Conclusions

Negative ion mode HILIC LC/FT-ICR MS was developed to compare metabolic profiles of untreated and small molecule (oligomycin, 2-deoxyglucose, and Bz-423) treated Jurkat cells. HILIC column was used to separate highly polar metabolites involved in glycolysis and TCA cycle. Oligomycin-treated Jurkat cells did not show any changes compared to untreated cells. By contrast, 2-deoxyglucose and Bz-423 treatment caused significant metabolic changes. However, many of the metabolites observed in LC/FT-ICR MS could not be identified using currently available metabolite databases. Thus, improved small organic molecule (e.g. metabolites, lipids, fatty acids, and peptides) characterization and identification methods involving various kinds of

MS/MS strategies were explored in this thesis work.

CID, IRMPD, and EID of phosphate-containing metabolites provided valuable complementary structural information, which can aid in the identification of such compounds. Generally, IRMPD provided the most extensive fragmentation because the phosphate group is a good chromophore for CO₂ IR laser (10.6 μm).

Metal-adducted fatty acids were analyzed to investigate the utility of EID for determining double bond locations. Various metals (Li, Zn, Co, Ag, Ni, Mg, Ca, Fe, and Mn) were used to fix one charge at the carboxylate end of fatty acids to promote charge-remote fragmentation. Ion abundances of $[C_xH_yO_2 + \text{Met}]^+$ in EID of Mn(II)-adducted fatty acids allowed determination of all double bond positions in the fatty acids investigated. However, other metal-adducted fatty acids did not generally provide characteristic product ion abundances at all double bond locations.

CID and IRMPD of Ag-adducted phospholipids were investigated to determine the fatty acyl groups attached to the sn-1 and sn-2 esterification sites. CID and IRMPD of Ag-adducted phospholipids resulted in headgroup loss as the most abundant fragmentation pathway. However, in addition to headgroup loss, $[R_x\text{COOH} + \text{Ag}]^+$ product ions were observed along with their neutral losses, $[R_x\text{COOH} - \text{H}_2\text{O} + \text{Ag}]^+$ and

$[R_x\text{COOH} - \text{CO}_2 - \text{H}_2 + \text{Ag}]^+$, in which $R_x\text{COOH}$ is an unsaturated acyl chain. Thus, CID and IRMPD of Ag-adducted phospholipids could be used to identify the acyl chains at the sn-1 and sn-2 esterification sites as well as to identify the phospholipid type.

In addition, ECD of divalent metal-adducted phospholipids was explored to obtain phospholipid structural information. $[R_2\text{COOH} - \text{H} + \text{Ni}]^+$ (and $[\text{M} - R_2\text{COOH}]^+$ (for phosphatidylcholine) were consistently observed due to closer distance of the sn-2 position to electron capture sites compared to the sn-1 position, and weak Lewis acidic-basic interactions between Ni^{2+} and acyl chains. Thus, phospholipid regiochemistry could be determined from these characteristic product ions. For Ba^{2+} -adducted phospholipids, the ratio of total product ion abundances involving cleavage at the sn-2 position to the total product ion abundance involving cleavage at the sn-1 esterification site was consistently larger than 1, correlating with its hard Lewis acidic property and large ionic radius.

Lastly, we have shown that negatively charged peptides can capture 6-7 eV electrons, forming unique radical species, $[\text{M} - n\text{H}]^{(n+1)-}$ and *c*- and *z*-type product ions from peptide backbone cleavage, analogous to positive ion mode ECD. This novel reaction, termed niECD, appears particularly promising for acidic phosphorylated and

sulfated peptides, which yielded extensive *c*- and *z*-type product ions retaining PTMs, thus allowing determination of PTM sites. In addition, niECD showed higher sequence coverage than CID of the same peptide precursor ions.

8.2. Future Directions

8.2.1. Applications of Developed Alternative MS/MS Strategies and LC/FT-ICR MS/MS

The developed methods should improve metabolite structural characterization and identification, because metabolite identification still remains a major challenge in metabolomics.^{1, 2-4, 5} FT-ICR MS can be used without CID (which is the most commonly used MS/MS technique)^{3, 6-9} due to its low ppm level accuracy and high resolution.^{6, 10-13} However, many metabolites share very similar masses, thus MS/MS is required to uniquely assign metabolite structure and the developed alternative MS/MS strategies should aid metabolite identification and provide further confirmation of metabolite identities.

LC is often coupled with MS to allow use of retention time as another component of metabolite identification, or to reduce ion suppression. The developed MS/MS strategies could be combined with both on- and off-line LC/FT-ICR MS. For off-line

LC/FT-ICR MS, LC eluants can be fractionated using TriVersa™ NanoMate (Advion, Ithaca, NY). Individual fractions are diluted 2-3 fold with spraying solvent for ESI-FT-ICR MS/MS.¹⁴⁻¹⁶ If necessary, metal ions can be added to the spraying solvent and metal adduction reaction can occur for MS/MS of metal-adducted fatty acids or phospholipids.

8.2.2. Study of niECD Mechanism

I have shown that negatively charged peptides can capture 6-7 eV electrons and form unique radical species, $[M - nH]^{(n+1)-}$. In addition, *c*- and *z*-type product ions, which are typical in positive ion mode ECD, are observed in niECD of negatively charged peptide ions. More interestingly, PTMs such as phosphorylation and sulfation were all preserved in the niECD process. However, the mechanism of niECD is still not understood, even though we suspect that zwitterionic properties may play a role in niECD, based on experimental data to date. To understand the niECD mechanism, derivatization of peptide N-termini could be performed to remove potential protonation sites. For example, acetylation of peptides void of arginine should reduce the probability of gas-phase zwitterionic structures,¹⁷ whereas addition of fixed charges would promote zwitterionic structures.¹⁸ niECD of derivatized peptides can then be

performed to explore the effect of zwitterionic structures in the niECD process.

8.2.3 Application of niECD to Other Biomolecules

Carbohydrates and their conjugates, such as glycoproteins and glycolipids, are involved in immune system recognition, nervous system development, and many other critical biological processes. However, methods for their full structural characterization are less developed than for linear biopolymers such as proteins and oligonucleotides, because of their non-linear, branched structures. IRMPD, ECD, and EDD have been applied for structural analysis of carbohydrates or glycoproteins.¹⁹⁻²¹ niECD may provide complementary structural information for complex carbohydrate structures compared to other MS/MS methods. Further, niECD may be valuable in carbohydrate analysis because ionization of carbohydrates is often more efficient in negative ion mode, particularly for sialylated and sulfated species, which have important biological functions. In addition, niECD of oligonucleotides, DNA, and RNA may be useful for providing structural information on such biomolecules.

8.3. References

1. Aharoni, A.; Ric de Vos, C. H.; Verhoeven, H. A.; Maliepaard, C. A.; Kruppa, G.; Bino, R.; Goodenowe, D. B. *Omic*s **2002**, *6*, 217-234.

2. Bino, R. J.; Hall, R. D.; Fiehn, O.; Kopka, J.; Saito, K.; Draper, J.; Nikolau, B. J.; Mendes, P.; Roessner-Tunali, U.; Beale, M. H.; Trethewey, R. N.; Lange, B. M.; Wurtele, E. S.; Sumner, L. W. *Trends Plant Sci* **2004**, *9*. 418-425.
3. Edwards, J. L.; Chisolm, C. N.; Shackman, J. G.; Kennedy, R. T. *J Chromatogr A* **2006**, *1106*. 80-88.
4. Krieger, C. J.; Zhang, P.; Mueller, L. A.; Wang, A.; Paley, S.; Arnaud, M.; Pick, J.; Rhee, S. Y.; Karp, P. D. *Nucleic Acids Res* **2004**, *32*. D438-442.
5. Smith, C. A.; O'Maille, G.; Want, E. J.; Qin, C.; Trauger, S. A.; Brandon, T. R.; Custodio, D. E.; Abagyan, R.; Siuzdak, G. *Ther Drug Monit* **2005**, *27*. 747-751.
6. Brown, S. C.; Kruppa, G.; Dasseux, J. L. *Mass Spectrom Rev* **2005**, *24*. 223-231.
7. Buchholz, A.; Takors, R.; Wandrey, C. *Anal Biochem* **2001**, *295*. 129-137.
8. Byrd, G. D.; Ogden, M. W. *J Mass Spectrom* **2003**, *38*. 98-107.
9. Triolo, A.; Altamura, M.; Dimoulas, T.; Guidi, A.; Lecci, A.; Tramontana, M. *J Mass Spectrom* **2005**, *40*. 1572-1582.
10. Amster, I. J. *J Mass Sepctrom*. **1996**, *31*. 1325.
11. Comisarow, M. B.; Marshall, A. G. *Chem. Phys. Lett* **1974**, *26*. 489.
12. Marshall, A. G.; Hendrickson, C. L.; Jackson, G. S. *Mass Spectrom Rev* **1998**, *17*. 1-35.
13. Sleno, L.; Volmer, D. A.; Marshall, A. G. *J Am Soc Mass Spectrom* **2005**, *16*. 183-198.
14. Dettmer, K.; Aronov, P. A.; Hammock, B. D. *Mass Spectrom Rev* **2007**, *26*. 51-78.
15. Renfrow, M. B.; Mackay, C. L.; Chalmers, M. J.; Julian, B. A.; Mestecky, J.; Kilian, M.; Poulsen, K.; Emmett, M. R.; Marshall, A. G.; Novak, J. *Anal Bioanal Chem* **2007**, *389*. 1397-1407, DOI: 10.1007/s00216-007-1500-z.
16. Zamfir, A.; Vakhrushev, S.; Sterling, A.; Niebel, H. J.; Allen, M.; Peter-Katalinic, J. *Anal Chem* **2004**, *76*. 2046-2054, DOI: 10.1021/ac035320q.
17. Lindh, I.; Sjovall, J.; Bergman, T.; Griffiths, W. J. *J Mass Spectrom* **1998**, *33*. 988-993.
18. Adamczyk, M.; Gebler, J. C.; Wu, J. *Rapid Commun Mass Spectrom* **1999**, *13*. 1413-1422.
19. Adamson, J. T.; Hakansson, K. *J Proteome Res* **2006**, *5*. 493-501.
20. Adamson, J. T.; Hakansson, K. *Anal Chem* **2007**, *79*. 2901-2910.
21. Adamson, J. T.; Hakansson, K. *J Am Soc Mass Spectrom* **2007**, *18*. 2162-2172.

Appendix A

Phosphate-containing Metabolite Enrichment with TiO₂ Micro-tips

A.1. Introduction

Metabolites are essential to living cells. Metabolite levels represent integrative information of cellular function, and define the phenotype of a cell or tissue in response to genetic or environmental changes. mRNA levels do not always correlate with protein levels, and translated protein may or may not be enzymatically active. Therefore, changes observed in the transcriptome or proteome do not always correspond to phenotypic alterations. Thus measurement of the metabolites synthesized by a biological system is very important to assess genetic function and also aids the understanding of the proteome.¹⁻⁶ Metabolomics is the study of the full arsenal of endogenous small molecules in biological systems, with the ultimate goal of identifying biomarkers and enzymatic pathways related to human disease.¹⁻³ The size of the metabolome is extraordinary (although not as vast as the proteome). For example, most eukaryotic organisms possess 4,000-20,000 distinct metabolites.⁷ Also, metabolites have wide

variations in chemical (e.g., molecular weight, polarity, acidity) and physical (e.g., volatility) properties, which makes metabolome analysis highly challenging. Thus, targeted metabolite analysis would be valuable to selectively detect a few members of compound classes within a cell or tissue.⁸ Enrichment of specific subsets of small molecules from biological systems would greatly benefit targeted approaches.

Mass spectrometry remains the most suitable technology for measurement of metabolites because of its wide dynamic range, good sensitivity, and the ability to observe a diverse number of molecular species. Mass spectrometry coupled with chromatography (LC/MS) is preferred in metabolomics, due to reduction of sample complexity and additional information for metabolite identification.^{4, 7, 9-11}

Phosphate-containing metabolites are important in life activities such as phosphate metabolism and energy conversion. Phosphates are most commonly found in the form of nucleotides, cofactors, and phosphorylated carbohydrates. Phosphate-containing metabolites are highly polar, and poorly retained with reverse phase liquid chromatography (RPLC). Therefore, additional chromatographic techniques such as hydrophilic interaction liquid chromatography (HILIC) are required, however, HILIC offers only moderate separation capacity.¹²⁻¹³ Incomplete separation of polar metabolites may cause ion suppression in LC/MS due to co-elution. Thus metabolite enrichment can be beneficial to metabolomics due to removal of co-eluted unwanted analytes. Recently, chemoselective probes based on functional groups have been used to enrich amine, acid, aldehyde, and thiol-containing compounds among polar metabolites.¹⁴⁻¹⁵ However, this approach alters metabolite structure as well as tandem mass spectra. Thus, current metabolite databases cannot be used.

Phosphopeptides are also important in many cellular processes, including metabolism and cellular signaling. The important role of phosphopeptides emphasizes the need for a highly selective and efficient method for enriching phosphopeptides and identifying the phosphorylation sites in these peptides. Several strategies have been developed to enrich phosphopeptides from complex biological matrices.¹⁶ Titanium oxide (TiO₂) has been successfully applied to phosphopeptide enrichment, where weak Lewis acidic-basic interactions between phosphates and TiO₂ are utilized for phosphate retention.¹⁷⁻²⁰ Thus, this approach may also allow enrichment of phosphate-containing metabolites.

Here, we present enrichment of phosphate-containing metabolites with titanium dioxide microtips, which have been successfully applied for phosphopeptide enrichment.¹⁹⁻²¹ Metabolite enrichment is expected to maximize the number of observed phosphate-containing metabolites from a biological system and to expand the dynamic range for detection of these metabolites.

A.2. Experimental Section

A.2.1. Sample Preparation

Phosphate-containing metabolites investigated in this work were purchased from Sigma-Aldrich (St. Louis, MO) and used without further purification. TiO₂ micro-tips were purchased from Glygen (Columbia, MD). Metabolites were bound to micro-tips in 10 µl acidic solution (formic or acetic acid, pH 2 - 3). The micro-tips were subsequently washed with 50 µl of H₂O or H₂O/acetonitrile (50/50 or 20/80, v/v) and bound metabolites were eluted with 50 µl of 0.5 % piperidine (pH 11).

Standard metabolite mixture, composed of 17-20 polar metabolites, including seven phosphate-containing metabolites (shown in Table A.1) and several non phosphate-containing metabolites (asparagine, aspartic acid, glutamic acid, glutamine, citrate, tryptophan, Trp-Gly-Gly, Thr-Ser-Lys, Glu-Ala, Glu, and phosphatidylserine) was used to explore enrichment performance of TiO₂. The concentrations of non phosphate-containing metabolites (e.g., aspartic acid, glutamic acid, and the tripeptide Thr-Ser-Lys) were at most 120 times higher than those of phosphate-containing metabolites (e.g., glycerol 3-phosphate, glucose 6-phosphate, and ADP) in the standard metabolite mixture. ADP-ribose was used as an internal standard to compare signal abundances of phosphate-containing metabolites before and after enrichment.

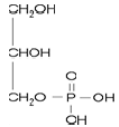
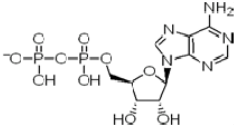
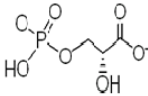
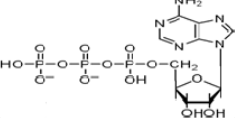
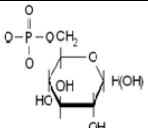
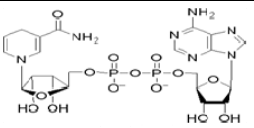
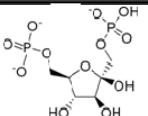
Name	Structure	[M - H] ⁻	Name	Structure	[M - H] ⁻
Glycerol 3-phosphate (G3P)		171.0059	ADP		426.0216
3-phosphoglyceric acid (3PG)		184.9851	ATP		505.9879
Glucose 6-phosphate (G6P)		259.0219	NADH		664.1169
Fructose 1,6-diphosphate (F1,6BP)		338.9882			

Table A.1. Phosphate-containing metabolites and their structures.

A.2.2. Fourier Transform Ion Cyclotron Resonance Mass Spectrometry

Mass spectra were acquired with a 7 Tesla quadrupole-Fourier transform ion cyclotron resonance (FT-ICR) mass spectrometer (Bruker, Daltonics, MA) using H₂O/acetonitrile (50/50, v/v) as spraying solvent for direct infusion. LC/MS was also performed with a HILIC TSK GEL amide-80 column (Tosoh bioscience, Japan) and isocratic mobile phase conditions (40 % A: 7.5 mM ammonium acetate in H₂O, 60 % B: 7.5 mM ammonium acetate in acetonitrile) with 15 min LC run time. All data were obtained in negative ion mode.

For ESI, N₂ was used as both nebulizing gas (4 L/s) and drying gas (1.5 L/s). The drying gas temperature was set to 200°C. Briefly, ions produced by electrospray ionization were mass-selectively externally accumulated²²⁻²³ in a hexapole for 1 s, transferred via high voltage ion optics, and captured in the ICR cell by dynamic trapping. This accumulation sequence was looped three times to improve ion abundance. For direct infusion, mass spectra were acquired with XMASS software (version 6.1, Bruker Daltonics) in broadband mode from m/z 21 to 1000 with 256K data points and summed over 5-10 scans. Data processing was performed with the MIDAS analysis software.²⁴ For LC/MS, data were acquired with Hystar (version 3.1, Bruker Daltonics) and Apex control (version 1.0, Bruker Daltonics). Data processing was performed with Data Analysis software (version 3.4, Bruker Daltonics).

A.3. Results and Discussion

Table A.1 shows the phosphate-containing metabolites used in this study and their structures. Standard metabolite mixture, with higher amount of non phosphate-

containing metabolites to mimic competitive environment in biological systems, was prepared to evaluate enrichment performance. The amount of non phosphate-containing metabolites was much higher than that of phosphate-containing metabolites in the standard metabolite mixture. No base was added to the ESI spraying solvent for mass analysis because weakly acidic mobile phase is preferred in LC. Also, phosphate-containing metabolites are rather acidic, and exist in deprotonated form, $[M - H]^-$, at neutral pH.

A.3.1. Comparison of Signal Abundances of Phosphate-containing Metabolites Before and After Enrichment

Non phosphate-containing metabolites were dominant in ESI mass spectra before enrichment, due to their higher concentrations. However, phosphate-containing metabolites were observed at low abundances. In particular, glucose 6-phosphate (G6P) and fructose 1,6-bisphosphate (F1,6BP) were barely observed before enrichment as shown in the inset in Figure A.1a. The low abundance of these two metabolites is probably due to ion suppression and the presence of closely adjacent peaks. However, G6P and F1,6BP ion signals were highly abundant after enrichment, as shown in the inset of Figure A.1b. Signal abundances of the closely adjacent peaks were reduced to the noise level, although it was difficult to compare signal abundances for each metabolite quantitatively due to lack of an internal standard. The most abundant metabolites before enrichment were peptides including Trp-Gly-Gly, which was about 40-fold more intense than ADP. However, TiO_2 treatment could selectively eliminate non phosphate-containing metabolites, including Trp-Gly-Gly, and, after treatment, signal abundance of this tripeptide was much lower than that of ADP. The data shown in Figure A.1 was obtained with an acetic acid loading solution. Very similar results were obtained with

formic acid, as shown in Figure A.2. Thus, the pH (optimum at 2-3) rather than the acid type appears to have the largest effect on metabolite enrichment efficiency.

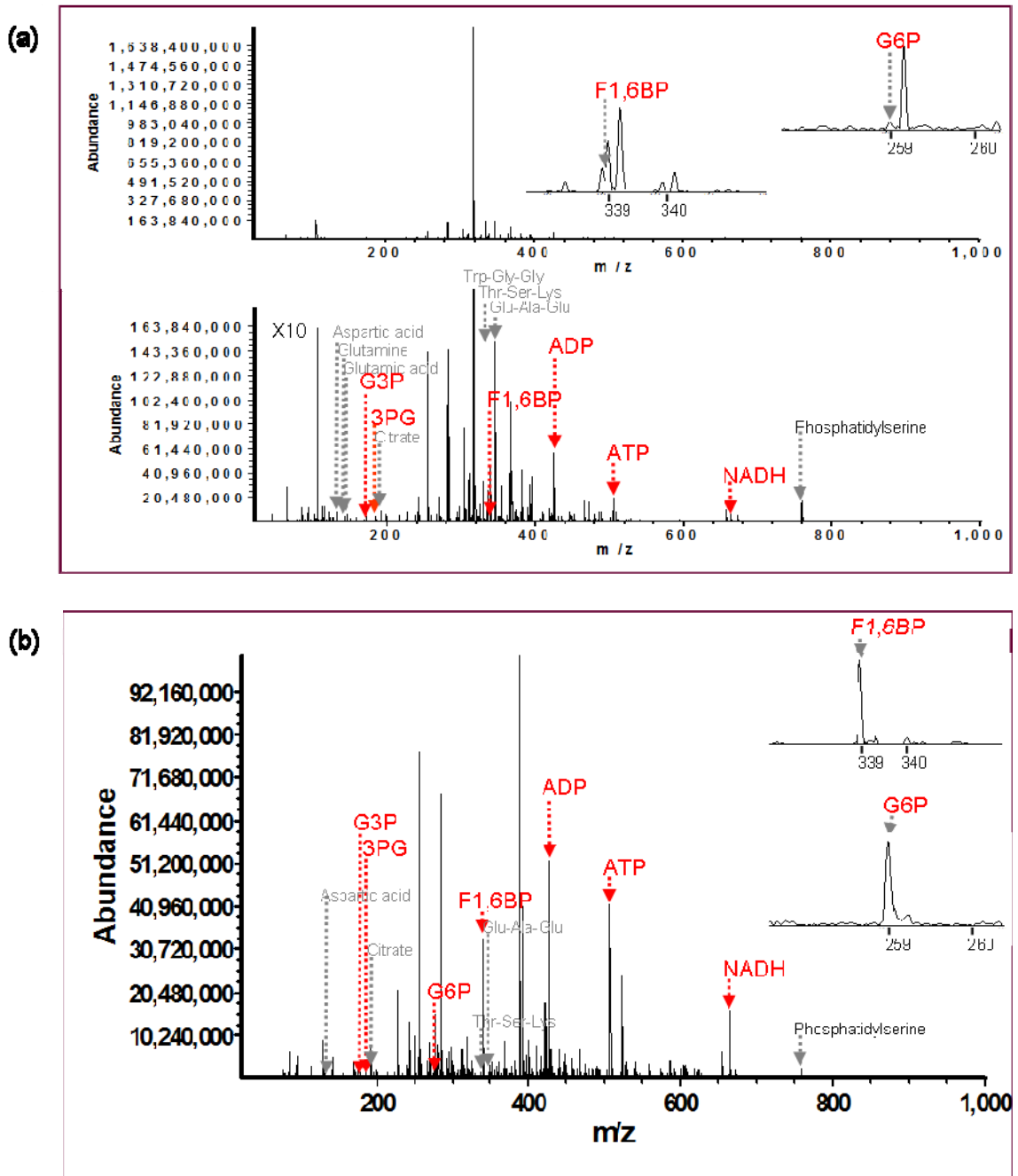


Figure A.1. Comparison of signal abundances of phosphate-containing metabolites before (a) and after (b) TiO₂ enrichment using 7 % CH₃COOH as loading solution. Washing solution was 100 % H₂O and elution solution was 0.5 % piperidine (pH 11).

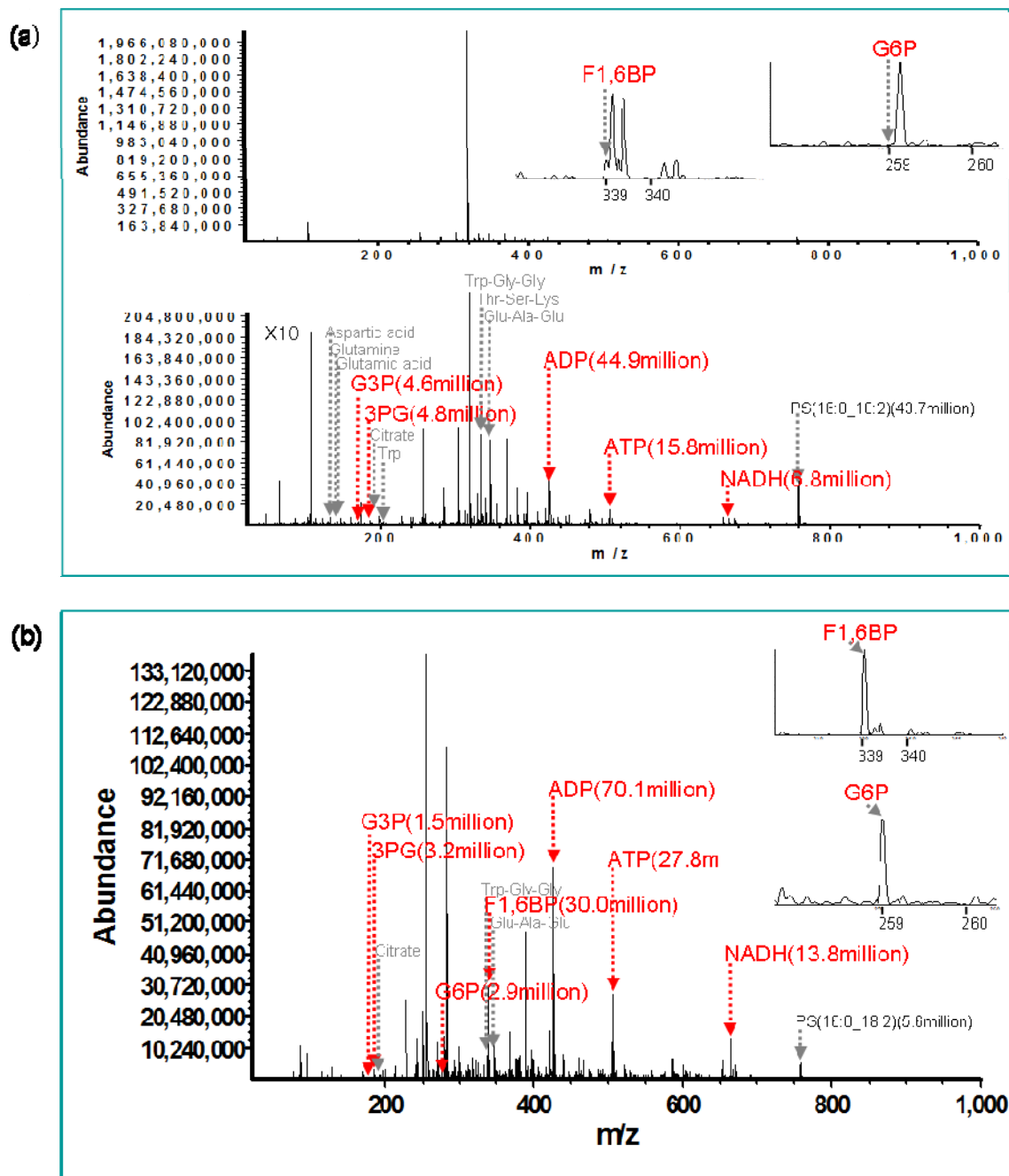


Figure A.2. Comparison of signal abundances of phosphate-containing metabolites before (a) and after (b) TiO_2 enrichment using 3.3 % HCOOH as loading solution. Washing solution was 100 % H_2O and elution solution was 0.5 % piperidine (pH 11).

To evaluate enrichment performance quantitatively, ADP-ribose was added into the spraying solvent as an internal standard and metabolite signal abundances were normalized to that of ADP-ribose. For this experiment, equal concentrations of phosphate-containing metabolites (2 μM) was used, except for G6P, which was at a 3-fold higher concentration, as shown in Table A.2. Higher concentration of G6P was used due to the relatively low signal abundance of G6P compared to other phosphate-containing metabolites with the same concentration. However, the signal abundance of G6P increased much more than 3 fold, implying that signal abundance is not a linear function of concentration, as expected when ion suppression is at play.

A.3.2. Quantitative Comparison of Enrichment Performance using Internal Standard

Metabolite signal abundances before and after enrichment, normalized to internal standard (ADP-ribose) are shown in Figure A.3. Similar to the data discussed above, non phosphate-containing metabolites were dominant before enrichment, however, phosphate-containing metabolites were the most dominant peaks after enrichment. Without enrichment, most of the phosphate-containing metabolites were difficult to observe. Other metabolites, which were included at much higher concentration in the sample, should cause ion suppression of phosphate-containing metabolites. Mostly non phosphate-containing metabolites were observed to remain in the loading solution (Figure A.3) and thus they did not bind to TiO_2 . This observation provided further support for selective binding of phosphate-containing metabolites to TiO_2 .

Enrichment performance was increased when the number of phosphates in the metabolites increased: ATP and F1,6BP were not detected before enrichment, but were very abundant after enrichment. ADP, which has two phosphates, was observed with

[M-H] ⁻	Standard mixture		Spraying solvent
	Metabolites	Conc.(μ M)	Conc.(μ M)
131.0457	Asparagine	237	
132.0297	Aspartic acid	237	
145.0814	Glutamine	237	
146.0454	Glutamic acid	237	
171.0059	Glycerol 3-phosphate	2	
184.9851	3-phosphoglyceric acid	2	
191.0192	Citrate	5	
195.0294	4-methylsophthalic acid	4	
203.0824	Tryptophan	2	
259.0219	Glucose 6-phosphate/F6P	6	
333.1775	Thr-Ser-Lys	4	
338.9882	Fructose 1,6-diphosphate	2	
346.1251	Glu-Ala-Glu	8	
426.0216	ADP	2	
505.9879	ATP	2	
558.0840	ADP-r		1
664.1169	NADH	2	
758.4972	PS(16:0_18:2)	5	
765.5544	PC(16:0_18:2)	5	

Table A.2. The concentrations of phosphate-containing metabolites in standard metabolite mixture.

moderate abundance even before enrichment, however, its signal abundance was increased significantly (~ 7-fold) after enrichment. On the other hand, NADH did not show enrichment with TiO₂ micro-tips, even though it contains two phosphate groups. By contrast, both ADP and F1,6BP, which also contain two phosphate groups, were enriched. This difference in behavior may be explained by steric effects: ADP and F1,6BP have terminal phosphates which should be able to freely interact with TiO₂,

whereas the two phosphate groups in NADH are located at the center of the molecule and their interaction with TiO₂ may therefore be hindered.

TiO₂, 3.3 % HCOOH in H₂O / H₂O / 0.5 % Piperidine

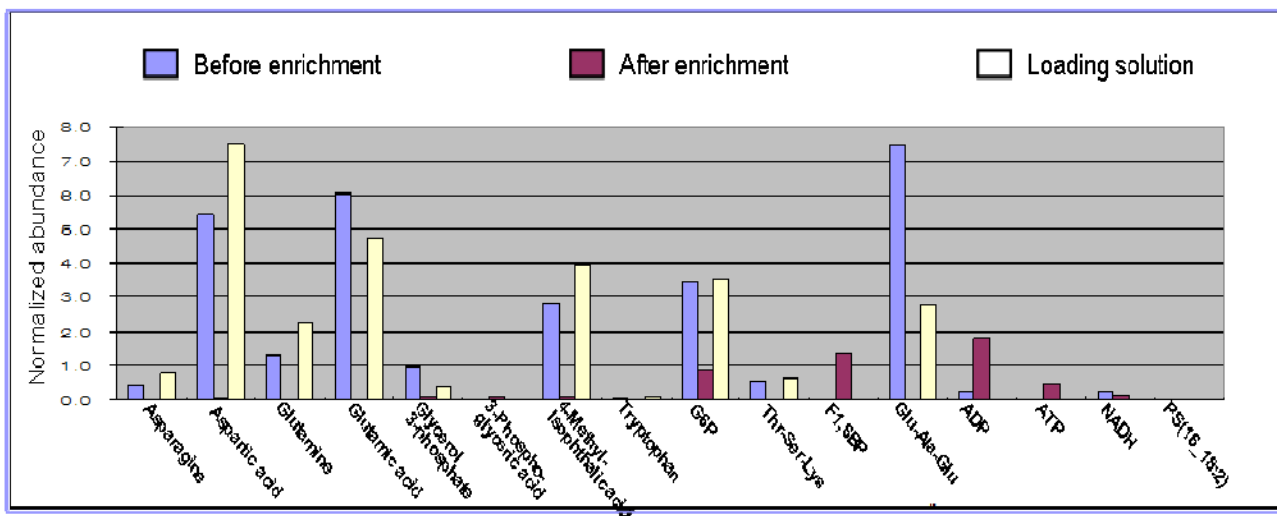


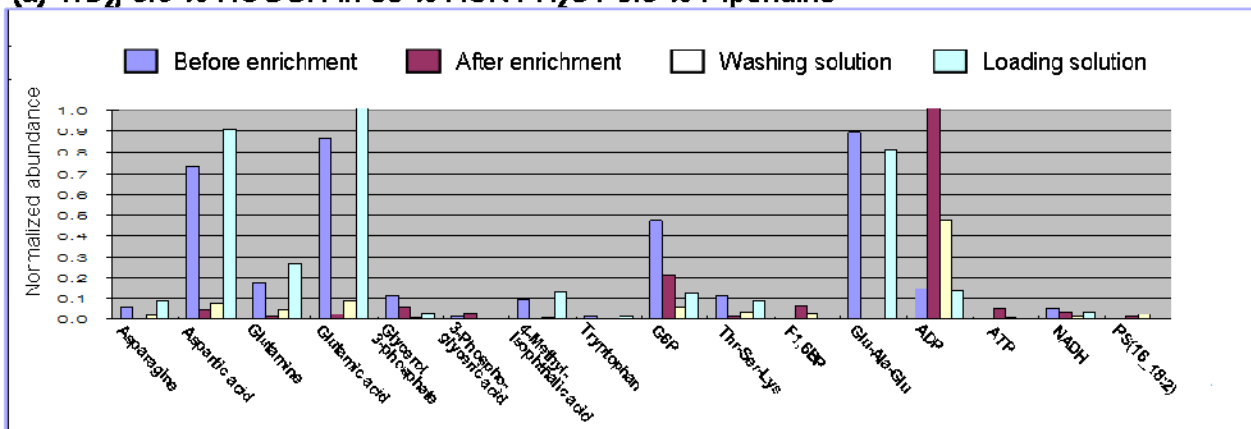
Figure A.3. Quantitative comparison of enrichment performance using an internal standard (ADP-ribose). Loading solution was 3.3 % HCOOH, washing solution was 100 % H₂O, and elution solution was 0.5 % piperidine (pH 11).

A.3.3. Effect of Acetonitrile in Loading and Washing Solution

Organic solvent such as acetonitrile contained in washing and loading solution affected enrichment efficiencies, as shown in Figures A.4a and A.4b. When acetonitrile was included in the loading solution, enrichment performance of phosphate-containing metabolites was improved (Figure A.4a), compared to enrichment without acetonitrile (Figure A.3). For example, signal abundance of ADP increased ~ 5-fold after enrichment using 100% H₂O as loading solution (Figure A.3), however, up to ~ 7-fold ADP signal abundance increase was seen after adding acetonitrile to the loading solution (Figure A.4a). When acetonitrile was added to both loading and washing solutions, enrichment

performance of G6P increased significantly (Figure A.4b). Significant amount of G6P was lost from TiO₂ during the washing step when 100 % H₂O was used as washing solution, as shown in Figure A.4a, which includes analyses of the washing solutions. However, no G6P was observed in the washing solution when TiO₂ micro-tips were washed with acetonitrile/H₂O (80/20, v/v), as shown in Figure A.4b. There was no significant difference in enrichment performance when the acetonitrile percentage was varied from 50-80 % in the loading and washing solutions.

(a) TiO₂, 3.3 % HCOOH in 80 % ACN / H₂O / 0.5 % Piperidine



(b) TiO₂, 3.3 % HCOOH in 80 % ACN / 80 % ACN / 0.5 % Piperidine

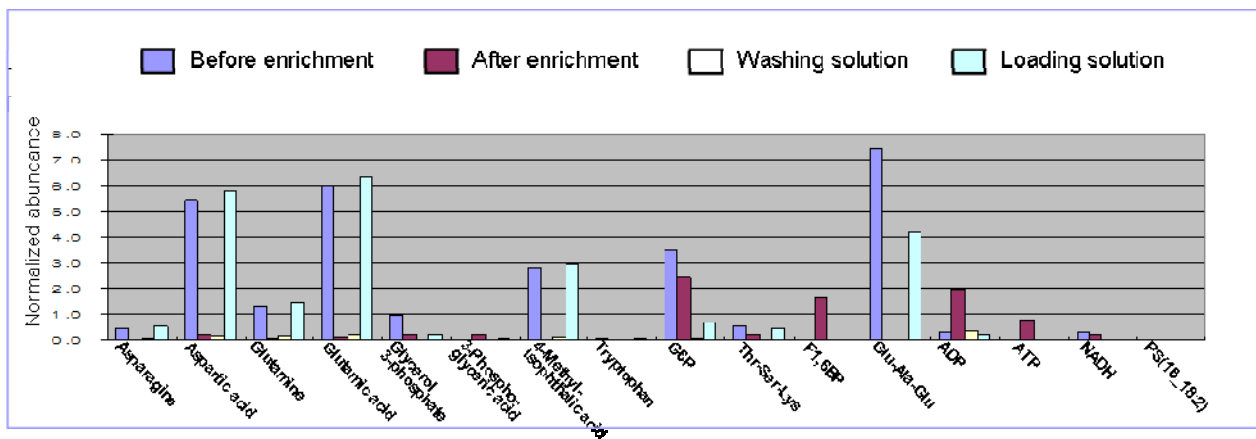
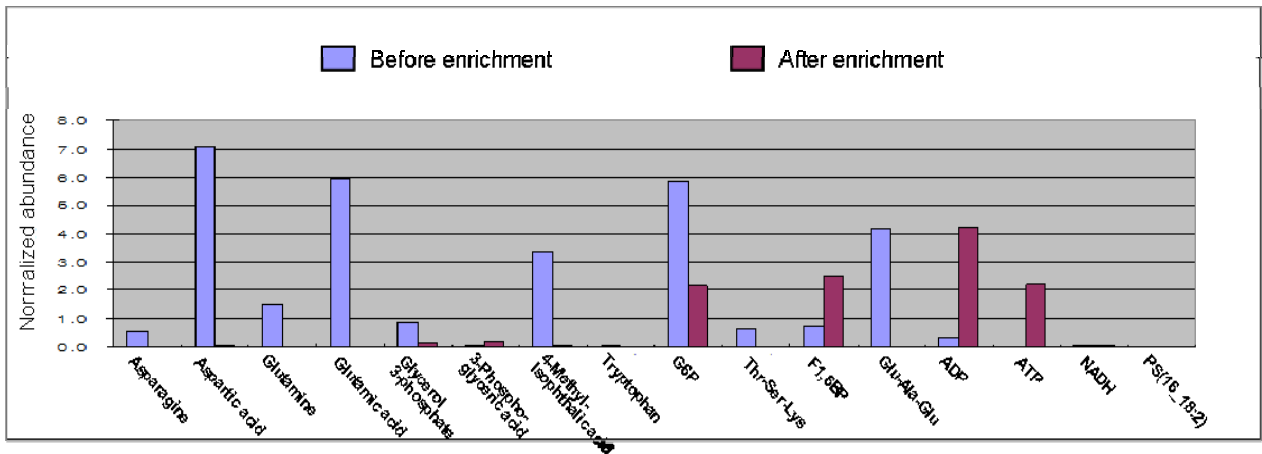


Figure A.4. Effect of acetonitrile in loading and washing solutions; (a) acetonitrile (80 %) was used in loading solution, (b) acetonitrile (80 %) was used in loading and washing solutions. Other conditions were the same as in Figure A.3 (including the internal standard).

A.3.4. Benefit of Phosphate-containing Metabolite Enrichment in LC/MS

Figure A.5 shows that targeted metabolite enrichment can benefit LC/MS as well as direct injection (DI)/MS. LC/MS cannot completely eliminate ion suppression due to co-elution, particularly when LC run times are not long enough for efficient separation of all analytes. Some phosphate-containing metabolites, such as ADP and ATP, were observed at good signal abundance in LC/MS even without enrichment, as shown in Figure A.5b. On the contrary, G6P was observed at low abundance in LC/MS, where other co-eluting

(a) DI-MS



(b) LC-MS

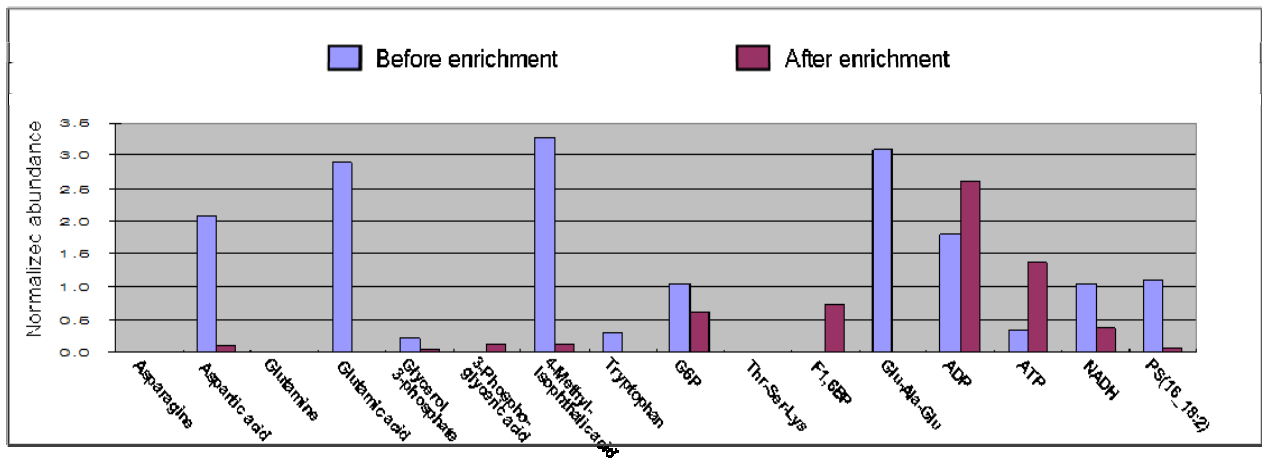


Figure A.5. Comparison of the enrichment performance of phosphate-containing metabolites between DI/MS (a) and LC/MS (b).

analytes may suppress G6P signal abundance. Only four out of seven phosphate-containing metabolites were observed at higher abundance in LC/MS before compared to after enrichment. However, Figure A.5b still shows that enrichment increased signal abundances of phosphate-containing metabolites in LC/MS. Similar to DI/MS, the enrichment performance increased with the number of phosphate groups in phosphate-containing metabolites.

A.4. Conclusions

Non phosphate-containing metabolites, such as aspartic and glutamic acid, were dominant in mass spectra of metabolite mixture before enrichment of phosphate-containing metabolites with TiO₂, due to their higher concentrations. However, phosphate-containing metabolites were observed at low abundances. Signal magnitudes of more than half of the phosphate-containing metabolites increased after enrichment. By contrast, most of the non phosphate-containing metabolites remained in the loading solution. Enrichment performance generally increased with the number of phosphate groups of phosphate-containing metabolites. In addition, enrichment performance was affected by the acetonitrile content in loading and washing solutions.

In many cases, HILIC could not separate polar metabolites completely, and some of the polar metabolites therefore coeluted, which likely caused ion suppression of phosphate-containing metabolites. Signal abundances of phosphate-containing metabolites in LC/MS also increased after enrichment. These results clearly show that TiO₂ selectively binds phosphate-containing metabolites, and therefore should be useful for enriching phosphate-containing metabolites from complex biological samples.

A.5. References

1. Villas-Boas, S. G.; Mas, S.; Akesson, M.; Smedsgaard, J.; Nielsen, J. *Mass Spectrom Rev* **2005**, *24*. 613-646.
2. Rochfort, S. *J Nat Prod* **2005**, *68*. 1813-1820.
3. Cascante, M.; Boros, L. G.; Comin-Anduix, B.; de Atauri, P.; Centelles, J. J.; Lee, P. W. *Nat Biotechnol* **2002**, *20*. 243-249.
4. Kell, D. B. *Curr Opin Microbiol* **2004**, *7*. 296-307.
5. Lindon, J. C.; Holmes, E.; Bollard, M. E.; Stanley, E. G.; Nicholson, J. K. *Biomarkers* **2004**, *9*. 1-31.
6. van der Greef, J.; Stroobant, P.; van der Heijden, R. *Curr Opin Chem Biol* **2004**, *8*. 559-565.
7. Fernie, A. R.; Trethewey, R. N.; Krotzky, A. J.; Willmitzer, L. *Nat Rev Mol Cell Biol* **2004**, *5*. 763-769.
8. Fiehn, O. *Comp Funct Genomics* **2001**, *2*. 155-168.
9. Brown, S. C.; Kruppa, G.; Dasseux, J. L. *Mass Spectrom Rev* **2005**, *24*. 223-231.
10. Dettmer, K.; Aronov, P. A.; Hammock, B. D. *Mass Spectrom Rev* **2007**, *26*. 51-78.
11. Dunn, W. B.; Ellis, D. I. *TrAC* **2005**, *24*. 285-294.
12. Bajad, S. U.; Lu, W.; Kimball, E. H.; Yuan, J.; Peterson, C.; Rabinowitz, J. D. *J Chromatogr A* **2006**, *1125*. 76-88.
13. Hemstrom, P.; Irgum, K. *J Sep Sci* **2006**, *29*. 1784-1821.
14. Carlson, E. E.; Cravatt, B. F. *Nat Methods* **2007**, *4*. 429-435.
15. Carlson, E. E.; Cravatt, B. F. *J Am Chem Soc* **2007**, *129*. 15780-15782.
16. Han, G.; Ye, M.; Zou, H. *Analyst* **2008**, *133*. 1128-1138.
17. Cantin, G. T.; Shock, T. R.; Park, S. K.; Madhani, H. D.; Yates, J. R., 3rd *Anal Chem* **2007**, *79*. 4666-4673.
18. Kweon, H. K.; Hakansson, K. *Anal Chem* **2006**, *78*. 1743-1749.
19. Larsen, M. R.; Thingholm, T. E.; Jensen, O. N.; Roepstorff, P.; Jorgensen, T. J. *Mol Cell Proteomics* **2005**, *4*. 873-886.
20. Thingholm, T. E.; Jorgensen, T. J.; Jensen, O. N.; Larsen, M. R. *Nat Protoc* **2006**, *1*. 1929-1935.
21. Schmidt, A.; Csaszar, E.; Ammerer, G.; Mechtler, K. *Proteomics* **2008**, *8*. 4577-4592.
22. Belov, M. E.; Nikolaev, E. N.; Anderson, G. A.; Udseth, H. R.; Conrads, T. P.; Veenstra, T. D.; Masselon, C. D.; Gorshkov, M. V.; Smith, R. D. *Anal Chem* **2001**, *73*. 253-261.
23. Hendrickson, C. L.; Quinn, J. P.; Emmett, M. R.; Marshall, A. G., in *49th ASMS Conference on Mass Spectrometry and Allied Topics*. Chicago, IL, 2001; CD-ROM.
24. Senko, M. W.; Canterbury, J. D.; Guan, S.; Marshall, A. G. *Rapid Commun Mass Spectrom* **1996**, *10*. 1839-1844.

Appendix B

Comparison of Collision Induced Dissociation and Infrared Multiphoton Dissociation for Structural Characterization of Lipid A

B.1. Introduction

Endotoxic lipopolysaccharides (LPS), in addition to phospholipids and proteins, are the major components of the outer membrane of all Gram-negative bacteria. The LPS of Gram-negative bacteria is composed of three main parts: (i) the O-antigen polysaccharide (O-PS); (ii) the relatively conserved core polysaccharide (core-PS); and (iii) lipid A, the hydrophobic lipid component responsible for biological activities within the host.¹⁻² Toll-like receptors in a host recognize the lipid A portion of LPS and stimulate inflammation to attract immune cells and clear bacterial infections.³⁻⁴ The strong immune response to lipid A is the reason that LPS has been historically referred to as “endotoxin”. Some pathogens regulate the structure of their lipid A and its acylation patterns in order to adapt to the host environment, thereby contributing to greater fitness within the host.⁵ While its toxic effects can be damaging, the sensing of lipid A by the human immune system may also be critical for the onset of immune responses to Gram-negative

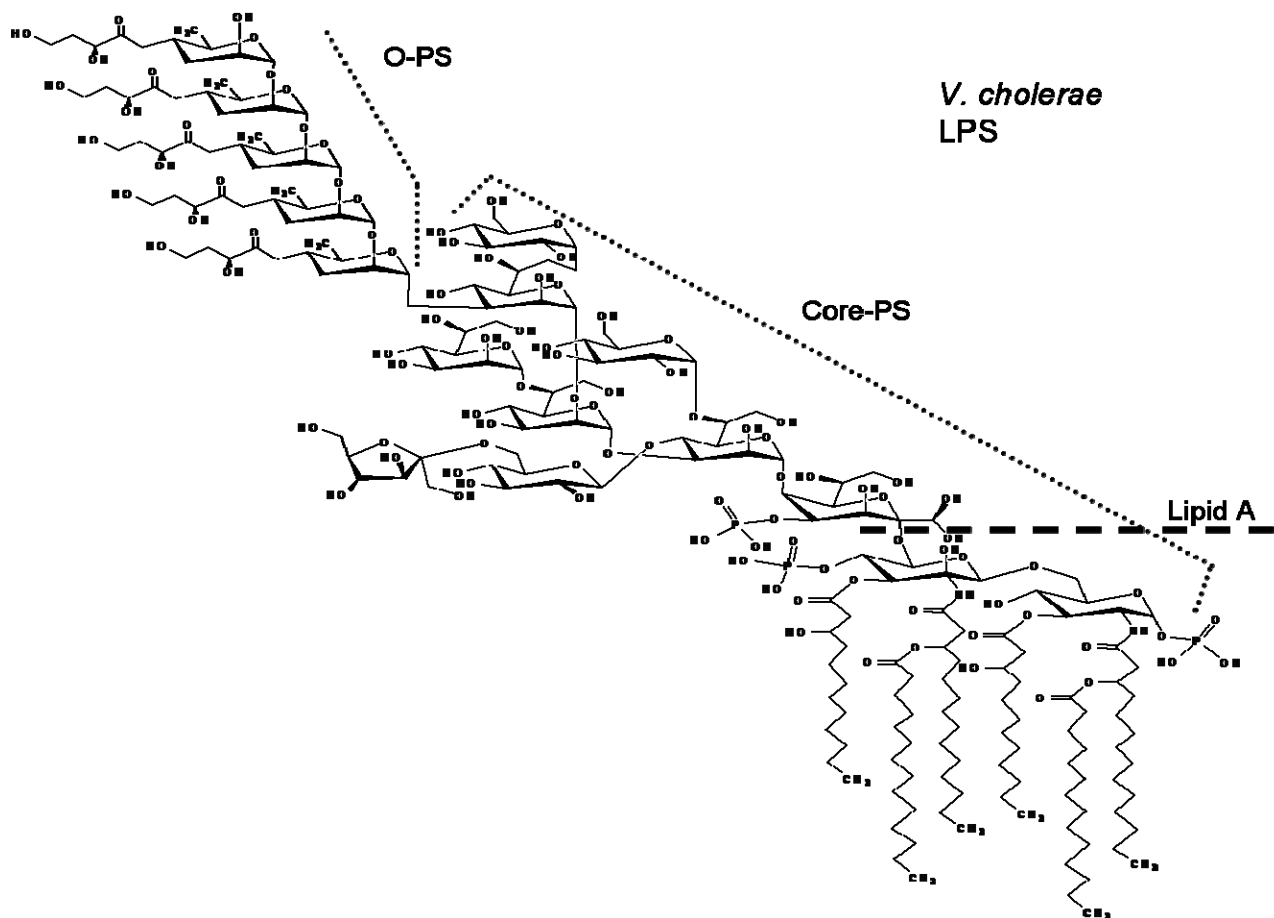
infection. Many of the immune activating abilities of LPS can be attributed to the lipid A unit.⁶

Vibrio cholerae (*V. cholerae*) causes the epidemic diarrheal disease cholera. Disease occurs when contaminated food or water is ingested, resulting in a voluminous secretory diarrhea that can lead to dehydration and death if left untreated. *V. cholerae* strains can be further subdivided into two biotypes, classical and El Tor, which differ biochemically and clinically.⁷ The first cholera pandemics were caused by the classical biotype, however, the current pandemic was caused by the El Tor biotype.⁸ Classical strains typically cause a more severe disease, while El Tor cause less severe and sometimes even asymptomatic cases. However, El Tor strains appear to have increased fitness in the environment, which may be why they have largely replaced classical strains as the cause of disease in recent years.⁹ Classical strains are very sensitive to polymyxin B, while El Tor strains are relatively resistant. Our collaborators hypothesized that differences in surface structures of the two biotypes are responsible for differential sensitivity, and chose to characterize the role of *msbB*, a lipid IV_A acyltransferase, with regard to antimicrobial peptide resistance and virulence in *V. cholerae*. Dr. Jyl Matson in Prof. DiRita's group in the University of Michigan Medical School carried out genetic screens to identify genes associated with resistance and sensitivity to polymyxin B in El Tor and classical *V. cholerae*, respectively. They found that *msbB* contributes to the resistance of El Tor strains to several antimicrobial peptides and is necessary for wild type colonization of mice. In contrast, classical strains lacking *msbB* show wild type resistance and colonization phenotypes. Mass spectrometric analysis was necessary to

characterize the structure of lipid A from classical *V. cholerae* (O395) as well as El Tor *V. cholerae* (C6706).

Lipid A is a glucosamine dimer, which is N- and O-acylated at the C-2, C-3, C-2' and C-3' positions by up to seven C₁₀-C₁₈ fatty acids. It is also phosphorylated at the C-1 and/or C-4' positions of the disaccharide ring as shown in Scheme B.1. Structural characterization of lipid A has been performed by NMR spectroscopy¹⁰⁻¹¹ and by mass spectrometry using various ionization techniques.¹²⁻¹⁵ Soft ionization, such as electrospray ionization (ESI) can reduce the internal energy of desorbed molecular species, and hinder gas-phase fragmentation. Thus, soft ionization allows more complete structural determination of biomolecules compared to less soft technique (e.g., MALDI). ESI combined with collision induced dissociation (CID) has been employed to fragment lipid A gas-phase ions, providing structural information regarding the structure of intact lipid A.¹⁵⁻¹⁶

In this study, ESI-Fourier transform ion cyclotron resonance (FT-ICR) mass spectrometry was used to characterize the structure of lipid A by accurate molecular mass. A further aim was to compare CID and infrared multiphoton dissociation (IRMPD) for structural characterization of lipid A. CID is the most commonly used tandem mass spectrometric technique and has been used for lipid A analysis.¹⁵⁻¹⁶ IRMPD has also been applied to obtain structural information of lipid A.¹⁷ Generally, CID and IRMPD provided similar structural information for lipid A. However, fragmentation efficiency was dependent upon the number of lipid A fatty acids, and its charge state.



Scheme B.1. Lipopolysaccharide (LPS) of *V. cholerae*. As shown here, LPS is composed of three main parts: (i) the O-antigen polysaccharide (O-PS); (ii) the relatively conserved core polysaccharide (core-PS); and (iii) lipid A, the hydrophobic lipid component responsible for biological activities within the host.

B.2. Experimental Section

B.2.1. Sample Preparation

LPS (lipopolysaccharide) of *E. coli* K-235 was purchased from Sigma-Aldrich (St. Louis, MO) and used without further purification. LPS of *V. cholerae* was prepared and provided by Dr. DiRita's group at the University of Michigan Medical School.¹⁸

B.2.2. Fourier Transform Ion Cyclotron Resonance Mass Spectrometry

ESI-FTICR MS was performed using an Apollo II ion source and an APEX-Q instrument (Bruker Daltonics) in negative ion mode. Lipid samples were dissolved in a 49.95/49.95/0.1 (v/v/v) mixture of isopropanol/water/triethylamine (pH ~9), and electrosprayed at a flow rate of 70 $\mu\text{L/h}$ with a capillary voltage of 3.7 kV and a drying gas temperature of 130 $^{\circ}\text{C}$. The final concentration of lipid A was 0.4-0.5 mg/ml in spraying solvent. Ions produced by ESI were mass-selectively externally accumulated¹⁹⁻²⁰ in a hexapole for 0.2-2 s, transferred via high voltage ion optics, and captured in the ICR cell by dynamic trapping. This accumulation sequence was looped three times to improve precursor ion abundance.

For tandem mass spectrometry (MS/MS) experiments, CID was performed at a collision cell DC offset of 30-40 V with Ar as collision gas. IRMPD was performed inside the ICR cell with a 25 W, 10.6 μm , CO_2 laser (Synrad, Mukilteo, WA). The laser beam was deflected by two mirrors for alignment through a hollow dispenser cathode to the center of the ICR cell. The beam entered the vacuum system through a BaF_2 window. Photon irradiation was performed for 100-180 ms at 7.5-10 W laser power. Also, electron detachment dissociation (EDD) was performed for comparison. An indirectly heated hollow dispenser cathode was used for electron generation.²¹ A heating current of 1.8 A was applied to a heater element located behind the cathode. For EDD, performed inside the ICR cell, the cathode bias voltage was pulsed to 20 V for 4 s. All mass spectra were acquired with XMASS software (version 6.1, Bruker Daltonics) in broadband mode from m/z 200 to 5000 with 256K data points and summed over 20-60 scans. Data processing was performed with the MIDAS analysis software²² LPS from *E.*

coli K-235 (Sigma-Aldrich) was used to perform external calibration with two lipid A anionic species (m/z 1796.212 for lipid A_{hexa} and m/z 1017.639 for lipid A_{tri-PO₄H₃}). All mass spectral peaks were assigned within 10 ppm mass accuracy.

B.3. Results and Discussion

The structure of *V. cholerae* LPS is shown in Scheme B.1. As indicated, lipid A is the hydrophobic component of LPS. Lipid A from four different strains (two wild types and two mutants for each wild type) of *V. Cholerae* were compared as shown in Figure B.1. Peaks were assigned using exact mass obtained from FT-ICR MS and tandem mass spectrometric methods (CID and IRMPD). MS analysis showed that classical *V. cholerae* lacking *msbB* produced hexa-acylated lipid A, where deletion of *msbB* in El Tor (C6706 $\Delta msbB$) and classical *V. Cholerae* (O395 $\Delta msbB$) resulted in loss of an acyl chain, as expected.¹⁸

Figure B.1 shows that two wild types (C6706 and O395) have lipid A_{hexa} (hexa-acylated lipid A), but two mutants (O395 $\Delta msbB$ and C6707 $\Delta msbB$) do not. Peak assignment was based on exact mass obtained by FT-ICR MS, and MS/MS. As an example, Figure B.2 shows MS/MS of lipid A_{penta} (penta-acylated lipid A) from the mutant O395. Both CID and IRMPD provided acyl chain loss from lipid A_{penta}, forming lipid A_{tetra} (tetra-acylated lipid A). Phosphate loss from both lipid A_{penta} and lipid A_{tetra} was also observed. These MS/MS results confirmed the peak assignment. However, CID and IRMPD spectra of lipid A_{hexa} were more different, as shown in Figure B.3. CID did not provide any fragmentation, regardless of collision energy. On the contrary,

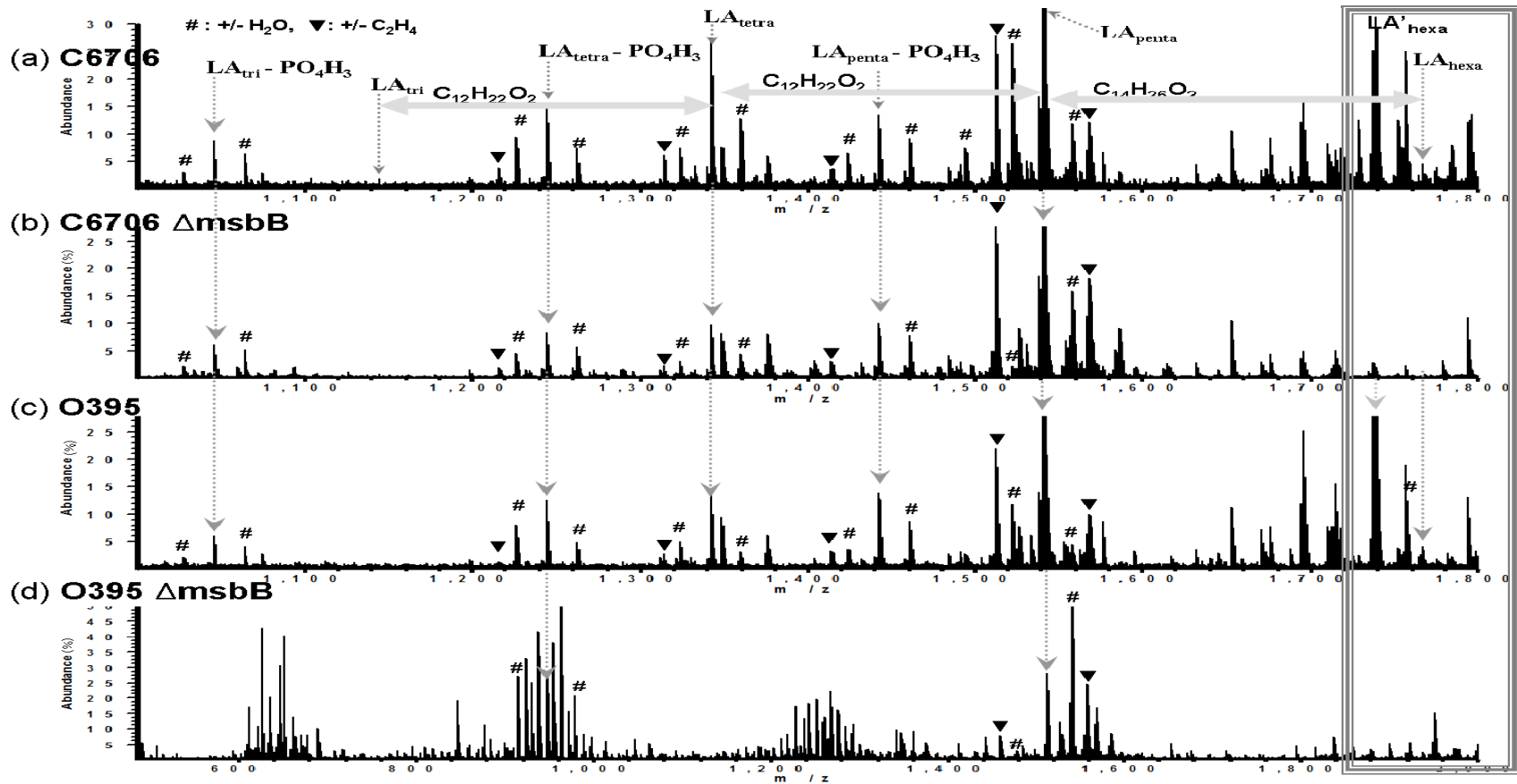


Figure B.1. Mass spectra of lipid A from four strains of *V. cholerae* (two wild types and two mutants); (a) C6706, (b) C6706 $\Delta msbB$, (c) O395, and (d) O395 $\Delta msbB$. LA_{hexa} indicates hexa-acylated lipid A, LA_{penta} indicates penta-acylated lipid A, and so on. LA'_{hexa} indicates hexa-acylated lipid A containing fatty acid with different number of carbons. # indicates H_2O adduct or loss, and ▲ indicates difference of C_2H_4 between adjacent abundant peaks. The m/z region highlighted with a box shows the major difference among four strains of *V. cholerae*.

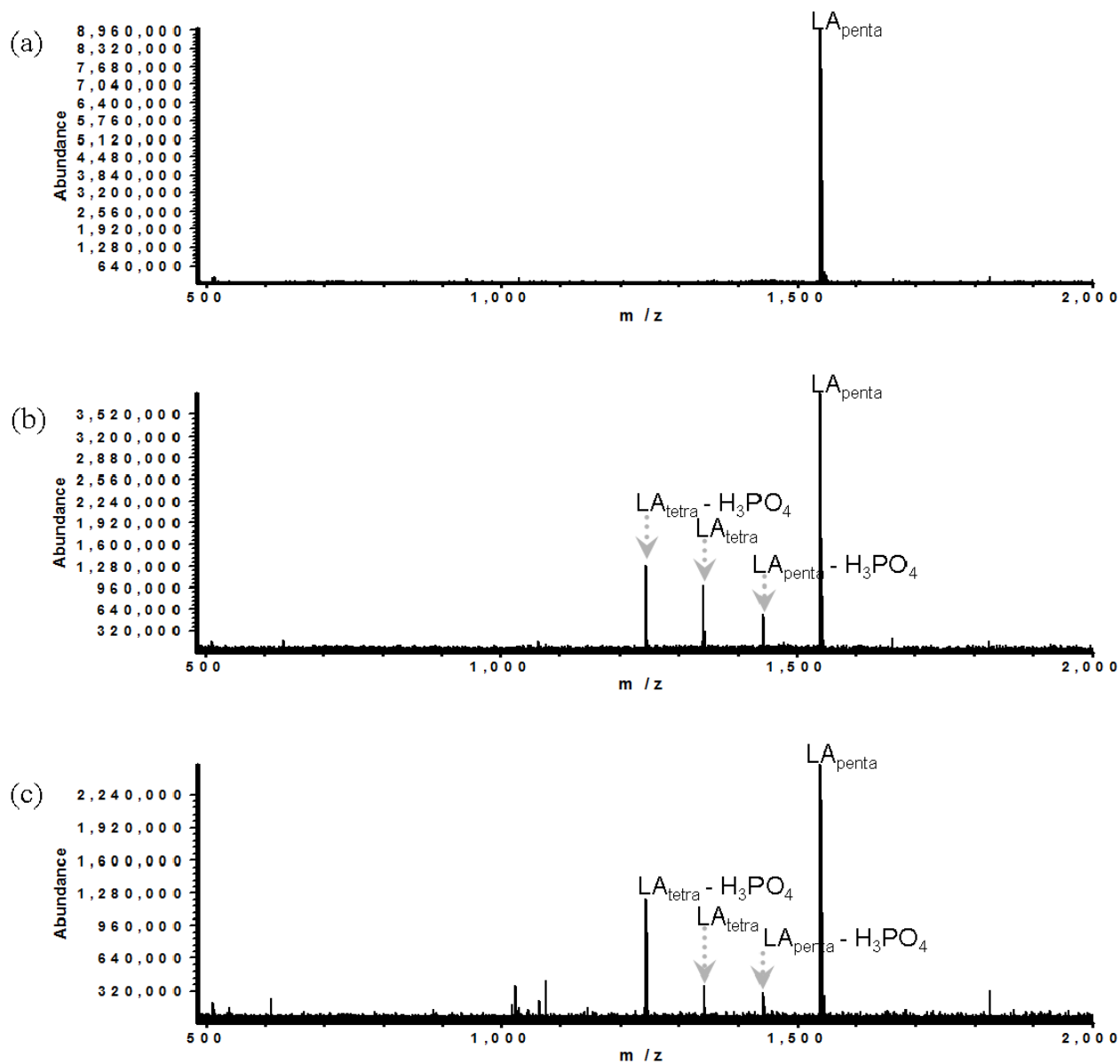


Figure B.2. MS/MS of lipid A_{penta} from *V. cholerae* O395; (a) isolation of singly deprotonated lipid A_{penta}, (b) CID of lipid A_{penta} (collision voltage 35 V), (c) IRMPD of lipid A_{penta}, (10 W laser power for 120 ms).

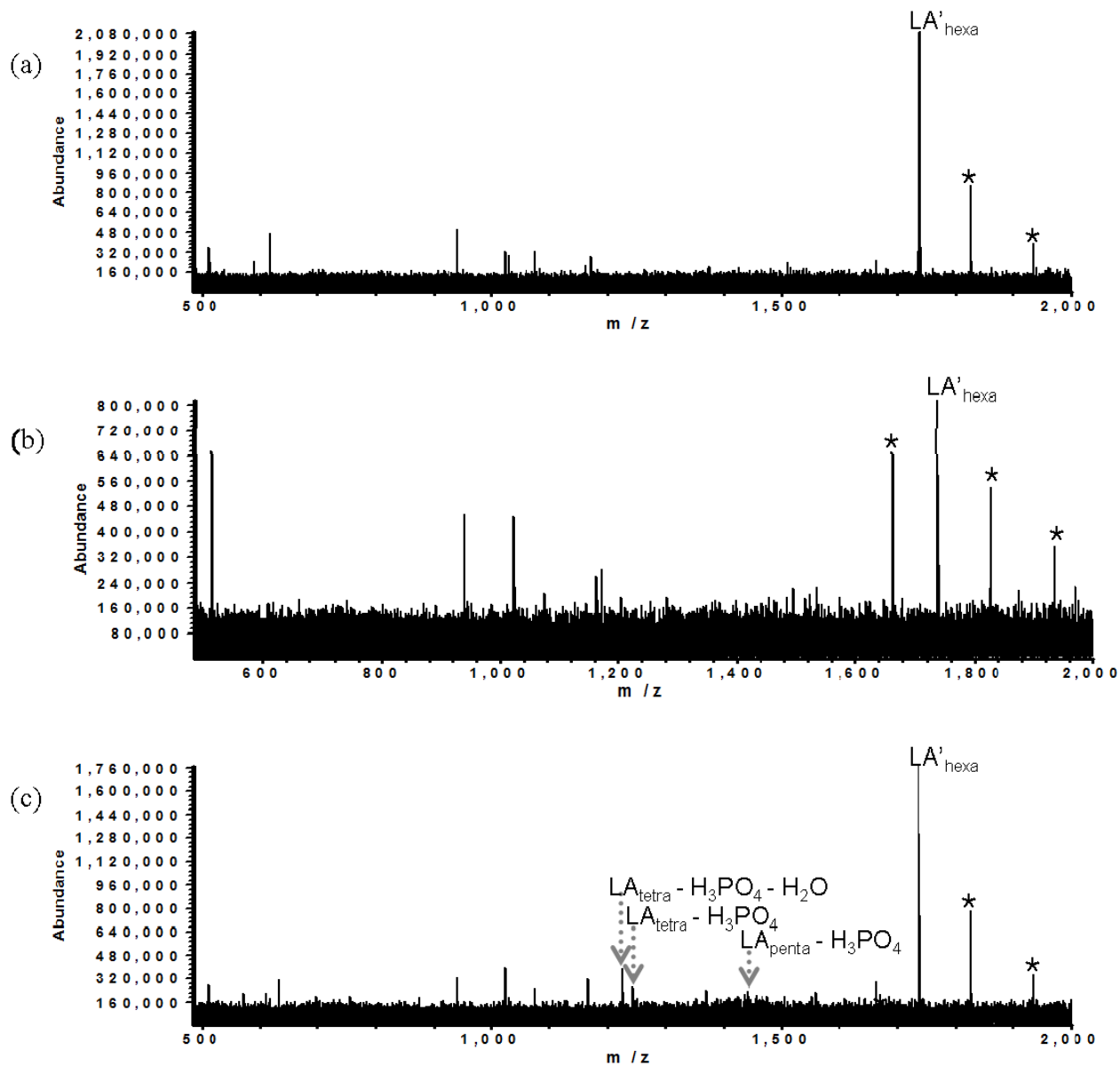


Figure B.3. MS/MS of lipid A_{hexa} from *V. cholerae* O395; (a) isolation of singly deprotonated lipid A_{hexa} , (b) CID of lipid A_{hexa} (collision voltage 40 V), (c) IRMPD of lipid A_{hexa} (10 W laser power for 180 ms).

IRMPD of lipid A_{hexa} provided structural information in a similar manner as CID and IRMPD of lipid A_{penta}.

As a comparison, lipid A from *E. coli* K-235 was also subjected to CID and IRMPD. Similar fragmentation patterns were observed in CID and IRMPD of Lipid A_{penta}, as shown in Figure B.4. As expected (based on the results for *V. cholerae* lipid A), lipid A_{hexa} yielded very limited fragmentation in CID, however, extensive fragmentation was observed in IRMPD, as shown in Figure B.5. It is currently unclear what causes this difference in fragmentation of lipid A_{hexa} in CID and IRMPD. It is assumed that hexa-acylated lipid A would have more non-covalent interactions between the six fatty acids. Thus, it is expected that more energy may be needed to break these interactions and generate fragments during the CID process for hexa-acylated lipid A, compared to penta- or tetra-acylated lipid A. On the other hand, molecular ions remain in the ICR cell during IRMPD, which may aid deprotonated lipid A in absorbing energy more efficiently. In addition, IRMPD activation can be carefully controlled simply by changing the IR irradiation time. Thus, IRMPD may be more efficient at breaking non-covalent interactions among the six fatty acyl chains, thereby providing valuable structural information of lipid A_{hexa}. Also, lipid A contains phosphate groups, well known chromophores in the IR region,²³⁻²⁴ which render IRMPD a more preferable MS/MS strategy for lipid A analysis.

Lipid A_{penta} or lipid A_{tetra} should need less energy to break non-covalent interactions among fatty acid chains due to the smaller number of fatty acids compared to lipid A_{hexa}. The collision energies used in this study may be sufficient to break non-covalent interactions in lipid A_{penta} or lipid A_{tetra}, but not in lipid A_{hexa}. Thus, explaining the

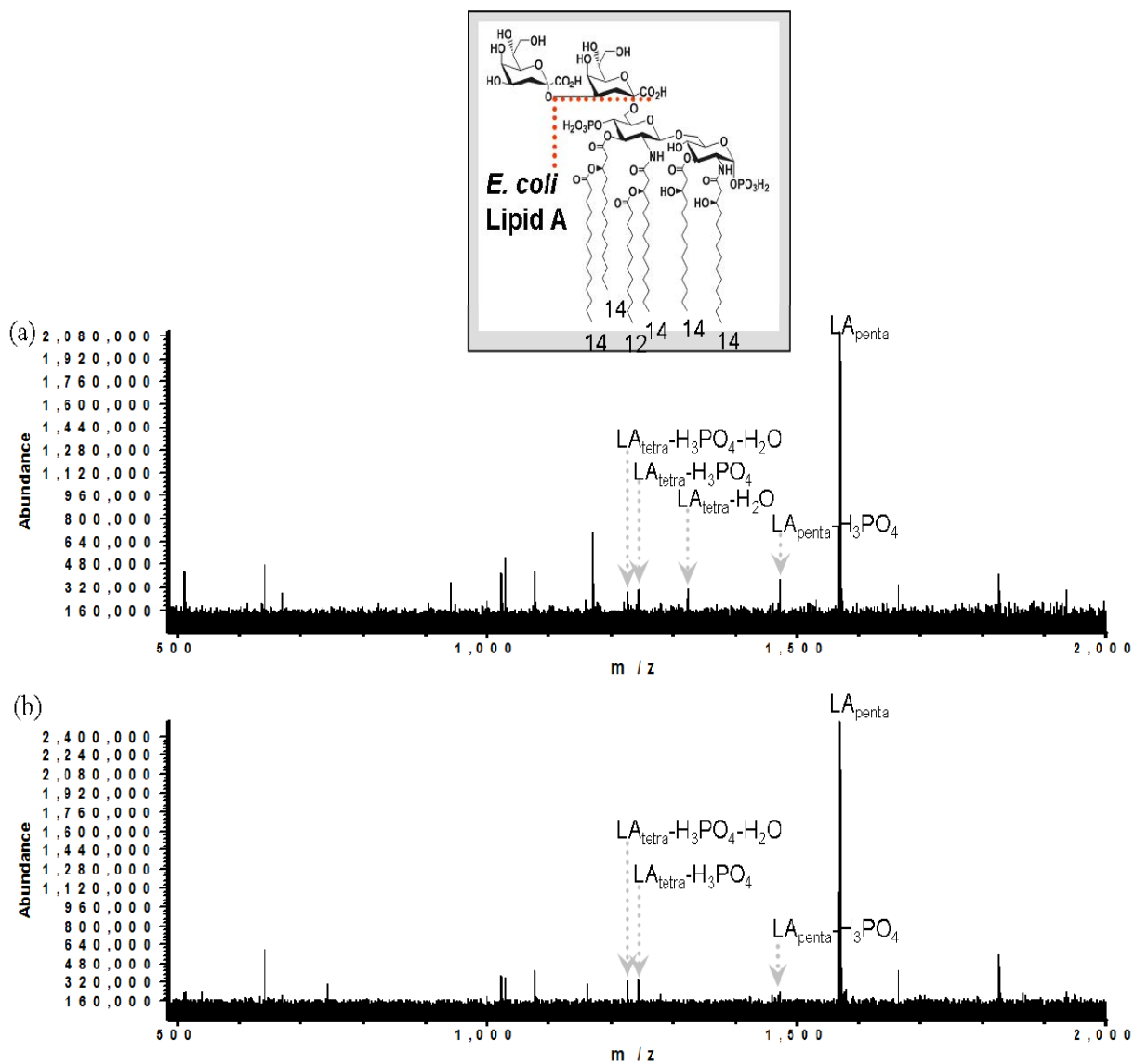


Figure B.4. MS/MS of lipid A_{penta} from *E. coli* K-235; (a) CID of lipid A_{penta} (collision voltage 35 V), (b) IRMPD of lipid A_{penta} (10 W laser power for 100 ms). The inset shows the structure of lipid A from *E. coli* K-235.

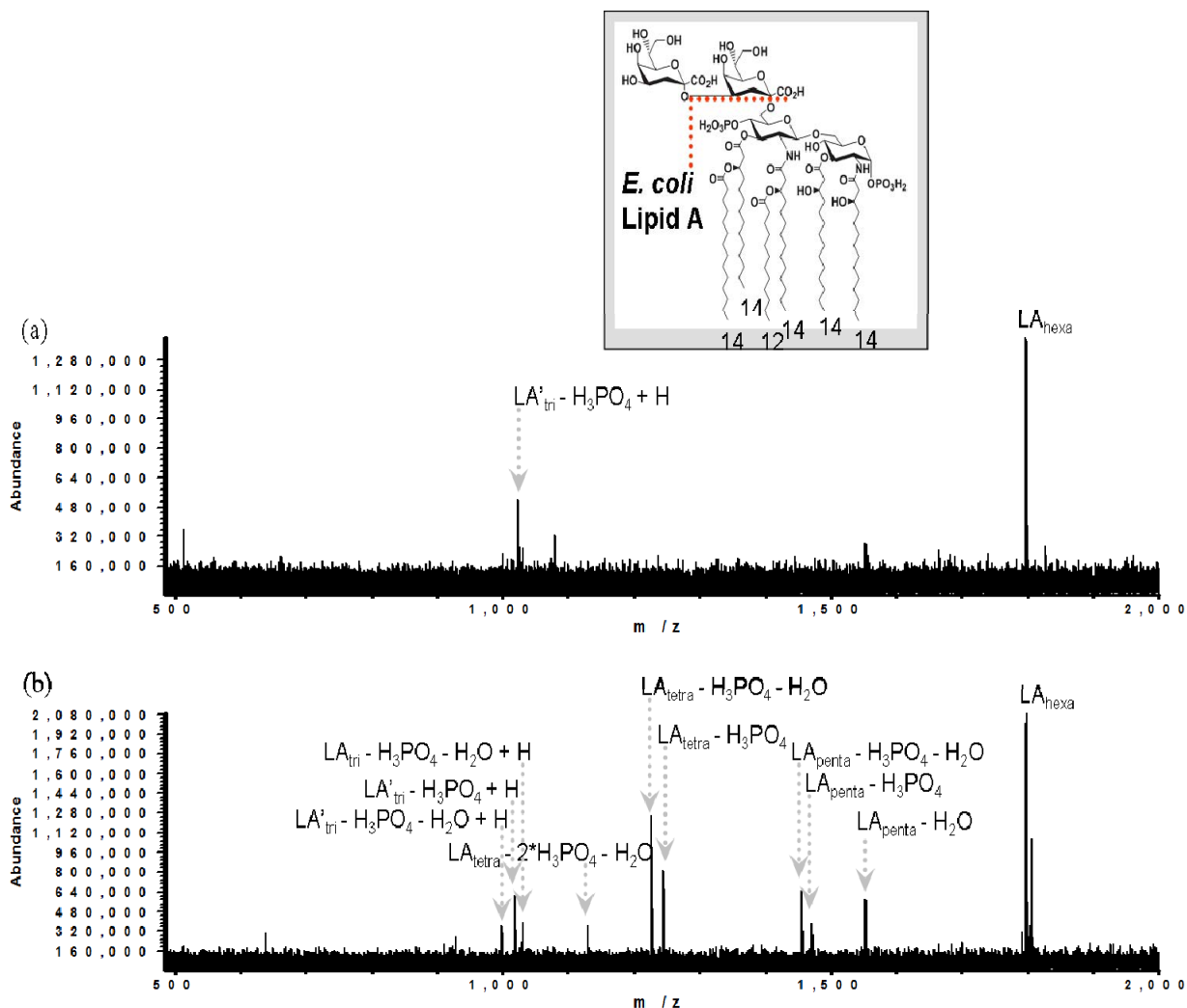


Figure B.5. MS/MS of lipid A_{hexa} from *E. coli* K-235; (a) CID of lipid A_{hexa} (collision voltage 40 V), (b) IRMPD of lipid A_{hexa} (7.5 W laser power for 100 ms). The inset shows the structure of lipid A from *E. coli* K-235.

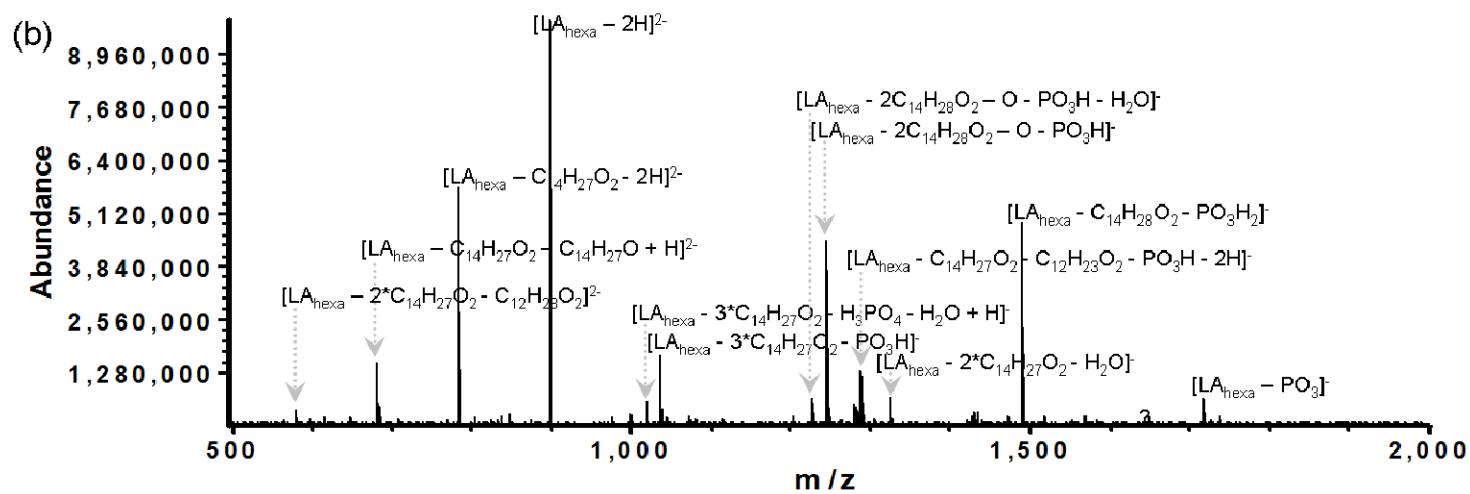
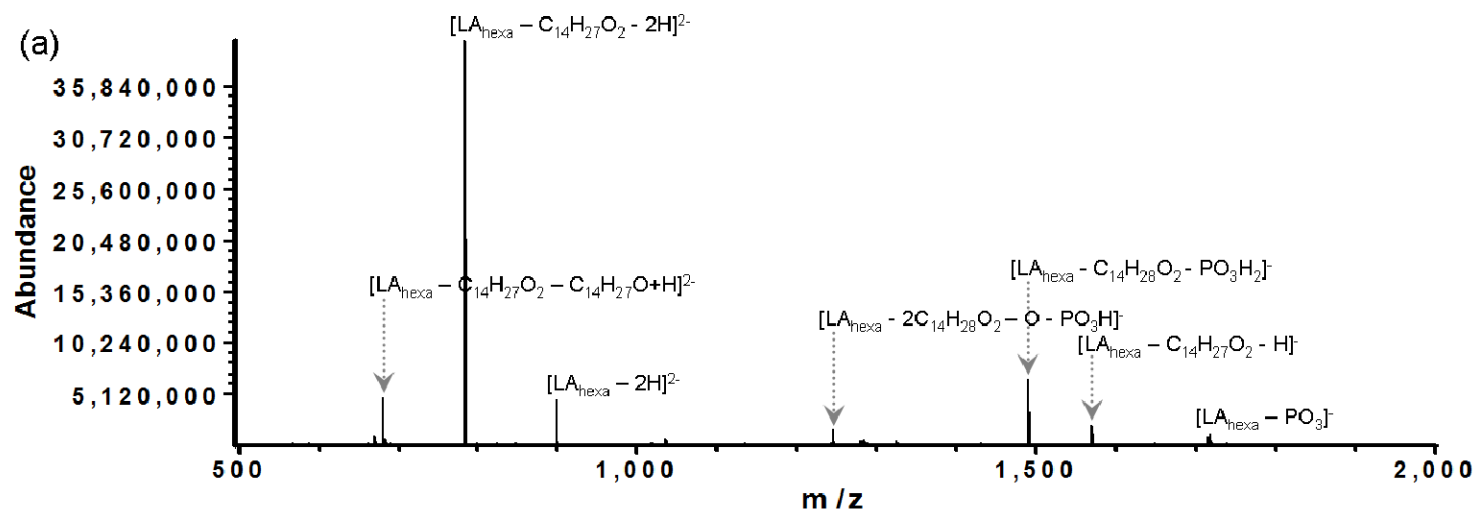
similar fragmentation behavior in CID and IRMPD of lipid A_{penta} and lipid A_{tetra}. However, there were obvious differences observed between CID and IRMPD of lipid A_{hexa}. Madalinski et. al. also studied lipid A structure using low energy CID.¹⁶ In their study, product ions generated from lipid A_{hexa} were observed but with low abundances. The amount of lipid A used for CID was not stated in their study. If more *V. cholerae* lipid A was available in my study, several product ions might be observed in CID spectra,

however, fragmentation efficiency may still be much lower than that in IRMPD. When the same amount of lipid A_{hexa} was used (from *E. coli*), IRMPD provided more structural information than CID, as shown in Figure B.5.

Figure B.6 shows a comparison between CID, IRMPD, and EDD of doubly deprotonated lipid A_{hexa} from *E. coli*. CID of doubly deprotonated lipid A_{hexa} (Figure B.6a) provided more fragmentation compared to CID of singly deprotonated lipid A_{hexa} (Figure B.5a). Higher charge states reach higher kinetic energy during acceleration and are less stable due to intramolecular Coulomb repulsion. Consequently, more abundant fragmentation was observed in CID of doubly deprotonated lipid A_{hexa} compared to singly deprotonated lipid A_{hexa} .²⁵ However, the preferred fragmentation pathway in CID was loss of one fatty acyl group from precursor ions. Other fragmentation pathways were much less prevalent. On the other hand, IRMPD resulted in more evenly abundant fragments, and a larger variety of fragmentation pathways were observed compared to CID. EDD provided very similar structural information as CID and its fragmentation efficiency was significantly lower than other MS/MS strategies.

B.4. Conclusions

CID and IRMPD were compared for the purpose of lipid A structural characterization. IRMPD appears preferable over CID for structural determination of lipid A_{hexa} because CID resulted in limited fragmentation, possibly due to strong non-covalent interactions between the six fatty acyl groups of lipid A_{hexa} . However, CID and IRMPD provided similar fragmentation efficiencies for lipid A containing less than five



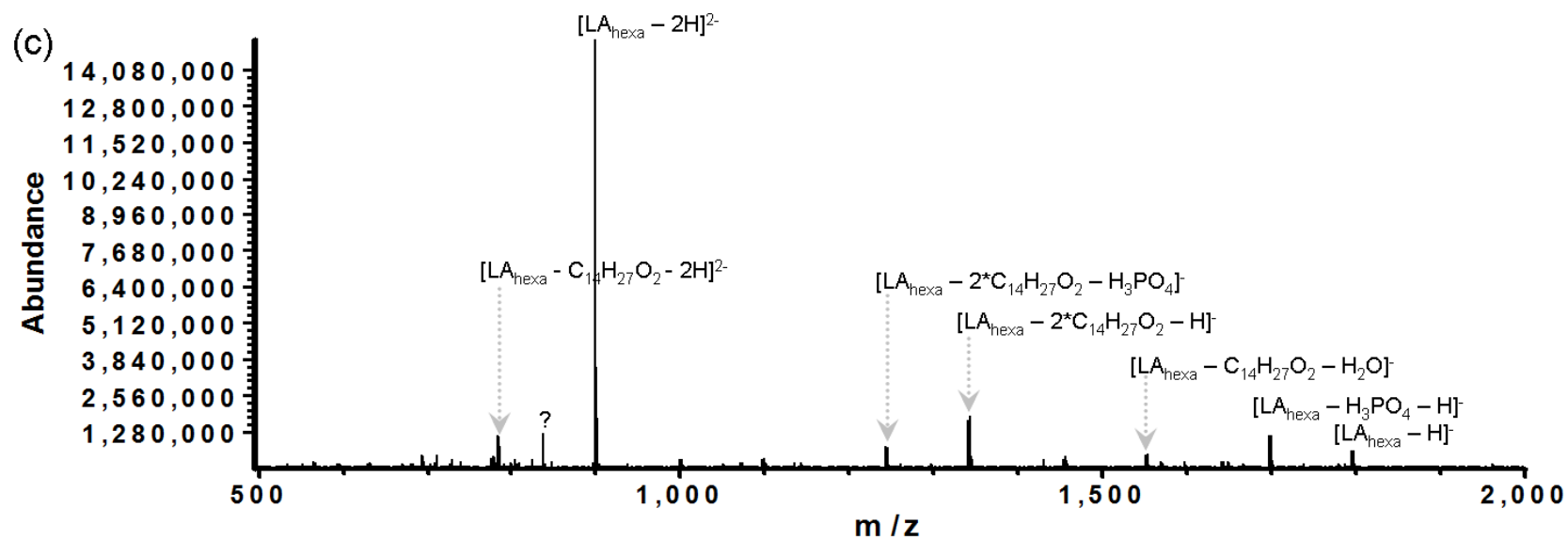


Figure B.6. MS/MS of doubly deprotonated lipid A_{hexa} from *E. coli* K-235; (a) CID of lipid A_{hexa} (collision voltage 15 V), (b) IRMPD of lipid A_{hexa} (10 W laser power for 100 ms). (C) EDD of lipid A_{hexa} (~20 eV electrons for 4 s).

fatty acyl groups. In addition, for doubly deprotonated lipid A, IRMPD provided more efficient and extensive fragmentation compared to CID and EDD.

B.5. References

1. Luderitz, O.; Westphal, O. *Angew Chem Int Ed Engl* **1966**, *5*. 198-210.
2. Gmeiner, J.; Luderitz, O.; Westphal, O. *Eur J Biochem* **1969**, *7*. 370-379.
3. Darveau, R. P. *Curr Opin Microbiol* **1998**, *1*. 36-42.
4. Netea, M. G.; van Deuren, M.; Kullberg, B. J.; Cavaillon, J. M.; Van der Meer, J. W. *Trends Immunol* **2002**, *23*. 135-139.
5. Dotson, G. D.; Kaltashov, I. A.; Cotter, R. J.; Raetz, C. R. *J Bacteriol* **1998**, *180*. 330-337.
6. Raetz, C. R.; Whitfield, C. *Annu Rev Biochem* **2002**, *71*. 635-700.
7. Chatterjee, S. N.; Chaudhuri, K. *Biochim Biophys Acta* **2003**, *1639*. 65-79.
8. Sack, R. B.; Siddique, A. K.; Longini, I. M., Jr.; Nizam, A.; Yunus, M.; Islam, M. S.; Morris, J. G., Jr.; Ali, A.; Huq, A.; Nair, G. B.; Qadri, F.; Faruque, S. M.; Sack, D. A.; Colwell, R. R. *J Infect Dis* **2003**, *187*. 96-101.
9. Yoon, S. S.; Mekalanos, J. J. *Infect Immun* **2006**, *74*. 6547-6556.
10. Zahringer, U.; Lindner, B.; Rietschel, E. T. *Adv Carbohydr Chem Biochem* **1994**, *50*. 211-276.
11. Czaja, J.; Jachymek, W.; Niedziela, T.; Lugowski, C.; Aldova, E.; Kenne, L. *Eur J Biochem* **2000**, *267*. 1672-1679.
12. Qureshi, N.; Mascagni, P.; Ribi, E.; Takayama, K. *J Biol Chem* **1985**, *260*. 5271-5278.
13. Cole, R. B.; Domelsmith, L. N.; David, C. M.; Laine, R. A.; DeLucca, A. J. *Rapid Commun Mass Spectrom* **1992**, *6*. 616-622.
14. Kaltashov, I. A.; Doroshenko, V.; Cotter, R. J.; Takayama, K.; Qureshi, N. *Anal Chem* **1997**, *69*. 2317-2322.
15. Boue, S. M.; Cole, R. B. *J Mass Spectrom* **2000**, *35*. 361-368.
16. Madalinski, G. F., F.; Wind, F. C.; Afonso, C.; Tabet, J. C. *Int. J. of Mass Spectrom.* **2006**, *249-250*. 77-92.
17. Muller-Loennies, S.; Lindner, B.; Brade, H. *J Biol Chem* **2003**, *278*. 34090-34101.
18. Matson, J. S.; Yoo, H. J.; Hakansson, K.; Dirita, V. J. *J Bacteriol* **2010**, *192*. 2044-2052.
19. Belov, M. E.; Nikolaev, E. N.; Anderson, G. A.; Udseth, H. R.; Conrads, T. P.; Veenstra, T. D.; Masselon, C. D.; Gorshkov, M. V.; Smith, R. D. *Anal Chem* **2001**, *73*. 253-261.
20. Hendrickson, C. L.; Quinn, J. P.; Emmett, M. R.; Marshall, A. G., in *49th ASMS Conference on Mass Spectrometry and Allied Topics*. Chicago, IL, 2001; CD-ROM.
21. Tsybin, Y. O.; Hakansson, P.; Budnik, B. A.; Haselmann, K. F.; Kjeldsen, F.; Gorshkov, M.; Zubarev, R. A. *Rapid Commun Mass Spectrom* **2001**, *15*. 1849-1854.
22. Senko, M. W.; Canterbury, J. D.; Guan, S.; Marshall, A. G. *Rapid Commun Mass Spectrom* **1996**, *10*. 1839-1844.

23. Yoo, H. J.; Liu, H.; Hakansson, K. *Anal Chem* **2007**, *20*. 7858-7866.
24. Flora, J. W.; Muddiman, D. C. *J Am Chem Soc* **2002**, *124*. 6546-6547.
25. Chen, M.; Su, X.; Yang, J.; Jenkins, C. M.; Cedars, A. M.; Gross, R. W. *Anal Chem* *82*. 163-171.